

Mechanistic Studies of Two Ni-Catalyzed Reactions: Reductive Amidation of Esters with Nitroarenes and Hydrosilylation of Alkenes

Présentée le 28 août 2020

à la Faculté des sciences de base
Laboratoire de synthèse et de catalyse inorganique
Programme doctoral en chimie et génie chimique

pour l'obtention du grade de Docteur ès Sciences

par

Marten Leendert PLOEGER

Acceptée sur proposition du jury

Prof. T. Rizzo, président du jury
Prof. X. Hu, directeur de thèse
Prof. M. Costas, rapporteur
Dr C. Scarborough, rapporteur
Prof. K. Severin, rapporteur

Acknowledgements

First, I would like to thank my supervisor, professor Xile Hu for giving me the opportunity to work in his group and for the guidance he has given me over the past four years. I enjoyed the large amount of freedom with which I was able to conduct research in his group, but also deeply appreciate his understanding of when it is time to wrap up a project rather than spending more time to discover additional details about a mechanism.

I would also like to thank the members of my jury, professor Kai Severin, professor Miquel Costas, Dr. Chris Scarborough and my jury president professor Thomas Rizzo, for their willingness to evaluate my work.

I would also like to thank the members of the magasin in the BCH for keeping the supplies running smoothly and always being available for questions regarding ordering chemicals or dealing with waste. I am also thankful to our secretary Christina Zamanos-Epremian for all the help with administrative issues and the many trips I have had to take throughout my PhD.

I am grateful to the members of the ISIC NMR, X-Ray and mass spectrometry teams for maintaining excellent facilities for analytical techniques. In particular, I would like to thank Dr. Daniel Ortiz, who was always very willing to help me with my many attempts to characterize highly sensitive intermediates with HRMS. Although it has unfortunately not worked out in the end, it certainly was not because of a lack of trying. Special thanks also go out to Dr. Aurélien Bornet, who was always more than willing to help me set up special NMR experiments and to educate me a bit more on some of the technical details behind them. I am also very grateful to Dr. Euro Solari, who performed the elemental analysis and could often do so at a moments notice.

I'd like to thank my current and former group members for the pleasant working atmosphere that I have enjoyed over the last four years. I am especially grateful to Aliko and Guido, with whom I have shared such a large portion of these four years. I have always enjoyed your company both inside and outside the lab. I am also very happy to have met Zach, Salome and Jade in my final year. Although I only just got to know you during the tail end of my PhD, I always enjoyed the climbing sessions and various other social outings with you. I am also very happy with Jade's help with the translation of the abstract to French.

I am also grateful to all the people involved with NoNoMeCat. Professor Bert Klein-Gebbink and Dr. Johann Jastrzebski have done a great job in keeping things going smoothly. I feel the

group always got along together great and the meetings we've had together were always a lot of fun. Of course, I am especially grateful to Andréa. Our collaboration was an incredible amount of work, but it never felt bad and I really enjoyed the informal manner with which we were able to work together.

Finally, I would like to thank some people from back home in The Netherlands. Monalisa, I am very happy we have reconnected after I missed my chance to work at Homkat. I always enjoy our meetings whenever we manage to find some time for them and our discussions about life and academia always give me a lot to think about.

Tjerk, Mayke, Janne en Jerinike, it is hard to overstate how important your support has been in the years leading up to and during my PhD. I can honestly say I would not be where I am now without you and for that I am deeply grateful.

Abstract

Mechanistic investigations into homogeneously catalyzed reactions are essential for the further development of synthetic methodologies. Insights in the overall reaction pathway and vital steps such as the rate-determining and selectivity-determining steps allow for rational design of improved catalysts. Moreover, mechanistic investigations may reveal the existence of unexpected intermediates in the catalytic cycle. The discovery of such intermediates may inspire new methodologies that would not have been considered if their formation was unknown.

Because of economic advantages over heavier congeners, there has been a recent surge in the use of nickel -based homogeneous catalysts. Although much progress has been made into methodology development, the mechanistic understanding of the new reactivities is relatively primitive. In-depth mechanistic investigations into nickel catalyzed reactions are therefore of considerable interest.

Chapters 2-4 deal with the mechanism of reductive coupling of nitroarenes and esters to form amides. In chapter 2, the initial reduction pathway that occurs before the reaction with ester is investigated, revealing the crucial intermediate to be azobenzene and the source of the proton in the final amide product. In chapter 3, kinetics, Hammett plots, competition experiments and stoichiometric reactions with a potential intermediate are described. These studies reveal azobenzene is reductively cleaved by low-valent nickel before the ester gets involved in the reaction. Moreover, ZnCl_2 , a byproduct of the reduction of the nickel precursor by zinc, is revealed to play an important role in several steps of the reaction. In chapter 4, the computational investigation based on the experimental data is discussed. By combining the computational exploration of the potential energy surface with qualitative kinetic analysis, a catalytic cycle for the reaction between azobenzene and ester could be proposed.

The finding that the reaction between azobenzene and ester goes through nickel imide intermediates is intriguing as nickel imides are known to react with a variety of substrates and azobenzene would be a relatively benign precursor to them. Chapter 5 reports a preliminary exploration of several types of reactivities can be expected to work on the basis that the reactivity with imides is already known. Several types of these reactivities seem to be inaccessible as they are incompatible with the highly reductive nature of the nickel catalyst that is required for the azobenzene activation. However, some other reactivities show promise.

Chapter 6 reports an investigation in the alkene hydrosilylation catalyzed by a nickel pincer complex developed in our group. Previous investigations had indicated a nickel alkyl complex

was the resting state. However, a combination of reaction progress analysis, transmission electron microscopy and competition reactions reveal that this is merely a precatalyst. Under catalytic conditions, it slightly decomposes to form the true catalyst, which is tentatively identified as nickel nanoparticles.

Key words: mechanistic studies, nitrobenzene, amidation, azobenzene, nickel imide, hydrosilylation, nickel nanoparticles

Résumé

Les recherches mécanistes sur les réactions catalysées de manière homogène sont essentielles pour le développement ultérieur des méthodologies synthétiques. Les informations concernant la voie de réaction globale et de ces étapes cruciales telles que les étapes déterminantes de vitesse et de sélectivité permettent une conception rationnelle de catalyseurs améliorés. En outre, les études mécanistiques peuvent révéler l'existence d'intermédiaires inattendus dans le cycle catalytique. La découverte de tels intermédiaires peut inspirer de nouvelles méthodologies qui n'auraient pas été envisagées si leur formation était inconnue.

En raison des avantages économiques par rapport aux congénères plus lourds, l'utilisation de catalyseurs homogènes à base de nickel a récemment connu une forte augmentation. Bien que de nombreux progrès aient été réalisés dans le développement de méthodologies, la compréhension mécanistique des nouvelles réactivités est relativement primitive. Des études mécanistiques approfondies sur les réactions catalysées par le nickel présentent donc un intérêt considérable.

Les chapitres 2 à 4 traitent du mécanisme de couplage réducteur des nitroarènes et des esters pour former des amides. Dans le chapitre 2, la voie de réduction initiale qui se produit avant la réaction avec l'ester est étudiée, révélant que l'intermédiaire crucial est l'azobenzène et la source du proton dans le produit amide final. Au chapitre 3, la cinétique, le diagramme de Hammett, les expériences de compétition et les réactions stoechiométriques avec un intermédiaire potentiel sont décrits. Ces études révèlent que l'azobenzène est clivé par réduction par le nickel de faible valence avant que l'ester ne soit impliqué dans la réaction. De plus, le ZnCl_2 , un sous-produit de la réduction du précurseur du nickel par le zinc, se révèle jouer un rôle important dans plusieurs étapes de la réaction. Au chapitre 4, l'étude computationnelle basée sur les données expérimentales est discutée. En combinant l'exploration computationnelle de la surface d'énergie potentielle avec une analyse cinétique qualitative, un cycle catalytique pour la réaction entre l'azobenzène et l'ester a pu être proposé.

La constatation selon laquelle la réaction entre l'azobenzène et l'ester passe par des intermédiaires d'imides de nickel est intrigante car les imides de nickel sont connus pour réagir avec une variété de substrats et l'azobenzène serait un précurseur relativement bénin pour ceux-ci. Le chapitre 5 rapporte exploration préliminaire de plusieurs types de réactivités qui devraient fonctionner sur la base du fait que la réactivité avec les imides est déjà connue. Plusieurs types de ces réactivités semblent être inaccessibles car ils sont incompatibles avec la nature hautement

réductrice du catalyseur au nickel nécessaire à l'activation de l'azobenzène. Cependant, certaines autres réactivités semblent prometteuses.

Le chapitre 6 rapporte une recherche mécanistique sur l'hydrosilylation d'alcène catalysée par un complexe en nickel développé dans notre groupe. Les recherches antérieures avaient indiqué un état de repos de l'alkyle de nickel. Cependant, une combinaison d'analyse de la progression de la réaction, de microscopie électronique à transmission et de réactions de compétition révèle qu'il s'agit simplement d'un précatalyseur. Il se décompose ensuite légèrement dans les conditions catalytiques pour former le véritable catalyseur, qui est provisoirement identifié comme étant des nanoparticules de nickel.

Mots Clés: études mécanistiques, nitrobenzène, amidation, azobenzène, imide de nickel, hydrosilylation, nanoparticules de nickel

List of symbols and abbreviations

°C	degrees Celsius
Å	Angstrom
acac	acetylacetonate
ATR-IR	attenuated total reflection infra red
azo	azobenzene
azoxy	azoxybenzene
BDE	bond dissociation energy
bipy	2,2'-bipyridine
BS	basis set
cat	catalyst
CCSD(T)	coupled cluster single double triple
cm ⁻¹	wavenumber
COD	1,4-biscyclooctadiene
Cp	cyclopentadienyl
CV	column volume
DCM	dichloromethane
dd	doublet of doublet
DFT	density functional theory
DHA	9,10-dihydroanthracene
DKH	Douglas-Kroll-Hess Hamiltonian
DME	dimethoxyethane
DMF	dimethylformamide
DMSO	dimethylsulfoxide
dtbpe	1,2-bis(ditertbutylphosphino)ethane
EDX	energy dispersive x-ray spectroscopy
ee	enantiomeric excess
Eelec	electronic energy
ene	1-octene
EPFL	Ecole Polytechnique Fédérale de Lausanne
EPR	electron paramagnetic resonance
equiv.	equivalents
FID	flame ionization detector
G	free energy
GC	gas chromatography
GC/MS	gas chromatography/mass spectrometry
G _{corr}	free energy corrections based on frequency calculations
h	hour
H	enthalpy
HRMS	high resolution mass spectrometry
K	Kelvin
kcal	kilocalorie
KIE	kinetic isotope effect
k _{obs}	observed rate constant
L	ligand

M	molar
m	multiplet
Me	methyl
Mes	2,4,6-trimethylphenyl
mg	milligram
MHz	megahertz
mL	milliliter
NLE	non-linear effect
NMP	N-methyl-2-pyrrolidinone
NMR	nuclear magnetic resonance
Nu	nucleophile
ON	overnight
PES	potential energy surface
phen	1,10-phenanthroline
ppm	parts per million
PTFE	Polytetrafluoroethylene
R ²	Coefficient of determination
RMSE	root mean square error
RPKA	reaction progress kinetic analysis
S	entropy
s	second
S ²	spin contamination
S _N 1	monomolecular nucleophilic substitution
t	time
t	triplet
T	temperature
td	triplet of doublet
TEM	Transmission electron microscopy
TEMPO	(2,2,6,6-Tetramethylpiperidin-1-yl)oxyl
THF	tetrahydrofuran
TMS	trimethylsilyl
TON	turnover number
ν	reaction rate
V_{burr}	% of volume of sphere with radius r around metal center occupied by ligand
VTNA	variable time normalization analysis
δ	chemical shift
θ	Cone angle
μL	microliter
ρ	Hammett reaction parameter
σ	Hammett substituent constant

Contents

Chapter 1	Introduction.....	1
1.1	Homogeneous Catalysis	2
1.1.1	Mechanistic Research in Homogeneous Catalysis	2
1.2	Selected methods in mechanistic research	3
1.2.1	Kinetics	3
1.2.2	Hammett plots.....	8
1.2.3	Isotope labelling.....	10
1.2.4	Non-linear effects.....	12
1.2.5	Differential selectivity experiments.....	13
1.2.6	Computational modelling.....	14
1.3	Application of nickel in homogeneous catalysis.....	15
1.4	Mechanistic aspects of homogeneous nickel catalysis.....	16
1.4.1	Radical nature of cross coupling.....	16
1.4.2	Oxidation state	18
1.4.3	Speciation.....	18
1.4.4	Ligand design.....	19
1.5	Aim of the project.....	20
1.6	References	22
Chapter 2	Identification of intermediates in nickel catalysed amidation of esters with nitroarenes	33
2.1	Introduction	34
2.2	Identification of reactive species.....	35
2.3	Proton source.....	37
2.4	Insights into reduction pathway	39
2.5	Conclusions	41
2.6	Experimental	42

2.6.1	General remarks	42
2.6.2	Comments on GC analysis.....	42
2.6.3	General remarks on re-optimization of reaction conditions nitrobenzene-derived substrates.....	42
2.6.4	Reaction profile of nitrobenzene-ester coupling.....	45
2.6.5	Reaction profile of azoxybenzene-ester coupling.....	46
2.6.6	Quenching experiment	46
2.6.7	Reaction profile of nitrobenzene reduction.....	47
2.7	References	47
Chapter 3	Mechanism of Ni-catalyzed reductive amidation of unactivated esters with azobenzenes: experimental study.....	51
3.1	Introduction	52
3.2	In Situ ATR-IR monitoring	52
3.3	Kinetic studies	53
3.3.1	Standard conditions.....	53
3.3.2	Influence of ZnCl ₂	54
3.3.3	Kinetics at high [ZnCl ₂]	55
3.3.4	Reason for rate law change	56
3.4	Hammett plots	57
3.5	Search for Nickel-azoarene species.....	58
3.5.1	Reactivity of a Ni(0)-azoarene adduct	59
3.6	Discussion of decay pathway for 8^F	60
3.6.1	Involvement in catalytic cycle	60
3.6.2	Proposed decay product	61
3.7	Conclusions	62
3.8	Experimental	63
3.8.1	General experimental methods	63
3.8.2	General remarks of kinetic measurements.....	63

3.8.3	Stirring rate influence under low-[ZnCl ₂] conditions	66
3.8.4	Competition between an aromatic ester and an aliphatic ester	66
3.8.5	Reaction rate Hammett study	67
3.8.6	Competition Hammett study	69
3.8.7	Synthesis of 8^F	72
3.8.8	Reactivity 8^F with ester 1a	72
3.9	References	73
Chapter 4	Mechanism of Ni-catalyzed reductive amidation of unactivated esters with azobenzenes: computational study and overall conclusions.....	77
4.1	Introduction	78
4.2	Reduction of Ni(II) complex by Zn	78
4.3	Pathway for splitting azobenzene	80
4.4	Reactivity with ester	81
4.5	Qualitative Kinetic Analysis	83
4.5.1	Pathway via TS4	84
4.5.2	Pathway via TS4_Zn :	85
4.5.3	Pathway via TS5 :	86
4.6	Catalytic cycle	87
4.7	Conclusions	88
4.8	Experimental	89
4.8.1	Computational methods	89
4.8.2	Treatment of solid zinc	90
4.8.3	Coupled Cluster calculations for benchmarking	91
4.8.4	Spin state analysis	94
4.8.5	Solvation analysis for the complexes I , II and III	97
4.9	References	99
Chapter 5	Exploring reactivity of nickel-imide species derived from Ni-mediated activation of azobenzene.....	103

5.1	Introduction	104
5.2	Ligand considerations.....	105
5.3	Reaction with isonitrile	105
5.4	Amidation of aldehydes.....	106
5.5	C-H amination at acidic positions	107
5.5.1	α -Amination of nitroalkane.....	108
5.5.2	Ketone α -amination.....	108
5.5.3	Amination of terminal alkynes.....	109
5.6	Benzylic C-H amination.....	109
5.7	Discussion & Conclusion	112
5.8	Experimental	113
5.8.1	Computational details	113
5.8.2	Equipment.....	113
5.8.3	Materials	113
5.8.4	Synthesis N-cyclohexyl-1,10-phenanthroline-2-carboxamide (L4)	114
5.8.5	Screening with Ni(II)	114
5.8.6	Screening with Ni(0).....	115
5.8.7	Screening nickel-copper cocatalysis	115
5.9	References	116
 Chapter 6 Mechanistic Investigations of Nickamine-Catalyzed Hydrosilylation of Alkenes 123		
6.1	Introduction	124
6.2	Reaction progress monitoring by <i>in situ</i> ^1H NMR	126
6.3	Determination of true catalyst	129
6.3.1	Ex situ TEM.....	130
6.3.2	Mercury test	130
6.3.3	Competition experiments	131

6.4	Mechanism of decomposition 11-octyl	133
6.5	Discussion on TOF	136
6.6	Conclusions	137
6.7	Experimental	137
6.7.1	General experimental methods	137
6.7.2	Synthesis 11-octyl	138
6.7.3	NMR-followed hydrosilylation of 1-octene.....	138
6.7.4	Hydrosilylation of <i>trans</i> -(2-vinylcyclopropyl)benzene	139
6.7.5	Mercury test	139
6.7.6	Alkene competition.....	139
6.7.7	TEM sample preparation.....	140
6.7.8	Study of 11-octyl decompostion.....	140
6.7.9	Spectroscopic characterisation 1-(2-phenylethyl)	141
6.7.10	NMR-followed hydrosilylation of styrene.....	141
6.8	References	142

Chapter 1

Introduction

1.1 Homogeneous Catalysis

Homogeneous catalysis is of vital importance to the synthesis of valuable fine chemicals such as drugs or agrochemicals. Through careful design of the catalyst, reactions can be made more efficient, or more selective. The importance of research in homogeneous catalysis is clearly apparent from the Nobel prizes that have been awarded in recent decades to reactions enabled by homogeneous catalysis, such as asymmetric hydrogenation and epoxidation,¹ olefin metathesis² and palladium-catalyzed cross coupling.³ In order to address continuously increasing demands on sustainability and economic efficiency of chemical processes, the field of homogeneous catalysis constantly strives for improvements to better catalyst design and new reaction development.

1.1.1 Mechanistic Research in Homogeneous Catalysis

A vital part of the search for improvement of catalytic processes is development of a good understanding of the reaction mechanism. By knowing which reactivities are part of the catalytic cycle, what factors influence them and which steps are the slowest of the catalytic cycle, the protocol may be improved in a rational way rather than by broad screening of conditions.

One example of this is the finding that Suzuki-Miyaura reactions of aryl chlorides and aryl bromides are particularly efficient with tris(*tert*-butyl)phosphine. Mechanistic studies on the catalytic system suggested that this is due to formation of monoligated palladium complexes.⁴ With this in mind, Buchwald developed exceptionally bulky (dialkylphosphanyl)biaryls. Palladium(0) preferentially only binds one of these ligands, whereas most phosphines tend to form $L_2Pd(0)$ complexes. As a result the extremely bulky ligands are indeed extraordinarily effective for Suzuki coupling, allowing catalyst loadings of less than 1 mol% and non-activated aryl chlorides as substrates.^{5,6} The ligands proved to be effective for amination of aryl halides as well⁷ and is now a staple for screening palladium cross coupling catalysis.

Another example of the utility of mechanistic understanding of reactions for improving them is the development of better catalysts for olefin metathesis. Mechanistic studies have shown that both initiation and decomposition of the catalyst depend on the competition between substrate and a phosphine ligand. Tuning of the stability of the ruthenium phosphine bond therefore

provide the best way to strike the right balance between these two processes.^{8,9} Thus, a good understanding of the mechanism can provide good directions for improving catalysis.

1.2 Selected methods in mechanistic research

In the following subsections, various methods applied for elucidating reaction mechanisms are discussed. Like any scientific question, the elucidation of a reaction mechanism should be approached by posing a potential hypothesis and subsequently finding the appropriate method to attempt to refute this. Therefore, the discussed topics cannot be viewed as a catch-all guideline to approach reaction mechanisms, nor is it a comprehensive list of possible options. Rather, it is meant to provide a broad overview of the most generally applicable methods and showing their strengths and potential weaknesses.

1.2.1 Kinetics

Kinetic studies are instrumental to the understanding of reaction mechanisms. By thorough kinetic analysis, the reaction order of reactants, catalysts and additives and thus the reaction rate law can be revealed. The rate law provides insight into which molecules interact with each other during the rate determining step and the equilibria prior to it.^{10,11} While this won't outright point into the direction of a single reaction mechanism, it can immediately exclude hypotheses that are incompatible with the found rate law.

Kinetics of reactions involving a single substrate (*e.g.* solvolysis, or the decay of an isolated intermediate) have relatively simple rate laws. For example, the rate law of first and second order decay are given by equations 1.1 and 1.2, respectively, where $[A]$ is the concentration of the substrate and k is a rate constant dependent on the reaction conditions.

$$\frac{-d[A]}{dt} = k[A] \quad (1.1)$$

$$\frac{-d[A]}{dt} = k[A]^2 \quad (1.2)$$

Integrating these equations gives the relation between the substrate concentration and time (equations 1.3 and 1.4 for a first and a second order reaction, respectively).

$$\ln([A]_t) = \ln([A]_0) - kt \quad (1.3)$$

$$\frac{1}{[A]_t} = \frac{1}{[A]_0} - kt \quad (1.4)$$

$[A]_t$ is the concentration of A at time point t and $[A]_0$ is the starting concentration of A. Note that both equations 1.3 and 1.4 are written in a linear form with respect to time. This allows for a straightforward method to determine the rate law experimentally. The concentration of A can be monitored with either *in situ* spectroscopic techniques, or by analyzing aliquots. A plot can then be constructed with the left-hand side of the integrated rate law on the y-axis (*i.e.* $\ln([A]_t)$ for a first order reaction and $1/[A]_t$ for a second order reaction) and time on the x-axis. The plot will be linear if the right order is considered.¹² Otherwise, a different integrated rate law may be considered in a similar manner.

In reactions with multiple substrates, kinetic analysis can become too complicated for this approach, as there are now multiple variables (equation 1.5).

$$\frac{d[P]}{dt} = k[A]^x[B]^y[C]^z \quad (1.5)$$

In this equation, $[P]$ is the product concentration, A, B and C are reaction parameters such as reactants, reagents and/or catalysts, and x , y and z are the respective reaction orders of these molecules.

Traditionally, two methods were used to address the multivariability of such rate laws. In one method, all but one parameter may be kept approximately constant, by studying the reaction with those molecules in large excess.^{11,12} This leads to an approximated rate law (equation 1.6) where the rate constant k' now includes the variables that are quasi-invariant (equation 1.7). Naturally, catalysts that don't undergo considerable decomposition during the reaction can be included in k' without using a large excess.

$$\frac{d[P]}{dt} = k'[A]^x \quad (1.6)$$

$$k' = k[B]^y[C]^z \quad \text{valid when } [B]_t \approx [B]_0 \text{ and } [C]_t \approx [C]_0 \quad (1.7)$$

As the approximated rate law (equation 1.6) now has a similar form as rate laws for reactions involving a single substrate (equations 1.1 and 1.2), it can be analyzed in a similar manner (*vide supra*). After repeating this methodology for each variable, all unknown reaction orders (x , y and z in equation 1.5) can be determined. However, a downside of this approach is that the reaction conditions used for the kinetic study differ strongly from those under which the reaction is normally conducted, which could lead to misleading results.

In the second traditional method, data may be collected only from the initial state of the reaction. As the conversions of the substrates are still low at this point, they are approximately equal to their starting concentrations. This leads to an approximately linear plot of product versus time, of which the slope can be defined as the observed rate constant (k_{obs} , equation 1.8 and 1.9).

$$[P] = k_{obs} \cdot t \quad \text{Only valid in during the initial part of the reaction} \quad (1.8)$$

$$k_{obs} = k[A]_0^x[B]_0^y[C]_0^z \quad (1.9)$$

k_{obs} can then be further analyzed by repeating the reaction several times with a slight variation in the starting concentration of one of the reaction parameters, while keeping all others constant. In this manner, a relation between k_{obs} and the varied parameter can be found (equation 1.10), which can be transformed into its logarithmic form (equation 1.11).

$$k_{obs} = k'_{obs}[A]_0^x \quad \text{where } k'_{obs} = [B]_0^y[C]_0^z \quad (1.10)$$

$$\log(k_{obs}) = \log(k'_{obs}) + \log([A]_0) \cdot x \quad (1.11)$$

Thus, if the logarithm of the initial rate k_{obs} is plotted against the logarithm of the parameter with varied initial concentration (A), a linear graph is obtained, of which the slope is the reaction order in the varied parameter (x). This procedure can then be repeated for the other parameters to derive y and z as well.¹¹

Disadvantages of this approach include the vast amount of experiments that are required to get the order of even a single variable and the fact that initial rates may not be representative of the reaction mechanism, for example if an induction period occurs.

Because of the downsides of the traditional approaches, new methods have been developed that allow analysis of the data over the entire duration of the reaction, while staying close to the standard reaction conditions. This so-called reaction progress kinetic analysis (RPKA) was initially developed by Blackmond and coworkers. The methodology relies on two basic principles. Firstly, Blackmond introduced the constant called excess. This constant is based on the difference in initial concentrations of the substrates. If proper stoichiometry is applied and a clean reaction occurs, this value does not change during the reaction progress. Thus, the introduction of excess in rate laws allows to reduce the number of variables in the rate law. Secondly, RPKA relies on the direct plotting of the rate law, i.e. reaction rate versus substrate concentra-

tion, rather than the traditional substrate (or product) concentration versus time. Order in substrates can then be derived by interrogating the data by plotting different versions of the rate law (*i.e.* adjusting the rate on the y-axis by division by concentration of one substrate, with the other substrate on the x-axis). If the correct rate law is plotted, this should lead to overlapping graphs even when the conditions are varied.¹³

An example of this is shown in Figure 1.1 for the reaction between chalcone and diethylzinc. Figure 1.1A shows the rate data plotted versus the concentration of chalcone. By dividing the y-axis by the diethylzinc concentration for each point, Figure 1.1B is obtained. Now all traces overlap, despite all having a different Et_2Zn concentration at every point. This indicates the rate law is first order in diethylzinc. The overlapping graphs are not linear, but flatten to a plateau, which indicates saturation kinetics for chalcone.

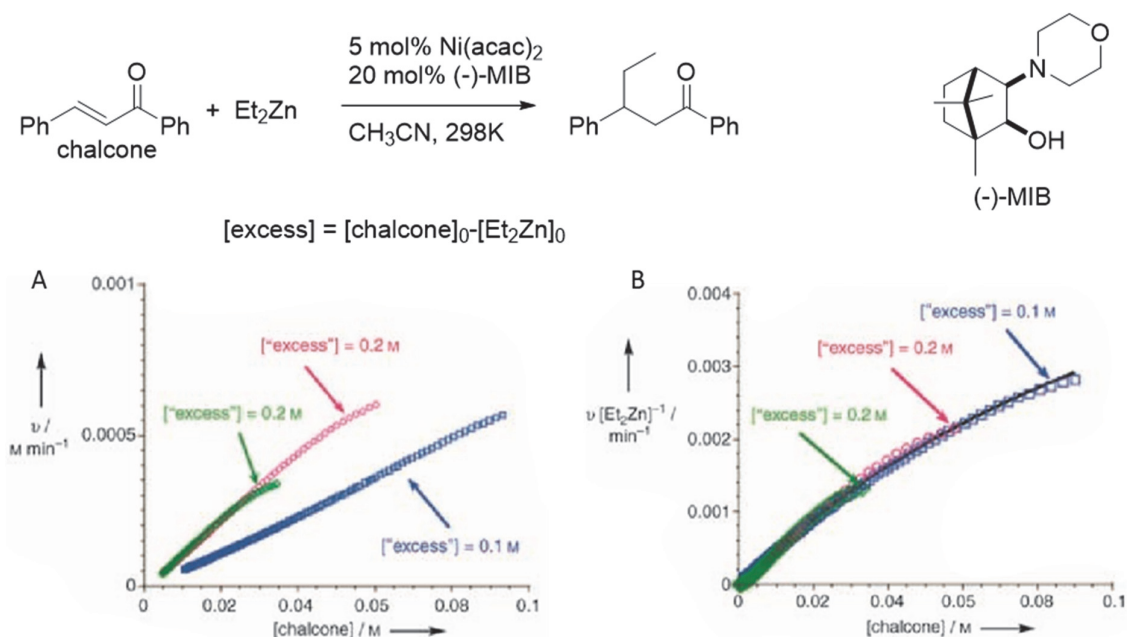


Figure 1.1: Application of RPKA to a reaction between chalcone and Et_2Zn . (A) rate data plotted against chalcone concentration for three different reaction conditions. (B) Same data as in (A), but with the y-axis divided by the Et_2Zn concentration for each point. The graphs are reproduced with permission from ref.13.

RPKA has great advantages over traditional approaches, since it requires fewer experiments to reach the same conclusions and avoids problems like induction periods. However, it still requires accurate measurements of both the reaction rate and the concentration of different species in the reaction mixture. Knowing the reaction rate at different time points is especially challenging, as it either requires specialized experimental setups such as reaction calorimetry, or advanced fitting of the measured concentration data.

To make the principles of RPKA more accessible to less specialized laboratories, Burés developed a time normalization method. With this technique, the reactivity data are plotted either with substrate or product on the y-axis and time multiplied by an investigated reaction parameter (*e.g.* catalyst concentration) on the x-axis. Reaction conditions that vary only in the investigated reaction parameter should then overlap, provided that the power applied to the variable used to modify the x-axis is equal to the power of that variable that appears in the rate law.¹⁴ Burés further demonstrated that the technique can also work if the investigated reaction parameter changes over the course of the reaction conditions, by multiplying the time-axis with a Riemann integral of the reaction parameter. Once again, the goal is to find the power that makes reaction traces that vary in initial concentration of the investigated parameter overlap, as this is the same power that appears in the rate law (Figure 2.2). This technique, named variable time normalization analysis (VTNA), is applicable to substrates¹⁵ as well as to the catalyst, if its concentration is variable, but known.¹⁶

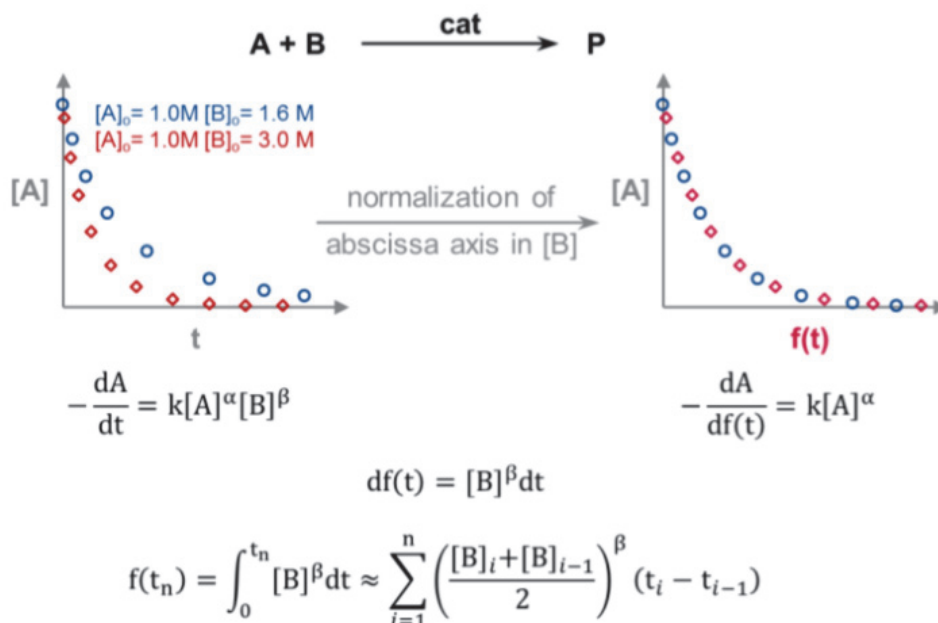


Figure 1.2: General example of the VTNA method. The time axis is changed into the Riemann integral of the concentration of B. This leaves $[A]$ as the only variable in the equation for $-dA/df(t)$. The reaction traces will overlap if the chosen value of β corresponds to the order in B. Reproduced with permission from ref.15.

VTNA is a powerful method that can reveal the rate law with just a few measured reaction traces. However, it should be noted that the methodology relies on judging by eye if the traces overlap and the found orders in substrates, catalysts and additives therefore lack an estimation of error. Although this doesn't pose a problem for more traditionally encountered orders like zero, one, two, or half, more complex reaction mechanisms may give fractional orders for which

no precise number can be given. In such a case VTNA will give an order that may for example be described as “between 1 and 2”. If a more accurate understanding of the order is required to distinguish between mechanistic hypotheses, traditional kinetic experiments that can provide estimates of errors may therefore still be necessary. Furthermore, although VTNA is in principle compatible with any technique to determine the concentration of the reaction parameters, accuracy of the Riemann integral improves with shorter time intervals, which means that *in situ* monitoring should generally be preferred.

1.2.2 Hammett plots

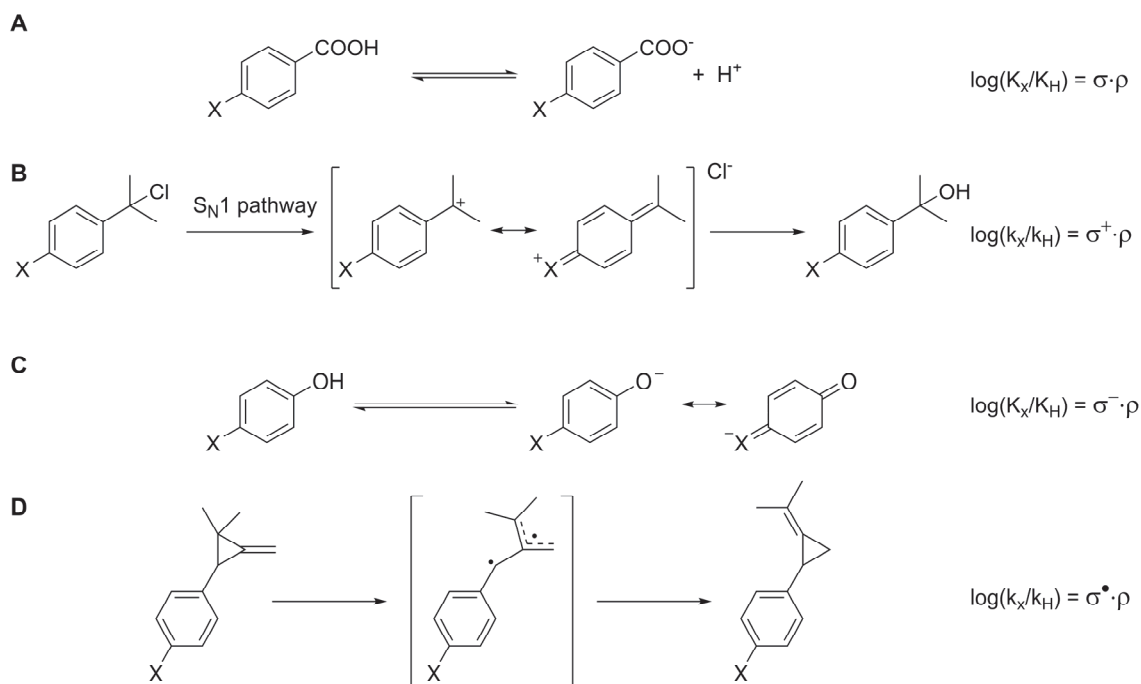
In the first half of the 20th century, it was recognized that substituents on aromatic reactants can have similar effect on the reactivity of these substrates for various reaction types. Hammett formalized these findings with equation 1.12.¹⁷

$$\text{Log}K - \text{Log}K^0 = \sigma \cdot \rho \quad (1.12)$$

Here, K and K^0 represent either equilibrium or rate constants and σ and ρ are constants that relate specifically to the substituent on the substrate and to the studied reaction, respectively. The power of this equation lies in the strict separation of factors specific to the substrate and those specific to the reaction type. Thus, the substrate-specific constants can be derived from a reference reaction, after which they may be applied to other reactions to gain information on the nature of those reactions.

Hammett originally chose the acid-base equilibrium for benzoic acids (Scheme 1.1A) as the main basis for his sigma constants,¹⁷ as a wide variety of accurate data was available for this. However, he soon realized that the sigma constants derived this way were not entirely universal.¹⁸ Since Hammett’s initial seminal papers, several different sigma constants have been developed to account for the shortcomings of Hammett’s original ones, such as accounting for electron donating resonance effects (Scheme 1.1B),¹⁹ electron withdrawing resonance effects (Scheme 1.1C)²⁰ and radical reactivity (Scheme 1.1D).²¹ It should be noted that radical Hammett constants are also represented by dibenzylmercury decomposition reactions²² and EPR hyperfine coupling constants.²³ Full consideration of all three of these radical-based radical Hammett constants can therefore be required.²⁴

Scheme 1.1: reactions that form the basis for several Hammett constants.



Mechanistic information can be gained by performing the reaction under study with various substrates that vary only in their aryl substituent and attempting to correlate measured rate constants with reported sigma-constants.

The first piece of valuable information can be gained by considering which type of constant creates the best linear correlation. Good correlation with σ^{\bullet} that cannot be obtained with the non-radical constants can indicate the substrate has some radical character in the rate determining step.²⁴ Conversely, poor correlation with the radical constants excludes a radical nature of the rate determining step. If the correlation is especially good with the σ^+ or σ^- , this provides a good indication that resonance stabilization by the substituent plays an important role. In addition it indicates if the benzylic position gains or loses electron density in the rate determining step, respectively.^{25,26} This latter conclusion can also be drawn if Hammett's original constant provides the best fit, by considering the slope: a positive slope indicates charge buildup whereas a negative slope indicates charge depletion. However, if the correlation is not improved by using σ^+ or σ^- , this charge buildup likely does not occur in a position that allows for resonance stabilization.

Special cases may also arise in a Hammett substituent study. On the one hand, it may occur, that a V-shape Hammett plot is obtained, where two parts of the plot have a slope with opposite

sign. This indicates a shift in the mechanism. For example, with increasingly electron withdrawing substituents, a nucleophilic substitution may shift from S_N1 to S_N2 .²⁷ Another situation that may arise is lack of variance on the y-axis. This can indicate there is no change in electron center near the aryl position, or that the substrate only gets involved in the reaction after the rate determining step.

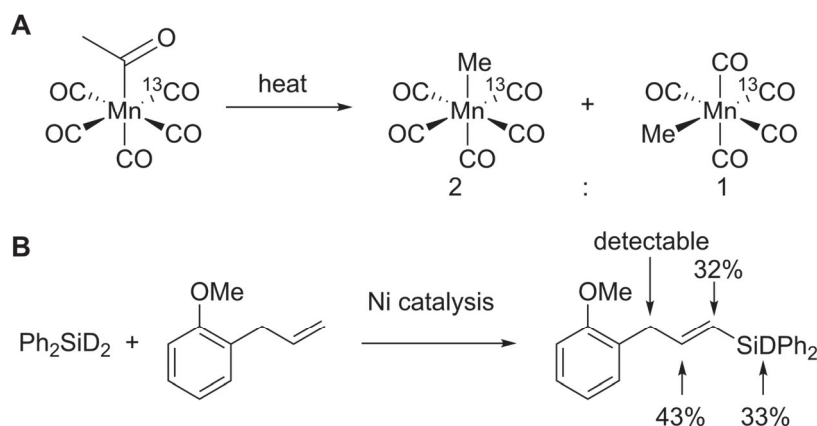
A final notion on Hammett plots is that they may be set up either with parallel reactions, where the rate is determined for different substrates, or by a direct competition between the studied substrates with the reference substrate. The two setups may lead to different results, if the selectivity-determining step is different from the rate-determining step and thus provide additional mechanistic information.²⁸

1.2.3 Isotope labelling

Labelling substrates with naturally non-abundant isotopes allows to track the movement of specific atoms from reactant to product. This type of tracking has been used to investigate whether alkyl insertion reactions into metal-bound carbonyl occur with movement of carbonyl, or movement of alkyl. It was studied by looking at the deinsertion reaction (which should go through the same pathway as insertion due to microreversibility) of isotopically labeled acetylpentacarbonylmanganese(I). The labeled product of the thermal deinsertion reaction is a 2:1 cis:trans mixture of pentacarbonylmethylmanganese(I) (Scheme 1.2A).²⁹ If the carbonyl part of the acetyl moiety would move during deinsertion, the trans product could not be made. Thus, the isotopic labelling proved that the alkyl is the part that moves during the insertion and deinsertion reactions with metal bound carbonyls.

An additional aspect of reactions that may be gauged with isotope labelling is reversibility of a certain step. For instance, hydrosilylation with a silane containing Si-D bonds rather than Si-H bonds, leads to deuteration of multiple positions in the product, rather than just at a single position (Scheme 1.2B). Therefore, the insertion of hydride into the double bond must be reversible, so it can migrate over the carbon chain via repeated β -hydride elimination and insertion cycles.³⁰

Scheme 1.2: isotope labelling experiments for (A) proving methyl moves in migratory insertion and for (B) showing reversibility of hydride insertion in nickel catalyzed hydrosilylation.



Another benefit of working with isotopically labelled compounds is that they allow to study kinetic isotope effects (KIE), *i.e.* the phenomenon that there is a difference in rate between substrates that contain different isotopes. KIEs arise from a difference in bond strength between a minimum on the potential energy surface (PES) and a transition state. As such they can provide valuable information on what happens during a certain transition state. Large KIEs indicate a bond cleavage, whereas weak KIEs indicate a change in hybridization instead.³¹ The reaction setup determines on which transition state the information is gained: if the KIE is determined by running two reactions with labeled and unlabeled substrate in parallel and measuring the rate of each reaction, information on the rate determining step is obtained. On the other hand, if the labeled and unlabeled substrate are present in the same reaction mixture, the KIE can be determined by the product ratio, or the conversion ratio and it will provide insight into the steps that are specifically related to the reaction step that irreversibly involves the substrate. For carbon KIEs, the competition experiment can also be performed at natural abundance of the isotope.³²

1.2.4 Non-linear effects

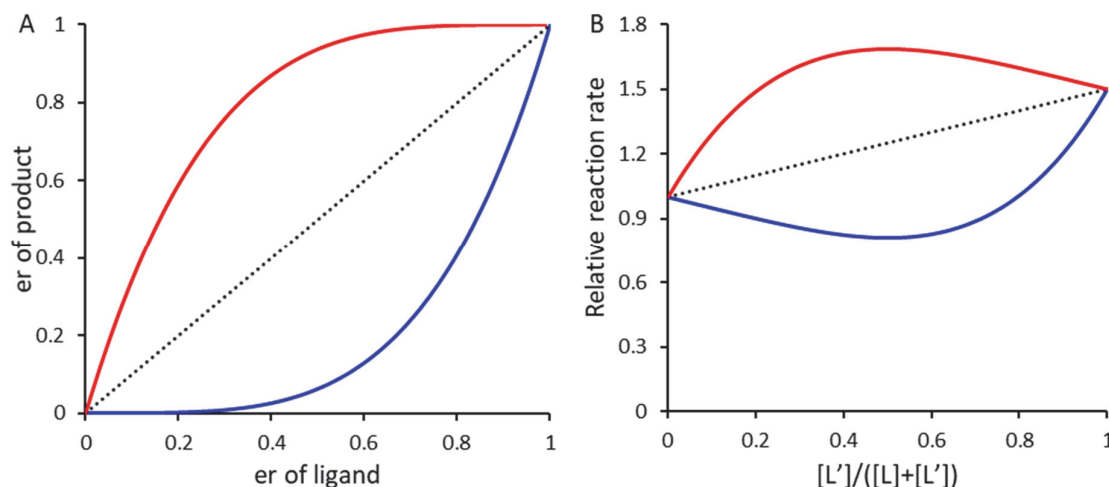


Figure 1.3: NLE for (A) enantioselectivity with a chiral ligand where only the er of the ligand is varied and (B) NLE on reaction rate where two similar achiral ligands L and L' are used. The black dashed line represents how the graph would look in absence of an NLE. The red line represents a positive NLE. The blue line represents a negative NLE.

Traditionally, the term non-linear effect (NLE) is a descriptor for phenomena that can occur in the study of asymmetric catalysis. In principle, when the enantiomeric excess (ee) of the chirality-inducing entity (*e.g.* a chiral ligand) is increased, the enantiomeric excess of the product should also increase linearly. However, certain phenomena, such as the involvement of multiple molecules of the chirality-inducing entity in the selectivity-determining step, or aggregation of catalytic species can lead to non-linearity (Figure 1.3A).^{33–35} Since these types of phenomena can easily go unnoticed by other mechanistic experiments, consideration of NLE has become a staple in mechanistic research into asymmetric reactions. Some care must be taken though, since certain types of reactions may inherently lead to an NLE, as has been demonstrated for dynamic kinetic resolution where the substrate does not isomerize directly.³⁶

In principle non-linear effects may also occur outside of asymmetric catalysis. Indeed, Sigman and coworkers have shown that the relative amount of Heck coupling side product generated in their asymmetric diarylation of alkenes increases as the ee of the chiral acid cocatalyst is lowered, even though the ee of the target product showed no NLE. The authors postulated that while only one molecule of chiral phosphoric acid is involved in the enantioselectivity-determining step, the side reaction does involve an additional phosphoric acid molecule, thus leading to an NLE outside of product ee.³⁷

The concept of NLE is taken even further away from its origins by Pollice and Schürch. They have demonstrated that an NLE can also occur when no selectivity concerns exist, as the catalytic reaction rate can depend non-linearly on the ratio between two similar, non-chiral ligands (Figure 1.3B).³⁸ If the use of two different ligands would simply lead to the coexistence of two independent catalytic cycles, a weighted average of the catalytic rates of the pure catalysts and therefore a linear dependence on the ligand ratio is expected. Non-linearity of the reaction rate can therefore point to similar phenomena as are already well-known for asymmetric catalysis. Although the study of NLEs is not yet widely used in non-chiral chemistry, it may be useful if agglomeration of catalytic species is suspected.

1.2.5 Differential selectivity experiments

In the previous three sections we have already described several examples of how setting up direct competition in the reaction mixture can provide information on steps that are not rate-determining. Besides these relatively simple probes, the group of Alexander Schmidt has developed a general technique for considering selectivities of the studied catalytic system and deriving a variety of useful mechanistic insights from them. The core principle of the methodology is to employ an equimolar mixture of two similar substrates with a combined concentration equal to what would be the concentration of one of those substrates under standard conditions. The reaction is then followed in time and selectivity between the two substrates is visualized by plotting the concentration of the product from one substrate versus the concentration of the product of the other substrate (conversions of each substrate may also be used). Such a plot allows for consideration of the selectivity over the course of the whole reaction, which makes it less sensitive to changes in selectivity due to changes in relative concentration of the substrates over the course of the reaction. These types of plots can then be made under different conditions and compared. If the change in conditions leads to non-overlapping selectivity graphs, this indicates that the change has an influence on the nature of the catalytic intermediate that governs the selectivity.³⁹

One application of this methodology is to investigate whether the active catalyst is a molecular species, or rather a nanoparticle or bulk metal. This question is generally difficult to answer, since a catalytic mixture may contain a mixture of all three types of species.⁴⁰ Differential selectivity graphs generated under varying catalyst precursor concentration can provide insight.

While the nature of a molecular catalyst should remain unchanged at different precursor concentrations, shape and morphology of particulate catalysts are dependent on nucleation and propagation kinetics, which are linked to precursor concentrations. Thus, if a catalytic system has a molecular active species, the differential selectivity graphs will be invariant to catalyst concentration, while changes are expected for particulate catalysts.³⁹

Another application of the differential selectivity measurements is to consider if certain steps in the reaction occur reversibly or irreversibly. If a reaction occurs irreversibly, the subsequent steps will not have an influence on the selectivity. However, if a non-negligible amount of equilibration occurs, the relative rate of the second step will depend at least on the identity of the species that interacts in the second step. Thus changing the nature of the species that interacts during the second step will lead to changes in the selectivity graph only if the first step is reversible.⁴¹

1.2.6 Computational modelling

The utility of a lot of experimental methods for mechanistic analysis is limited by species that are relatively long-lived in the catalytic cycle, or isolable. In addition, while some of the methods described above may get around such limitations, information on reactivity is often limited to the reaction sequence, along with some general observations, such as increase of electron density at a certain point, or that a particular bond may be broken in a particular step.

In contrast, computational modelling in principle allows for the calculation of any species that may be hypothesized to be part of the catalytic cycle, regardless of how short-lived may be. In this manner, a full PES of the hypothesized reactivity may be constructed, by calculating all structures and their corresponding electronic and free energies.⁴² Information on the rate determining step may then be obtained by applying the activation span model.⁴³

In addition, information may be garnered that is physically impossible to access via experimental methods. For instance, calculations of transition states allow for direct visualization of the manner in which reactants interact with the catalyst in any given step. Techniques like the activation strain model,⁴⁴ or natural orbitals for chemical valence⁴⁵ can even deconstruct the factors that influence binding energies in transition states and PES minima into terms that chemists are used to, such as steric and electronic interactions, or bonding and back bonding to transition metals.

Finally, computational modelling allows for insights into ligand effects on catalysis in a considerably more straightforward manner than would be possible experimentally. If two ligand systems are compared experimentally, a global difference may be observed in reaction efficiency or selectivity, but these observations are the result of a combination of factors in each of the reaction steps. Conversely, calculation of the reaction pathway with two different ligands shows all the influences that apply to the different reaction steps individually. Computational studies with varied ligands may therefore provide valuable insight into what ligand design may be the most valuable to target to improve a certain reaction. For example, a study by Houk and coworkers on oxidative addition of esters to nickel provides valuable insights into which ligand characteristics have the greatest influence on selectivity.⁴⁶

Despite all these advantages, computational modelling also has a few weaknesses. Firstly, while experimental studies gain information from reaction mixtures that closely resemble the standard conditions and are therefore bound to reveal information about the studied mechanism, in computational modelling, results can only be obtained on the species that the chemist decides to model. It is therefore possible that computational modelling leads to a certain model, simply because an alternative, more favorable pathway was not imagined by the researcher and therefore not treated. Another problem with computational modelling comes with the errors that are necessarily involved in the calculated energies. These errors are generally understood to be around 3 kcal/mol when methods are used that allow for reasonable computational costs.^{47,48} Errors of this size can have considerable impact for example on predicted kinetic profiles.⁴⁹ Because of these limitations, best results are likely obtained when computational results are compared to experimental ones, to minimize the chance of missing the inclusion of important factors in the calculations and to have several different experimental results that the computational model must be able to explain, before it can be accepted.

1.3 Application of nickel in homogeneous catalysis

Nickel is a considerably more abundant element than the heavier transition metals most often used in catalysis: while the accessible resources worldwide for nickel are estimated at 130 million tons, this is only 100,000 tons for platinum group metals (a general term for Ru, Rh, Pd, Os, Ir, Pt) and 33,000 tons for gold.⁵⁰ Due to the higher abundance, the cost of nickel compounds is generally lower than that of similar compounds based on heavier congeners.

For the production of pharmaceuticals, the higher abundance of nickel has an additional effect:

because of the relatively high abundance, nickel is a common contaminant in starting materials. As a result, testing for trace nickel is always required, regardless of whether it has been used in the synthesis. Conversely, testing for the heavier metals is only necessary if they have been used in the synthetic process.⁵¹ Avoiding use of the heavier transition metals in drug products can therefore be cheaper, as the amount of required quality control that needs to be performed goes down.

In addition to economic advantages, there are some key reactivity differences between nickel and its heavier congener palladium. Nickel has relatively low electronegativity, which makes it highly reactive in oxidative addition reactions.⁵² This makes nickel especially useful for cross-coupling reactions with substrates that are generally resistant to oxidative addition, such as phenol derivatives like ethers and esters,^{53,54} nitriles,^{55–57} or aryl fluorides.⁵⁸ Another way in which the low electronegativity manifests is the strong capacity to back bond, leading to strong binding to unsaturated molecules.⁵⁹ Nickel is also less proficient at β -hydride elimination than palladium.⁶⁰ This is useful to prevent byproduct formation in cross coupling with aliphatic substrates.^{61,62}

Both the economic advantages and the particular reactivity of nickel complexes have led to considerable interest in the development of nickel-catalyzed synthetic methodologies. The large body of work performed for development of nickel catalysis is highlighted in several recent reviews on cross coupling,^{63–67} reductive coupling,⁶⁸ dehydrogenative coupling,⁶⁹ C-H activation,^{70,71} cycloaddition⁷² and formation of heterocycles.⁷³

1.4 Mechanistic aspects of homogeneous nickel catalysis

As mentioned in the previous section, nickel has a couple of properties that make its reactivity distinct from its heavier congeners. This section will highlight some of the mechanistic implications these differences have on nickel chemistry.

1.4.1 Radical nature of cross coupling

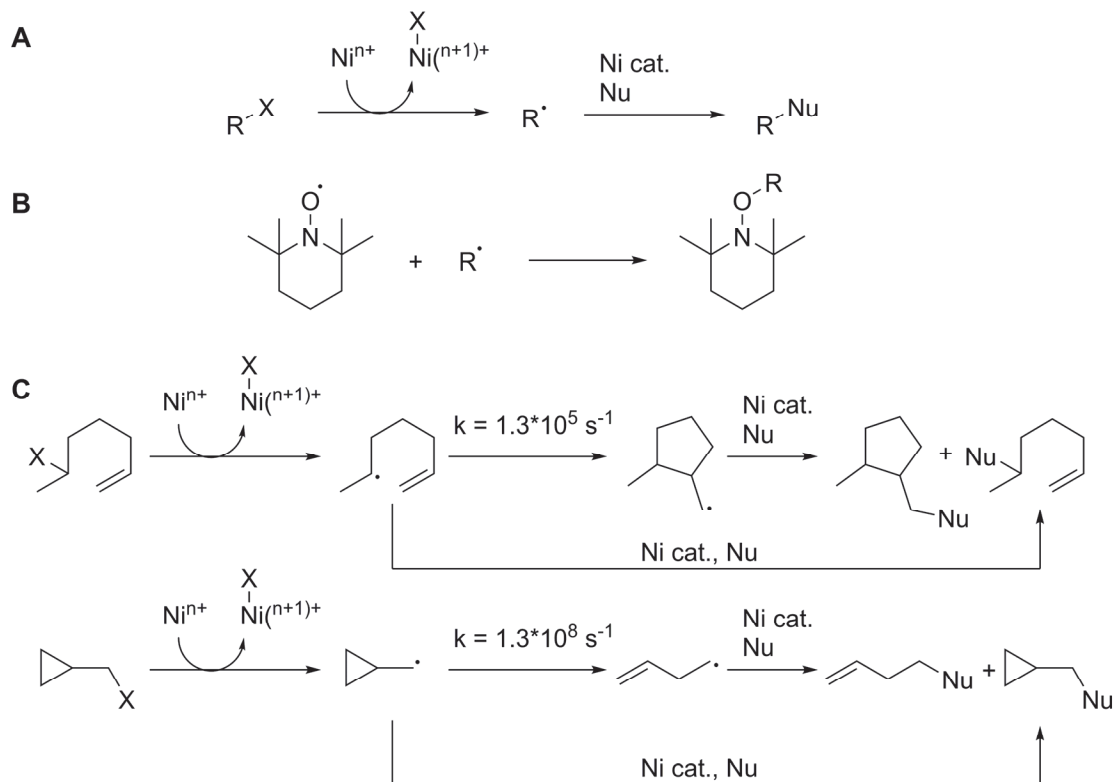
Compared to its heavier congeners, nickel forms particularly weak bonds with carbon, that are prone to homolytic cleavage.⁷⁴ Because of this, mechanisms of nickel catalyzed reactions often include free radical reactions (Scheme 1.3A). One indication of such reactivity could be stereoinconvergent reactivity of a chiral substrates,⁷⁵ or the formation of two diastereomer products

from a diastereomerically pure substrate.⁷⁶

To probe intermediacy of free radicals, the reaction can be performed in the presence of a radical trapping reagents such as stable persistent radicals like (2,2,6,6-Tetramethylpiperidin-1-yl)oxyl (TEMPO). The presence of a trapping reagent should suppress the reaction. Moreover, the trapped radical can be characterized by identifying the TEMPO-adduct.⁷⁷

Alternatively, substrates containing a radical clock may be used. Radical clocks contain structural features that can rapidly undergo reorganization of the carbon framework through (de)cyclization if a radical is generated in specific positions.^{78,79} The use of substrates with such structural features therefore reveal if free radicals are formed in the catalytic cycle: if radicals are formed, some amount of the observed products should have a reorganized carbon framework. Moreover, the ratio of reorganized versus non-reorganized product is dependent on the rate with which the radical is trapped. By varying the conditions and checking the product ratio, the species responsible for trapping the radical in the catalytic cycle can be identified.⁸⁰

Scheme 1.3: (A) General representation of radical intermediacy in nickel catalysis. (B) Trapping of the radical by TEMPO, preventing the reaction with the nucleophile Nu. (C) Two examples of radical clocks. After the activation by nickel, the radical intermediate can (de)cyclize to give an isomeric product.



1.4.2 Oxidation state

Nickel can reach a wide variety of oxidation state. Aside from the common nickel precursors that have oxidation state 0 (bis-(1,4-cyclooctadiene)nickel(0), $\text{Ni}(\text{COD})_2$) and II (commercially available nickel salts), various complexes have been isolated in oxidation state I,^{77,81–84} III^{85–87} and even IV.^{87–89}

For reactions that occur with free radical intermediates, catalytic cycles where nickel exists in oxidation states I, II and III are generally proposed.^{77,80} Reactions without radical intermediates on the other hand, are generally proposed to occur with catalytic cycles wherein nickel switches in two-electron redox changes between oxidation state 0 and II,^{90,91} or between states I and III.^{81–83}

For the two-electron catalytic cycles, com- or disproportionation reactions present an additional mechanistic complication. For 0/II cycles, comproportionation reactions are known to form Ni(I) species that are inactive in the catalytic cycle,^{90,92} thus limiting the turnover number (TON). Conversely, I/III cycles require the comproportionation to occur to generate the active species.^{81–83} Investigations into this type of behavior is rather recent, which makes it currently difficult to consider any generalities about which reactions fare better with 0/II cycles and which one with I/III cycles, nor is it clear what factors may favor comproportionation. Further mechanistic studies that consider the redox behavior of the nickel catalyst are therefore of considerable interest.

1.4.3 Speciation

Aside from molecular nickel catalysis, nickel can also be effective as a heterogeneous catalyst^{93,94} or as nanoparticle.^{95–97} The nanoparticles may be formed from both Ni(II)^{95,97} or Ni(0) precursors.⁹⁸ In addition to nanoparticle formation, nickel may also form small aggregates, as has been observed with the common catalyst precursor $\text{Ni}(\text{acac})_2$ (acac = acetylacetonate).⁹⁹ Although these processes are now well known a thorough consideration of the nature of the active catalyst is generally not considered with nickel catalysis. Since interconversion between heterogeneous species, aggregates and molecular species is well-documented for palladium and platinum,⁴⁰ it would be wise to consider potential formation of particulate nickel from molecular precursors, or leaching of nickel atoms from heterogeneous precursors. Methods that can be

used to study these phenomena include the differential selectivity experiments (as discussed above)³⁹ and by studying the reaction of substrates embedded in nanoporous polymer beads.¹⁰⁰

1.4.4 Ligand design

Only quite recently, attention has been paid to the fact that screening of catalysts is generally done with ligands that were originally designed with Pd catalysis in mind. This can create inherent shortcomings, due to the different nature of the elements (*vide supra*). Hence, tailored design of ligands for nickel is now highly required.^{101–104} Parameterization of a set of phosphine ligands giving varying performance for nickel catalyzed Suzuki coupling of acetals revealed an increased yield with increased Tolman's cone angle, but an upper limit on the V_{burr} parameter that signifies the steric hindering near the metal centre (Figure 1.4). Traditionally, the ligands with a large cone angle were designed by increasing steric hindrance (Johnphos, PCyp(Mes₂)), which also tend to increase V_{burr} . This explains why the ligands designed for palladium don't necessarily work well in nickel reactions: the requirement for nickel is that the ligand has steric bulk remote from the metal center, rather than close by.¹⁰¹

While this conclusion may provide inspiration of new reactivity, it should not be considered a rule of thumb for nickel catalysis in general. For example, the nickel catalyzed Suzuki coupling of benzylic ethers could be realized with nickel ligated by sterically relatively unencumbered cyclohexyl-substituted N-heterocyclic carbenes. Moreover, the reaction outcome was very sensitive to the exact nature of the ligand.¹⁰⁵ This example illustrates that considerably more effort is required in ligand design and mechanistic understanding to improve the efficiency and scope of nickel catalysis.

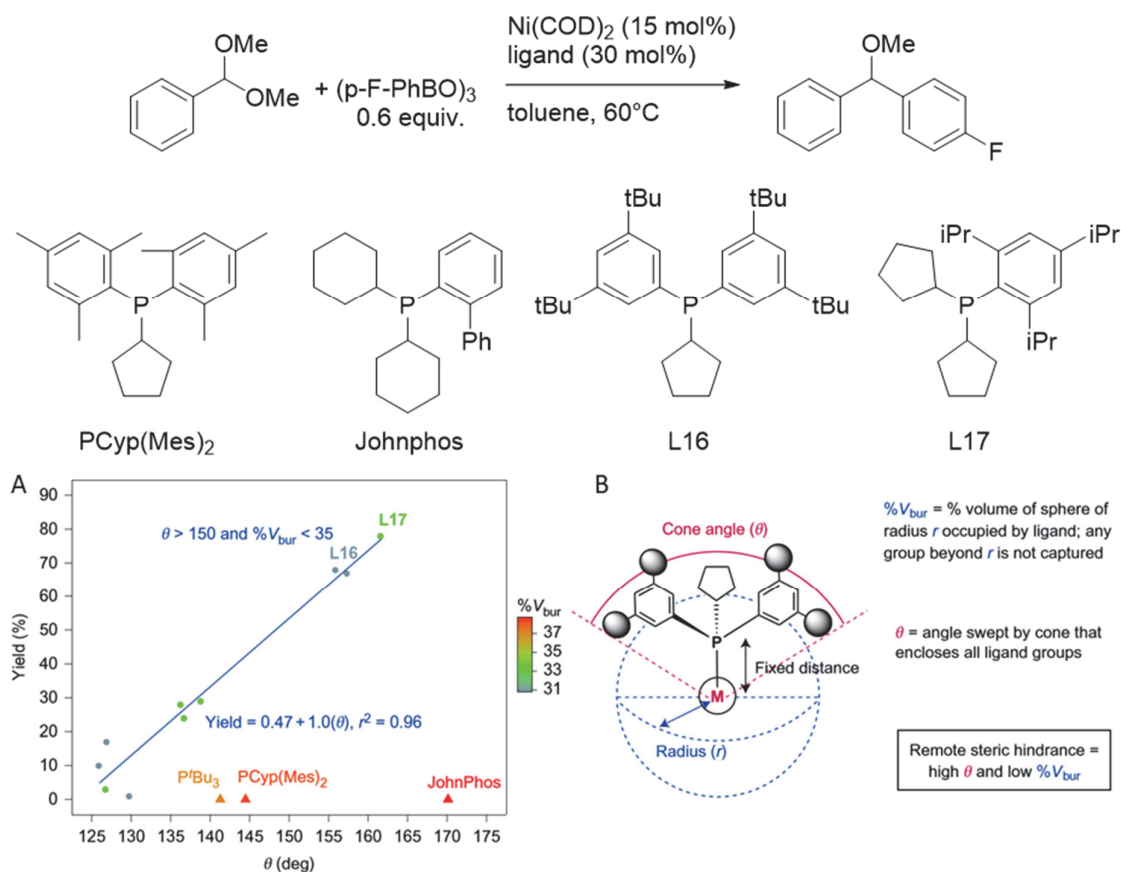


Figure 1.4: (A) Correlation between cone angle θ and yield for arylation of a dimethylacetal. The correlation breaks down for ligands with too high V_{bur} . (B) Visual representation of the parameters θ and V_{bur} . (A) and (B) are reproduced from ref. 101.

1.5 Aim of the project

Sections 1.4.2-1.4.4 demonstrate that recent mechanistic studies on nickel catalysis have laid bare several particularities about nickel chemistry that had not fully been considered before. This highlights our incomplete understanding on the factors that may influence nickel catalysis. This thesis aims to further develop this understanding by studying nickel catalyzed reactions with nitroarenes as nitrogen source for amidation recently developed in our group,^{106–111} applying several of the techniques discussed in section 1.2. In addition, we will study hydrosilylation catalyzed by a nickel pincer complex developed in our group.¹¹²

Chapter 2 deals with the identification of the true reactive intermediate generated from the nitroarenes.

Chapter 3 and 4 investigate in depth how the intermediate azobenzene reacts with esters under nickel catalysis. Chapter 3 discusses the applied experimental techniques, while chapter 4 focuses on the computational study.

These three chapters reveal a heretofore unknown reactivity of nickel. Moreover, it is revealed that ZnCl_2 plays a pivotal role in the reaction. Given the propensity of using Zn as reductant for nickel catalyzed reductive coupling, the notion that ZnCl_2 is not merely a byproduct of the reaction could have broad implications.

Chapter 5 explores how the knowledge obtained in chapters 2-4 could be used to further the utility of nickel catalysis with nitroarenes.

Finally, chapter 6 explores the reactivity of nickel catalyzed hydrosilylation previously disclosed by our group.¹¹² It reveals the reaction is governed by nickel nanoparticles, rather than by a discrete nickel complex, as previously believed.

Overall, the results presented in this thesis build on the mechanistic understanding of nickel chemistry and underscore the importance of mechanistic research for the discovery of new reactivity patterns in homogeneous catalysis.

1.6 References

- (1) The Nobel Prize in Chemistry 2001. NobelPrize.Org. Nobel Media AB 2020. Sun. 22 Mar 2020. <<https://Www.Nobelprize.Org/Prizes/Chemistry/2001/Summary/>>.
- (2) The Nobel Prize in Chemistry 2005. NobelPrize.Org. Nobel Media AB 2020. Mon. 23 Mar 2020. <<https://Www.Nobelprize.Org/Prizes/Chemistry/2005/Summary/>>.
- (3) The Nobel Prize in Chemistry 2010. NobelPrize.Org. Nobel Media AB 2020. Sun. 22 Mar 2020. <<https://Www.Nobelprize.Org/Prizes/Chemistry/2010/Summary/>>.
- (4) Littke, A. F.; Dai, C.; Fu, G. C. Versatile Catalysts for the Suzuki Cross-Coupling of Arylboronic Acids with Aryl and Vinyl Halides and Triflates under Mild Conditions. *J. Am. Chem. Soc.* **2000**, *122* (17), 4020–4028. <https://doi.org/10.1021/ja0002058>.
- (5) Walker, S. D.; Barder, T. E.; Martinelli, J. R.; Buchwald, S. L. A Rationally Designed Universal Catalyst for Suzuki–Miyaura Coupling Processes. *Angew. Chem. Int. Ed.* **2004**, *43* (14), 1871–1876. <https://doi.org/10.1002/anie.200353615>.
- (6) Barder, T. E.; Walker, S. D.; Martinelli, J. R.; Buchwald, S. L. Catalysts for Suzuki–Miyaura Coupling Processes: Scope and Studies of the Effect of Ligand Structure. *J. Am. Chem. Soc.* **2005**, *127* (13), 4685–4696. <https://doi.org/10.1021/ja042491j>.
- (7) Fors, B. P.; Watson, D. A.; Biscoe, M. R.; Buchwald, S. L. A Highly Active Catalyst for Pd-Catalyzed Amination Reactions: Cross-Coupling Reactions Using Aryl Mesylates and the Highly Selective Monoarylation of Primary Amines Using Aryl Chlorides. *J. Am. Chem. Soc.* **2008**, *130* (41), 13552–13554. <https://doi.org/10.1021/ja8055358>.
- (8) Sanford, M. S.; Ulman, M.; Grubbs, R. H. New Insights into the Mechanism of Ruthenium-Catalyzed Olefin Metathesis Reactions. *J. Am. Chem. Soc.* **2001**, *123* (4), 749–750. <https://doi.org/10.1021/ja003582t>.
- (9) Sanford, M. S.; Love, J. A.; Grubbs, R. H. Mechanism and Activity of Ruthenium Olefin Metathesis Catalysts. *J. Am. Chem. Soc.* **2001**, *123* (27), 6543–6554. <https://doi.org/10.1021/ja010624k>.
- (10) Espenson, J. H. Chapter 5: Deduction of Reaction Mechanisms. In *Chemical Kinetics and Reaction Mechanisms*; McGraw-Hill Book Company, 1981; pp 89–115.
- (11) Anslyn, E. V.; Dougherty, D. A. Chapter 7: Energy Surfaces and Kinetic Analyses. In *Modern Physical Organic Chemistry*; University Science Books, 2006.
- (12) Espenson, J. H. Chapter 2: Reactions with a Simple Kinetic Form. In *Chemical Kinetics and Reaction Mechanisms*; McGraw-Hill Book Company, 1981; pp 12–41.
- (13) Blackmond, D. G. Reaction Progress Kinetic Analysis: A Powerful Methodology for Mechanistic Studies of Complex Catalytic Reactions. *Angew. Chem. Int. Ed.* **2005**, *44* (28), 4302–4320. <https://doi.org/10.1002/anie.200462544>.

-
- (14) Burés, J. A Simple Graphical Method to Determine the Order in Catalyst. *Angewandte Chemie International Edition* **2016**, 55 (6), 2028–2031. <https://doi.org/10.1002/anie.201508983>.
- (15) Burés, J. Variable Time Normalization Analysis: General Graphical Elucidation of Reaction Orders from Concentration Profiles. *Angewandte Chemie International Edition* **2016**, 55 (52), 16084–16087. <https://doi.org/10.1002/anie.201609757>.
- (16) Martínez-Carrión, A.; Howlett, M. G.; Alamillo-Ferrer, C.; Clayton, A. D.; Bourne, R. A.; Codina, A.; Vidal-Ferran, A.; Adams, R. W.; Burés, J. Kinetic Treatments for Catalyst Activation and Deactivation Processes Based on Variable Time Normalization Analysis. *Angew. Chem. Int. Ed.* **2019**, 58 (30), 10189–10193. <https://doi.org/10.1002/anie.201903878>.
- (17) Hammett, L. P. The Effect of Structure upon the Reactions of Organic Compounds. Benzene Derivatives. *J. Am. Chem. Soc.* **1937**, 59 (1), 96–103. <https://doi.org/10.1021/ja01280a022>.
- (18) Hammett, L. P. Linear Free Energy Relationships in Rate and Equilibrium Phenomena. *Trans. Faraday Soc.* **1938**, 34, 156. <https://doi.org/10.1039/tf9383400156>.
- (19) Brown, H. C.; Okamoto, Y. Electrophilic Substituent Constants. *J. Am. Chem. Soc.* **1958**, 80 (18), 4979–4987. <https://doi.org/10.1021/ja01551a055>.
- (20) Hansch, Corwin.; Leo, A.; Taft, R. W. A Survey of Hammett Substituent Constants and Resonance and Field Parameters. *Chem. Rev.* **1991**, 91 (2), 165–195. <https://doi.org/10.1021/cr00002a004>.
- (21) Creary, X.; Mehrsheikh-Mohammadi, M. E.; McDonald, S. Methylene cyclopropane Rearrangement as a Probe for Free Radical Substituent Effects. .Sigma..Bul. Values for Commonly Encountered Conjugating and Organometallic Groups. *J. Org. Chem.* **1987**, 52 (15), 3254–3263. <https://doi.org/10.1021/jo00391a015>.
- (22) Dinçtürk, S.; Jackson, R. A.; Townson, M.; Ağırbaş, H.; Billingham, N. C.; March, G. Free Radical Reactions in Solution. Part 6. Thermal Decomposition of Substituted Dibenzyl Mercurials in Solution. An Improved Σ^{\cdot} Scale. *J. Chem. Soc., Perkin Trans. 2* **1981**, No. 8, 1121–1126. <https://doi.org/10.1039/P29810001121>.
- (23) Dust, J. M.; Arnold, D. R. Substituent Effects on Benzyl Radical ESR Hyperfine Coupling Constants. The .Sigma..Alpha..Cndot. Scale Based upon Spin Delocalization. *J. Am. Chem. Soc.* **1983**, 105 (5), 1221–1227. <https://doi.org/10.1021/ja00343a024>.
- (24) Kong, C.; Jana, N.; Jones, C.; Driver, T. G. Control of the Chemoselectivity of Metal *N*-Aryl Nitrene Reactivity: C–H Bond Amination versus Electrocyclization. *J. Am. Chem. Soc.* **2016**, 138 (40), 13271–13280. <https://doi.org/10.1021/jacs.6b07026>.
- (25) Banerjee, S.; Sathyamoorthi, S.; Du Bois, J.; Zare, R. N. Mechanistic Analysis of a Copper-Catalyzed C–H Oxidative Cyclization of Carboxylic Acids. *Chem. Sci.* **2017**, 8 (10), 7003–7008. <https://doi.org/10.1039/C7SC02240A>.

-
- (26) Freitag, F.; Irrgang, T.; Kempe, R. Mechanistic Studies of Hydride Transfer to Imines from a Highly Active and Chemoselective Manganate Catalyst. *J. Am. Chem. Soc.* **2019**, *141* (29), 11677–11685. <https://doi.org/10.1021/jacs.9b05024>.
- (27) Richard, J. P.; Jencks, W. P. A Simple Relationship between Carbocation Lifetime and Reactivity-Selectivity Relationships for the Solvolysis of Ring-Substituted 1-Phenylethyl Derivatives. *J. Am. Chem. Soc.* **1982**, *104* (17), 4689–4691. <https://doi.org/10.1021/ja00381a037>.
- (28) Schmidt, A. F.; Al-Halaiqa, A.; Smirnov, V. V. Heck Reactions of Alkenes with Aryl Iodides and Aryl Bromides: Rate-Determining Steps Deduced from a Comparative Kinetic Study of Competing and Noncompeting Reactions. *Kinet Catal* **2007**, *48* (5), 716–727. <https://doi.org/10.1134/S0023158407050175>.
- (29) Noack, K.; Calderazzo, F. Carbon Monoxide Insertion Reactions V. The Carbonylation of Methylmanganese Pentacarbonyl with ^{13}CO . *Journal of Organometallic Chemistry* **1967**, *10* (1), 101–104. [https://doi.org/10.1016/S0022-328X\(00\)81721-0](https://doi.org/10.1016/S0022-328X(00)81721-0).
- (30) Zhang, Z.; Bai, L.; Hu, X. Alkene Hydrosilylation Catalyzed by Easily Assembled Ni(II)-Carboxylate MOFs. *Chem. Sci.* **2019**, *10* (13), 3791–3795. <https://doi.org/10.1039/C9SC00126C>.
- (31) Anslyn, E. V.; Dougherty, D. A. Chapter 8.1 Isotope Effects. In *Modern Physical Organic Chemistry*; University Science Books, 2006; pp 421–441.
- (32) Kwan, E. E.; Park, Y.; Besser, H. A.; Anderson, T. L.; Jacobsen, E. N. Sensitive and Accurate ^{13}C Kinetic Isotope Effect Measurements Enabled by Polarization Transfer. *J. Am. Chem. Soc.* **2017**, *139* (1), 43–46. <https://doi.org/10.1021/jacs.6b10621>.
- (33) Blackmond, D. G. Kinetic Aspects of Nonlinear Effects in Asymmetric Catalysis. *Acc. Chem. Res.* **2000**, *33* (6), 402–411. <https://doi.org/10.1021/ar990083s>.
- (34) Puchot, C.; Samuel, O.; Dunach, E.; Zhao, S.; Agami, C.; Kagan, H. B. Nonlinear Effects in Asymmetric Synthesis. Examples in Asymmetric Oxidations and Aldolization Reactions. *J. Am. Chem. Soc.* **1986**, *108* (9), 2353–2357. <https://doi.org/10.1021/ja00269a036>.
- (35) Guillaneux, D.; Zhao, S.-H.; Samuel, O.; Rainford, D.; Kagan, H. B. Nonlinear Effects in Asymmetric Catalysis. *J. Am. Chem. Soc.* **1994**, *116* (21), 9430–9439. <https://doi.org/10.1021/ja00100a004>.
- (36) Kalek, M.; Fu, G. C. Caution in the Use of Nonlinear Effects as a Mechanistic Tool for Catalytic Enantioconvergent Reactions: Intrinsic Negative Nonlinear Effects in the Absence of Higher-Order Species. *J. Am. Chem. Soc.* **2017**, *139* (11), 4225–4229. <https://doi.org/10.1021/jacs.7b01826>.
- (37) Orlandi, M.; Hilton, M. J.; Yamamoto, E.; Toste, F. D.; Sigman, M. S. Mechanistic Investigations of the Pd(0)-Catalyzed Enantioselective 1,1-Diarylation of Benzyl Acrylates. *J. Am. Chem. Soc.* **2017**, *139* (36), 12688–12695. <https://doi.org/10.1021/jacs.7b06917>.

- (38) Pollice, R.; Schnürch, M. Expansion of the Concept of Nonlinear Effects in Catalytic Reactions Beyond Asymmetric Catalysis. *Chem. Eur. J.* **2016**, *22* (16), 5637–5642. <https://doi.org/10.1002/chem.201504970>.
- (39) Schmidt, A. F.; Kurokhtina, A. A.; Larina, E. V. Differential Selectivity Measurements and Competitive Reaction Methods as Effective Means for Mechanistic Studies of Complex Catalytic Reactions. *Catal. Sci. Technol.* **2014**, *4* (10), 3439–3457. <https://doi.org/10.1039/C4CY00479E>.
- (40) Eremin, D. B.; Ananikov, V. P. Understanding Active Species in Catalytic Transformations: From Molecular Catalysis to Nanoparticles, Leaching, “Cocktails” of Catalysts and Dynamic Systems. *Coordination Chemistry Reviews* **2017**, *346*, 2–19. <https://doi.org/10.1016/j.ccr.2016.12.021>.
- (41) Kurokhtina, A. A.; Larina, E. V.; Yarosh, E. V.; Lagoda, N. A.; Schmidt, A. F. Mechanistic Study of Direct Arylation of Indole Using Differential Selectivity Measurements: Shedding Light on the Active Species and Revealing the Key Role of Electrophilic Substitution in the Catalytic Cycle. *Organometallics* **2018**, *37* (13), 2054–2063. <https://doi.org/10.1021/acs.organomet.8b00216>.
- (42) Cramer, C. J. *Essentials of Computational Chemistry: Theories and Models*, 2nd ed.; Wiley: Chichester, West Sussex, England ; Hoboken, NJ, 2004.
- (43) Kozuch, S.; Shaik, S. How to Conceptualize Catalytic Cycles? The Energetic Span Model. *Acc. Chem. Res.* **2011**, *44* (2), 101–110. <https://doi.org/10.1021/ar1000956>.
- (44) Bickelhaupt, F. M.; Houk, K. N. Analyzing Reaction Rates with the Distortion/Interaction-Activation Strain Model. *Angew. Chem. Int. Ed.* **2017**, *56* (34), 10070–10086. <https://doi.org/10.1002/anie.201701486>.
- (45) Mitoraj, M.; Michalak, A. Natural Orbitals for Chemical Valence as Descriptors of Chemical Bonding in Transition Metal Complexes. *J Mol Model* **2007**, *13* (2), 347–355. <https://doi.org/10.1007/s00894-006-0149-4>.
- (46) Hong, X.; Liang, Y.; Houk, K. N. Mechanisms and Origins of Switchable Chemoselectivity of Ni-Catalyzed C(Aryl)–O and C(Acyl)–O Activation of Aryl Esters with Phosphine Ligands. *J. Am. Chem. Soc.* **2014**, *136* (5), 2017–2025. <https://doi.org/10.1021/ja4118413>.
- (47) Harvey, J. N.; Himo, F.; Maseras, F.; Perrin, L. Scope and Challenge of Computational Methods for Studying Mechanism and Reactivity in Homogeneous Catalysis. *ACS Catalysis* **2019**, *9* (8), 6803–6813. <https://doi.org/10.1021/acscatal.9b01537>.
- (48) Liu, Z.; Patel, C.; Harvey, J. N.; Sunoj, R. B. Mechanism and Reactivity in the Morita–Baylis–Hillman Reaction: The Challenge of Accurate Computations. *Physical Chemistry Chemical Physics* **2017**, *19* (45), 30647–30657. <https://doi.org/10.1039/C7CP06508F>.
- (49) Pérez-Soto, R.; Besora, M.; Maseras, F. The Challenge of Reproducing with Calculations Raw Experimental Kinetic Data for an Organic Reaction. *Org. Lett.* **2020**, *acs.orglett.0c00367*. <https://doi.org/10.1021/acs.orglett.0c00367>.

- (50) Mineral Commodity Summaries 2020.
<https://pubs.usgs.gov/periodicals/mcs2020/mcs2020.pdf>.
- (51) ICH Guideline Q3D (R1) on Elemental Impurities.
https://www.ema.europa.eu/en/documents/scientific-guideline/international-conference-harmonisation-technical-requirements-registration-pharmaceuticals-human-use_en-32.pdf
- (52) Tsou, T. T.; Kochi, J. K. Mechanism of Oxidative Addition. Reaction of Nickel(0) Complexes with Aromatic Halides. *J. Am. Chem. Soc.* **1979**, *101* (21), 6319–6332. <https://doi.org/10.1021/ja00515a028>.
- (53) Mesganaw, T.; Garg, N. K. Ni- and Fe-Catalyzed Cross-Coupling Reactions of Phenol Derivatives. *Org. Process Res. Dev.* **2013**, *17* (1), 29–39. <https://doi.org/10.1021/op300236f>.
- (54) Guo, L.; Rueping, M. Decarbonylative Cross-Couplings: Nickel Catalyzed Functional Group Interconversion Strategies for the Construction of Complex Organic Molecules. *Acc. Chem. Res.* **2018**, *51* (5), 1185–1195. <https://doi.org/10.1021/acs.accounts.8b00023>.
- (55) Garcia, J. J.; Brunkan, N. M.; Jones, W. D. Cleavage of Carbon–Carbon Bonds in Aromatic Nitriles Using Nickel(0). *J. Am. Chem. Soc.* **2002**, *124* (32), 9547–9555. <https://doi.org/10.1021/ja0204933>.
- (56) Yu, P.; Morandi, B. Nickel-Catalyzed Cyanation of Aryl Chlorides and Triflates Using Butyronitrile: Merging Retro-Hydrocyanation with Cross-Coupling. *Angew. Chem. Int. Ed.* **2017**, *56* (49), 15693–15697. <https://doi.org/10.1002/anie.201707517>.
- (57) Fang, X.; Yu, P.; Willems, S.; Morandi, B. Nickel-Catalyzed Cascade Annulation for the Rapid Synthesis of Carbocyclic Nitriles. *HCA* **2019**, *102* (5), e1900059. <https://doi.org/10.1002/hlca.201900059>.
- (58) Tobisu, M.; Xu, T.; Shimasaki, T.; Chatani, N. Nickel-Catalyzed Suzuki–Miyaura Reaction of Aryl Fluorides. *J. Am. Chem. Soc.* **2011**, *133* (48), 19505–19511. <https://doi.org/10.1021/ja207759e>.
- (59) Massera, C.; Frenking, G. Energy Partitioning Analysis of the Bonding in $L_2 TM-C_2H_2$ and $L_2 TM-C_2H_4$ ($TM = Ni, Pd, Pt$; $L_2 = (PH_3)_2, (PMe_3)_2, H_2PCH_2PH_2, H_2P(CH_2)_2PH_2$)[†]. *Organometallics* **2003**, *22* (13), 2758–2765. <https://doi.org/10.1021/om0301637>.
- (60) Lin; Liu, L.; Fu, Y.; Luo, S.-W.; Chen, Q.; Guo, Q.-X. Comparing Nickel- and Palladium-Catalyzed Heck Reactions. *Organometallics* **2004**, *23* (9), 2114–2123. <https://doi.org/10.1021/om034067h>.
- (61) Vechorkin, O.; Hu, X. Nickel-Catalyzed Cross-Coupling of Non-Activated and Functionalized Alkyl Halides with Alkyl Grignard Reagents. *Angewandte Chemie International Edition* **2009**, *48* (16), 2937–2940. <https://doi.org/10.1002/anie.200806138>.

- (62) Joshi-Pangu, A.; Ganesh, M.; Biscoe, M. R. Nickel-Catalyzed Negishi Cross-Coupling Reactions of Secondary Alkylzinc Halides and Aryl Iodides. *Org. Lett.* **2011**, *13* (5), 1218–1221. <https://doi.org/10.1021/ol200098d>.
- (63) Han, F.-S. Transition-Metal-Catalyzed Suzuki–Miyaura Cross-Coupling Reactions: A Remarkable Advance from Palladium to Nickel Catalysts. *Chem. Soc. Rev.* **2013**, *42* (12), 5270. <https://doi.org/10.1039/c3cs35521g>.
- (64) Ritleng, V.; Henrion, M.; Chetcuti, M. J. Nickel N-Heterocyclic Carbene-Catalyzed C–Heteroatom Bond Formation, Reduction, and Oxidation: Reactions and Mechanistic Aspects. *ACS Catal.* **2016**, *6* (2), 890–906. <https://doi.org/10.1021/acscatal.5b02021>.
- (65) Henrion, M.; Ritleng, V.; Chetcuti, M. J. Nickel N-Heterocyclic Carbene-Catalyzed C–C Bond Formation: Reactions and Mechanistic Aspects. *ACS Catal.* **2015**, *5* (2), 1283–1302. <https://doi.org/10.1021/cs5014927>.
- (66) Rosen, B. M.; Quasdorf, K. W.; Wilson, D. A.; Zhang, N.; Resmerita, A.-M.; Garg, N. K.; Percec, V. Nickel-Catalyzed Cross-Couplings Involving Carbon–Oxygen Bonds. *Chem. Rev.* **2011**, *111* (3), 1346–1416. <https://doi.org/10.1021/cr100259t>.
- (67) Iwasaki, T.; Kambe, N. Ni-Catalyzed C–C Couplings Using Alkyl Electrophiles. *Top Curr Chem (Z)* **2016**, *374* (5), 66. <https://doi.org/10.1007/s41061-016-0067-6>.
- (68) Wang, X.; Dai, Y.; Gong, H. Nickel-Catalyzed Reductive Couplings. *Top Curr Chem (Z)* **2016**, *374* (4), 43. <https://doi.org/10.1007/s41061-016-0042-2>.
- (69) Arun, V.; Mahanty, K.; De Sarkar, S. Nickel-Catalyzed Dehydrogenative Couplings. *ChemCatChem* **2019**, *11* (9), 2243–2259. <https://doi.org/10.1002/cctc.201900254>.
- (70) Harry, N. A.; Saranya, S.; Ujwaldev, S. M.; Anilkumar, G. Recent Advances and Prospects in Nickel-Catalyzed C–H Activation. *Catal. Sci. Technol.* **2019**, *9* (8), 1726–1743. <https://doi.org/10.1039/C9CY00009G>.
- (71) Yamaguchi, J.; Muto, K.; Itami, K. Nickel-Catalyzed Aromatic C–H Functionalization. *Top Curr Chem (Z)* **2016**, *374* (4), 55. <https://doi.org/10.1007/s41061-016-0053-z>.
- (72) Thakur, A.; Louie, J. Advances in Nickel-Catalyzed Cycloaddition Reactions To Construct Carbocycles and Heterocycles. *Acc. Chem. Res.* **2015**, *48* (8), 2354–2365. <https://doi.org/10.1021/acs.accounts.5b00054>.
- (73) Kurahashi, T.; Matsubara, S. Nickel-Catalyzed Reactions Directed toward the Formation of Heterocycles. *Acc. Chem. Res.* **2015**, *48* (6), 1703–1716. <https://doi.org/10.1021/acs.accounts.5b00041>.
- (74) Ananikov, V. P. Nickel: The “Spirited Horse” of Transition Metal Catalysis. *ACS Catal.* **2015**, *5* (3), 1964–1971. <https://doi.org/10.1021/acscatal.5b00072>.
- (75) Dudnik, A. S.; Fu, G. C. Nickel-Catalyzed Coupling Reactions of Alkyl Electrophiles, Including Unactivated Tertiary Halides, To Generate Carbon–Boron Bonds. *J. Am. Chem. Soc.* **2012**, *134* (25), 10693–10697. <https://doi.org/10.1021/ja304068t>.

- (76) Zultanski, S. L.; Fu, G. C. Nickel-Catalyzed Carbon–Carbon Bond-Forming Reactions of Unactivated Tertiary Alkyl Halides: Suzuki Arylations. *J. Am. Chem. Soc.* **2013**, *135* (2), 624–627. <https://doi.org/10.1021/ja311669p>.
- (77) Schley, N. D.; Fu, G. C. Nickel-Catalyzed Negishi Arylations of Propargylic Bromides: A Mechanistic Investigation. *Journal of the American Chemical Society* **2014**, *136* (47), 16588–16593. <https://doi.org/10.1021/ja508718m>.
- (78) Griller, D.; Ingold, K. U. Free-Radical Clocks. *Acc. Chem. Res.* **1980**, *13* (9), 317–323. <https://doi.org/10.1021/ar50153a004>.
- (79) Newcomb, M.; Toy, P. H. Hypersensitive Radical Probes and the Mechanisms of Cytochrome P450-Catalyzed Hydroxylation Reactions. *Acc. Chem. Res.* **2000**, *33* (7), 449–455. <https://doi.org/10.1021/ar960058b>.
- (80) Breitenfeld, J.; Ruiz, J.; Wodrich, M. D.; Hu, X. Bimetallic Oxidative Addition Involving Radical Intermediates in Nickel-Catalyzed Alkyl–Alkyl Kumada Coupling Reactions. *J. Am. Chem. Soc.* **2013**, *135* (32), 12004–12012. <https://doi.org/10.1021/ja4051923>.
- (81) Cornella, J.; Gómez-Bengoa, E.; Martin, R. Combined Experimental and Theoretical Study on the Reductive Cleavage of Inert C–O Bonds with Silanes: Ruling out a Classical Ni(0)/Ni(II) Catalytic Couple and Evidence for Ni(I) Intermediates. *J. Am. Chem. Soc.* **2013**, *135* (5), 1997–2009. <https://doi.org/10.1021/ja311940s>.
- (82) Kalvet, I.; Guo, Q.; Tizzard, G. J.; Schoenebeck, F. When Weaker Can Be Tougher: The Role of Oxidation State (I) in P- vs N-Ligand-Derived Ni-Catalyzed Trifluoromethylthiolation of Aryl Halides. *ACS Catal.* **2017**, *7* (3), 2126–2132. <https://doi.org/10.1021/acscatal.6b03344>.
- (83) Zhang, K.; Conda-Sheridan, M.; R. Cooke, S.; Louie, J. N-Heterocyclic Carbene Bound Nickel(I) Complexes and Their Roles in Catalysis. *Organometallics* **2011**, *30* (9), 2546–2552. <https://doi.org/10.1021/om200090d>.
- (84) Miyazaki, S.; Koga, Y.; Matsumoto, T.; Matsubara, K. A New Aspect of Nickel-Catalyzed Grignard Cross-Coupling Reactions: Selective Synthesis, Structure, and Catalytic Behavior of a T-Shape Three-Coordinate Nickel(i) Chloride Bearing a Bulky NHC Ligand. *Chem. Commun.* **2010**, *46* (11), 1932. <https://doi.org/10.1039/b924716e>.
- (85) Smith, S. M.; Planas, O.; Gómez, L.; Rath, N. P.; Ribas, X.; Mirica, L. M. Aerobic C–C and C–O Bond Formation Reactions Mediated by High-Valent Nickel Species. *Chem. Sci.* **2019**, *10* (44), 10366–10372. <https://doi.org/10.1039/C9SC03758F>.
- (86) Smith, S. M.; Rath, N. P.; Mirica, L. M. Axial Donor Effects on Oxidatively Induced Ethane Formation from Nickel–Dimethyl Complexes. *Organometallics* **2019**, *38* (19), 3602–3609. <https://doi.org/10.1021/acs.organomet.9b00438>.
- (87) Watson, M. B.; Rath, N. P.; Mirica, L. M. Oxidative C–C Bond Formation Reactivity of Organometallic Ni(II), Ni(III), and Ni(IV) Complexes. *J. Am. Chem. Soc.* **2017**, *139* (1), 35–38. <https://doi.org/10.1021/jacs.6b10303>.

- (88) Martinez, G. E.; Ocampo, C.; Park, Y. J.; Fout, A. R. Accessing Pincer Bis(Carbene) Ni(IV) Complexes from Ni(II) via Halogen and Halogen Surrogates. *J. Am. Chem. Soc.* **2016**, *138* (13), 4290–4293. <https://doi.org/10.1021/jacs.5b12827>.
- (89) Bour, J. R.; Camasso, N. M.; Sanford, M. S. Oxidation of Ni(II) to Ni(IV) with Aryl Electrophiles Enables Ni-Mediated Aryl–CF₃ Coupling. *J. Am. Chem. Soc.* **2015**, *137* (25), 8034–8037. <https://doi.org/10.1021/jacs.5b04892>.
- (90) Yin, G.; Kalvet, I.; Englert, U.; Schoenebeck, F. Fundamental Studies and Development of Nickel-Catalyzed Trifluoromethylthiolation of Aryl Chlorides: Active Catalytic Species and Key Roles of Ligand and Traceless MeCN Additive Revealed. *J. Am. Chem. Soc.* **2015**, *137* (12), 4164–4172. <https://doi.org/10.1021/jacs.5b00538>.
- (91) Hie, L.; Fine Nathel, N. F.; Hong, X.; Yang, Y.-F.; Houk, K. N.; Garg, N. K. Nickel-Catalyzed Activation of Acyl C–O Bonds of Methyl Esters. *Angewandte Chemie International Edition* **2016**, *55* (8), 2810–2814. <https://doi.org/10.1002/anie.201511486>.
- (92) Mohadjer Beromi, M.; Banerjee, G.; Brudvig, G. W.; Charboneau, D. J.; Hazari, N.; Lant, H. M. C.; Mercado, B. Q. Modifications to the Aryl Group of Dppf-Ligated Ni σ -Aryl Precatalysts: Impact on Speciation and Catalytic Activity in Suzuki–Miyaura Coupling Reactions. *Organometallics* **2018**, *37* (21), 3943–3955. <https://doi.org/10.1021/acs.organomet.8b00589>.
- (93) Frieman, B. A.; Taft, B. R.; Lee, C.-T.; Butler, T.; Lipshutz, B. H. Nickel-in-Charcoal (Ni/C): An Efficient Heterogeneous Catalyst for the Construction of C–C, C–N, and C–H Bonds. *Synthesis* **2005**, *2005* (17), 2989–2993. <https://doi.org/10.1055/s-2005-872145>.
- (94) Lipshutz, B. H.; Butler, T.; Swift, E. C–C Bond Formation Catalyzed Heterogeneously by Nickel-on-Graphite (Ni/C_g). *Org. Lett.* **2008**, *10* (5), 697–700. <https://doi.org/10.1021/ol702453q>.
- (95) Buslov, I.; Song, F.; Hu, X. An Easily Accessed Nickel Nanoparticle Catalyst for Alkene Hydrosilylation with Tertiary Silanes. *Angew. Chem. Int. Ed.* **2016**, *55* (40), 12295–12299. <https://doi.org/10.1002/anie.201606832>.
- (96) Galeandro-Diamant, T.; Suleimanov, I.; Veyre, L.; Bousquié, M.; Meille, V.; Thieuleux, C. Alkene Hydrosilylation with Supported and Unsupported Ni Nanoparticles: Strong Influence of the Ni Environment on Activity and Selectivity. *Catal. Sci. Technol.* **2019**, *9* (7), 1555–1558. <https://doi.org/10.1039/C8CY01487F>.
- (97) Ananikov, V. P.; Beletskaya, I. P. Preparation of Metal “Nanosalts” and Their Application in Catalysis: Heterogeneous and Homogeneous Pathways. *Dalton Trans.* **2011**, *40* (16), 4011. <https://doi.org/10.1039/c0dt01277g>.
- (98) Baudouin, D.; Szeto, K. C.; Laurent, P.; De Mallmann, A.; Fenet, B.; Veyre, L.; Rodemerck, U.; Copéret, C.; Thieuleux, C. Nickel–Silicide Colloid Prepared under Mild Conditions as a Versatile Ni Precursor for More Efficient CO₂ Reforming of CH₄ Catalysts. *J. Am. Chem. Soc.* **2012**, *134* (51), 20624–20627. <https://doi.org/10.1021/ja3111797>.

- (99) Eremin, D. B.; Ananikov, V. P. Exceptional Behavior of Ni₂O₂ Species Revealed by ESI-MS and MS/MS Studies in Solution. Application of Superatomic Core To Facilitate New Chemical Transformations. *Organometallics* **2014**, *33* (22), 6352–6357. <https://doi.org/10.1021/om500637k>.
- (100) Sonnenberg, J. F.; Coombs, N.; Dube, P. A.; Morris, R. H. Iron Nanoparticles Catalyzing the Asymmetric Transfer Hydrogenation of Ketones. *J. Am. Chem. Soc.* **2012**, *134* (13), 5893–5899. <https://doi.org/10.1021/ja211658t>.
- (101) Wu, K.; Doyle, A. G. Parameterization of Phosphine Ligands Demonstrates Enhancement of Nickel Catalysis via Remote Steric Effects. *Nature Chem* **2017**, *9* (8), 779–784. <https://doi.org/10.1038/nchem.2741>.
- (102) Nielsen, D. K.; Doyle, A. G. Nickel-Catalyzed Cross-Coupling of Styrenyl Epoxides with Boronic Acids. *Angew. Chem. Int. Ed.* **2011**, *50* (27), 6056–6059. <https://doi.org/10.1002/anie.201101191>.
- (103) Lavoie, C. M.; MacQueen, P. M.; Rotta-Loria, N. L.; Sawatzky, R. S.; Borzenko, A.; Chisholm, A. J.; Hargreaves, B. K. V.; McDonald, R.; Ferguson, M. J.; Stradiotto, M. Challenging Nickel-Catalysed Amine Arylations Enabled by Tailored Ancillary Ligand Design. *Nat Commun* **2016**, *7* (1), 11073. <https://doi.org/10.1038/ncomms11073>.
- (104) Marín, M.; Moreno, J. J.; Navarro-Gilabert, C.; Álvarez, E.; Maya, C.; Peloso, R.; Nicasio, M. C.; Carmona, E. Synthesis, Structure and Nickel Carbonyl Complexes of Dialkylterphenyl Phosphines. *Chem. Eur. J.* **2019**, *25* (1), 260–272. <https://doi.org/10.1002/chem.201803598>.
- (105) Tobisu, M.; Yasutome, A.; Kinuta, H.; Nakamura, K.; Chatani, N. 1,3-Dicyclohexylimidazol-2-Ylidene as a Superior Ligand for the Nickel-Catalyzed Cross-Couplings of Aryl and Benzyl Methyl Ethers with Organoboron Reagents. *Org. Lett.* **2014**, *16* (21), 5572–5575. <https://doi.org/10.1021/ol502583h>.
- (106) Cheung, C. W.; Ploeger, M. L.; Hu, X. Direct Amidation of Esters with Nitroarenes. *Nature Communications* **2017**, *8*, 14878. <https://doi.org/10.1038/ncomms14878>.
- (107) Cheung, C. W.; Ploeger, M. L.; Hu, X. Amide Synthesis via Nickel-Catalysed Reductive Aminocarbonylation of Aryl Halides with Nitroarenes. *Chemical Science* **2018**, *9* (3), 655–659. <https://doi.org/10.1039/C7SC03950F>.
- (108) Cheung, C. W.; Ploeger, M. L.; Hu, X. Nickel-Catalyzed Reductive Transamidation of Secondary Amides with Nitroarenes. *ACS Catalysis* **2017**, *7* (10), 7092–7096. <https://doi.org/10.1021/acscatal.7b02859>.
- (109) Cheung, C. W.; Ma, J.-A.; Hu, X. Manganese-Mediated Reductive Transamidation of Tertiary Amides with Nitroarenes. *Journal of the American Chemical Society* **2018**, *140* (22), 6789–6792. <https://doi.org/10.1021/jacs.8b03739>.
- (110) Cheung, C. W.; Ploeger, M. L.; Hu, X. Direct Amidation of Esters with Nitroarenes. *Nature Communications* **2017**, *8* (1). <https://doi.org/10.1038/ncomms14878>.

- (111) Cheung, C. W.; Shen, N.; Wang, S.-P.; Ullah, A.; Hu, X.; Ma, J.-A. Manganese-Mediated Reductive Amidation of Esters with Nitroarenes. *Organic Chemistry Frontiers* **2019**. <https://doi.org/10.1039/C8QO01405A>.
- (112) Buslov, I.; Becouse, J.; Mazza, S.; Montandon-Clerc, M.; Hu, X. Chemoselective Alkene Hydrosilylation Catalyzed by Nickel Pincer Complexes. *Angewandte Chemie International Edition* **2015**, 54 (48), 14523–14526. <https://doi.org/10.1002/anie.201507829>.

Chapter 2 Identification of intermediates in nickel catalysed amidation of esters with nitroarenes

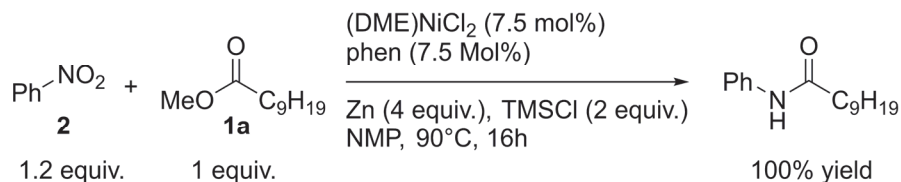
Part of the data were reproduced with permission from Cheung, C.W.; Ploeger, M.L.; Hu, X. Direct amidation of esters with nitroarenes *Nature Communications*. 2017, 8, 14878. Copyright the authors and from Ploeger, M.L.; Darù, A.; Harvey, J.N.; Hu, X. Reductive Cleavage of Azoarene as a Key step in Nickel-Catalyzed Amidation of Esters with Nitroarenes *ACS Catalysis*. 2020, 10, 2845-2854. Copyright 2020 American Chemical Society.

2.1 Introduction

Nitroarenes are important synthetic intermediates for nitrogen-containing aromatic compounds, due to their ease of preparation and a variety of potential transformations.^{1,2} The most common conversion of nitroarenes is the reduction to anilines.² However, a number of groups have recently started to develop synthetic methods that lead to N-functionalized compounds directly from nitroarenes.^{3–10} Our group has contributed to this field as well, by developing reactions for amidation of various substrates with nitroarenes as nitrogen source.^{11–15} The original motivation of this reactivity was to improve step economy of amidations, as these are often done with anilines that are themselves derived from nitroarenes. However, we found that aniline was an inferior substrate to nitroarenes in several cases.^{11,14,15} This phenomenon has been observed by others as well^{3,8,9} and indicates that the reaction mechanism does not involve a straightforward reduction of nitroarene followed by well-established amine chemistry.

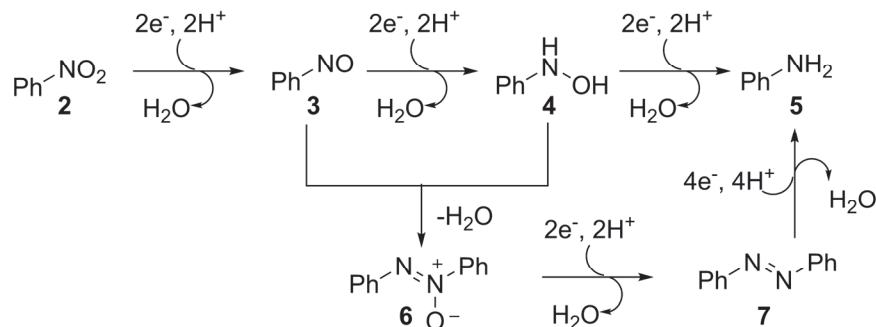
Given the recent surge in using nitroarenes directly for formation of C-N coupled products and the finding that the reaction pathway is not via well-established pathways, a more in-depth mechanistic understanding of this type of reactivity is of interest. We chose to study the coupling between methyl decanoate (**1a**) and nitrobenzene (**2**) catalyzed by nickel as a model reaction (Scheme 2.1). The yield is quantitative, which minimizes complications due to side reactions. The choice of model reaction also meant Zn could be used as reductant instead of Mn, which avoids the complication of Mn-mediated amidation.^{8,14,15}

Scheme 2.1: Model reaction studied in this chapter



2.2 Identification of reactive species

Scheme 2.2: A simplified pathway for nitroarene reduction.



Several species could form upon reduction of nitrobenzene (Scheme 2.2).¹⁶ To understand which of these might be responsible for the amidation of esters, we tested if these compounds could be used as nitrogen source in lieu of nitrobenzene. Since reduction towards these species would lead to depletion of the reductants and formation of byproducts, a slight re-optimization was performed for these substrates (see Section 2.6.3 for details). The conversions of the nitrogen source and the yield of amide under optimized conditions for each potential intermediate are listed in Table 2.1. Aniline (**5**) gave poor yields regardless of the conditions, excluding it as a potential intermediate. Phenylhydroxylamine (**4**) gave reasonable yields, but these deteriorated if fewer equivalents of Zn and trimethylsilylchloride (TMSCl) than for the nitrobenzene reaction were used. Since some amount of Zn and TMSCl should be consumed to generate the hydroxylamine from nitrobenzene, the required reductant stoichiometry shown in table 2.1 rules out hydroxylamine as intermediate as well.

Good yields were obtained for nitrosobenzene (**3**), azoxybenzene (**6**) and azobenzene (**7**). Importantly, as these intermediates become more reduced (from nitrosobenzene to azoxybenzene to azobenzene), fewer equivalents of Zn and TMSCl are required to make the reaction work. This supports a mechanistic scenario wherein nitrosobenzene is a precursor to azoxybenzene, which is subsequently reduced to azobenzene, which is in turn the species to react with the ester.

Table 2.1: Amidation with various nitrobenzene reduction products under reoptimized conditions.

<div style="display: flex; align-items: center; justify-content: center;"> <div style="text-align: center;"> intermediate + x equiv. </div> <div style="margin: 0 10px;"> $\text{MeO}-\text{C}(=\text{O})-\text{C}_9\text{H}_{19}$ </div> <div style="text-align: center;"> $\xrightarrow[\text{NMP, 90}^\circ\text{C, 16h}]{\begin{array}{l} (\text{DME})\text{NiCl}_2 \text{ (7.5 mol\%)} \\ \text{phen (7.5 mol\%)} \\ y \text{ equiv. Zn, } z \text{ equiv. TMSCl} \end{array}}$ </div> <div style="text-align: center;"> $\text{Ph}-\text{N}(\text{H})-\text{C}(=\text{O})-\text{C}_9\text{H}_{19}$ </div> </div>				
Intermediate	x	y	z	GC yield (ester conversion)
PhNO	1.2	3	2	~100 (100)
$\text{Ph}-\text{N}(\text{H})-\text{OH}$	1.2	4	2	74 (78)
PhNH ₂ + 2 equiv. ZnCl ₂	1.2	2	0	43 (45)
$\text{Ph}-\text{N}^+(\text{O}^-)=\text{N}-\text{Ph}$	0.5	3	0.5	~100 (96)
$\text{Ph}-\text{N}=\text{N}-\text{Ph}$	0.5	2	0.09	~100 (97)

To ascertain if such a reduction chain is indeed operative under the catalytic conditions, the reaction starting from nitrobenzene was followed in time by GC/MS (Figure 2.1A). While nitrobenzene is converted rapidly, amide product formation is not observed in the first 50 minutes of the reaction. Of the potential intermediates on the reduction pathway, only azoxybenzene and azobenzene are observed. Azoxybenzene increases at the beginning of the reaction to a steady state concentration, until finally decreasing near the end of the reaction, while azobenzene starts to form in minor quantities around the time that product formation occurs.

To determine whether azoxybenzene is converted to azobenzene before reacting with ester, or could itself be a potent intermediate, the reaction starting from azoxybenzene was followed in time by GC/MS (Figure 2.1B). Under these conditions, azoxybenzene is rapidly converted, while the formation of amide product is once again delayed by an induction period. Azobenzene initially builds up, reaching a maximum concentration as the azoxybenzene is nearly depleted and the product amide has started to form.

The results in Figure 2.1 suggest that there is indeed a reduction chain via azoxybenzene to azobenzene and that azobenzene is the intermediate that reacts with ester under our conditions.

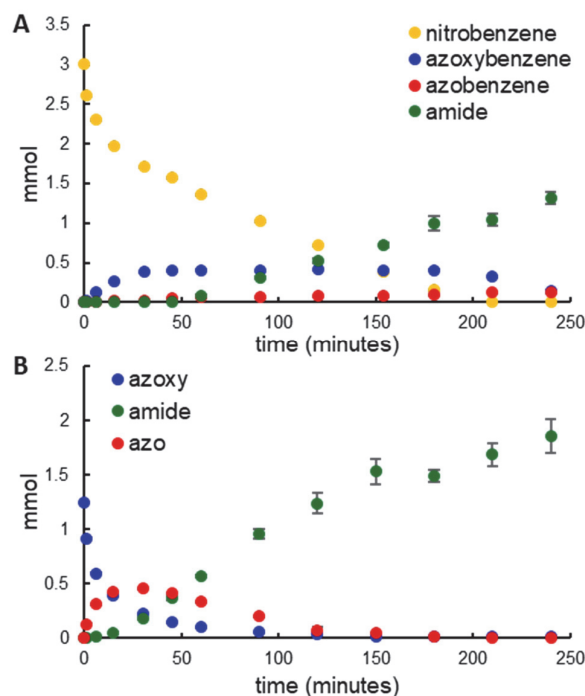
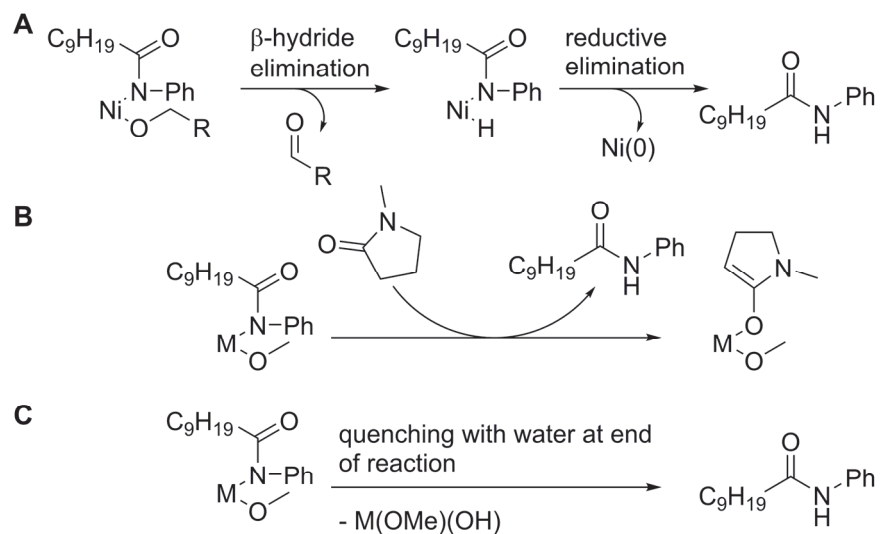


Figure 2.1: Reaction profiles of the amidation. (A) The evolution of the amount of different species present (in mmol) during the reductive amidation of **1a** with nitrobenzene. Conditions according to Scheme 2.1. (B) The evolution of the amount of different species present (in mmol) during the reductive amidation of **1a** with azoxybenzene. Conditions: 0.5 M **1a**, 0.3 M azoxybenzene, 3 eq Zn, 0.5 eq TMSCl, 7.5 mol% Ni(DME)Cl₂, 7.5 mol% phenanthroline in 5 ml NMP at 90°C. For both graphs, sampling was performed in triplicate; the error bars indicate the sample standard error

2.3 Proton source

As the reactive intermediate azobenzene contains no N-H bonds, the origin of the amide proton is not directly clear. It could in principle be derived from the alkoxy leaving group on the ester, the solvent or from water introduced at the end of the reaction (Scheme 2.3). Given the ease of proton exchange at the amide position, determining its origin through deuterium labelling is complicated. We therefore applied different probes to refute pathway A in scheme 2.3 and lend credence to pathway C.

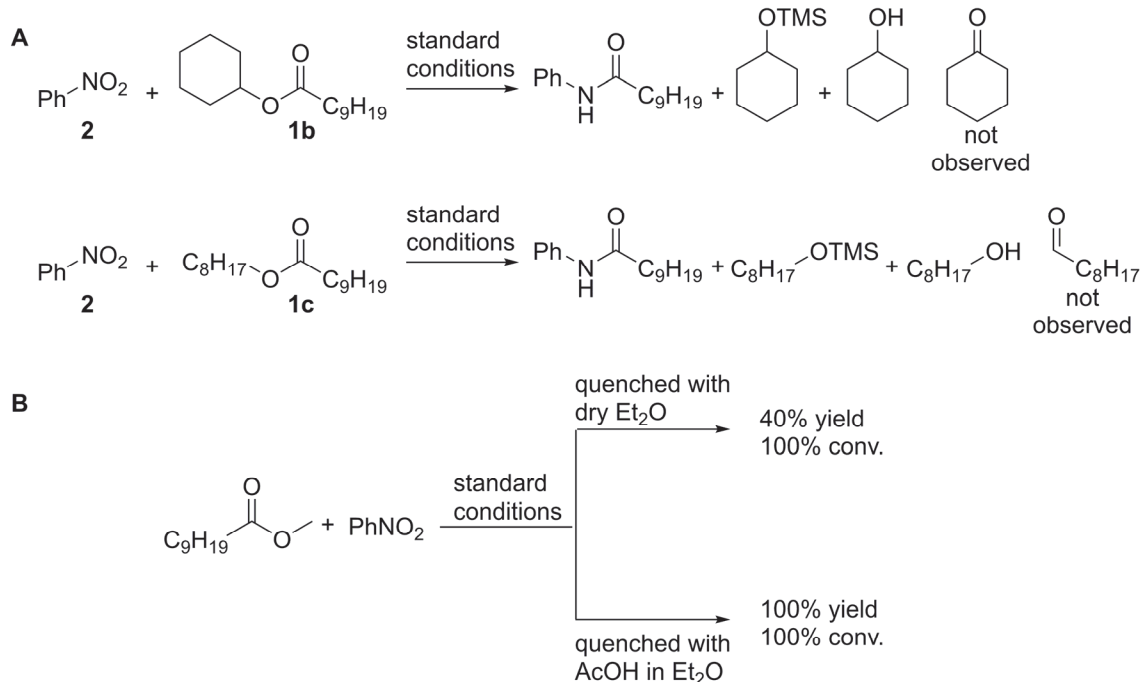
Scheme 2.3: Three possible pathways to explain the origin of the proton on the amide nitrogen.



Ester substrates with alkoxy-substituents heavier than methoxy facilitated the observation of byproducts derived from the leaving group with GC/MS. For substrates containing a secondary cyclohexoxy (**1b**) or a primary *n*-octoxy (**1c**) leaving group, the only byproducts derived from these groups observed by GC/MS are their alcohols and trimethylsilyl ethers (Scheme 2.4A). Beta-hydride elimination to provide the amide proton (Scheme 2.3A) does not seem to occur.

Scheme 2.4: (A) Lack of ketone or aldehyde formation when esters with bigger leaving groups are employed.

(B) Quenching influences the yield of amide.



When aliquots from a reaction between nitrobenzene and methyl decanoate under standard conditions were diluted with dry diethyl ether in the glove box to prepare a GC/MS sample, a yield of only 40% was determined, despite 100% conversion of both substrates. From samples prepared from the same reaction mixture by dilution with 0.5 M acetic acid in diethyl ether 100% yield of amide was determined (Scheme 2.4B). These results suggest the pathway depicted in Scheme 2.3C does indeed occur.

The presence of some amount of amide product in the sample prepared with dry diethyl ether suggests different pathways might be occurring. However, when 3 samples were prepared in triplicate, an upward trend in the GC yield was observed among samples that should be identical in all respects, except for the amount of time that had elapsed between preparation and GC analysis. This indicates that samples may react with atmospheric water as they stand on the sample tray.

Thus, while we were unable to definitively exclude pathway of Scheme 2.3B, the most important proton source appears to be the quenching at the end of the reaction. The product initially formed in the reaction mixture is therefore likely a metal amidate. Since zinc ions should be stoichiometrically available in the reaction mixture, it is the most likely candidate for the metal in this amidate. Possibly it is formed after transmetalation from catalytically formed nickel amidate.

2.4 Insights into reduction pathway

Reduction pathways of nitrobenzene are well documented in the presence of acidic protons and a reductant.¹⁶ However, the fact that the quenching medium is the proton source for the amide in this reaction indicates that acidic protons are not present under our conditions. Therefore, an adjusted reduction pathway should be operative under our catalytic conditions. Given recent efforts to prepare valuable azoarenes through reduction of nitroarenes,^{17–20} an investigation into our acid-free reduction may provide valuable insights. We therefore performed some preliminary mechanistic investigations into the mechanism of azobenzene formation from nitrobenzene, by omitting the ester from the reaction mixture.

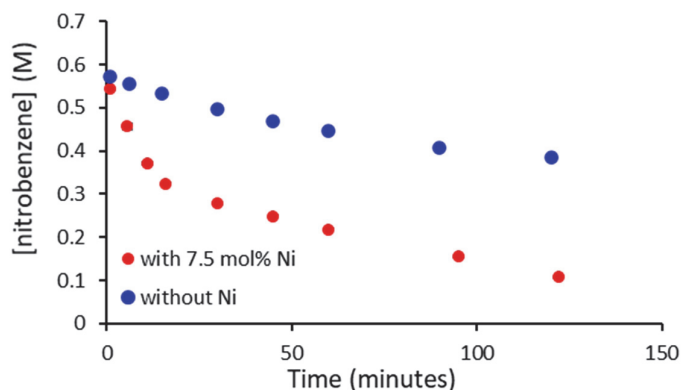


Figure 2.2: Nitrobenzene conversion followed with GC in the absence and presence of catalytic nickel

Although nitrobenzene can apparently be converted by Zn alone (Figure 2.2), the rate of conversion is considerably higher in the presence of nickel catalyst. With nickel catalyst the nitrobenzene is fully converted within 3.5 hours, whereas conversion is not complete without nickel even after heating at 90°C overnight. Moreover, azoxybenzene is the only observed product when the reduction is performed without nickel, whereas azobenzene can be observed as well if catalytic nickel is present. Thus, nickel plays an important role in the reduction of nitrobenzene under our conditions.

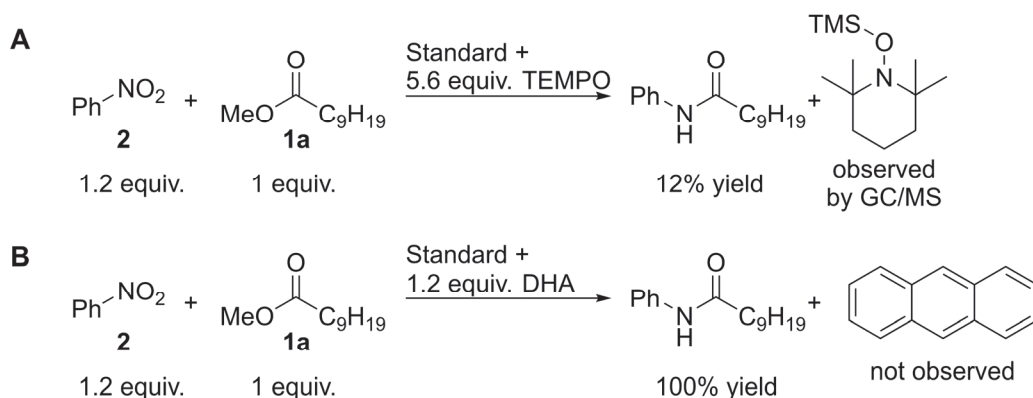
One possible role that nickel might fulfil is the activation of intermediate nitrosobenzene. Although we never observed nitrosobenzene in the reactions monitored by GC/MS, its intermediacy can be inferred from the failure of our catalytic system to convert nitroalkanes, likely due to tautomerization of nitrosoalkanes to oximes.^{21,22} Indeed, successful conversion of nitroalkanes in reductive amination reactions is considered important evidence for lack of nitroso intermediates.^{10,23}

Low-valent nickel nitroso-adducts have been reported, although with different ligand systems.^{24,25} Metal-nitroso complexes have also been shown to play a role in C-N coupling with nitroarenes catalyzed by iron.²⁶ Unfortunately, we were unable to isolate a nickel nitroso adduct with phenanthroline, or the closely related bipyridine as a ligand.

An alternative role for nickel would be the activation of trimethylsilylchloride. When the amidation of **1a** with nitrobenzene is performed in the presence of 1.2 equivalents of TEMPO, the reaction is suppressed and silylated TEMPO can be observed (Scheme 2.5A). This may indicate intermediacy of the trimethylsilyl radical. Generation of alkyl radicals from alkyl halides by low-valent nickel species is well-established,^{27,28} and radical addition to nitrobenzene is known to cause deoxygenative reduction.²⁹ Similar reactivity may therefore be envisioned with silyl radicals formed from a silyl halide. However, some care must be taken with this conclusion, as

another radical scavenger, 9,10-dihydroanthracene (DHA), did not suppress the reaction at all, or lead to formation of anthracene (Scheme 2.5B). The C-H bond dissociation energy (BDE) of DHA is 79.3 kcal/mol,³⁰ while the of Si-H BDE of trimethylsilane is 94.7±1.7 kcal/mol, so the thermodynamic driving force should be strong enough.³¹

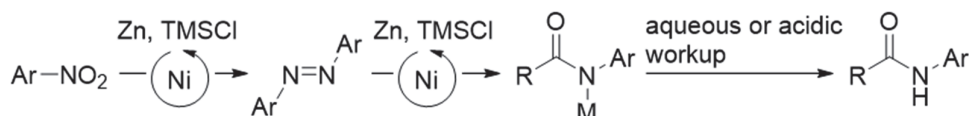
Scheme 2.5: Influence of radical scavengers (A) TEMPO and (B) DHA on the reaction yield.



2.5 Conclusions

We have demonstrated the nickel-catalyzed amidation of esters with nitroarenes occurs with intermediacy of azobenzene as key intermediate. In addition, we unveiled that the nitrogen-bound proton in the product amide isn't introduced until the reaction mixture is quenched, which indicates a metal amidate as initial product. Finally, we briefly looked into the reduction pathway, since the lack of acidic protons means this pathway is different from the well-established reduction pathway. We revealed nickel plays an important role already in the reduction pathway, although the nature of the nickel catalysis for this pathway can only be speculated on at this point. The findings in this chapter can be summarized in Scheme 2.6: first, nitrobenzene is converted to azobenzene through Zn/TMSCl reduction and nickel catalysis. Then, azobenzene reacts with ester under the influence of nickel to form a metal amidate. Finally, this metal amidate is converted to the product amide upon quenching the reaction medium. The conversion of azobenzene to amide is intriguing in its own right and the mechanism thereof will be further explored in chapters 3 and 4.

Scheme 2.6: Reaction pathway for amidation of esters with nitrobenzene.



2.6 Experimental

2.6.1 General remarks

All reactions were set up and performed under inert nitrogen atmosphere using standard glove box and Schlenk techniques. Anhydrous N-methyl-2-pyrrolidinone (NMP) stored over molecular sieves was purchased from Acros and stored in a glove box. Diethyl ether was purified using a two column solid-state purification system (Innovative Technology, NJ, USA) and transferred to the glovebox without exposure to air. Anhydrous 1,10-phenanthroline, (DME)NiCl₂, zinc, TMSCl, naphthalene, methyl decanoate, nitrobenzene, nitrosobenzene, phenylhydroxylamine, azoxybenzene, azobenzene, TEMPO and 9,10-dihydroanthracene were purchased from commercial sources and used without further purification.

2.6.2 Comments on GC analysis

GC/MS was measured on an Agilent 7890B GC coupled to an Agilent 5977B Mass Spectrometer equipped with an Agilent J&W DB-5MS Ultra Inert column with 0.25 mm internal diameter. GC was measured on a Perkin Elmer Clarus 400 Gas chromatographer equipped with the same column. The carrier gas for the GC/MS is helium; for the GC it is hydrogen. Quantification was done by integrating the flame ionization detector (FID) chromatogram. The ratio between the analyte peak integral and the naphthalene internal standard peak integral was multiplied by a factor (f) to account for difference in FID response for different compounds: f_{az} : 0.82, f_{azoxy} : 0.92, f_{amide} : 0.87, f_{nitro} : 1.67. f_{nitro} was determined by the ratio of the number of carbon atoms in nitrobenzene divided by the number of carbon atoms in naphthalene, which gave reasonable results for early time points. The other correction factors were determined by measuring calibration curves over 2 orders of magnitude concentrations of the analyte.

2.6.3 General remarks on re-optimization of reaction conditions nitrobenzene-derived substrates

For all intermediates, the reaction was performed with 7.5 mol% Ni(glyme)Cl₂ / phen catalyst loading. 0.5 M ester (= 1 equiv) in 0.5 ml NMP was used. Reactants were introduced to the

reaction mixtures via freshly prepared stock solutions containing the substrates and the internal standard. The reactions were performed with naphthalene as internal standard. Amide yields and ester conversions were analyzed by preparation of GC samples from the crude reaction mixtures and measuring the ratio of peak area of the ester and amide versus naphthalene. Sample preparation was done by adding a few drops of the reaction mixture to diethyl ether, shaking and filtering the resulting suspension with 0.22 μm ptfe syringe filters. The screening results are summarized in Tables 2.2-2.6.

Table 2.2: Re-optimization for amidation with aniline.

$\text{Ph-NH}_2 + \text{MeO-C(=O)-C}_9\text{H}_{19}$		(DME)NiCl ₂ (7.5 mol%) phen (7.5 Mol%) Zn (equiv.), TMSCl (equiv.), ZnCl ₂ (equiv.) NMP, 90°C, 16h			$\text{Ph-NH-C(=O)-C}_9\text{H}_{19}$
1.2 equiv.	1 equiv.				
Zn (equiv.)	TMSCl (equiv.)	ZnCl ₂ (equiv.)	Conversion (%) ^a	Yield (%) ^b	
4	2	0	14	12	
2	1	0	27	28	
2	0	0	0	0	
2	2	0	20	17	
1	0	0	0	0	
4	2	2	18	3	
2	1	2	25	19	
2	0	2	45	44	
1	1	2	21	20	
1	0	2	44	39	
0	0	2	0	0	

^aDetermined with GC by difference in ester/naphthalene ratio between product mixture and stock solution. ^bDetermined by GC from amide/naphthalene ratio multiplied by 0.87

Table 2.3: Re-optimization for amidation with nitrosobenzene.

$\text{Ph-NO} + \text{MeO-C(=O)-C}_9\text{H}_{19} \xrightarrow[\text{Zn (equiv.), TMSCl (equiv.)}]{\text{(DME)NiCl}_2 \text{ (7.5 mol\%) phen (7.5 Mol\%)}} \text{Ph-NH-C(=O)-C}_9\text{H}_{19}$
 1.2 equiv. 1 equiv.
 NMP, 90°C, 16h

Zn (equiv.)	TMSCl (equiv.)	Conversion (%) ^a	Yield (%) ^b
4	2	100	100
3	2	100	100
3	1	91	87
2	1	22	12

^aDetermined with GC by difference in ester/naphthalene ratio between product mixture and stock solution. ^bDetermined by GC from amide/naphthalene ratio multiplied by 0.87

Table 2.4: Re-optimization for amidation with phenylhydroyamine.

$\text{Ph-NH-OH} + \text{MeO-C(=O)-C}_9\text{H}_{19} \xrightarrow[\text{Zn (equiv.), TMSCl (equiv.)}]{\text{(DME)NiCl}_2 \text{ (7.5 mol\%) phen (7.5 Mol\%)}} \text{Ph-NH-C(=O)-C}_9\text{H}_{19}$
 1.2 equiv. 1 equiv.
 NMP, 90°C, 16h

Zn (equiv.)	TMSCl (equiv.)	Conversion (%) ^a	Yield (%) ^b
4	2	78	74
3	2	60	59
2	2	17	15
2	1	11	4

^aDetermined with GC by difference in ester/naphthalene ratio between product mixture and stock solution. ^bDetermined by GC from amide/naphthalene ratio multiplied by 0.87

Table 2.5: Re-optimization for amidation with azoxybenzene.

0.5 equiv.		1 equiv.		Conversion (%) ^a	Yield(%) ^b
Zn (equiv.)	TMSCl (equiv.)	Zn (equiv.)	TMSCl (equiv.)		
4	1	4	0.5	85	81
4	1	4	0.5	95	93
4	1	4	0.091	2	6
3	1	4	0.5	96	99
2	1	4	0.5	91	81
1	1	4	0.5	53	45

^aDetermined with GC by difference in ester/naphthalene ratio between product mixture and stock solution. ^bDetermined by GC from amide/naphthalene ratio multiplied by 0.87

Table 2.6: Re-optimization for azidation with azobenzene.

0.5 equiv.		1 equiv.		Conversion (%) ^a	Yield (%) ^b
Zn (equiv.)	TMSCl (equiv.)	Zn (equiv.)	TMSCl (equiv.)		
4	1	4	0.09	65	48
4	1	4	0.09	90	69
3	1	4	0.09	97	76
2	1	4	0.09	97	~100
1	1	4	0.09	72	60

^aDetermined with GC by difference in ester/naphthalene ratio between product mixture and stock solution. ^bDetermined by GC from amide/naphthalene ratio multiplied by 0.87

2.6.4 Reaction profile of nitrobenzene-ester coupling

655 mg Zn (10 mmol, 4 equiv.), 41.7 mg (DME)NiCl₂ (0.1875 mmol, 0.075 equiv.), 34.4 mg 1,10-phenanthroline (0.1875 mmol, 0.075 equiv.), 63.2 mg naphthalene (0.5 mmol, 0.2 equiv.), 5 mL NMP, 553 mg TMSCl (5 mmol, 2 equiv.), 465 mg methyl decanoate (2.5 mmol, 1 equiv.)

and 370 mg nitrobenzene (3 mmol, 1.2 equiv.) were added to an oven-dried Schlenk flask in the glove box. Closed with a greased stopper. Outside the glove box, the stopper was replaced with a septum under nitrogen flow and the system was purged for a few minutes. The mixture was then submerged in a pre-heated 90°C oil bath. This moment is considered $t=0$. GC samples were prepared in triplicate at the time points indicated in Figure 2.1A by adding an aliquot to 0°C diethyl ether and filtering the resulting suspension.

2.6.5 Reaction profile of azoxybenzene-ester coupling

250 mg Zn (3.75 mmol, 1.5 equiv.), 40.2 mg (DME)NiCl₂ (0.1875 mmol, 0.075 equiv.), 33.5 mg 1,10-phenanthroline (0.1875 mmol, 0.075 equiv.), 64.0 mg naphthalene (0.5 mmol, 0.2 equiv.), 248 mg azoxybenzene (1.25 mmol, 0.5 equiv.), 5 mL NMP, 154 mg TMSCl (1.25 mmol, 0.5 equiv.) and 467 mg methyl decanoate (2.5 mmol, 1 equiv.) were added to an oven-dried Schlenk flask in the glove box. Closed with a greased stopper. Outside the glove box, the stopper was replaced with a septum under nitrogen flow and the system was purged for a few minutes. The mixture was then submerged in a pre-heated 90°C oil bath. This moment is considered $t=0$. GC samples were prepared in triplicate at the time points indicated in Figure 2.1B by adding an aliquot to 0°C diethyl ether and filtering the resulting suspension.

2.6.6 Quenching experiment

65.3 mg Zn (1 mmol, 4 equiv.), 4.0 mg (DME)NiCl₂ (0.01875 mmol, 0.075 equiv.), 3.3 mg 1,10-phenanthroline (0.01875 mmol, 0.075 equiv.), 10.5 mg naphthalene (0.05 mmol, 0.2 equiv.), 0.5 mL NMP, 53.7 mg TMSCl (0.5 mmol, 2 equiv.), 46.4 mg methyl decanoate (0.25 mmol, 1 equiv.) and 37.2 mg nitrobenzene (0.3 mmol, 1.2 equiv.) were added to an oven-dried scintillation vial in the glove box. Stirred on a pre-heated 90°C heating plate for 16 hours. After cooling down, 15 μ L of the reaction mixture was added to each of six oven dried vials. To three of them, dry Et₂O was added. These mixtures were shaken and filtered into GC-vials through 0.22 μ m PTFE syringe filters. The three other mixtures were treated with 0.5 M AcOH in Et₂O. After shaking, these mixtures were filtered into GC-vials through 0.22 μ m PTFE syringe filters. Samples were analyzed by GC.

2.6.7 Reaction profile of nitrobenzene reduction

Zn (10 mmol, 4 equiv.), (DME)NiCl₂ (0 or 0.1875 mmol, 0 or 0.075 equiv.), phenanthroline (0 or 0.1875 mmol, 0 or 0.075 equiv.), 5 mL NMP and TMSCl (5 mmol, 2 equiv.) were added to an oven-dried Schlenk flask in the glove box. After stirring for 2 hours, nitrobenzene (3 mmol, 1.2 equiv.) was added. The schlenk was closed with a greased stopper. Outside the glove box, the stopper was replaced with a septum under nitrogen flow and the system was purged for a few minutes. The mixture was then submerged in a pre-heated 90°C oil bath. This moment is considered t=0. GC samples were prepared in triplicate at the time points indicated in Figure 2.2 by adding an aliquot to 0°C diethyl ether and filtering the resulting suspension. Both the reaction conditions (with and without catalytic nickel) were repeated twice, giving 9 data points per time point, which were averaged to give the data presented in Figure 2.2.

2.7 References

- (1) Ono, N. *The Nitro Group in Organic Synthesis*; Wiley-VCH: New York, 2001.
- (2) Booth, G. Nitro Compounds, Aromatic. In *Ullmann's Encyclopedia of Industrial Chemistry*; Wiley-VCH: New York, 2012; p 301.
- (3) Tong, S.; Xu, Z.; Mamboury, M.; Wang, Q.; Zhu, J. Aqueous Titanium Trichloride Promoted Reductive Cyclization of *o*-Nitrostyrenes to Indoles: Development and Application to the Synthesis of Rizatriptan and Aspidospermidine. *Angew. Chem. Int. Ed.* **2015**, *54* (40), 11809–11812. <https://doi.org/10.1002/anie.201505713>.
- (4) Gui, J.; Pan, C.-M.; Jin, Y.; Qin, T.; Lo, J. C.; Lee, B. J.; Spergel, S. H.; Mertzman, M. E.; Pitts, W. J.; La Cruz, T. E.; Schmidt, M. A.; Darvatkar, N.; Natarajan, S. R.; Baran, P. S. Practical Olefin Hydroamination with Nitroarenes. *Science* **2015**, *348* (6237), 886–891. <https://doi.org/10.1126/science.aab0245>.
- (5) Rauser, M.; Ascheberg, C.; Niggemann, M. Electrophilic Amination with Nitroarenes. *Angew. Chem. Int. Ed.* **2017**, *56* (38), 11570–11574. <https://doi.org/10.1002/anie.201705356>.
- (6) Zhu, K.; Shaver, M. P.; Thomas, S. P. Chemoselective Nitro Reduction and Hydroamination Using a Single Iron Catalyst. *Chem. Sci.* **2016**, *7* (5), 3031–3035. <https://doi.org/10.1039/C5SC04471E>.
- (7) Shen, N.; Cheung, C. W.; Ma, J.-A. Direct Amide Synthesis via Ni-Mediated Aminocarbonylation of Arylboronic Acids with CO and Nitroarenes. *Chem. Commun.* **2019**, *55* (91), 13709–13712. <https://doi.org/10.1039/C9CC06638A>.

-
- (8) Wang, S.-P.; Cheung, C. W.; Ma, J.-A. Direct Amidation of Carboxylic Acids with Nitroarenes. *J. Org. Chem.* **2019**, *84* (21), 13922–13934. <https://doi.org/10.1021/acs.joc.9b02068>.
- (9) Nykaza, T. V.; Li, G.; Yang, J.; Luzung, M. R.; Radosevich, A. T. $P^{III}/P^V=O$ Catalyzed Cascade Synthesis of N-Functionalized Azaheterocycles. *Angew. Chem. Int. Ed.* **2020**, *59* (11), 4505–4510. <https://doi.org/10.1002/anie.201914851>.
- (10) Roscales, S.; Csáky, A. G. Transition-Metal-Free Three-Component Synthesis of Tertiary Aryl Amines from Nitro Compounds, Boronic Acids, and Trialkyl Phosphites. *Adv. Synth. Catal.* **2020**, *362* (1), 111–117. <https://doi.org/10.1002/adsc.201901009>.
- (11) Cheung, C. W.; Ploeger, M. L.; Hu, X. Direct Amidation of Esters with Nitroarenes. *Nat. Commun.* **2017**, *8*, 14878. <https://doi.org/10.1038/ncomms14878>.
- (12) Cheung, C. W.; Ploeger, M. L.; Hu, X. Nickel-Catalyzed Reductive Transamidation of Secondary Amides with Nitroarenes. *ACS Catal.* **2017**, *7* (10), 7092–7096. <https://doi.org/10.1021/acscatal.7b02859>.
- (13) Cheung, C. W.; Ploeger, M. L.; Hu, X. Amide Synthesis via Nickel-Catalysed Reductive Aminocarbonylation of Aryl Halides with Nitroarenes. *Chem. Sci.* **2018**, *9* (3), 655–659. <https://doi.org/10.1039/C7SC03950F>.
- (14) Cheung, C. W.; Ma, J.-A.; Hu, X. Manganese-Mediated Reductive Transamidation of Tertiary Amides with Nitroarenes. *J. Am. Chem. Soc.* **2018**, *140* (22), 6789–6792. <https://doi.org/10.1021/jacs.8b03739>.
- (15) Cheung, C. W.; Shen, N.; Wang, S.-P.; Ullah, A.; Hu, X.; Ma, J.-A. Manganese-Mediated Reductive Amidation of Esters with Nitroarenes. *Org. Chem. Front.* **2019**, *6* (6), 756–761. <https://doi.org/10.1039/C8QO01405A>.
- (16) Mahata, A.; Rai, R. K.; Choudhuri, I.; Singh, S. K.; Pathak, B. Direct vs. Indirect Pathway for Nitrobenzene Reduction Reaction on a Ni Catalyst Surface: A Density Functional Study. *Phys Chem Chem Phys* **2014**, *16* (47), 26365–26374. <https://doi.org/10.1039/C4CP04355C>.
- (17) Sakai, N.; Fujii, K.; Nabeshima, S.; Ikeda, R.; Konakahara, T. Highly Selective Conversion of Nitrobenzenes Using a Simple Reducing System Combined with a Trivalent Indium Salt and a Hydrosilane. *Chem. Commun.* **2010**, *46* (18), 3173. <https://doi.org/10.1039/c000383b>.
- (18) Gund, S. H.; Shelkar, R. S.; Nagarkar, J. M. An Efficient Catalyst-Free and Chemoselective Synthesis of Azobenzenes from Nitrobenzenes. *RSC Adv* **2014**, *4* (81), 42947–42951. <https://doi.org/10.1039/C4RA06027J>.
- (19) Liu, X.; Li, H.-Q.; Ye, S.; Liu, Y.-M.; He, H.-Y.; Cao, Y. Gold-Catalyzed Direct Hydrogenative Coupling of Nitroarenes To Synthesize Aromatic Azo Compounds. *Angew. Chem. Int. Ed.* **2014**, *53* (29), 7624–7628. <https://doi.org/10.1002/anie.201404543>.

-
- (20) Zhang, X.; Yao, J.; Ke, X. Tuning Catalytic Selectivity in Cascade Reactions by Light Irradiation. *Catal. Lett.* **2018**, *148* (4), 1124–1129. <https://doi.org/10.1007/s10562-018-2320-9>.
- (21) Johnson, Kenneth.; Degering, Ed. F. The Utilization of Aliphatic Nitro Compounds. (I) The Production of Amines and (II) The Production of Oximes. *J. Am. Chem. Soc.* **1939**, *61* (11), 3194–3195. <https://doi.org/10.1021/ja01266a061>.
- (22) Ohe, K.; Uemura, S. Sodium Arenetellurolate-Catalyzed Reduction of Nitroalkanes to Oximes. *Heteroat. Chem.* **1991**, *2* (4), 507–511. <https://doi.org/10.1002/hc.520020414>.
- (23) Rauser, M.; Eckert, R.; Gerbershagen, M.; Niggemann, M. Catalyst-Free Reductive Coupling of Aromatic and Aliphatic Nitro Compounds with Organohalides. *Angew. Chem. Int. Ed.* **2019**, *58* (20), 6713–6717. <https://doi.org/10.1002/anie.201814197>.
- (24) Otsuka, S.; Yoshida, T.; Tatsuno, Y. Isocyanide-Nickel(0) and -Palladium(0) Complexes Involving Unsaturated Ligands. *J. Am. Chem. Soc.* **1971**, *93* (24), 6462–6469. <https://doi.org/10.1021/ja00753a021>.
- (25) Berman, R. S.; Kochi, J. K. Kinetics and Mechanism of Oxygen Atom Transfer from Nitro Compounds Mediated by Nickel(0) Complexes. *Inorg. Chem.* **1980**, *19* (1), 248–254. <https://doi.org/10.1021/ic50203a050>.
- (26) Song, H.; Yang, Z.; Tung, C.-H.; Wang, W. Iron-Catalyzed Reductive Coupling of Nitroarenes with Olefins: Intermediate of Iron–Nitroso Complex. *ACS Catal.* **2020**, *10* (1), 276–281. <https://doi.org/10.1021/acscatal.9b03604>.
- (27) Schley, N. D.; Fu, G. C. Nickel-Catalyzed Negishi Arylations of Propargylic Bromides: A Mechanistic Investigation. *J. Am. Chem. Soc.* **2014**, *136* (47), 16588–16593. <https://doi.org/10.1021/ja508718m>.
- (28) Breitenfeld, J.; Ruiz, J.; Wodrich, M. D.; Hu, X. Bimetallic Oxidative Addition Involving Radical Intermediates in Nickel-Catalyzed Alkyl–Alkyl Kumada Coupling Reactions. *J. Am. Chem. Soc.* **2013**, *135* (32), 12004–12012. <https://doi.org/10.1021/ja4051923>.
- (29) Russell, G. A.; Yao, C.-F. Deoxygenation of Nitro and Nitrosoaromatics by Photolysis With t -BuHgI/KI. Regiochemistry of t -Butyl Radical Addition to Nitrosoaromatics [1]. *Heteroat. Chem.* **1993**, *4* (5), 433–444. <https://doi.org/10.1002/hc.520040505>.
- (30) Rossi, M. J.; McMillen, D. F.; Golden, D. M. Aliphatic Carbon-Hydrogen Bond Scission Processes in Diphenylmethane and 2-Benzyl- and 4-Benzylpyridine. The Heat of Formation of the Diphenylmethyl and α -Phenylethyl Radical in the Gas Phase. *J. Phys. Chem.* **1984**, *88* (21), 5031–5039. <https://doi.org/10.1021/j150665a048>.
- (31) Rumble, J. R., ed. Physical Constants of Organic Compounds. In *CRC Handbook of Chemistry and Physics, 100th Edition (Internet Version 2019)*; CRC press/Taylor&Francis, Boca Raton, FL; p Table 3, Entry 1015.

Chapter 3

Mechanism of Ni-catalyzed reductive amidation of unactivated esters with azobenzenes: experimental study

Part of the data were reproduced with permission from Ploeger, M.L.; Darù, A.; Harvey, J.N.; Hu, X. Reductive Cleavage of Azoarene as a Key step in Nickel-Catalyzed Amidation of Esters with Nitroarenes *ACS Catalysis*. 2020, 10, 2845-2854. Copyright 2020 American Chemical Society.

3.1 Introduction

Azobenzene and its derivatives have been heavily utilized as organic dyes¹ and recently they have been of growing interest for various applications in functional materials.^{2,3} For this reason, their synthesis has been an active field of research⁴ and they are now readily available from common functional groups, such as nitroarenes,^{5,6} or anilines.^{7,8} In addition, C-H activation methods may be employed to further functionalize the azoarenes after their synthesis.⁹

As a result of their ease of synthesis, azoarenes are now also of interest as synthetic intermediates. For example, they can be converted into triazoles by reaction with silyl azides,¹⁰ to benzimidazoles by reaction with methyl triflate¹¹ and to quinolones with allyl halides.¹²

Recently, we reported nickel catalyzed amidation of esters with nitroarenes.¹³ This type of chemistry was later successfully expanded to transamidation with nitroarenes.¹⁴ In chapter 2, initial mechanistic studies revealed the following reaction sequence: first, the nitroarene is converted to azoarene under the reductive conditions. The azoarene subsequently reductively couples with a carbonyl electrophile through nickel catalysis to form a metal amide, which is finally converted to the amide upon quenching the reaction.

These findings indicate that the nickel catalysts we used may be effective for further increase of the synthetic utility of azoarenes. However, the way the azoarenes react with esters under the influence of nickel catalysis is still poorly understood, hindering reaction design. A more thorough mechanistic model of the Ni-catalyzed reductive amidation of unactivated esters with azobenzenes (called azo-ester coupling from now) is therefore of interest. In this chapter, we further elucidate the mechanism, through kinetic studies, linear free energy relationships and stoichiometric studies, using para-substituted azoarenes and methyl decanoate as model substrates. The findings reported in this chapter were instrumental to inform detailed computational studies, which led to a comprehensive mechanistic model (see chapter 4).

3.2 In Situ ATR-IR monitoring

The reaction of azobenzene (**7**) and methyl decanoate (**1a**) under relevant reductive coupling conditions (Figure 3.1A) was chosen as the model reaction for the detailed mechanistic study, since it yields the product quantitatively.¹³ The reaction was monitored by in situ attenuated total reflection infrared (ATR-IR) (Figure 3.1B). As the reaction proceeded, signals of **1a** at

1145-1209 cm^{-1} and 1738 cm^{-1} decayed (labeled **1a** in Figure 3.1B). Meanwhile, two peaks at 1055 cm^{-1} and 1537 cm^{-1} grew, which were tentatively attributed to the Zn-amide product (**P**), which was previously identified as the end product of amidation before quenching with a proton source in the workup (see chapter 2). As the reaction gave the amide product quantitatively with respect to **1a**, the conversion of **1a** reflected the reaction progress well. The concentrations of **1a** was estimated by the intensity of the IR peak at 1735 cm^{-1} .

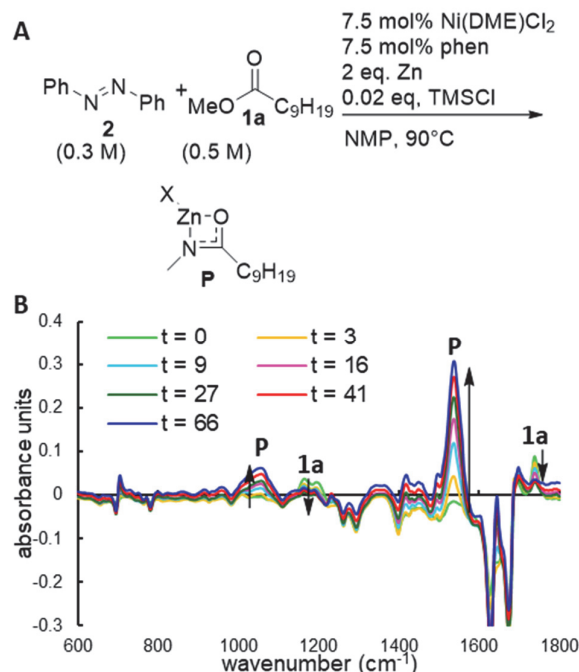


Figure 3.1: (A) Reaction scheme for Ni-catalyzed reductive coupling of azobenzene with **1a**. X = Cl or OMe. (B) Time-dependent IR spectra of the reaction mixture. The arrows indicate growth and decay of the assigned peaks. The indicated times are in minutes.

3.3 Kinetic studies

3.3.1 Standard conditions

Under standard conditions (Figure 3.1A), **1a** underwent a linear decay (Figure 3.2A). This result indicated that the reaction was zero order in both **1a** and azobenzene under these conditions. The reactions were conducted under different loadings of catalysts and a log/log plot of the reaction rate versus catalyst concentration (Figure 3.2B) indicated an order of about 1.5 in Ni catalyst. The rates varied with the stirring rates, which suggested some involvement of heterogeneous Zn species in the rate determining step (see the methods section for details).

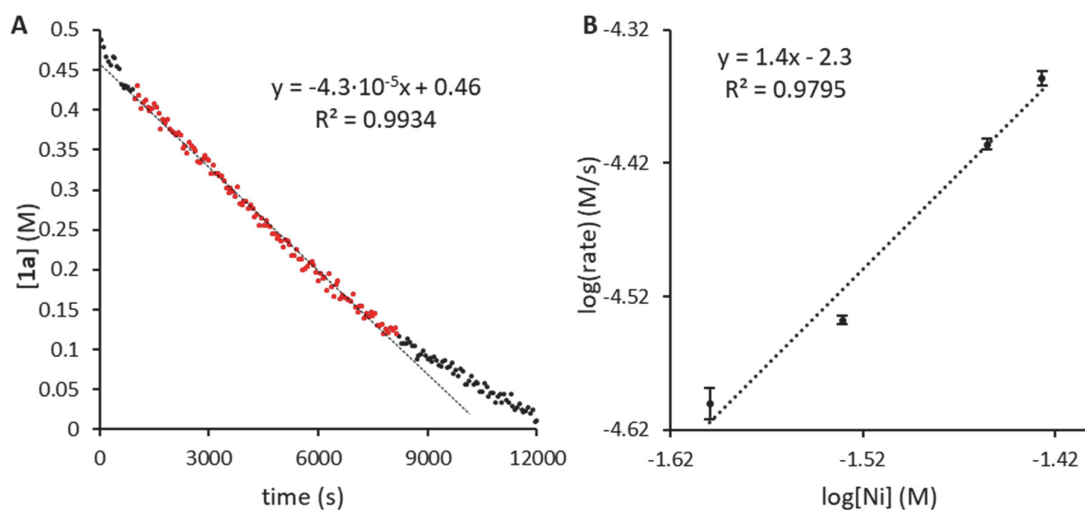


Figure 3.2: (A) A plot showing the decay of **1a** over the reaction time; conditions as in Figure 3.1A; Red dots indicate the data used for the linear regression to determine the rate of the reaction. (B) log/log plot of reaction rate versus the concentration of nickel catalyst. Values are averages over two runs. The error bars represent the standard error.

3.3.2 Influence of ZnCl_2

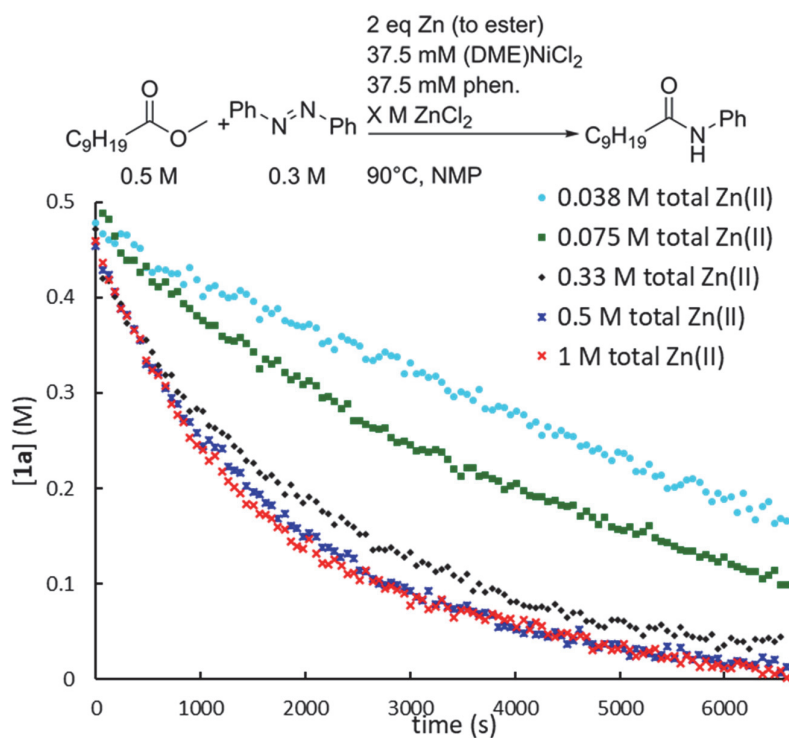


Figure 3.3: Influence of total ZnCl_2 concentration on the reaction rate. Conditions according to Figure 3.1A, with additional ZnCl_2 . The total Zn(II) concentration is estimated from the sum of added ZnCl_2 and Ni(DME)Cl_2 .

Since ZnCl_2 was generated *in situ* from oxidation of Zn by a Ni species in this reaction, its influence was then probed by adding external ZnCl_2 . An increase of the total concentration of ZnCl_2 (from both external and *in situ* sources) had two significant effects (Figure 3.3): (i) it accelerated the reaction; (ii) it changed the order of at least one of the substrates to non-zero so that the decay of **1a** was no longer linear when a significant amount of external ZnCl_2 was added. A saturation point was reached at a total ZnCl_2 concentration of 0.5M.

3.3.3 Kinetics at high $[\text{ZnCl}_2]$

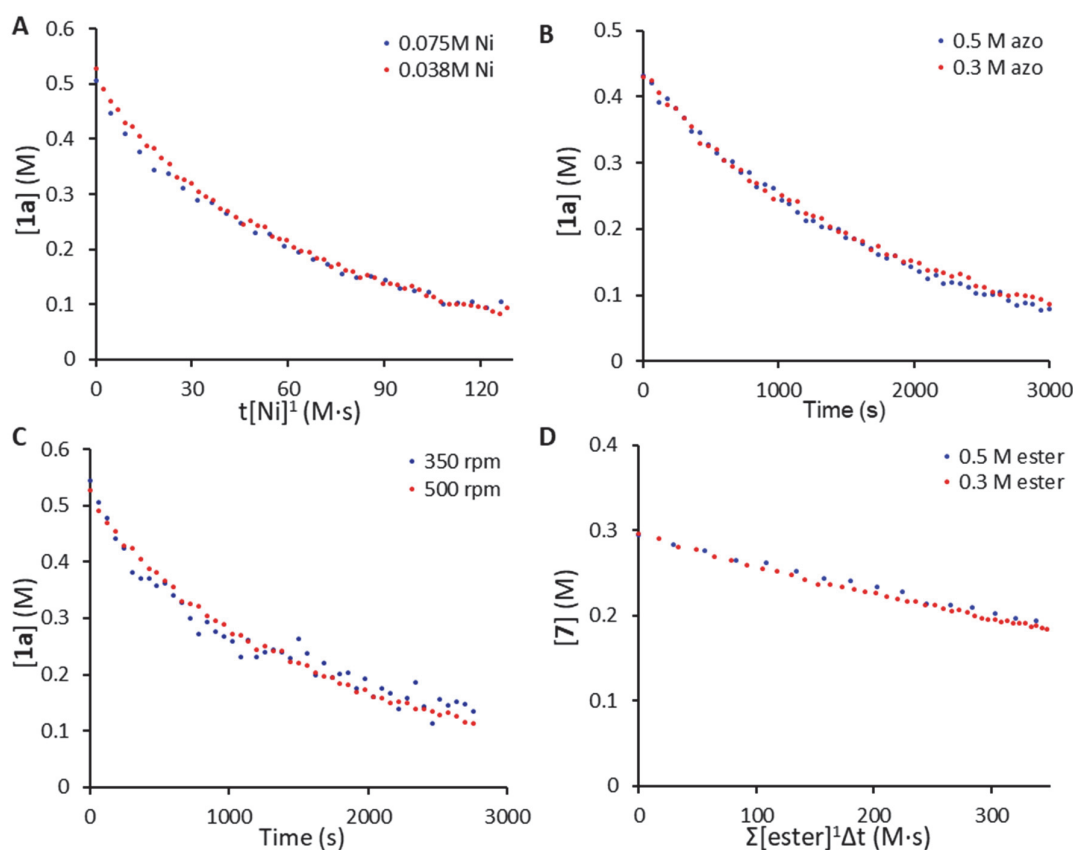


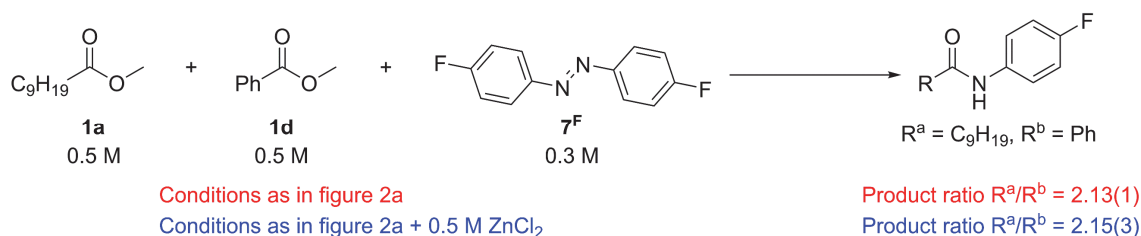
Figure 3.4: Kinetics at high total ZnCl_2 concentrations. General conditions: similar to Figure 3.1A, but with additional ZnCl_2 to reach saturation with total Zn(II) concentration of 0.5 M. (A) Overlaying VTNA plots at two different concentrations of Ni catalyst. The X axis is $t[\text{Ni}]$, where $[\text{Ni}]$ is the total concentration of nickel, as determined by the weight of added Ni(DME)Cl_2 . Overlap occurs only when the reaction is first order in nickel. (B) Overlaying VTNA plots at two different concentrations of **7** (azo). The X axis is time. Overlap occurs only if the reaction is zeroth order in **7**. (C) Overlaying reaction rate profiles at two different stirring rates. (D) Overlaying VTNA plots at different concentrations of **1a** (ester). The X axis is time multiplied by the approximate integral of $[\mathbf{1a}]$, where $[\mathbf{1a}]$ is the concentration of ester determined by FT-IR. Overlap occurs only if the reaction is first order in **1a**.

The kinetics of the reaction were then measured at high total ZnCl_2 concentrations, and analyzed by VTNA (Figure 3.4).^{15,16} Two sets of experimental data were sufficient to deduce the reaction order by VTNA. The overlaying graphs indicated that the reaction was first order in Ni catalyst and zero order in azobenzene (Figure 3.4A-B). The reaction rates were the same under different stirring rates (Figure 3.4C), suggesting that only homogenous species were involved in the rate determining step when significant external ZnCl_2 was added. This result also suggested the stirring-rate dependence of the rates under no external ZnCl_2 addition was due to ZnCl_2 formation from heterogeneous Zn particles. To determine the order in ester, the initial amount of **1a** was varied. The concentration of azobenzene was estimated by deducing the reacted amount from the initial concentration assuming a perfect reaction stoichiometry. VTNA plot showed that the reaction was first order in **1a** (Figure 3.4D) at high total ZnCl_2 concentrations.

3.3.4 Reason for rate law change

The observed change in rate law with added ZnCl_2 could be a result of relative acceleration of the rate determining step, which changes the resting state, or it could be due to activation of a different catalytic cycle that is not operative at low concentrations of ZnCl_2 . To distinguish between the two scenarios, a competition experiment was conducted with and without external ZnCl_2 addition. An equal amount of **1a** and an aryl ester, methyl benzoate (**1d**), was treated with 1,2-bis(4-fluorophenyl)diazene (**7^F**), producing a mixture of alkyl and aryl amides (Scheme 3.1). Under standard conditions (shown in Figure 1A), the ratio of alkyl to aryl amide was about 2.1:1. Addition of external ZnCl_2 (to reach saturation with a total concentration of 0.5 M) did not change the outcome of the coupling. This result suggests that addition of ZnCl_2 did not change the nature of the intermediate that reacts with ester.¹⁷ As this species also involves activated azoarene (vide infra), the catalytic cycle should look the same under both conditions. Thus, the conditions can be conveniently manipulated to study different parts of the catalytic cycle experimentally.

Scheme 3.1: A competition experiment conducted with and without external ZnCl_2 . Product ratios are averaged over two runs. Reported error is the standard error.



3.4 Hammett plots

The rates of the reactions of **1a** with a series of azoarenes bearing different substituents at para-positions were measured at a high total ZnCl_2 concentration. A Hammett plot based on the observed rate constant is shown in Figure 3.5A. The reaction rate depends strongly on the nature of the para-substituent in a Volcano-like correlation. On the left side of the Volcano (NMe_2 , OMe , and Me), the more electron-donating substituents slow down the reaction, but on the right side (Me , F , H , and OCF_3), the more electron-withdrawing groups also slow down the reaction. This result suggests that two different rate laws or mechanisms apply: one for azoarenes with a strongly electron-donating group at the para-position, and the other one for other azoarenes (*i.e.* with Me , H , or electron-withdrawing para-substituents such as F and OCF_3). The majority of azoarenes substrates in the Ni-catalyzed reductive amidation belong to the latter category.

The choice of Hammett parameter on the x-axis is based on the quality of correlation of the 4 least electron-rich azoarenes: the coefficient of determination (R^2) improved from 0.945 to 0.987 when σ^+ was employed as Hammett parameter, rather than σ . The constant σ^+ was designed to reflect electron-donating resonance effects that are poorly represented in the Hammett constant based on benzoic acid derivative pKas. It is derived from the solvolysis of t-chumyl chloride derivatives.¹⁸ Therefore, it is particularly applicable for reactions that build up positive charge in the benzylic position para to the functional group. The good correlation with Hammett parameter σ^+ is therefore indicative of charge depletion from the nitrogen center in the transition state of the rate determining step.

The hammett plot shows that the azoarene is already activated by the nickel complex before the rate determining step. The strong influence of the identity of azoarene on the rate – the rate constant for the fastest measured azoarene is more than 4 times faster than the slowest measured one – would not be possible if the azobenzene got involved in the reaction after the rate determining step. As the rate is independent of the concentration of azoarene under these conditions (*vide supra*), the azobenzene must be activated by nickel before the rate determining step, either in an irreversible fashion, or in an equilibrium that is fully pushed towards activation under the reaction conditions.

The relative reaction rate of azoarenes sitting at the right side of the Volcano plot in Figure 3.5A was then determined in a set of competition experiments. An equal amount of azobenzene and another azoarene was reacted with **1a** to give a mixture of amide products originating from two different azoarene partners. The ratio of the products correlates to the relative reaction rates.

A Hammett plot of the relative rate determined in this manner is shown in Figure 3.5B. In this case, a reverse trend was observed compared to Figure 3.5A, with the more electron-withdrawing substituent leading to a higher relative reaction rate. The selectivity determining step must therefore be different from the rate determining step.

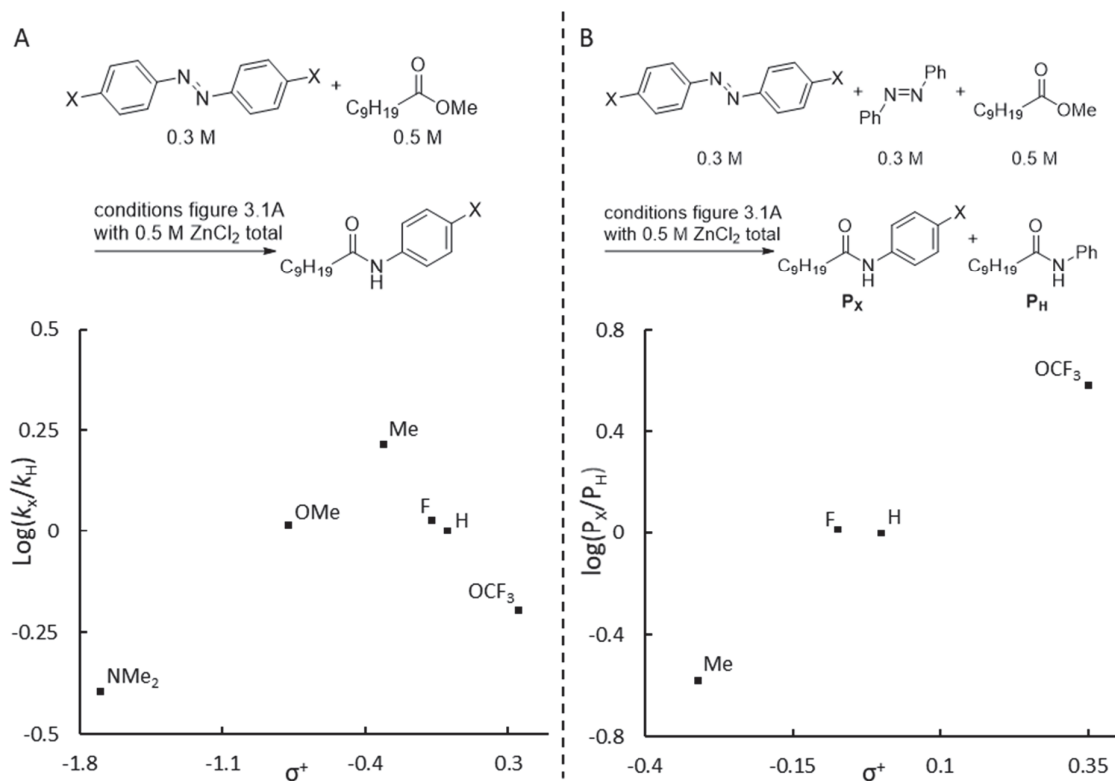


Figure 3.5: Hammett plots. (A) A plot using observed reaction rate constants; (B) A plot using relative reaction rate from competition experiments, determined by the product ratio at the end of the reaction. Conditions are similar to those in Figure 3.1A with additional ZnCl₂ to reach a total [Zn(II)] of 0.5 M.

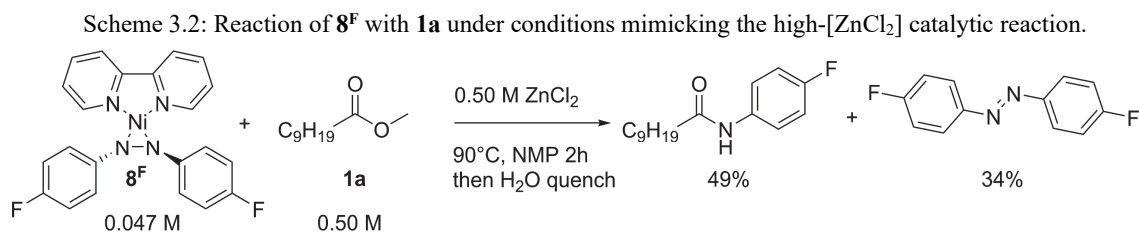
3.5 Search for Nickel-azoarene species

As the Hammett studies revealed that azoarene is activated by nickel before reaction with ester, we sought to identify this intermediate. A reaction between **7^F**, phenanthroline, (DME)NiCl₂ and Zn in NMP at 90°C did consume the azoarene if a 2:1 Ni:azoarene ratio was employed, but in ¹⁹F NMR, only a broad hump could be observed, alongside aniline, which may have formed due to adventitious water. Unfortunately, any attempts to isolate an intermediate from this product mixture through crystallization failed, as did further characterization

attempts with HRMS. Therefore, we sought to explore the reactivity in a more controlled manner.

3.5.1 Reactivity of a Ni(0)-azoarene adduct

Given that the coupling is conducted under strongly reducing conditions in the presence of an excess amount of Zn, a Ni(0)-azoarene species is a likely Ni-bound intermediate. Several such species with varying supporting ligands were reported in the literature,^{19–22} including one supported by a bipyridine ligand.²³ We tried to prepare an analogous species supported by phenanthroline, the preferred ligand for the amidation, but our attempts were unsuccessful. Recognizing that 2,2'-bipyridine (bipy) was also a viable ligand for the amidation with just a slightly lower yield than phen for a test reaction (94% versus 100%),¹³ we decided to employ a [Ni(0)(azoarene)(bipy)] complex as the model intermediate. To enable product identification by ¹⁹F NMR, we prepared the complex containing a para-F substituted azobenzene (**8^F**). Under conditions mimicking those of the catalytic reaction (e.g., high [ZnCl₂]) but in absence of free azobenzene and solid zinc, the amidation product was obtained in 49% yield (based on Ni; Scheme 3.2), in addition to some free azoarene **7^F** (34 %), indicating **8^F** does react with ester and could indeed be an intermediate on the catalytic cycle.



When **8^F** was heated in the presence of one equivalent of ZnCl₂, the complex quickly decayed (Figure 3.6A). The decomposition already starts before the target temperature of 90°C is reached and is complete in 270 seconds. Heating the NMR sample to 60°C, rather than 90°C slows down the reaction, so that enough data points can be collected to compare different conditions. Figure 3.6B shows that the reaction is sped up in the presence of a higher concentration of ZnCl₂. Under both conditions, the observed reaction products were the same. In ¹⁹F NMR, only **2^F** could be observed in approximately 50% yield (Figure 3.6C). ¹H NMR shows peaks in the paramagnetic range (Figure 3.6D). Any attempt to isolate the paramagnetic product of further characterize it with high resolution mass spectrometry (HRMS) failed. However, addition

of water to the product mixture generated aniline, as observed by ^{19}F NMR, indicating a cleavage of the azoarene may be part of the reactivity.

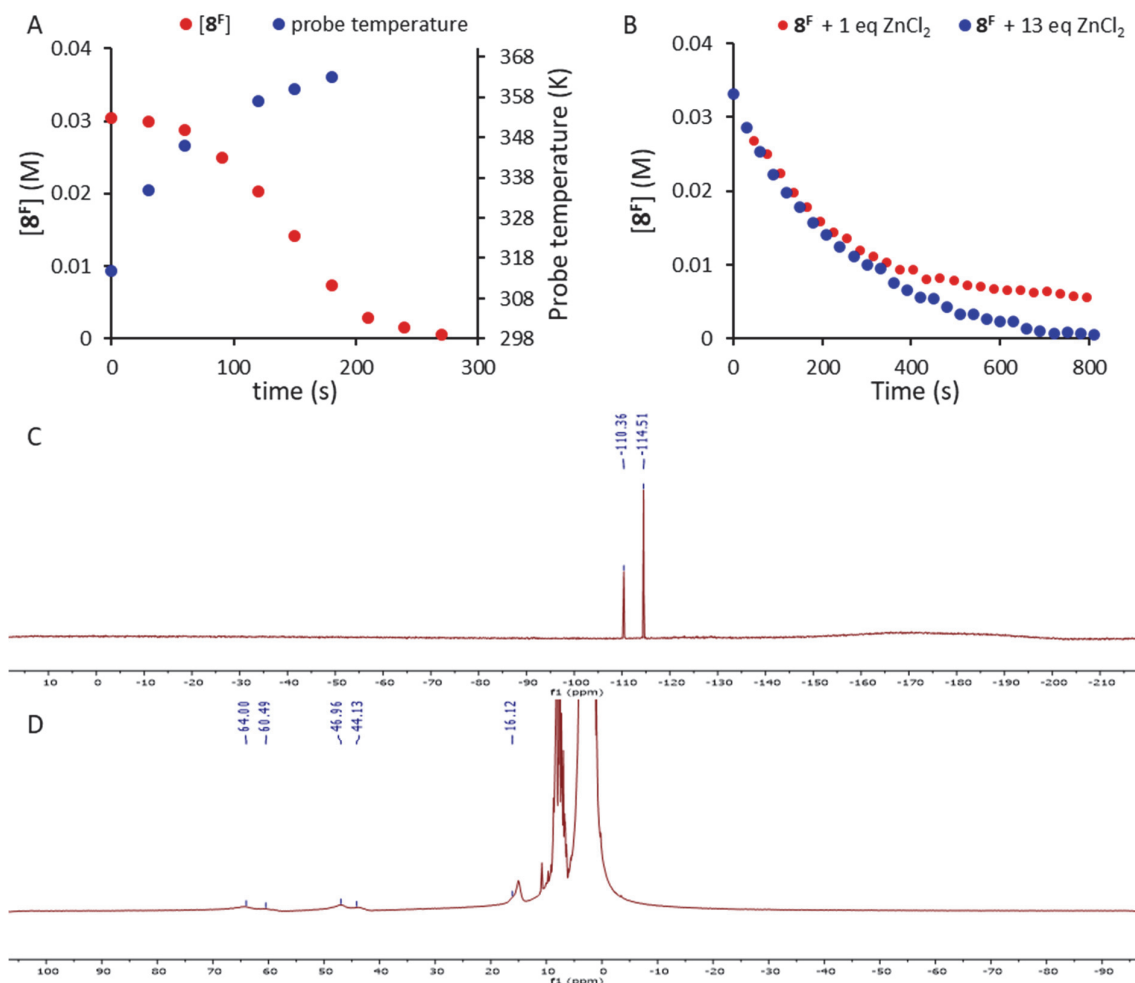


Figure 3.6: (A) *in situ* monitoring of the concentration of 8^{F} (left axis) while heating to 90°C. The probe temperature was noted at every measuring point (right axis). (B) Decay of 8^{F} at 60°C with different concentrations of ZnCl_2 . (C) ^{19}F NMR at the end of a decay reaction. (D) wide range ^1H NMR at the end of a decay reaction.

3.6 Discussion of decay pathway for 8^{F}

3.6.1 Involvement in catalytic cycle

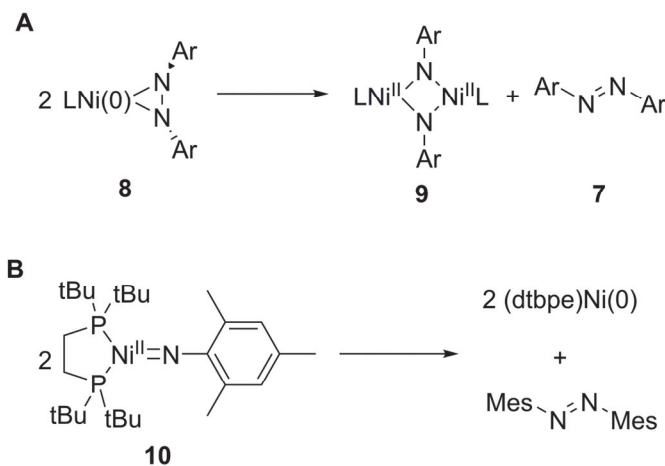
A clear comparison of the decay data with catalytic data is difficult because (i) the decay rate is very poorly defined for the reaction at 90°C; (ii) a different azoarene is used in the kinetic measurements for low- $[\text{ZnCl}_2]$ conditions; and (iii) a different ligand is used for the decay study than for kinetic measurements for both conditions. Despite these problems, rough estimates of

relative rates could still be useful, as it may help to determine if the observed reactivity could feasibly be part of the catalytic pathway, or should be considered deleterious to the catalyst.

Under low-[ZnCl₂] conditions with 0.029 M Ni, the TOF is 10⁻³ M **1a** s⁻¹ M⁻¹ catalyst (see figure 3.2B and experimental section). This translates to one turnover occurring every 1000 seconds. As **3^F** is fully decomposed within 270 seconds with a similar starting concentration for nickel, with part of the reactivity happening at less than 90°C, the decomposition should be faster than the rate determining step for these conditions. Under high-[ZnCl₂] conditions, the TOF is dependent on [**1a**]. at 0.3 M **1a** (40% conversion), the TOF for the reaction with **7^F** is 5·10⁻³ M **1a** s⁻¹ M⁻¹ catalyst (data from Hammett plot, see experimental section), which translates to one turnover occurring every 200 seconds, giving the same order of magnitude for the rate as decay of **8^F**. Overall, it seems the decay reaction is too fast in relation to catalysis to be a deleterious pathway, given the high yields obtained. Hence, the decay reactivity is likely a part of the catalytic cycle.

3.6.2 Proposed decay product

Scheme 3.3: (A) Proposed activation pathway for **8**. (B) Formation of azoarene from nickel(II) imide as reported by Hillhouse.



Scheme 3.3A describes a simplified activation pathway of a Ni(0)-azobenzene intermediate, neglecting the promotion of ZnCl₂ for simplicity. Dimerization of two molecules of Ni(0)-azobenzene species (**8**) followed by dissociation of a diazoarene gives a bridging Ni₂(NAr)₂ intermediate (**9**) which further reacts with ester to give the amide. Note that in the decay reactions of **8^F**, as well as in the stoichiometric reaction of **8^F** with **1a**, free azoarene **7^F** was also obtained

as a product, consistent with the proposed pathway. A similar dimerization pathway was proposed by Tonks and co-workers for the formation of a $\text{Ti}_2(\text{NAr})_2$ intermediate in the catalytic cycle of pyrrole synthesis from alkynes and azobenzene.^{24,25} An analogous reaction was observed between two Ta-azoarene complexes to give two Ta=NAr species.²⁶ In these reactions the 4-e reductive cleavage of azoarene is balanced by two 2-e oxidations of each metal center. This type of reactivity is also reported for iron,²⁷ silicon,²⁸ and aluminium.²⁹

For nickel, the cleavage of azobenzene has not been reported to the best of our knowledge, although Tonks recently reported the N=N cleavage of benzo[c]cinnoline by a Ni_2Ti complex.³⁰ The reverse reaction, i.e. the formation of an azoarene from two Ni=NAr moieties, has been reported by Hillhouse and co-workers: they showed that a diphosphine-ligated terminal nickel imide complex $(\text{dtbpe})\text{Ni}=\text{NMes}$ (**10**, dtbpe = 1,2-bis-(di-tert-butylphosphino)ethane, Mes = 2,4,6-trimethylphenyl) eliminated an azoarene at 80°C (scheme 3.3B).³¹ This example suggests the reverse reaction, the 4-electron reductive cleavage of an azoarene on Ni (as in Scheme 4A), is possible, given the appropriate ligand environment and reaction conditions (e.g., ZnCl_2 promotion). The dimeric form of **9** seems more appropriate for the ligands used in this study as opposed to the monomeric form of **10**, since Uyeda has published a nickel imide dimer supported by bipy, with a considerable amount of steric bulk around the imide.³²

3.7 Conclusions

From the experiments described in this chapter, several key features of the mechanism for the azobenzene-ester coupling reaction can be derived. (i) ZnCl_2 plays a key role in the reaction, accelerating the reaction and changing the rate law. The rate law change is due to a shift of the rate determining step, rather than a change in mechanism. (ii) Under the extreme conditions of high- and low- $[\text{ZnCl}_2]$, the reaction is zero order in both substrates, and first order in ester and zero order in azoarene, respectively. The order in nickel also changes from about 1.5 to 1 when excess ZnCl_2 is added to the reaction mixture. (iii) The azoarene must be activated by nickel before it reacts with ester. A reaction sequence where the ester undergoes oxidative addition to nickel followed by reaction with azoarene can therefore be excluded. (iv) A nickel(0) azoarene complex reacts in the presence of ZnCl_2 , likely involving the cleavage of the N=N bond. The rate with which this transformation occurs relative to the catalytic reaction rate suggests this reactivity is part of the catalytic cycle.

While these findings are not enough to postulate a catalytic cycle on their own, they provide useful input to computational study which is described in chapter 4.

3.8 Experimental

3.8.1 General experimental methods

All reactions were set up and performed under inert nitrogen atmosphere using standard glove box and Schlenk techniques. Anhydrous NMP stored over molecular sieves was purchased from Acros and stored in a glove box. The other solvents were purified using a two column solid-state purification system (Innovative Technology, NJ, USA) and transferred to the glovebox without exposure to air. Azobenzene, (DME)NiCl₂, 1,10-phenanthroline, trimethylsilylchloride and both methyl esters were purchased from commercial suppliers and used without further purification. Para-substituted azoarenes were prepared by oxidation of para-substituted anilines with air and copper(I) catalysis (OMe, Me, F, OCF₃)⁸ or DBU/NCS (NMe₂).⁷ ATR-IR measurements for *in situ* kinetics were performed with an IN350-T probe on a Bruker Vertex 80 spectrometer. NMR spectra were recorded on a Bruker Avance 400 Spectrometer. ¹H and ¹³C{¹H} chemical shifts were referenced internally to residual solvent signals. Quantitative ¹⁹F{¹H} NMR experiments were performed with a 30 degree pulse. Chemical shift values were referenced against fluorobenzene as internal standard using the value measured in DMF (-114.51 ppm).³³ Elemental analyses were performed on a Carlo Erba EA 1110 CHN instrument at EPFL.

3.8.2 General remarks of kinetic measurements

Concentration of methyl decanoate was measured with ATR-IR, using an IN350-T probe on a Bruker Vertex 80 spectrometer. Reactions were set up by mixing zinc (261 mg, 4 mmol), the appropriate amount of (DME)NiCl₂ and phenanthroline, 3.2 mL NMP and TMSCl (4.3 mg, 0.04 mmol) in an oven dried 2-neck Schlenk flask for 10-15 minutes in the glove box. During this time, the mixture turned from dark blue to black. Then, the appropriate amount of azoarene and (if required) ZnCl₂ were added. The Schlenk flask was taken out of the glove box and connected to a N₂ line. Under a nitrogen flow, a septum pierced with the infrared probe was installed to the main neck and a second septum was installed on the smaller neck (see Figure 3.7

for setup). The mixture was then submerged in a 90°C oil bath. After stirring for 10-15 minutes at this temperature, the infrared background was measured, and the periodic infrared monitoring was started. Within one minute of starting the monitoring, 0.80 mL of a NMP solution of methyldecanoate, which was prepared in the glove box, was added, after which the integral of the peak at 1742 cm^{-1} (see Figure 3.1B) was measured periodically. The integral was measured between 1716 and 1759 cm^{-1} with a baseline drawn from the average value between 610 and 628 cm^{-1} to the average value between 1777 and 1821 cm^{-1} . From the integral, the concentration of ester was obtained by multiplying by 0.254. This conversion factor was obtained by a calibration curve ranging from 0.12 to 0.48 M ester in NMP at 90°C.

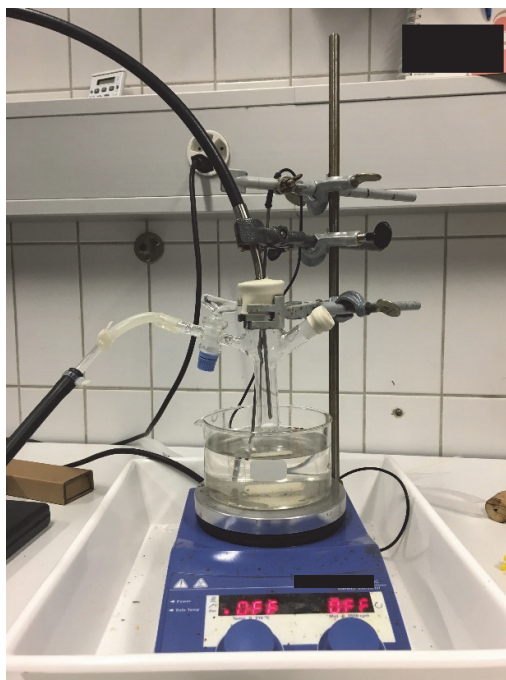


Figure 3.7: Picture of the setup used for kinetic measurements by IR. On the left side is the nitrogen line. The IR-probe connected to the Vortex 80 spectrometer is at the top and the septum through which the ester solution is added is at the right.

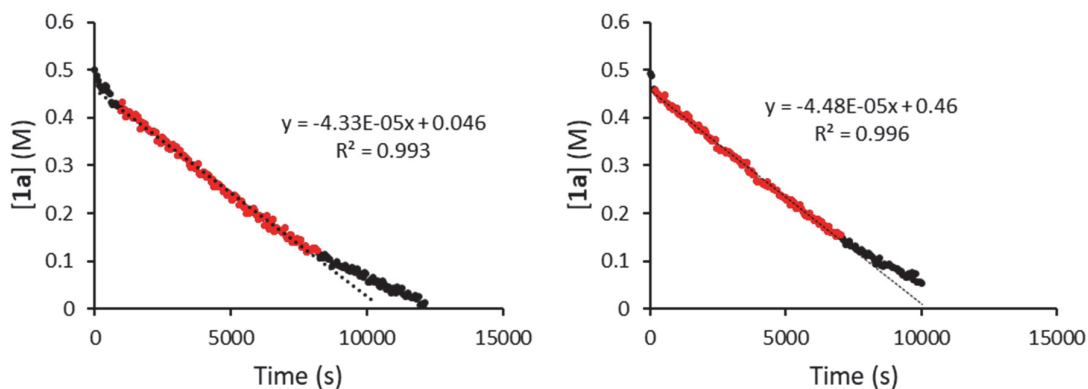


Figure 3.8: Reaction traces of FTIR-followed azobenzene-ester coupling with 0.037 M Ni-cat. Black points are the whole data set; the red points were used to obtain the slope, which was used as data point for Figure 3.2B.

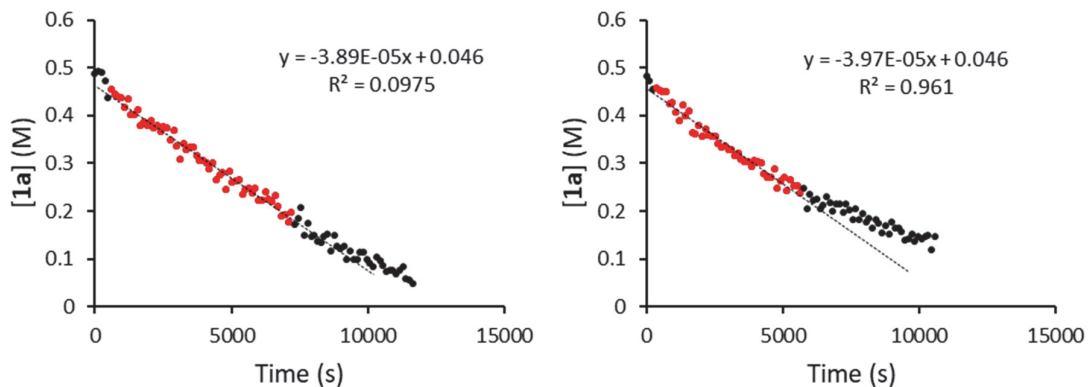


Figure 3.9: Reaction traces of FTIR-followed azobenzene-ester coupling with 0.035 M Ni-cat. Black points are the whole data set; the red points were used to obtain the slope, which was used as data point for Figure 3.2B.

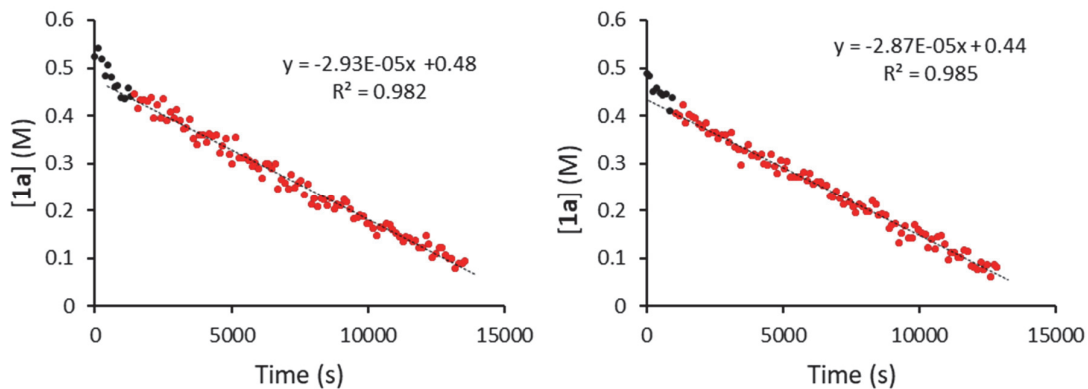


Figure 3.10: Reaction traces of FTIR-followed azobenzene-ester coupling with 0.035 M Ni-cat. Black points are the whole data set; the red points were used to obtain the slope, which was used as data point for Figure 3.2B.

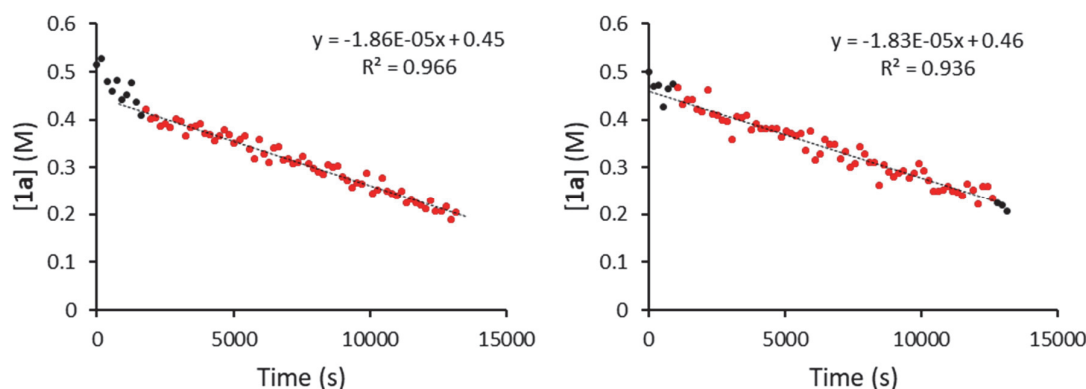


Figure 3.10: Reaction traces of FTIR-followed azobenzene-ester coupling with 0.037 M Ni-cat. Black points are the whole data set; the red points were used to obtain the slope, which was used as data point for Figure 3.2B.

3.8.3 Stirring rate influence under low-[ZnCl₂] conditions

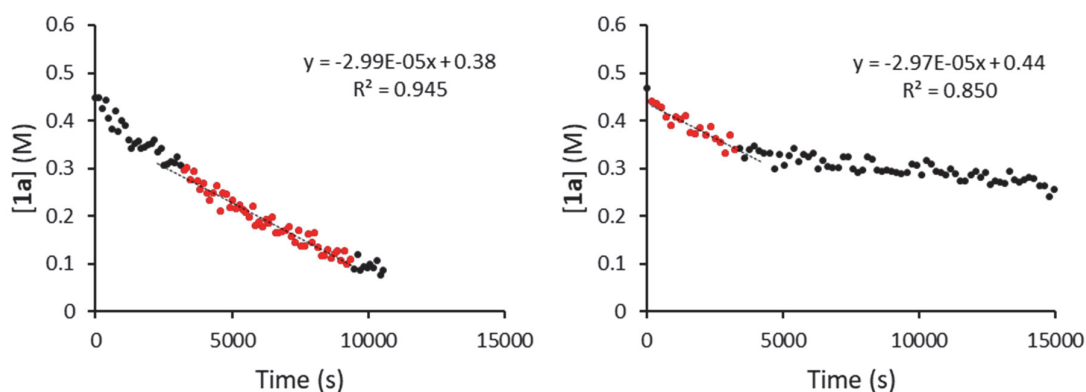


Figure 3.11: Reaction traces of FTIR-followed azobenzene-ester coupling under standard conditions, but at stirring rate of 350 rpm. For 500 rpm data, the reaction traces of Figure 3.8 were used. Note that the quality of fitting is not high; moreover, data reproducibility at the same stirring rate is not high. The data shown here are for indication purpose only. The conversion rate of ester at a stirring rate of 500 rpm was 4.41(8) 10⁻⁵ M s⁻¹, and it decreased to 2.98(1) 10⁻⁵ M s⁻¹ at a stirring rate of 350 rpm. Nevertheless, all data show the dependence of the reaction in stirring rate is significant.

3.8.4 Competition between an aromatic ester and an aliphatic ester

A NMP stock solution was prepared in the glove box in a 1 mL volumetric flask of 1,2-bis(4-fluorophenyl)diazene (**7^F** 161 mg, 0.74 mmol), methyldecanoate (231 mg, 1.24 mmol) and methyl benzoate (165 mg, 1.21 mmol). Four (4) reaction mixtures were set up by adding Zn (0.5 mmol), Ni(DME)Cl₂ (0.019 mmol), 1,10-phenanthroline (0.019 mmol), 0.10 ml NMP and 2 μ L

trimethylsilylchloride to oven dried scintillation vials. After stirring for a few minutes, the mixtures turned black. ZnCl_2 (0.23 mmol) was then added to two of the vials. Finally, 0.40 ml of the stock solution was added to all four mixtures and they were set to stir on a 90°C heating plate for 15 hours. After cooling down, 3 mL water and 3 ml ethyl acetate were added to each of the vials. After shaking the mixtures and settling of the resulting emulsion, 0.5 mL of the top layer was transferred to NMR tubes equipped with DMSO-d_6 capillaries, to measure Fluorine NMR (figure 3.12).

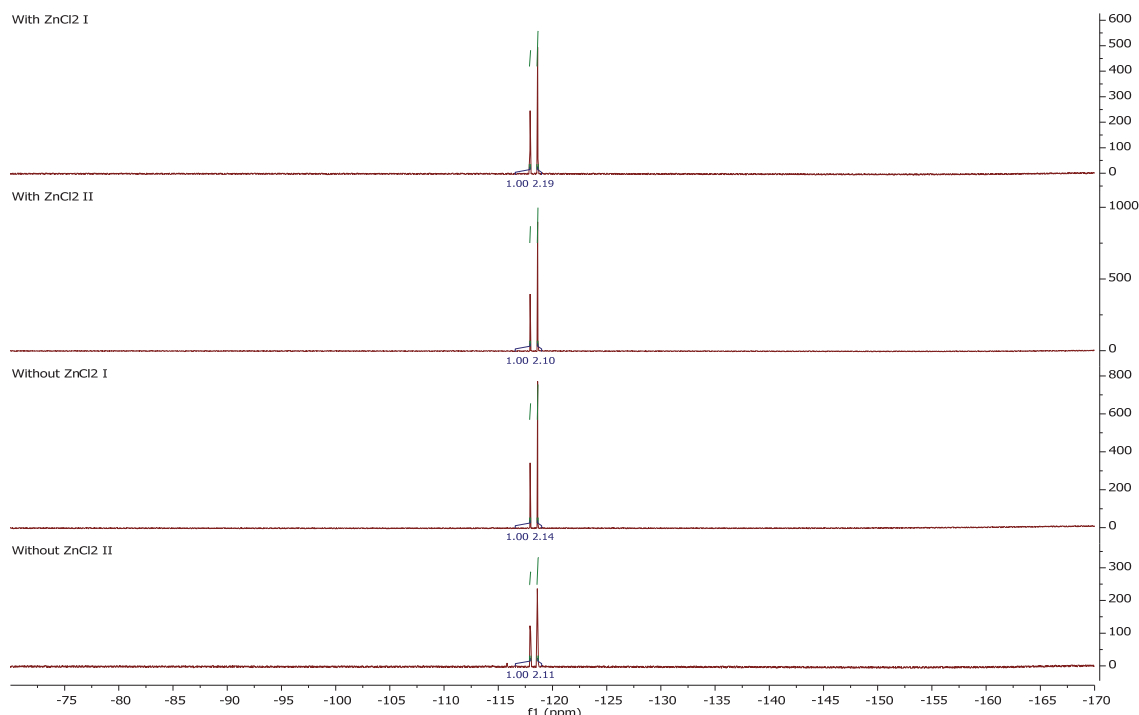


Figure 3.12: ^{19}F NMR spectra of the crude reaction mixtures for competition methyl decanoate and methyl benzoate in reaction with 7^{F}

3.8.5 Reaction rate Hammett study

The general procedure for infrared kinetic measurements was followed with 33.0 mg $(\text{DME})\text{NiCl}_2$ (0.15 mmol), 27.0 mg phenanthroline (0.15 mmol), 1.2 mmol of the appropriate azoarene, 252 mg ZnCl_2 (1.85 mmol). The ester solution was made in a 1 mL volumetric flask with 466 mg methyl decanoate (2.5 mmol). From the resulting reaction trace based on [ester], a straight line was generated by multiplying the time values on the x-axis with $[\text{Ni}]$ and with a Riemann sum approximation of the integral of [ester]. The slope of this straight line is taken as

the rate constant, which was used for generation of the Hammett plot depicted in Figure 3.5A. The raw and processed reaction traces are depicted in Figures 3.13-3.18.

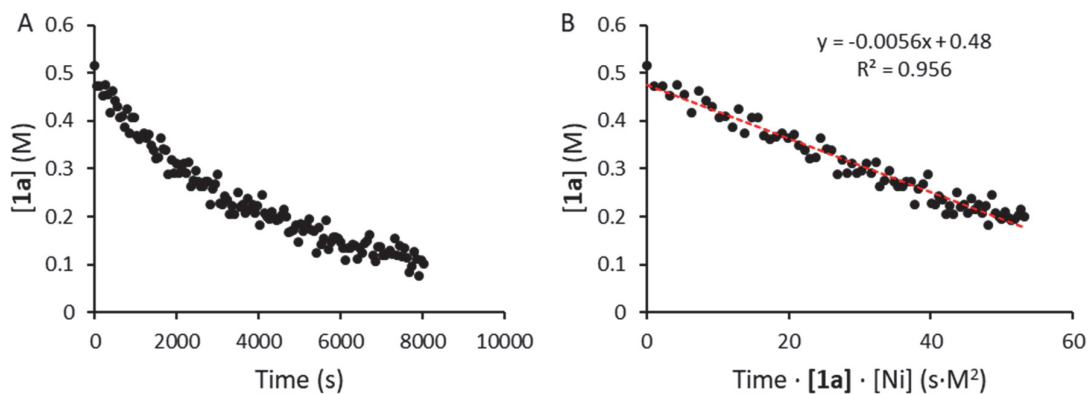


Figure 3.13: Raw (A) and processed (B) reaction trace for 1,2-bis(4-(dimethylamino)phenyl)diazene.

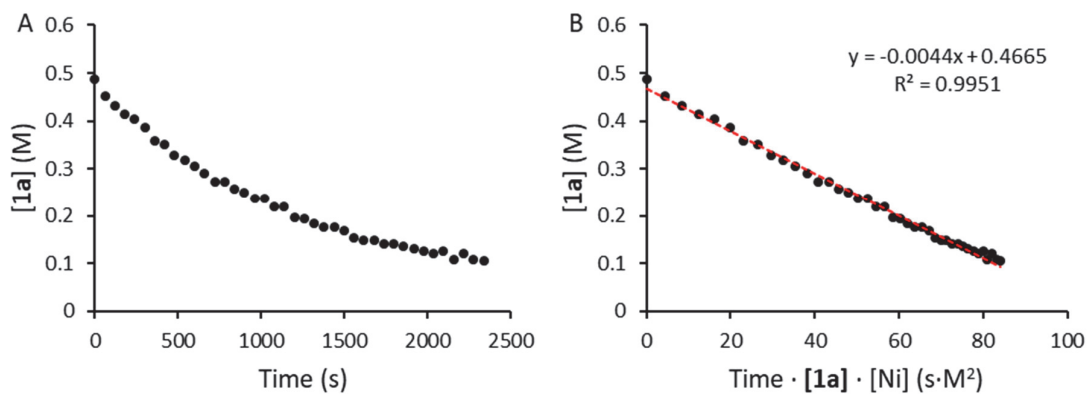


Figure 3.14: Raw (A) and processed (B) reaction trace for 1,2-bis(4-methoxyphenyl)diazene.

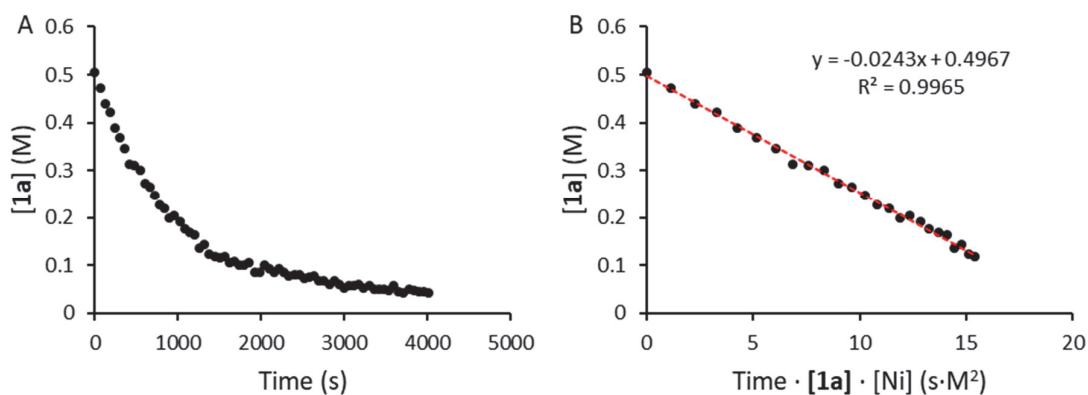


Figure 3.15: Raw (A) and processed (B) reaction trace for 1,2-bis(4-methylphenyl)diazene.

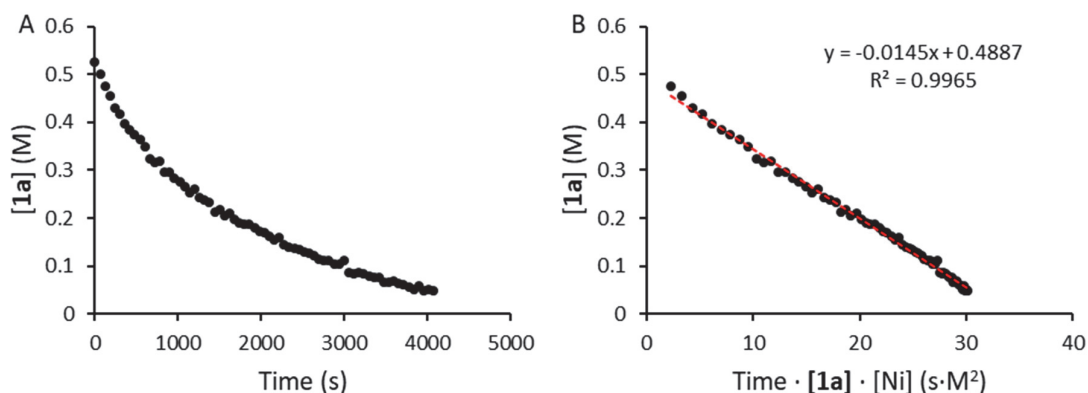


Figure 3.16 Raw (A) and processed (B) reaction trace for 1,2-bis(4-fluorophenyl)diazene.

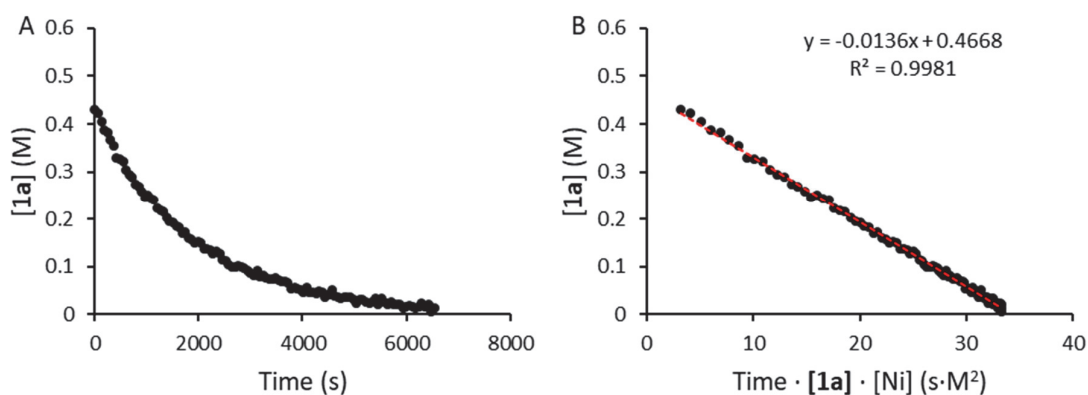


Figure 3.17: Raw (A) and processed (B) reaction trace for azobenzene

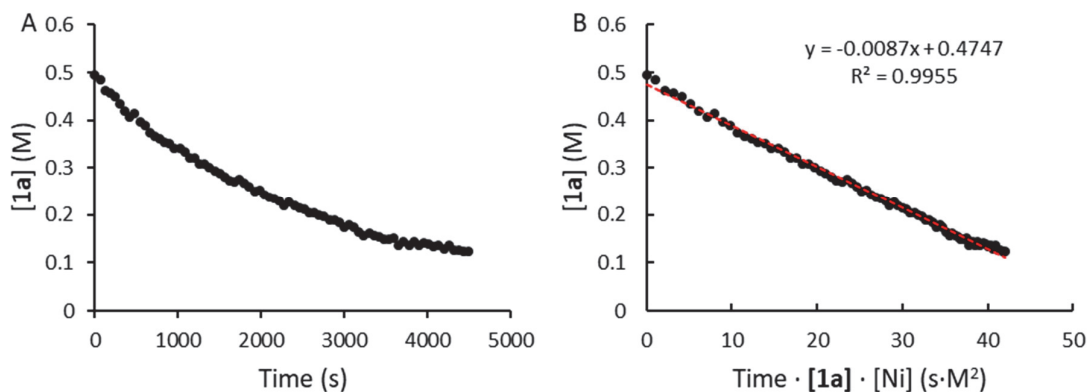


Figure 3.18: Raw (A) and processed (B) reaction trace for 1,2-bis(4-trifluoromethoxy)phenyl)diazene.

3.8.6 Competition Hammett study

A stock solution of azobenzene (150 mg, 0.823 mmol) and methyl decanoate (316 mg, 1.70 mmol) in NMP was prepared in a 2 mL volumetric flask. Zn (1 mmol), Ni(DME)Cl₂ (0.0375 mmol), 1,10-phenanthroline (0.0375 mmol), 0.40 mL NMP and 2 μ L trimethylsilylchloride were

added to 3 oven dried scintillation vials in the glove box. Stirred for a few minutes, which turned the mixtures from blue to black. Subsequently, ZnCl_2 (0.46 mmol), the appropriate substituted azoarene (0.25 mmol) and 0.60 mL of the azo/ester stock solution were added. The mixture was stirred on a 90°C heating plate for 21 hours. After cooling down, 5 mL water and 5 mL ethyl acetate were added to each vial. The mixtures were shaken and after the emulsion settled down 1 mL of the top layer was added to an NMR tube for each vial. The volatiles were removed in vacuo and NMR was measured after redissolution in CDCl_3 . The spectra were overlapped with spectra of the isolated amides to ascertain the correct peak intensities were compared. In cases where the crude mixture showed insufficient overlap with the spectra of isolated compounds to ascertain the peak identities, pure amide was added to the crude samples, identifying the grown peaks as the ones of interest.

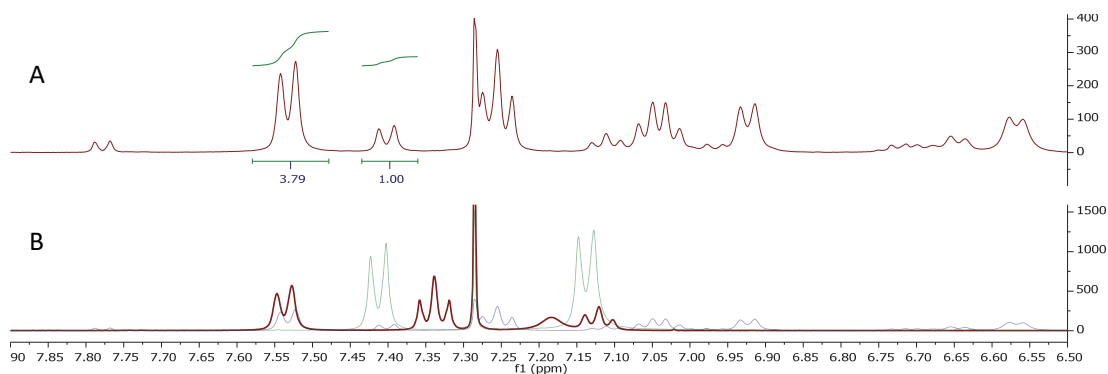


Figure 3.19 (A) Aromatic region from crude NMR of competition experiment between azobenzene and 1,2-bis(4-methylphenyl)diazene. (B) Overlap of crude NMR from competition (purple) with N-(p-toyl)decanamide (green) and N-phenyldecanamide (red), showing the integrals measured in A are representative of the two different product amides.

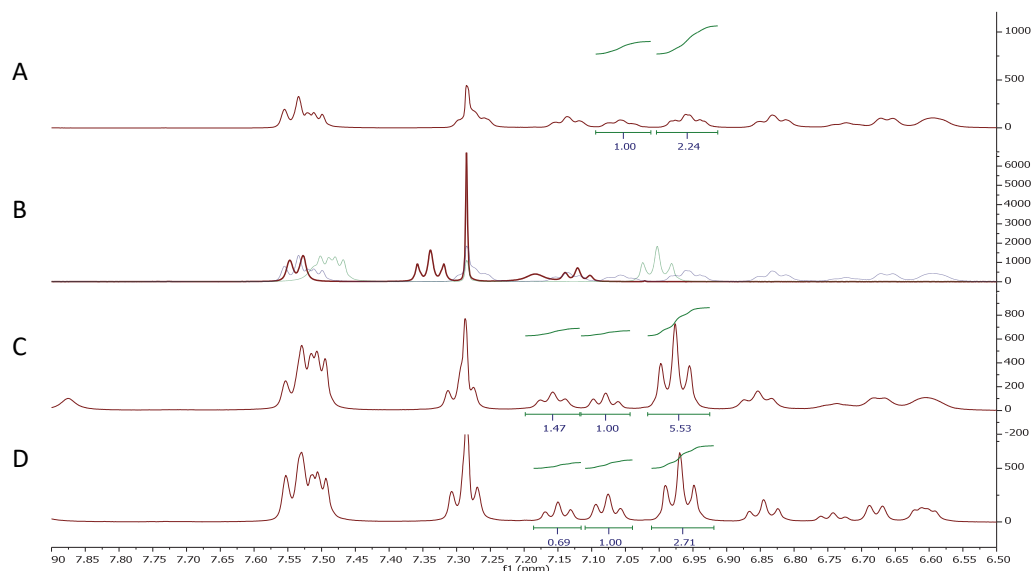


Figure 3.20: (A) Aromatic region from crude NMR of competition experiment between azobenzene and 1,2-bis(4-fluorophenyl)diazene. (B) Overlap of crude NMR from competition (purple) with N-(4-fluorophenyl)decanamide (green) and N-phenyldecanamide (red), showing it is ambiguous which integrals to measure in order to obtain the product ratio. (C) Crude NMR of competition experiment (A) with additional N-(4-fluorophenyl)decanamide, identifying one of the triplets as part of the added amide, since it has grown compared to the others. (D) Spectrum (C) with additional N-phenyldecanamide, identifying one of the triplets as part of the added amide, since it has grown compared to the others.

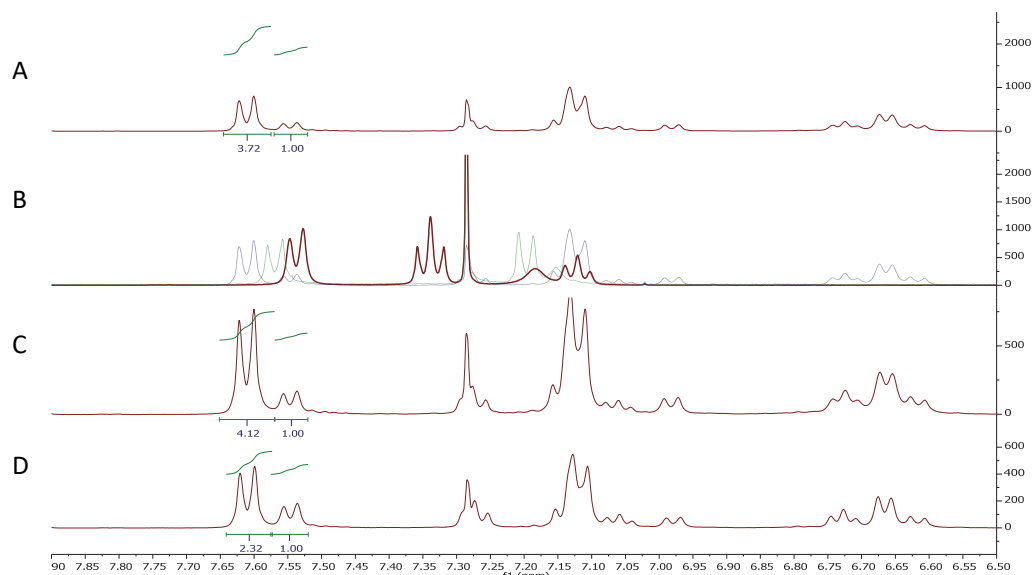


Figure 3.21: (A) Aromatic region from crude NMR of competition experiment between azobenzene and 1,2-bis(4-(trifluoromethoxy)phenyl)diazene. (B) Overlap of crude NMR from competition (purple) with N-(4-fluorophenyl)decanamide (green) and N-phenyldecanamide (red), showing the two most downfield doublets should belong to the two amide products, but leaving ambiguity regarding which peak belongs to which amide. (C) Crude NMR of competition experiment (A) with additional N-(4-(trifluoromethoxy)phenyl)decanamide, identifying the largest doublet as part of the added amide, since it has grown compared to the other. (D) Spectrum (C) with additional N-phenyldecanamide, confirming the other doublet as part of the added amide, since the ratio has now decreased again.

3.8.7 Synthesis of **8^F**

105 mg (Bipy)Ni(0)(COD)³⁴ (0.325 mmol) was dissolved in 24 mL THF in the glove box. 74.8 mg 1,2-bis(4-fluorophenyl)diazene (**7^F**, 0.343 mmol) was added via a weighing boat and the purple colour of the solution quickly turned darker. After stirring for 4.5 hours, the mixture was filtered over Celite. After washing with copious THF, the filtrate was concentrated to about 10 mL. 50 mL Et₂O was added and the mixture was stirred for 10 minutes. A dark brown residue was then filtered off and washed with Et₂O before drying under vacuum. 94 mg, 67% yield. ¹H NMR (400 MHz, DMF-*d*₇, ppm) δ = 9.13 – 8.86 (m, 1H), 8.40 – 8.25 (m, 1H), 8.18 (td, *J* = 7.8, 1.5 Hz, 1H), 7.70 (ddd, *J* = 7.5, 5.3, 1.3 Hz, 1H), 7.61 (dd, *J* = 9.0, 5.3 Hz, 2H), 6.89 (t, *J* = 8.9 Hz, 2H). ¹³C NMR (101 MHz, DMF-*d*₇, ppm) δ = 157.29 (d, *J*_{C,F} = 235.7 Hz), 156.89 (d, *J*_{C,F} = 2.2 Hz), 154.69, 151.46, 138.51, 128.54, 123.18, 121.11 (d, *J*_{C,F} = 7.3 Hz), 116.49 (d, *J*_{C,F} = 21.9 Hz). ¹⁹F NMR (376 MHz, NMP with DMSO-*d*₆ capillary for locking purposes, relative to internal standard fluorobenzene set to -114.51 ppm) δ = -127.06 ppm. The highly air sensitive nature of the compound precluded characterization by HRMS. Elemental analysis: Calculated for C₂₂H₁₆F₂N₄Ni: C, 61.01; H, 3.72; N, 12.94. Found: C, 58.22-58.94; H, 3.64-3.65; N, 12.12-12.36. Note that despite multiple trials we could not obtain perfect elemental analysis. The C content was about 3% lower than expected. The discrepancy might be due to the decomposition of samples during handling as the compound is quite sensitive to air. According to NMR, there are at most trace amounts of unidentified impurities. We think the samples are of sufficient purity for the stoichiometric model amidation reactions.

3.8.8 Reactivity **8^F** with ester **1a**

10.2 mg **8^F** (0.0236 mmol), 33.6 mg ZnCl₂ (0.247 mmol) and 53 μL methyl decanoate (**1a**, 0.25 mmol) and 0.50 mL NMP were added to a scintillation vial in the glove box. The mixture was stirred for 2 hours on a 90°C heating plate. After cooling down, the mixture was opened to air and 3.0 μL fluorobenzene (0.032 mmol), 0.5 mL CDCl₃ and 1 mL water were added. After shaking the mixture, the layers were separated by centrifugation. The bottom layer was then transferred to an NMR tube to measure ¹⁹F NMR. Yields were determined by comparing the integrals to that of the fluorobenzene internal standard. The experiment was performed twice with different batches of **3^F**, giving the same results.

3.9 References

- (1) Hunger, K. *Industrial Dyes: Chemistry, Properties, Application*; Wiley-VCH: Weinheim, 2003.
- (2) Ikeda, T. Photomodulation of Liquid Crystal Orientations for Photonic Applications. *J. Mater. Chem.* **2003**, *13* (9), 2037. <https://doi.org/10.1039/b306216n>.
- (3) Zhao, Y.; He, J. Azobenzene-Containing Block Copolymers: The Interplay of Light and Morphology Enables New Functions. *Soft Matter* **2009**, *5* (14), 2686. <https://doi.org/10.1039/b821589h>.
- (4) Merino, E. Synthesis of Azobenzenes: The Coloured Pieces of Molecular Materials. *Chem. Soc. Rev.* **2011**, *40* (7), 3835. <https://doi.org/10.1039/c0cs00183j>.
- (5) Gund, S. H.; Shelkar, R. S.; Nagarkar, J. M. An Efficient Catalyst-Free and Chemoselective Synthesis of Azobenzenes from Nitrobenzenes. *RSC Adv* **2014**, *4* (81), 42947–42951. <https://doi.org/10.1039/C4RA06027J>.
- (6) Sakai, N.; Fujii, K.; Nabeshima, S.; Ikeda, R.; Konakahara, T. Highly Selective Conversion of Nitrobenzenes Using a Simple Reducing System Combined with a Trivalent Indium Salt and a Hydrosilane. *Chem. Commun.* **2010**, *46* (18), 3173. <https://doi.org/10.1039/c000383b>.
- (7) Antoine John, A.; Lin, Q. Synthesis of Azobenzenes Using *N*-Chlorosuccinimide and 1,8-Diazabicyclo[5.4.0]Undec-7-Ene (DBU). *J. Org. Chem.* **2017**, *82* (18), 9873–9876. <https://doi.org/10.1021/acs.joc.7b01530>.
- (8) Zhang, C.; Jiao, N. Copper-Catalyzed Aerobic Oxidative Dehydrogenative Coupling of Anilines Leading to Aromatic Azo Compounds Using Dioxygen as an Oxidant. *Angew. Chem. Int. Ed.* **2010**, *49* (35), 6174–6177. <https://doi.org/10.1002/anie.201001651>.
- (9) Deng, H.; Li, H.; Wang, L. *Ortho* -Heteroarylation of Azobenzenes by Rh-Catalyzed Cross-Dehydrogenative Coupling: An Approach to Conjugated Biaryls. *Org. Lett.* **2016**, *18* (13), 3110–3113. <https://doi.org/10.1021/acs.orglett.6b01277>.
- (10) Khatun, N.; Modi, A.; Ali, W.; Patel, B. K. Palladium-Catalyzed Synthesis of 2-Aryl-2*H*-Benzotriazoles from Azoarenes and TMSN₃. *J. Org. Chem.* **2015**, *80* (19), 9662–9670. <https://doi.org/10.1021/acs.joc.5b01706>.
- (11) Yan, X.; Yi, X.; Xi, C. Direct Cleavage of the N–N Bond of Azobenzenes by MeOTf Leading to *N*-Arylbenzimidazoles. *Org. Chem. Front* **2014**, *1* (6), 657–660. <https://doi.org/10.1039/C4QO00056K>.
- (12) Yi, X.; Xi, C. Copper-Promoted Tandem Reaction of Azobenzenes with Allyl Bromides via N=N Bond Cleavage for the Regioselective Synthesis of Quinolines. *Org. Lett.* **2015**, *17* (23), 5836–5839. <https://doi.org/10.1021/acs.orglett.5b03009>.

- (13) Cheung, C. W.; Ploeger, M. L.; Hu, X. Direct Amidation of Esters with Nitroarenes. *Nat. Commun.* **2017**, *8*, 14878. <https://doi.org/10.1038/ncomms14878>.
- (14) Cheung, C. W.; Ploeger, M. L.; Hu, X. Nickel-Catalyzed Reductive Transamidation of Secondary Amides with Nitroarenes. *ACS Catal.* **2017**, *7* (10), 7092–7096. <https://doi.org/10.1021/acscatal.7b02859>.
- (15) Burés, J. A Simple Graphical Method to Determine the Order in Catalyst. *Angew. Chem. Int. Ed.* **2016**, *55* (6), 2028–2031. <https://doi.org/10.1002/anie.201508983>.
- (16) Burés, J. Variable Time Normalization Analysis: General Graphical Elucidation of Reaction Orders from Concentration Profiles. *Angew. Chem. Int. Ed.* **2016**, *55* (52), 16084–16087. <https://doi.org/10.1002/anie.201609757>.
- (17) Schmidt, A. F.; Kurokhtina, A. A.; Larina, E. V. Differential Selectivity Measurements and Competitive Reaction Methods as Effective Means for Mechanistic Studies of Complex Catalytic Reactions. *Catal. Sci. Technol.* **2014**, *4* (10), 3439–3457. <https://doi.org/10.1039/C4CY00479E>.
- (18) Brown, H. C.; Okamoto, Y. Electrophilic Substituent Constants. *J. Am. Chem. Soc.* **1958**, *80* (18), 4979–4987. <https://doi.org/10.1021/ja01551a055>.
- (19) Otsuka, S.; Yoshida, T.; Tatsuno, Y. Isocyanide-Nickel(0) and -Palladium(0) Complexes Involving Unsaturated Ligands. *J. Am. Chem. Soc.* **1971**, *93* (24), 6462–6469. <https://doi.org/10.1021/ja00753a021>.
- (20) Muetterties, E. L.; Pretzer, W. R.; Thomas, M. G.; Beier, B. F.; Thorn, D. L.; Day, V. W.; Anderson, A. B. Metal Clusters in Catalysis. 14. The Chemistry of Dinuclear Metal-Acetylene Complexes. *J. Am. Chem. Soc.* **1978**, *100* (7), 2090–2096. <https://doi.org/10.1021/ja00475a019>.
- (21) Link, H.; Reiss, P.; Chitsaz, S.; Pfistner, H.; Fenske, D. Synthese Und Molekülstrukturen von Amido- Und Imidoverbrückten Clustern Elektronreicher Übergangsmetalle. *Z. Für Anorg. Allg. Chem.* **2003**, *629* (5), 755–768. <https://doi.org/10.1002/zaac.200390138>.
- (22) Zurita, D. A.; Flores-Alamo, M.; García, J. J. Catalytic Transfer Hydrogenation of Azobenzene by Low-Valent Nickel Complexes: A Route to 1,2-Disubstituted Benzimidazoles and 2,4,5-Trisubstituted Imidazolines. *Dalton Trans.* **2016**, *45* (25), 10389–10401. <https://doi.org/10.1039/C6DT01674J>.
- (23) Dinjus, E.; Gorski, I.; Matschiner, H.; Uhlig, E.; Walther, D. Substitutionsreaktionen mit Gemischtligand-Komplexen des Nickel(0). I. Reaktionen mit Heteroolefinen. *Z. Für Anorg. Allg. Chem.* **1977**, *436* (1), 39–46. <https://doi.org/10.1002/zaac.19774360104>.
- (24) Gilbert, Z. W.; Hue, R. J.; Tonks, I. A. Catalytic Formal [2+2+1] Synthesis of Pyrroles from Alkynes and Diazenes via TiII/TiIV Redox Catalysis. *Nat. Chem.* **2016**, *8* (1), 63–68. <https://doi.org/10.1038/nchem.2386>.
- (25) Davis-Gilbert, Z. W.; Wen, X.; Goodpaster, J. D.; Tonks, I. A. Mechanism of Ti-Catalyzed Oxidative Nitrene Transfer in [2 + 2 + 1] Pyrrole Synthesis from Alkynes and

- Azobenzene. *J. Am. Chem. Soc.* **2018**, *140* (23), 7267–7281. <https://doi.org/10.1021/jacs.8b03546>.
- (26) Aubart, M. A.; Bergman, R. G. Tantalum-Mediated Cleavage of an NN Bond in an Organic Diazene (Azoarene) to Produce an Imidometal (MNR) Complex: An η^2 -Diazene Complex Is Not an Intermediate. *Organometallics* **1999**, *18* (5), 811–813. <https://doi.org/10.1021/om9809668>.
- (27) Bellows, S. M.; Arnet, N. A.; Gurubasavaraj, P. M.; Brennessel, W. W.; Bill, E.; Cundari, T. R.; Holland, P. L. The Mechanism of N–N Double Bond Cleavage by an Iron(II) Hydride Complex. *J. Am. Chem. Soc.* **2016**, *138* (37), 12112–12123. <https://doi.org/10.1021/jacs.6b04654>.
- (28) Takeuchi, K.; Ichinohe, M.; Sekiguchi, A. Access to a Stable Si₂N₂ Four-Membered Ring with Non-Kekulé Singlet Biradical Character from a Disilyne. *J. Am. Chem. Soc.* **2011**, *133* (32), 12478–12481. <https://doi.org/10.1021/ja2059846>.
- (29) Zhao, Y.; Liu, Y.; Yang, L.; Yu, J.-G.; Li, S.; Wu, B.; Yang, X.-J. Mechanistic Insight into the N=N Bond-Cleavage of Azo-Compounds That Was Induced by an Al–Al Bonded Compound [L₂–AlII–AlIIL₂]. *Chem. - Eur. J.* **2012**, *18* (19), 6022–6030. <https://doi.org/10.1002/chem.201103607>.
- (30) Dunn, P. L.; Chatterjee, S.; MacMillan, S. N.; Pearce, A. J.; Lancaster, K. M.; Tonks, I. A. The 4-Electron Cleavage of a N=N Double Bond by a Trimetallic TiNi₂ Complex. *Inorg. Chem.* **2019**, *58* (17), 11762–11772. <https://doi.org/10.1021/acs.inorgchem.9b01805>.
- (31) Mindiola, D. J.; Waterman, R.; Iluc, V. M.; Cundari, T. R.; Hillhouse, G. L. Carbon–Hydrogen Bond Activation, C–N Bond Coupling, and Cycloaddition Reactivity of a Three-Coordinate Nickel Complex Featuring a Terminal Imido Ligand. *Inorg. Chem.* **2014**, *53* (24), 13227–13238. <https://doi.org/10.1021/ic5026153>.
- (32) Powers, I. G.; Kiattisewee, C.; Mullane, K. C.; Schelter, E. J.; Uyeda, C. A 1,2-Addition Pathway for C(Sp²)–H Activation at a Dinickel Imide. *Chem. - Eur. J.* **2017**, *23* (32), 7694–7697. <https://doi.org/10.1002/chem.201701855>.
- (33) Rosenau, C. P.; Jeliet, B. J.; Gossert, A. D.; Togni, A. Exposing the Origins of Irreproducibility in Fluorine NMR Spectroscopy. *Angew. Chem. Int. Ed.* **2018**, *57* (30), 9528–9533. <https://doi.org/10.1002/anie.201802620>.
- (34) Dinjus, E.; Gorski, I.; Uhlig, E.; Walther, H. Nickel(0)-Komplexe mit der zentralen Koordinationseinheit NiN₂P₂. *Z. Für Anorg. Allg. Chem.* **1976**, *422* (1), 75–79. <https://doi.org/10.1002/zaac.19764220110>.

Chapter 4

Mechanism of Ni-catalyzed reductive amidation of unactivated esters with azobenzenes: computational study and overall conclusions

Part of the data were reproduced with permission from Ploeger, M.L.; Darù, A.; Harvey, J.N.; Hu, X. Reductive Cleavage of Azoarene as a Key step in Nickel-Catalyzed Amidation of Esters with Nitroarenes *ACS Catalysis*. 2020, 10, 2845-2854. Copyright 2020 American Chemical Society.

All calculations presented in this chapter have been performed by Andrea Darù at the KU Leuven. M.L. Ploeger has contributed through a close collaboration with discussions to relate the computational and experimental work. He also made qualitative kinetic analysis (section 4.5) and formulated the catalytic cycle (4.6) and conclusion (4.7).

4.1 Introduction

In chapter 3 mechanistic experiments provided some key insights into the mechanism of azobenzene-ester coupling: (i) azobenzene reacts with the nickel catalyst before the ester does; (ii) ZnCl_2 plays a key role in at least one of the catalytic steps and (iii) the rate determining step is either zero order in the substrates, while roughly 1.5 in nickel, or first order in nickel and ester, while zero order in azobenzene, depending on the ZnCl_2 concentration. Some interesting reactivity with a $\text{Ni}(0)$ azoarene adduct was also observed.

As these findings alone are insufficient to build a comprehensive mechanistic model, we turned to density functional theory (DFT) calculations to determine to explore pathways that cannot be discerned experimentally and to verify that some assumptions made in the experimental study are reasonable. Specifically, we sought to answer the following questions: (i) Can the experimentally tested $\text{Ni}(0)$ azoarene adduct be formed under our reaction conditions? (ii) Is there a pathway available that reductively splits the azoarene from this adduct intermediate as inferred from experimental results? (iii) What do the intermediate that reacts with ester and the transition state of this reaction look like? (iv) How does ZnCl_2 influence the reaction?

The experimental results served as input for these calculations, saving computational cost (e.g. a pathway of oxidative addition of ester before involvement of azoarene did not need to be investigated). In addition, the validity of the pathways that were found via computation was checked by comparing with the experimental results: the computational model would need to conform to the two rate laws that were found experimentally and give a reason for the shift from one rate law to the other upon addition of more ZnCl_2 to be considered reasonable.

4.2 Reduction of $\text{Ni}(\text{II})$ complex by Zn

By using a thermodynamic cycle involving experimental sublimation energy¹ and calculated solvation energy of a gaseous zinc atom, the thermodynamics of steps involving reduction of species by solid zinc could be considered.² Using this approach, the potential energy surface for reduction of $(\text{phen})\text{NiCl}_2$ (**I**) to lower valent nickel species could be calculated (Figure 4.1).

A one electron reduction to intermediate **II** is slightly downhill and is therefore expected to occur under catalytic conditions. Conversely, the direct reduction to solvent-ligated $\text{Ni}(0)$ complex **III** is more than 34 kcal mol^{-1} uphill. Since activation barriers towards and from **III** would

lead to an even higher overall activation energy, this step is considered inaccessible at the applied temperatures. Instead, **II** can bind azobenzene in a slightly uphill equilibrium with Ni(I) azobenzene adduct **IV**. The binding of azobenzene makes reduction to Ni(0) species **V** exothermic. Thus, the computational results shown in Figure 4.1 validate the assumption made in chapter 3 that a species like **8^F** can form in the reaction mixture.

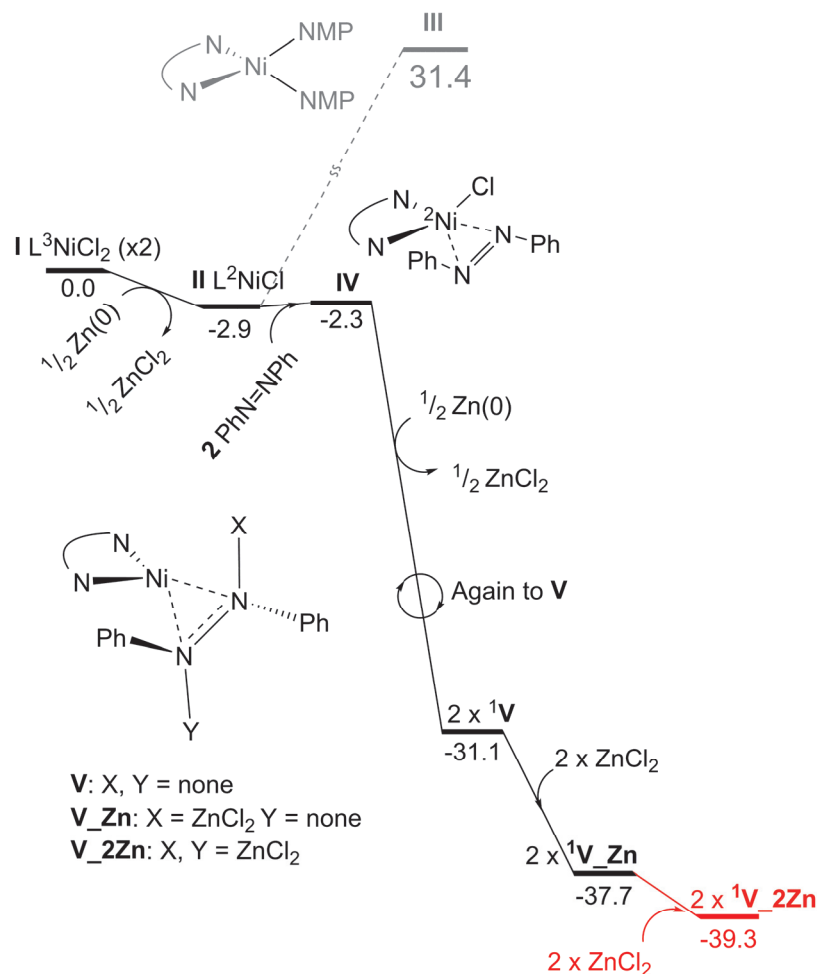


Figure 4.1: Ni(II) reduction by zinc powder, and possible coordination by $ZnCl_2$ as Lewis acid. Gibbs free energy values at 363 K in $kcal\ mol^{-1}$. Numbers in superscript before compound nomenclature and atoms denote spin pairing at that centre.

The change in redox behavior between Ni(I) species **II** and **IV** can be understood by considering the calculated properties of the reduced species **V**. Although this is formally a Ni(0) complex, it involves strong back-donation from Ni as can be seen by considering e.g. the N—N bond length, which is 1.39 Å (compared to 1.26 Å in free **2** and 1.35 Å in **IV**), suggesting donation from the high-energy nickel 3d orbitals to the N—N π^* orbital. Note that we do not

find that this complex has non-innocent Ni(I) character with transfer of one electron to the azo moiety; all attempts to calculate an open-shell singlet state with this bonding pattern revert to the closed-shell singlet described here.

Species **V** has quite nucleophilic azo nitrogen atoms, hence it can now coordinate to one or two ZnCl₂ metal centres through these nitrogen atoms, thereby generating **V_Zn** or **V_2Zn**. This complexation cannot fully occur in the absence of added ZnCl₂, since reduction of the nickel dichloride generates just one equivalent of ZnCl₂ upon forming **V**. Hence the second coordination requires additional ZnCl₂. This is shown in Figure 4.1 by highlighting the second coordination step in red.

4.3 Pathway for splitting azobenzene

Next, we attempted to validate the idea inferred from experimental work that reactivity of the Ni(0) azobenzene adduct could involve splitting of the azoarene. Indeed, we could find a reasonable pathway for cleaving the N=N bond, depicted in Figure 4.2.

The lowest-energy pathway we found starts from **V_Zn**. Two equivalents of **V_Zn** can react through transition state structure **TS1**, with N—N bond splitting in one of the two azo moieties, yielding an analogue of **VI** with a pendant azo moiety, referred to in Figure 4.2 as **PreVI**. **TS1** lies 27.0 kcal mol⁻¹ higher in free energy than two **V_Zn** (or a little bit more relative to two **V_2Zn**). The overall process is almost thermo-neutral, with **PreVI** lying just 3.8 kcal mol⁻¹ lower (in terms of Gibbs free energy) than two **V_Zn** complexes.

In order to obtain the nickel imide dimer **VI_2Zn** the azo-compound coordinated to one of the Ni centers in **PreVI** needs to be released. This is achieved by crossing **TS2** with a free energy barrier of 24.1 kcal mol⁻¹, with the dimer generated in a very exothermic process from **PreVI**. Overall, the formation of **VI_2Zn** is found to be downhill by 7.2 kcal mol⁻¹ from 2 equivalents of **V_Zn**, or by 5.6 kcal mol⁻¹ from 2 equivalents of **V_2Zn**. The pathway is reminiscent of the calculated pathway for Ti(II) by Tonks.³

The energy levels of reactants (**V**) and products (**VI**) of the splitting reaction without ZnCl₂ coordination are also displayed in Figure 4.2. Clearly, the splitting would be endothermic if ZnCl₂ is not present to stabilize the nickel imide dimer. Moreover, the ZnCl₂ binds more strongly to the nitrogen centres in **VI** than in **V**. Combined, these findings explain why the splitting is more efficient when a larger excess of ZnCl₂ is added, as reported in chapter 3: the

reaction requires ZnCl_2 to proceed smoothly, but as the product binds it more strongly than the starting material, available ZnCl_2 will become lower as the reaction proceeds.

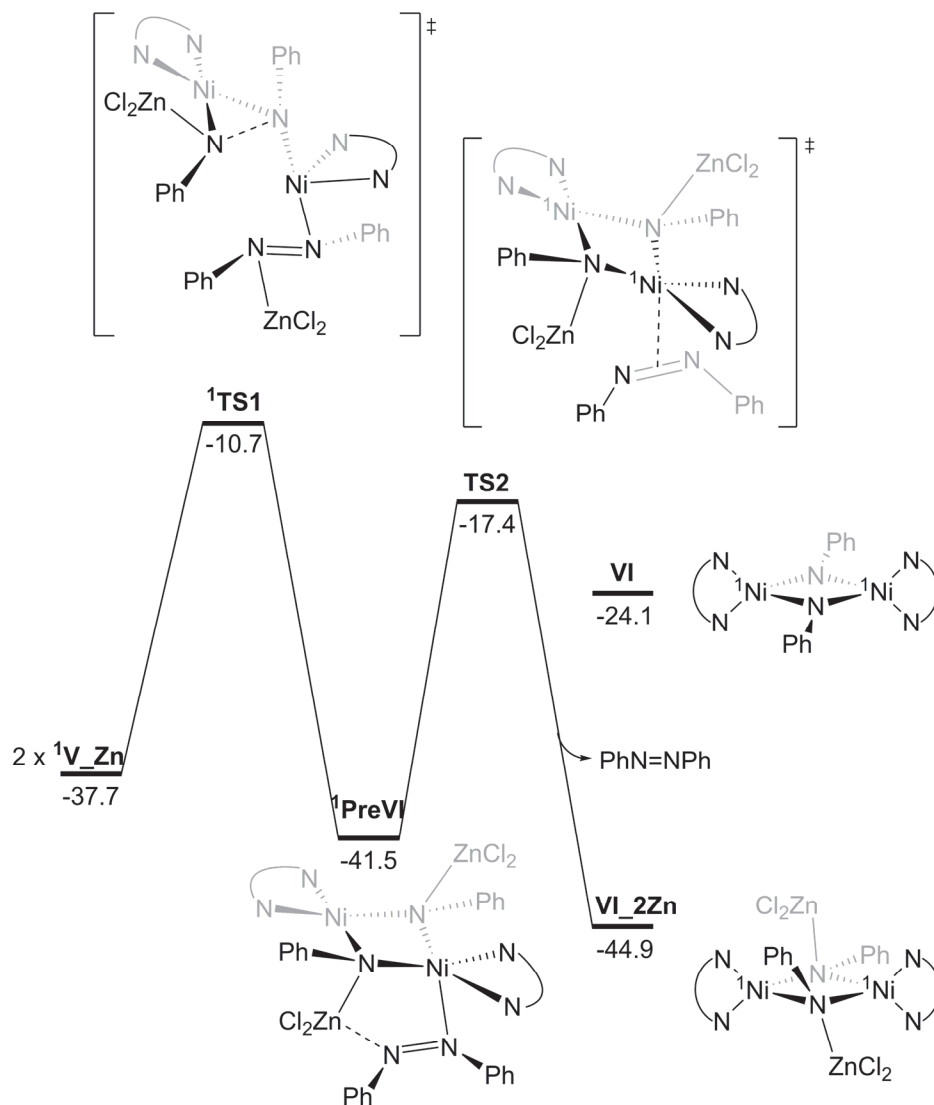


Figure 4.2: Pathway for reductive cleavage of azobenzene from Ni(0) azobenzene adduct. Gibbs free energy values at 363 K in kcal mol⁻¹. Numbers in superscript before compound nomenclature and atoms denote spin pairing at that centre.

4.4 Reactivity with ester

Figure 4.3 shows possible pathways for methyl propanoate (**1e**) with either **VI** or **VI_2Zn** towards the product zinc amide complex **P**. The highly stabilized **VI_2Zn** is calculated to react only very sluggishly with ester via **TS5_Zn** with an energy barrier of 36.9 kcal mol⁻¹. A reaction

pathway with **V** as starting point via **VI** and **TS5** would lead to a somewhat reasonable barrier of 31.9 kcal mol⁻¹. However, this barrier would increase by 20 kcal mol⁻¹ if the stabilization of **VI** through the binding of ZnCl₂ is taken into account. A splitting of the imide dimer, as suggested in Tonks' work³ is 31.1 kcal mol⁻¹ endothermic from the already disfavored intermediate **VI** and we therefore consider it inaccessible.

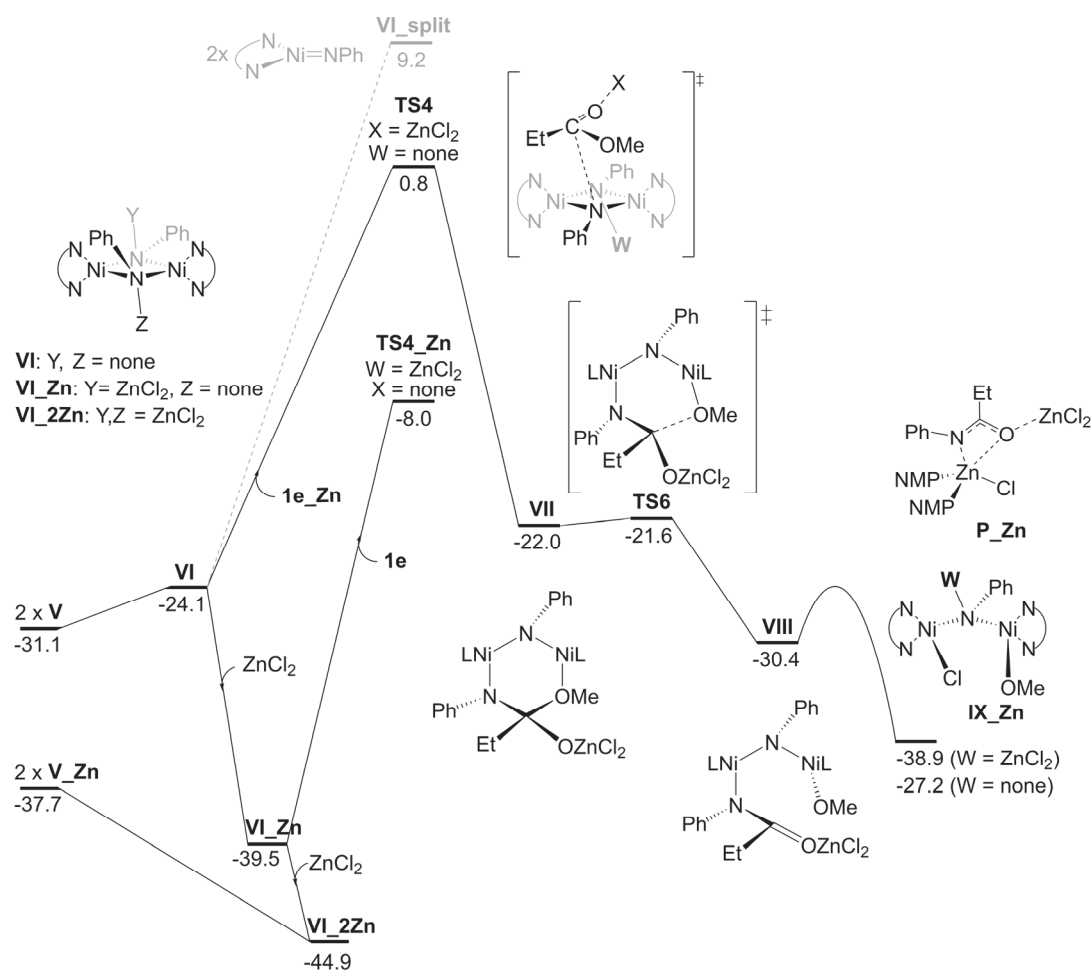


Figure 4.3: Possible pathways for reaction of **1e** with **V** or **VI**. Gibbs free energy values at 363 K in kcal mol⁻¹.

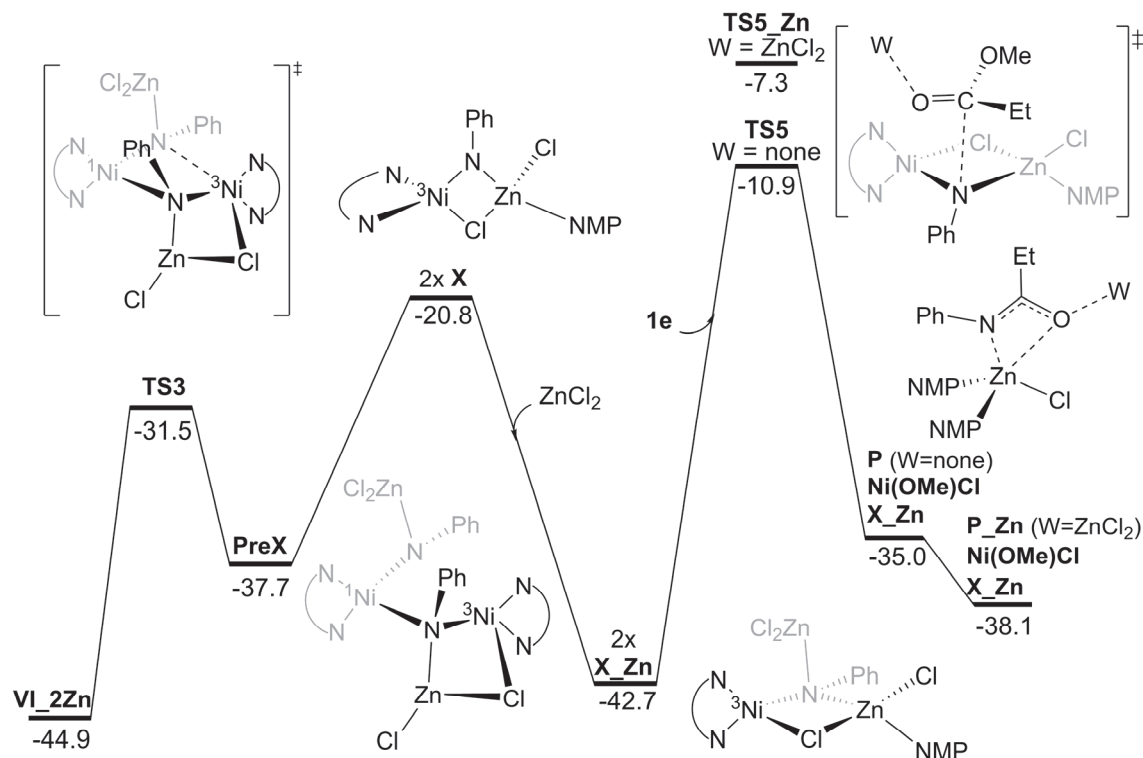


Figure 4.4 Pathway via splitting of **VI_2Zn**. Gibbs free energy values at 363 K in kcal mol⁻¹.

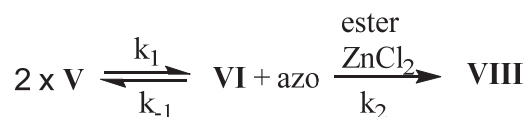
Because of the difficult reactivity directly from **VI_2Zn**, we also considered the splitting of complex **VI_2Zn** into two complexes of a nickel-zinc imide complex **X**. The intermediate **X** can also be stabilized by binding of an additional molecule of ZnCl_2 to the imide nitrogen, generating **X_Zn**. The conversion of **VI_2Zn** to two molecules of **X_Zn** is only slightly endothermic overall. The barrier towards product **P** is the lowest one we have found for reaction with **1c** (compare the value of -10.9 kcal mol⁻¹ with that of -8.0 kcal mol⁻¹ and 0.8 kcal mol⁻¹ of figure 4.3). The overall reaction barrier is now 34 kcal mol⁻¹. The expected free energy barrier for a process occurring in several hours at 363 K is roughly 28 kcal mol⁻¹, which is consistent with the value of 34 kcal mol⁻¹ considering the uncertainties involved in the calculations.^{4,5}

4.5 Qualitative Kinetic Analysis

The potential energy surfaces discussed in section 4.4 can only be considered to reasonably model the catalytic reaction, if they could feasibly predict the two rate laws observed experimentally and provide an explanation for the switch between the rate laws upon addition of

ZnCl₂. In this section, the rate laws that are expected based on the computed pathways are qualitatively analyzed and compared to the experimental findings reported in chapter 3.

4.5.1 Pathway via **TS4**



This reaction may be analyzed with the steady state approximation

$$\text{Rate} = k_2 [\mathbf{VI}][\text{ester} \cdot \text{ZnCl}_2] \quad (4.1)$$

$$d[\mathbf{VI}]/dt = k_1[\mathbf{V}]^2 - k_{-1}[\mathbf{VI}][\text{azo}] - k_2[\mathbf{VI}][\text{ester} \cdot \text{ZnCl}_2] = 0 \quad (4.2)$$

$$[\mathbf{VI}]_{\text{ss}} = \frac{k_1[\mathbf{V}]^2}{k_{-1}[\text{azo}] + k_2[\text{ester} \cdot \text{ZnCl}_2]} \quad (4.3)$$

Insert (4.3) into (4.1):

$$\text{Rate} = \frac{k_1 k_2 [\mathbf{V}]^2 [\text{ester} \cdot \text{ZnCl}_2]}{k_{-1}[\text{azo}] + k_2[\text{ester} \cdot \text{ZnCl}_2]} \quad (4.4)$$

Equation (4.4) may simplify under two limiting conditions.

a. The reverse reaction in the first equilibrium is much faster than the forward reaction with

$$\text{ester. Then, rate} = K_1 \frac{k_2[\mathbf{V}]^2[\text{ester} \cdot \text{ZnCl}_2]}{[\text{azo}]} \quad (4.5)$$

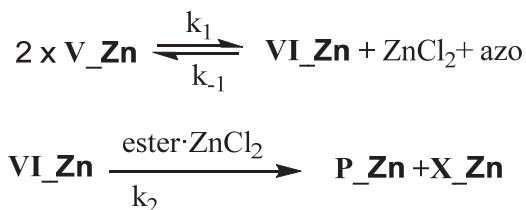
b. The forward reaction rate with ester is much faster than the reverse reaction of the equilibrium, rendering the formation of **VI** irreversible:

$$\text{Rate} = k_1[\mathbf{V}]^2 \quad (4.6)$$

In equations (4.4)-(4.6), the only nickel species that appears is **V**. Since **V** is the most stable nickel species before the rate limiting transition state by a considerable margin, it is reasonable to consider it as the resting state, i.e., $[\mathbf{V}] \approx [\text{Ni}]_{\text{total}}$. Hence, the pathway via **TS5** would certainly lead to a second order in nickel, which contradicts our experimental results. Furthermore, while

equation (4.6) would correctly predict 0th order in both substrates, it is unclear how ZnCl₂ would speed up the reaction, or result in a rate law with 1st order in ester, but 0th order in azobenzene. In fact, ZnCl₂ could lead to formation of **VI_Zn**, which would be a kinetic trap in this model.

4.5.2 Pathway via **TS4_Zn**:



Steady state approximation would again lead to an equation similar to (4.4), but with **[V]** substituted by **[V_Zn]**. In other words,

$$\text{Rate} = \frac{k_1 k_2 [\mathbf{V_Zn}]^2 [\text{ester} \cdot \text{ZnCl}_2]}{k_{-1} [\text{azo}] + k_2 [\text{ester} \cdot \text{ZnCl}_2]} \quad (4.7)$$

However, the computations suggest the energies of reactants and products of the first equilibrium are close to one another. As a result, the approximation $[\mathbf{V_Zn}] \approx [\text{Ni}]_{\text{total}}$ is invalid. Rather, we consider

$$[\text{Ni}]_{\text{total}} \approx 2[\mathbf{VI_Zn}] + [\mathbf{V_Zn}] \quad (4.8)$$

$$K_1 = \frac{[\mathbf{VI_Zn}][\text{azo}][\text{ZnCl}_2]}{[\mathbf{V_Zn}]^2} \quad (4.9)$$

Rearrangement of (4.8) followed by insertion into (4.9) leads to

$$2K_1[\mathbf{V_Zn}]^2 + [\text{azo}][\text{ZnCl}_2](\mathbf{V_Zn} - [\text{Ni}]_{\text{total}}) = 0 \quad (4.10)$$

Solution of equation (4.10) for **[V_Zn]** leads to a non-linear dependence of the rate (equations 4.7 and 4.9) on **[Ni]_{total}**, **[azo]**, and **[ZnCl₂]**.

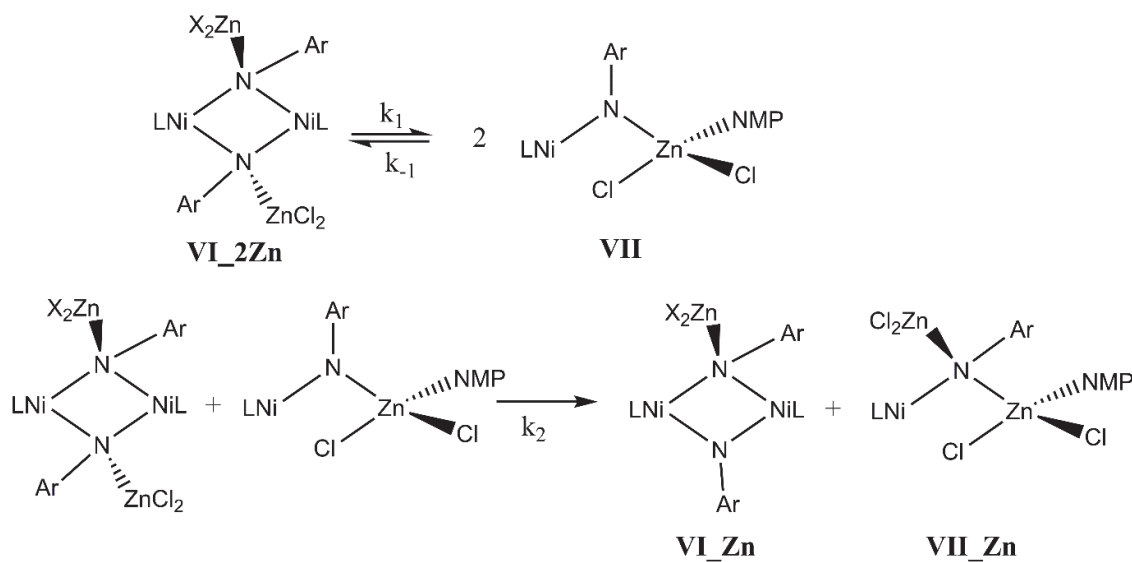
$$[\mathbf{V_Zn}] \approx \frac{-[\text{azo}][\text{ZnCl}_2] + \sqrt{([\text{azo}][\text{ZnCl}_2])^2 + 8K_1[\text{azo}][\text{ZnCl}_2][\text{Ni}]_{\text{total}}}}{4K_1} \quad (4.11)$$

Note that $[\text{ZnCl}_2]$ depends on $[\text{Ni}]_{\text{total}}$ when no additional amounts are added. As such, the square dependence of the rate on $[\text{V_Zn}]$ translates into a complicated dependence on nickel catalyst. The measured order of 1.4 does not contradict this. However, the rate also has a dependence on $[\text{azo}]$ (equation 4.11), which is not observed experimentally.

4.5.3 Pathway via TS5:

It is possible that the formation of **VII_Zn** is rate limiting under low- $[\text{ZnCl}_2]$ conditions, with the subsequent reaction with ester being faster than the equilibrium. In this case, a feasible reaction pathway towards the formation of **VII_Zn** is depicted in Scheme 4.1 (see also Figure 4.4).

Scheme 4.1: Formation pathway of **X_Zn**



Here a reversible uphill splitting of the dimer **VI_2Zn** into two monomeric **X** is followed by a reaction with **VI_2Zn** to give **VI_Zn** and **X_Zn**.

Applying a steady state approximation:

$$\text{Rate} = k_2[\text{VI_2Zn}][\text{VII}] \quad (4.12)$$

$$d[\text{VII}]/dt = k_1[\text{VI_2Zn}] - k_{-1}[\text{VII}]^2 - k_2[\text{VI_2Zn}][\text{VII}] = 0 \quad (4.13)$$

$$[\text{VII}]_{\text{ss}} = \frac{k_2[\text{VI_2Zn}] - \sqrt{k_2^2[\text{Ni_2Zn}]^2 + 4k_1k_{-1}[\text{VI_2Zn}]}}{-2k_{-1}} \quad (4.14)$$

If **VI_2Zn** is the resting state, $[\text{VI_2Zn}] \approx 0.5[\text{Ni}]_{\text{total}}$. Evaluating equation (4.14) shows that $[\text{VII}]_{\text{ss}}$ will increase with increasing $[\text{Ni}]_{\text{total}}$, but not linearly, so $[\text{VII}]_{\text{ss}} \propto ([\text{Ni}]_{\text{total}})^\alpha$, where $0 < \alpha < 1$. Inserting this relation into equation (4.12) leads to a relation where rate $\propto ([\text{Ni}]_{\text{total}})^{\alpha+1}$, which is in agreement with experiment. Under this model, the rate is 0th order in ester and azobenzene, which agree with experimental results under no additional $[\text{ZnCl}_2]$.

Upon addition of supplementary ZnCl_2 , **VII** could directly react with ZnCl_2 to give **VII_Zn**. At sufficiently high $[\text{ZnCl}_2]$, the formation of **VII_Zn** is fast and **VII_Zn** is the new resting state, i.e. $[\text{VII_Zn}] \approx [\text{Ni}]_{\text{total}}$. Thus,

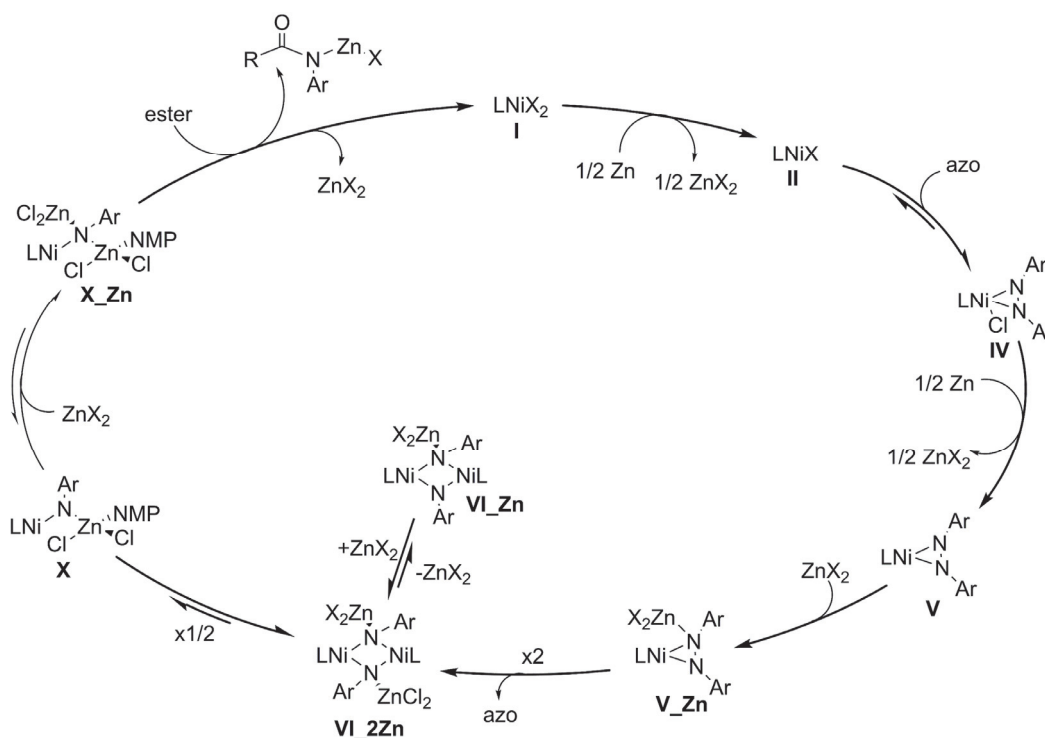
$$\text{Rate} = k[\text{ester}][\text{VII_Zn}] \quad (4.15)$$

So the reaction becomes first order in ester and nickel, and 0th order in azobenzene. This prediction agrees with the experimental results under high $[\text{ZnCl}_2]$.

4.6 Catalytic cycle

The complexity of the catalytic system hinders a decisive determination of the full catalytic cycle: compared to the vast amount of potential intermediate species, we have only managed to consider a limited number with DFT calculations. Nonetheless, the results from chapter 3 and the calculations on key intermediates presented in this chapter have provided valuable insights. Based on these, we propose the catalytic cycle depicted in Scheme 4.2. Nickel(II) (**I**, $\text{X} = \text{Cl}$ or $\text{X} = \text{OMe}$) is readily reduced to Ni(I) (**II**) by Zn. **II** can bind an azoarene, forming complex **IV**. While the adduct formation is uphill, it allows for facile reduction to Ni(0) azo adduct **V**, which readily binds a zinc salt to form **V_Zn**. Subsequently, two molecules of **V_Zn** combine to form dinickel bisimide **VI_2Zn**, releasing one equivalent of azoarene. **VI_2Zn** is in equilibrium with other Ni/Zn complexes **VI_Zn**, **VII** and **VII_Zn**, via the breaking up of dimers to monomers (**VI_2Zn** to **VII**) and the exchange of weakly binding zinc salts (**VI_2Zn** to **VI_Zn** and **VII** to **VII_Zn**). This equilibrating mixture is pushed forward by reaction of **VII_Zn** with an ester, forming a zinc complex of the product amide and regenerating **I**.

Scheme 4.2: Proposed catalytic cycle for azobenzene-ester coupling



4.7 Conclusions

The DFT calculations confirmed the accessibility of the Ni(0) azoarene complex studied in chapter 3. In addition, they showed that the suspected N=N cleavage is indeed feasible reactivity for this complex under catalytic conditions. Several roles of ZnCl₂ were uncovered. By functioning as a Lewis acid, several of the intermediates and transition states in the catalytic cycle are stabilized. Because of this, the catalytic mixture likely consists of a complicated equilibrating mixture of nickel-zinc imide complexes. This mixture can be pushed towards the species that is best capable of reactivity with esters, which explains the observed shift in rate law with increasing concentration of ZnCl₂. The combined results of chapter 3 and 4 allowed us to propose a catalytic cycle involving the formation of a nickel imide dimer from a strongly reductive nickel complex. Under the influence of ZnCl₂, the nickel imide dimer transforms into a nickel-zinc dimer, which finally reacts with ester to form the product and regenerate Ni(II). The discovery of nickel complexes that can cleave azobenzene is an inspiration for research into the application of azoarenes as nitrene-like nitrogen sources.

4.8 Experimental

4.8.1 Computational methods

Computations were performed using density functional theory (DFT) and the Gaussian 09 rev. E01 and Gaussian 16 rev A03 program packages.⁶ Geometry optimization was performed employing the hybrid meta-GGA functional TPSSh^{7,8} including the D3 empirical dispersion correction with Becke and Johnson damping D3BJ,⁹ together with the Def2SVP basis set on all atoms (BS1).¹⁰ In these DFT calculations, the effects of solvent (NMP) have been considered using the continuum solvent model with the SMD parameterization,¹¹ with the parameters for the related DMA solvent, which has a similar dielectric constant and shape to NMP (parameters for NMP are not available in the program package used). Explicit solvation using NMP molecules was also included when needed. Refined electronic energies were calculated by single point calculations, including scalar relativistic effects using the second-order (DKH)^{12,13} together with the TPSSh-D3BJ functional. For these single-point energy calculations, a larger basis set was used, based on the aug-cc-pwCVQZ-DK basis for Ni and Zn, the aug-cc-pVTZ-DK basis for Cl, cc-pVTZ-DK for all other heavy atoms, and cc-pVDZ-DK for H (BS2).¹⁴⁻¹⁶ This method has been validated for Ni redox chemistry based on coupled cluster single double triple CCSD(T)^{13,14,17,18} reference calculations carried out using the Molpro program package,¹⁵ again using the second-order DKH Hamiltonian to treat scalar relativistic effects, together with the same large basis set as in the DFT single point calculations. Vibrational frequency calculations were performed at the same level of theory as used for optimization and used to define the nature of the stationary points (minima and TSs) involved in the reaction mechanism. Free energy corrections (using a 1 M standard state reference, except for NMP where we used a standard state corresponding to the pure liquid, i.e. 10.4 M) were applied to the electronic energy and calculated based on the calculated rotational constants and vibrational frequencies, using the quasi-harmonic correction for small vibrational frequencies, with the cut-off set at 100 cm⁻¹.¹⁶ This correction is referred to in the following tables as G_{corr} where zero-point energy, thermal and entropic correction term are included. Therefore, the final Gibbs free energy value is obtained by $G = E_{\text{elec}} + G_{\text{corr}}$. In the main paper, this equation is used to obtain the presented relative free energies, with E_{elec} obtained with TPSSh-D3BJ as described above. Here, we also present energies computed with B3LYP-D3BJ and MN15.

4.8.2 Treatment of solid zinc

In order to calculate the free energy of the solid zinc we made use of the experimental value of the free energy of sublimation which we subtracted from the computed free energy of the zinc atom calculated in the gas phase. The calculation of these values was made at the temperature of 363 K in order to be consistent with the experimental conditions. The sublimation free energy was calculated based on the enthalpy and entropy values provided in NIST WebBook¹ with the following equations and values for gas and solid phase (Table 4.1).

Table 4.1: Values used for calculating the sublimation free energy of zinc.

Parameter	Gas phase	Solid
$H^\circ_{298.15} (\text{kJ mol}^{-1})$	130.42	0.00
$T (\text{K})$		363
$t = T / 1000 (\text{K})$		0.363
A	18.20166	25.60123
B	2.313999	-4.405292
C	-0.736547	20.42206
D	0.079950	-7.399697
E	1.073557	-0.045801
F	126.9388	-7.755964
G	184.6977	72.91373
H	130.4203	0.00000

Gas phase:

$$\Delta H^\circ_{363} = A*t + B*t^2/2 + C*t^3/3 + D*t^4/4 - E/t + F - H + H^\circ_{298.15} = 132.96673 \text{ kJ mol}^{-1} \quad (4.16)$$

$$= 31.76983 \text{ kcal mol}^{-1}$$

$$S^\circ_{363} = A*\ln(t) + B*t + C*t^2/2 + D*t^3/3 - E/(2*t^2) + G = 0.16297 \text{ kJ mol}^{-1} \text{ K}^{-1} \quad (4.17)$$

$$= 0.03894 \text{ kcal mol}^{-1}$$

$$\text{K}^{-1} \Delta G^\circ_{363} = 73.79786 \text{ kJ mol}^{-1} = 17.63390 \text{ kcal mol}^{-1} = 0.028101 \text{ hartree} \quad (4.18)$$

Solid phase:

$$\Delta H^\circ_{363} = A*t + B*t^2/2 + C*t^3/3 + D*t^4/4 - E/t + F - H + H^\circ_{298.15} = -2.38246 \text{ kJ mol}^{-1} \quad (4.19)$$

$$= -0.56929 \text{ kcal mol}^{-1}$$

$$S^\circ_{363} = A*\ln(t) + B*t + C*t^2/2 + D*t^3/3 - E/(2*t^2) + G = 0.046773 \text{ kJ mol}^{-1} \text{ K}^{-1} \quad (4.20)$$

$$= 0.01118 \text{ kcal mol}^{-1} \text{ K}^{-1}$$

$$\Delta G^\circ_{363} = -19.36101 \text{ kJ mol}^{-1} = -4.63629 \text{ kcal mol}^{-1} = -0.007372 \text{ hartree} \quad (4.21)$$

Once we obtained the experimental free energy values for the formation of zinc solid and gas the difference between these values provides the ΔG of sublimation:

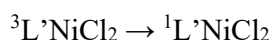
$$\begin{aligned} \Delta G^\circ_{363} (\text{s} \rightarrow \text{g}) &= \Delta G^\circ_{363} (\text{g}) - \Delta G^\circ_{363} (\text{s}) = -0.007372 - 0.028101 = 0.035482 \text{ hartree} \quad (4.22) \\ &= 22.27 \text{ kcal mol}^{-1} \end{aligned}$$

This value can then be subtracted from the free energy value of a zinc atom in the gas phase to obtain the free energy for a zinc atom in solid phase.

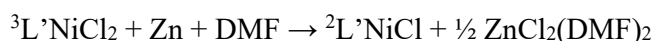
4.8.3 Coupled Cluster calculations for benchmarking

In order to test the quality of the functional TPSSh-D3BJ used to calculate the energy of the complex involved in the reaction mechanism, we carried out some coupled cluster calculations for some steps of the reaction mechanism suggested in the main text. Specifically, we calculated the following relative electronic energies for a simplified model system with a smaller mimic **L'** of the phenanthroline ligand (see details below):

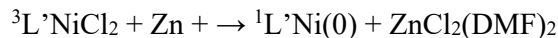
Step a: the energy difference between singlet and triplet for NiCl₂ complex **I**:



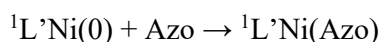
Step b: the reduction steps for the formation of **II**:



Step c: the reduction steps for the formation of a model of **III** without explicit solvation at nickel:



Step d: the formation of the Ni-azo complex **V** starting from **III**:



We used the CCSD(T) method^{17,18} including scalar relativistic effects by using the scalar-relativistic Douglas-Kroll-Hess (DKH) Hamiltonian for one-electron integrals,^{12,13} and the appropriate contracted correlation consistent basis set with correlated core electrons **BS2**. We performed single point calculations by taking the optimized structure for the model system obtained at the TPSSh-D3BJ/Def2SVP level of theory in gas phase. The model system is simplified and we also used the highest symmetry possible in order to reduce the computational costs. Therefore, the phenanthroline ligand has been substituted with (E)-N,N-(ethene-1,2-diyl)dime-thanimine (H_2CNCH)₂ that in this section will be abbreviated with **L'**; the explicit solvent NMP has been replaced by DMF; the azobenzene is modelled with 1,2-dimethyldiazene abbreviated as **Azo**, and the zinc is calculated as an atom in the gas phase. We then compared CCSD(T) electronic energy results with single-point calculations obtained for the same model system with the same structures by using the functionals TPSSh-D3BJ,⁷ B3LYP-D3BJ,^{19,20} BP86-D3BJ,^{19,21} MN15,²² PBEPBE-D3BJ,²³ and M06L²⁴ using the same basis set and relativistic Hamiltonian as the *ab initio* calculations. The obtained results are reported in Table 4.2-4.4

Table 4.2: Electronic energies E_{elec} obtained at the CCSD(T) and DFT level of theory. The empirical correction D3BJ is applied to all the functionals except for MN15 and M06L.

	Point group	CCSD(T)	TPSSh	B3LYP	BP86
¹ L'NiCl ₂	C _{2v}	-2707.533975	-2709.789465	-2709.823685	-2710.143168
³ L'NiCl ₂	C _{2v}	-2707.536065	-2709.792702	-2709.833032	-2710.128207
² L'NiCl	C _{2v}	-2246.333352	-2248.086224	-2248.122173	-2248.399725
¹ L'Ni	C _{2v}	-1785.045298	-1786.296179	-1786.322020	n.c.
¹ L'NiAzo	C ₂	-1974.177667	-1975.839288	-1975.852831	-1976.124238
ZnCl ₂ (DMF) ₂	C _{2v}	-3214.118204	-3216.821503	-3216.899361	-3217.201395
Zn	/	-1795.245770	-1795.862525	-1795.94704	-1796.192508
DMF	/	-248.197918	-248.7363855	-248.7350377	-248.7308431
Azo	/	-189.002452	-189.435526	-189.431795	-189.430383
	Point group	CCSD(T)	MN15	PBEPBE	M06L
¹ L'NiCl ₂	C _{2v}	-2707.533975	-2710.635077	-2708.837184	-2709.566801
³ L'NiCl ₂	C _{2v}	-2707.536065	-2710.615927	-2708.822480	-2709.573423
² L'NiCl	C _{2v}	-2246.333352	-2248.872372	-2247.330435	-2247.895154
¹ L'Ni	C _{2v}	-1785.045298	-1787.016496	n.c.	-1786.137756
¹ L'NiAzo	C ₂	-1974.177667	-1976.326075	-1975.045326	-1975.621579
ZnCl ₂ (DMF) ₂	C _{2v}	-3214.118204	-3217.71202	-3215.56229	-3216.56221
Zn	/	-1795.245770	-1797.188362	-1795.64528	-1795.81139
DMF	/	-248.197918	-248.4579837	-248.419764	-248.667612
Azo	/	-189.002452	-189.206201	-189.185824	-189.378161

Table 4.3: Relative electronic energy in kcal mol⁻¹ for the benchmark steps calculated with the electronic energy of Table 4.2

	ΔE_{elec}	ΔE_{elec}	ΔE_{elec}	ΔE_{elec}	ΔE_{elec}	ΔE_{elec}	ΔE_{elec}
	CCSD(T)	TPSSh	B3LYP	BP86	MN15	PBEPBE	M06L
Step a	1.31	2.03	5.87	-9.39	-12.02	-9.23	4.16
Step b	-22.33	-22.98	-18.99	-28.31	-37.83	-29.30	-18.53
Step c	8.89	6.47	18.05	/	-5.18	/	12.60
Step d	-81.52	-67.51	-62.13	/	-64.87	/	-66.30

Table 4.4: Electronic energy deviation in kcal mol⁻¹ and RMSE (root mean square error) calculated in respect of the CCSD(T) level of theory from data of Tab. S2a.

The color code is green < 3 kcal mol⁻¹; yellow < 5 kcal mol⁻¹; orange < 7 kcal mol⁻¹; red > 7 kcal mol⁻¹.

	ΔE_{elec}	ΔE_{elec}	ΔE_{elec}	ΔE_{elec}	ΔE_{elec}	ΔE_{elec}	ΔE_{elec}
	CCSD(T)	TPSSh	B3LYP	BP86	MN15	PBEPBE	M06L
Step a	0.00	0.72	4.55	-10.70	-13.33	-10.54	2.84
Step b	0.00	-0.65	3.34	-5.98	-15.50	-6.97	3.80
Step c	0.00	-2.42	9.16	/	-14.07	/	3.70
Step d	0.00	14.01	19.39	/	16.65	/	15.22
RMSE	0.00	7.13	11.09	11.51	14.95	11.63	8.18

From these benchmark results, we see first of all that the TPSSh, and M06L functionals account well for the energy differences in the spin-state change Step a and in the redox Steps b and c. B3LYP also provides reasonably accurate results for steps a and b, while the error for Step c is somewhat larger. The GGA functionals BP86 and PBE are less accurate, as is the meta-hybrid MN15. For step a, this is a clear case of the known trend whereby GGA functionals underestimate the stability of the high-spin state.¹⁴ The B3LYP functional appears to slightly overestimate the stability of the high-spin state. The best results are obtained with TPSSh-D3BJ and this motivates our use of this functional in the present study.

All the tested functionals yield less accurate energies for Step d, coordination of Azo with the Ni(0) species to create the V-like complex. This step is highly exothermic, showing the strong interaction between Ni(0) and Azo, confirming, as discussed in the main text, that this complex cannot be understood as involving only ligand to metal coordination. In fact, with the model used in the present benchmarking, this effect is very large, as shown by the change in the Ni-N distances (for N in the L' ligand) between the ¹L'Ni(0) and ¹L'NiAzo species (respectively 1.83 and 1.90 Å), or by the change in N-N bond length between the free Azo and the complex ¹L'Ni-Azo (respectively 1.24 and 1.37 Å). All of this denotes significant electronic donation from Ni to the Azo π^* orbitals. Unfortunately, this seems to create significant multi-reference character in ¹L'NiAzo, which shows up in the CCSD(T) calculations by high values of the T₁ and D₁

diagnostics, of 0.051 and 0.34 respectively. It is frequently argued that values exceeding 0.02 or perhaps 0.05 in the case of T_1 , and 0.15 in the case of D_1 , correlate with poor performance of the CCSD(T) method.²⁵ Accordingly, we consider that the Step d CCSD(T) benchmark is perhaps not completely reliable, and further work would be needed to obtain a reliable reference. As such extensive benchmarking goes beyond the scope of this work, we have here simply assumed that the good performance of TPSSh-D3BJ for the other steps can be taken as evidence to support its accuracy for the whole reactivity study.

4.8.4 Spin state analysis

While CCSD(T) benchmarking of the type reported cannot be carried out for the larger species studied in the main text, it is nevertheless instructive to compare energies predicted by different DFT functionals. In this section we are going to analyze the results of spin state multiplicity for the complexes LNiCl_2 **I**, Ni-dimer **VI**, and the Ni,Zn-heterodimer **X**. The values shown will be electronic and free energy by using the functionals TPSSh-D3BJ, B3LYP-D3BJ and BP86-D3BJ with the basis set **BS2** and relativistic effect.

4.8.4.1 (Phen)NiCl₂ (**I**)

We started the analysis by calculating the complex LNiCl_2 without any explicit solvation to know which spin state corresponds to the ground state. Therefore, we calculated the complex with singlet and triplet multiplicity and the results are reported in Table 4.5. We found that the triplet spin state is more stable for the hybrid functional TPSSh and B3LYP. The opposite result has been obtained by using BP86 as expected from the previous benchmark with CCSD(T). Therefore, the complex LNiCl_2 can be associated to a triplet ground state.

Table 4.5A: Absolute and relative electronic energy for the complex **I** in the singlet and triplet state.

	Electronic energy (/ hartree)		
	TPSSh-D3BJ	B3LYP-D3BJ	BP86-D3BJ
³ I	-3016.249737	-3016.277747	-3016.566464
¹ I	-3016.240606	-3016.263346	-3016.575264
Δ_{1-3}	-0.009131	-0.014401	0.0088
Δ_{1-3} in kcal mol ⁻¹	-5.7	-9.0	5.5

Table 4.5B: Absolute and relative Gibbs free energy for the complex **I** in the singlet and triplet state.

	Gcorr	Gibbs free energy (/ hartree)		
	(363K)	TPSSh-D3BJ	B3LYP-D3BJ	BP86-D3BJ
³I	0.124331	-3016.125406	-3016.153416	-3016.442133
¹I	0.128204	-3016.112402	-3016.135142	-3016.447060
Δ_{1-3}		-0.013004	-0.018274	0.004927
Δ_{1-3} in kcal mol ⁻¹		-8.2	-11.5	3.1

4.8.4.2 Nickel imide dimer **VI**

We now move on to the analysis of the Ni-dimer **VI**. This dimetallic Ni(II) species has 3 accessible multiplicities: singlet, triplet and quintet. The singlet can furthermore either correspond to an open-shell situation with antiparallel spins on the two nickel centres, or a closed-shell situation. All four options have been considered. In Table 4.6 we report the results for electronic and free energy.

Table 4.6A: Absolute and relative electronic energy for the Ni-dimer **VI** in the singlet, triplet, quintet and open-shell singlet states. [a]: $S^2 = 1.5045$

	Electronic energy (/ hartree)		
	TPSSh-D3BJ	B3LYP-D3BJ	BP86-D3BJ
¹VI	-4758.956120	-4758.949685	-4759.475259
³VI	-4758.948366	-4758.949167	-4759.455085
^{1open}VI_a	-4758.939921	-4758.939743	-4759.447670
⁵VI	-4758.936649	-4758.932078	-4759.442074
Δ_{1-1}	0.000000	0.000000	0.000000
Δ_{1-3}	0.007754	0.000519	0.020174
$\Delta_{1-1open}$	0.016199	0.009943	0.027589
Δ_{1-5}	0.019471	0.017608	0.033185
Δ_{1-1} in kcal mol ⁻¹	0.0	0.0	0.0
Δ_{1-3} in kcal mol ⁻¹	4.9	0.3	12.7
$\Delta_{1-1open}$ in kcal mol ⁻¹	10.2	6.2	17.3
Δ_{1-5} in kcal mol ⁻¹	12.2	11.0	20.8

Table 4.6B Absolute and relative Gibbs free energy for the Ni-dimer **VI** in the singlet, triplet, quintet and open-shell singlet states.

	Gcorr	Gibbs free energy (/ hartree)		
	(363K)	TPSSh-D3BJ	B3LYP-D3BJ	BP86-D3BJ
¹ VI	0.461872	-4758.494248	-4758.487813	-4759.013387
³ VI	0.457954	-4758.490412	-4758.491213	-4758.997131
¹ _{open} VI	0.457354	-4758.482567	-4758.482389	-4758.990316
⁵ VI	0.454701	-4758.481948	-4758.477377	-4758.987373
Δ_{1-1}		0.000000	0.000000	0.000000
Δ_{1-3}		0.003836	-0.003399	0.016256
$\Delta_{1-1\text{open}}$		0.011681	0.005425	0.023071
Δ_{1-5}		0.012300	0.010437	0.026014
Δ_{1-1} in kcal mol ⁻¹		0.0	0.0	0.0
Δ_{1-3} in kcal mol ⁻¹		2.4	-2.1	10.2
$\Delta_{1-1\text{open}}$ in kcal mol ⁻¹		7.3	3.4	14.5
Δ_{1-5} in kcal mol ⁻¹		7.7	6.5	16.3

The closed shell singlet form turns out to be the most stable state of dimer **VI** for almost all functionals. The only exception is for the case of free energy differences calculated using B3LYP-D3BJ, which yields a difference of 2.1 kcal mol⁻¹ in favor of the triplet. It should however be noted that even with B3LYP, the singlet is slightly more stable than the triplet in terms of the electronic energies. Therefore, assuming that TPSSh is the most accurate functional for the description of the nickel chemistry under study and that B3LYP overstabilizes the higher spin state, we are tempted to conclude that the singlet state is the ground state of species **VI**.

4.8.4.3 Nickel-zinc imide **X**

The last structure that will be analyzed in this section is the Ni,Zn-heterodimer **X**. This complex contains one Ni(II) metal and one Zn(II) center, connected by an amido group and a chloride group. The ground state can therefore be either a singlet or a triplet with the unpaired electrons located on the Ni center. The results are reported in Table 4.7

Table 4.7A: Absolute and relative electronic energy values for the Ni,Zn-heterodimer **X** in the singlet and triplet state.

	Electronic energy (/ hartree)		
	TPSSh-D3BJ	B3LYP-D3BJ	BP86-D3BJ
¹ X	-5425.081822	-5425.156945	-5425.715974
³ X	-5425.087202	-5425.169775	-5425.713551
Δ_{3-1}	-0.005380	-0.012830	0.002423
Δ_{3-1} in kcal mol ⁻¹	-3.4	-8.1	1.5

Table 4.7B: Absolute and relative Gibbs free energy values for the Ni,Zn-heterodimer **X** in the singlet and triplet state.

	Gcorr	Gibbs free energy (/ hartree)		
	(363K)	TPSSh-D3BJ	B3LYP-D3BJ	BP86-D3BJ
¹ X	0.339405	-5424.742417	-5424.817540	-5425.376569
³ X	0.337065	-5424.750137	-5424.832710	-5425.376486
Δ_{3-1}		-0.007720	-0.015170	0.000083
Δ_{3-1} in kcal mol ⁻¹		-4.8	-9.5	0.1

It is clear that a triplet ground state is the preferred one for the dimer **X** for both TPSSh and B3LYP. However, once again BP86 appears to underestimate the stability of the high spin state as for LNiCl₂ complex **I** previously discussed.

4.8.5 Solvation analysis for the complexes **I**, **II** and **III**

In this section we are going to analyze the results of solvation analysis for the complexes LNiCl₂ **I**, LNiCl **II** and LNi(0) **III**. The values shown will be electronic and free energy by using the functionals TPSSh-D3BJ, B3LYP-D3BJ and BP86-D3BJ with the basis set **BS2**. We used NMP as explicit solvent in order to know the more stable geometry of the 3 complexes under study. For the 3 Ni-complexes we calculated the bis-, mono-, and non- solvated structure and analyzed the final free energy value (Table 4.7). From these results we can notice the general agreement given by the 3 functionals used. The results allow us to conclude that the complexes LNiCl₂ **I** and LNiCl **II** most probably exist in solution without any additional solvent coordination to the nickel center, while the LNi(0) complex **III** appears to prefer bis-solvation. It is also reassuring that for such solvent coordination steps, which involve smaller changes in electronic structure at the metal center than do the redox or spin-state change steps, the different DFT functionals are in quite good agreement.

Table 4.8A: Absolute Gibbs free energy values for the complexes LNiCl₂ **I**, NiCl **II**, and the LNi(0) complex **III** coordinated with 0, 1 and 2 explicit NMP solvent(s).

	Gibbs free energy (/ hartree)		
	TPSSh-D3BJ	B3LYP-D3BJ	BP86-D3BJ
NMP	-326.140182	-326.133708	-326.127637
³ LNiCl ₂ _0NMP	-3016.125406	-3016.153416	-3016.442133
³ LNiCl ₂ _1NMP	-3342.256971	-3342.278711	-3342.558282
³ LNiCl ₂ _2NMP	-3668.390131	-3668.405895	-3668.67897
² LNiCl_0NMP	-2554.404373	-2554.42773	-2554.698846
² LNiCl_1NMP	-2880.535251	-2880.550328	-2880.819082
² LNiCl_2NMP	-3206.651933	-3206.661496	-3206.914005
¹ LNi_0NMP	-2092.598036	-2092.608365	-2092.874358
¹ LNi_1NMP	-2418.764206	-2418.766379	-2419.030131
¹ LNi_2NMP	-2744.904563	-2744.900806	-2745.152474

Table 4.8B: Gibbs free energy values for the complexes LNiCl₂ **I**, NiCl **II**, and the LNi(0) complex **III**, with free NMP molecules to get to a total of 2 NMP moieties for each entry for facile comparison.

	Gibbs free energy (/ hartree)		
	TPSSh-D3BJ	B3LYP-D3BJ	BP86-D3BJ
³ LNiCl ₂ _0NMP	-3668.405771	-3668.420832	-3668.697408
³ LNiCl ₂ _1NMP	-3668.397154	-3668.412419	-3668.685919
³ LNiCl ₂ _2NMP	-3668.390131	-3668.405895	-3668.678970
² LNiCl_0NMP	-3206.684738	-3206.695145	-3206.954121
² LNiCl_1NMP	-3206.675433	-3206.684036	-3206.946720
² LNiCl_2NMP	-3206.651933	-3206.661496	-3206.914005
¹ LNi_0NMP	-2744.878401	-2744.875781	-2745.129633
¹ LNi_1NMP	-2744.904389	-2744.900086	-2745.157768
¹ LNi_2NMP	-2744.904563	-2744.900806	-2745.152474

Table 4.8C: Relative Gibbs free energy values for the complexes LNiCl₂ **I**, NiCl **II**, and the LNi(0) complex **III**. Showing ³LNiCl₂_0NMP, ²LNiCl_0NMP, and ¹LNi_2NMP as more stable structures.

	Gibbs free energy (kcal mol ⁻¹)		
	TPSSh-D3BJ	B3LYP-D3BJ	BP86-D3BJ
³ LNiCl ₂ _0NMP	0.0	0.0	0.0
³ LNiCl ₂ _1NMP	5.4	5.3	7.2
³ LNiCl ₂ _2NMP	9.8	9.4	11.6
² LNiCl_0NMP	0.0	0.0	0.0
² LNiCl_1NMP	5.8	7.0	4.6
² LNiCl_2NMP	20.6	21.1	25.2
¹ LNi_0NMP	16.4	15.7	14.3
¹ LNi_1NMP	0.1	0.5	-3.3
¹ LNi_2NMP	0.0	0.0	0.0

4.9 References

- (1) <https://Webbook.Nist.Gov/Cgi/Inchi?ID=C7440666&Mask=2#Thermo-Condensed>.
- (2) Darù, A.; Hu, X.; Harvey, J. N. Iron-Catalyzed Reductive Coupling of Alkyl Iodides with Alkynes To Yield *Cis* -Olefins: Mechanistic Insights from Computation. *ACS Omega* **2020**, 5 (3), 1586–1594. <https://doi.org/10.1021/acsomega.9b03578>.
- (3) Davis-Gilbert, Z. W.; Wen, X.; Goodpaster, J. D.; Tonks, I. A. Mechanism of Ti-Catalyzed Oxidative Nitrene Transfer in [2 + 2 + 1] Pyrrole Synthesis from Alkynes and Azobenzene. *J. Am. Chem. Soc.* **2018**, 140 (23), 7267–7281. <https://doi.org/10.1021/jacs.8b03546>.
- (4) Liu, Z.; Patel, C.; Harvey, J. N.; Sunoj, R. B. Mechanism and Reactivity in the Morita–Baylis–Hillman Reaction: The Challenge of Accurate Computations. *Phys. Chem. Chem. Phys.* **2017**, 19 (45), 30647–30657. <https://doi.org/10.1039/C7CP06508F>.
- (5) Harvey, J. N.; Himo, F.; Maseras, F.; Perrin, L. Scope and Challenge of Computational Methods for Studying Mechanism and Reactivity in Homogeneous Catalysis. *ACS Catal.* **2019**, 9 (8), 6803–6813. <https://doi.org/10.1021/acscatal.9b01537>.
- (6) Frisch, M. J.; Trucks, G. W.; Schlegel, H. B.; Scuseria, G. E.; Robb, M. A.; Cheeseman, J. R.; Scalmani, G.; Barone, V.; Mennucci, B.; Petersson, G. A.; Nakatsuji, H.; Caricato, M.; Li, X.; Hratchian, H. P.; Izmaylov, A. F.; Bloino, J.; Zheng, G.; Sonnenberg, J. L.; Hada, M.; Ehara, M.; Toyota, K.; Fukuda, R.; Hasegawa, J.; Ishida, M.; Nakajima, T.; Honda, Y.; Kitao, O.; Nakai, H.; Vreven, T.; Montgomery, J. A., Jr.; Peralta, J. E.; Ogliaro, F.; Bearpark, M.; Heyd, J. J.; Brothers, E.; Kudin, K. N.; Staroverov, V. N.; Kobayashi, R.; Normand, J.; Raghavachari, K.; Rendell, A.; Burant, J. C.; Iyengar, S. S.; Tomasi, J.; Cossi, M.; Rega, N.; Millam, N. J.; Klene, M.; Knox, J. E.; Cross, J. B.; Bakken, V.; Adamo, C.; Jaramillo, J.; Gomperts, R.; Stratmann, R. E.; Yazyev, O.; Austin, A. J.; Cammi, R.; Pomelli, C.; Ochterski, J. W.; Martin, R. L.; Morokuma, K.; Zakrzewski, V. G.; Voth, G. A.; Salvador, P.; Dannenberg, J. J.; Dapprich, S.; Daniels, A. D.; Farkas, Ö.; Foresman, J. B.; Ortiz, J. V.; Cioslowski, J.; Fox, D. J. *Gaussian 09, Revision E.01*; Gaussian, Inc., Wallingford, CT, 2009.
- (7) Tao, J.; Perdew, J. P.; Staroverov, V. N.; Scuseria, G. E. Climbing the Density Functional Ladder: Nonempirical Meta–Generalized Gradient Approximation Designed for Molecules and Solids. *Phys. Rev. Lett.* **2003**, 91 (14). <https://doi.org/10.1103/PhysRevLett.91.146401>.
- (8) Staroverov, V. N.; Scuseria, G. E.; Tao, J.; Perdew, J. P. Comparative Assessment of a New Nonempirical Density Functional: Molecules and Hydrogen-Bonded Complexes. *J. Chem. Phys.* **2003**, 119 (23), 12129–12137. <https://doi.org/10.1063/1.1626543>.
- (9) Grimme, S.; Ehrlich, S.; Goerigk, L. Effect of the Damping Function in Dispersion Corrected Density Functional Theory. *J. Comput. Chem.* **2011**, 32 (7), 1456–1465. <https://doi.org/10.1002/jcc.21759>.

-
- (10) Weigend, F.; Ahlrichs, R. Balanced Basis Sets of Split Valence, Triple Zeta Valence and Quadruple Zeta Valence Quality for H to Rn: Design and Assessment of Accuracy. *Phys. Chem. Chem. Phys.* **2005**, *7* (18), 3297. <https://doi.org/10.1039/b508541a>.
- (11) Marenich, A. V.; Cramer, C. J.; Truhlar, D. G. Universal Solvation Model Based on Solute Electron Density and on a Continuum Model of the Solvent Defined by the Bulk Dielectric Constant and Atomic Surface Tensions. *J. Phys. Chem. B* **2009**, *113* (18), 6378–6396. <https://doi.org/10.1021/jp810292n>.
- (12) Douglas, M.; Kroll, N. M. Quantum Electrodynamical Corrections to the Fine Structure of Helium. *Ann. Phys.* **1974**, *82* (1), 89–155. [https://doi.org/10.1016/0003-4916\(74\)90333-9](https://doi.org/10.1016/0003-4916(74)90333-9).
- (13) Hess, B. A. Relativistic Electronic-Structure Calculations Employing a Two-Component No-Pair Formalism with External-Field Projection Operators. *Phys. Rev. A* **1986**, *33* (6), 3742–3748. <https://doi.org/10.1103/PhysRevA.33.3742>.
- (14) Dunning, T. H. Gaussian Basis Sets for Use in Correlated Molecular Calculations. I. The Atoms Boron through Neon and Hydrogen. *J. Chem. Phys.* **1989**, *90* (2), 1007–1023. <https://doi.org/10.1063/1.456153>.
- (15) Wilson, A. K.; Woon, D. E.; Peterson, K. A.; Dunning, T. H. Gaussian Basis Sets for Use in Correlated Molecular Calculations. IX. The Atoms Gallium through Krypton. *J. Chem. Phys.* **1999**, *110* (16), 7667–7676. <https://doi.org/10.1063/1.478678>.
- (16) Balabanov, N. B.; Peterson, K. A. Systematically Convergent Basis Sets for Transition Metals. I. All-Electron Correlation Consistent Basis Sets for the 3d Elements Sc–Zn. *J. Chem. Phys.* **2005**, *123* (6), 064107. <https://doi.org/10.1063/1.1998907>.
- (17) Čížek, J. On the Correlation Problem in Atomic and Molecular Systems. Calculation of Wavefunction Components in Ursell-Type Expansion Using Quantum-Field Theoretical Methods. *J. Chem. Phys.* **1966**, *45* (11), 4256–4266. <https://doi.org/10.1063/1.1727484>.
- (18) Watts, J. D.; Gauss, J.; Bartlett, R. J. Coupled-cluster Methods with Noniterative Triple Excitations for Restricted Open-shell Hartree–Fock and Other General Single Determinant Reference Functions. Energies and Analytical Gradients. *J. Chem. Phys.* **1993**, *98* (11), 8718–8733. <https://doi.org/10.1063/1.464480>.
- (19) Becke, A. D. Density-Functional Exchange-Energy Approximation with Correct Asymptotic Behavior. *Phys. Rev. A* **1988**, *38* (6), 3098–3100. <https://doi.org/10.1103/PhysRevA.38.3098>.
- (20) Becke, A. D. Density-functional Thermochemistry. IV. A New Dynamical Correlation Functional and Implications for Exact-exchange Mixing. *J. Chem. Phys.* **1996**, *104* (3), 1040–1046. <https://doi.org/10.1063/1.470829>.
- (21) Perdew, J. P. Density-Functional Approximation for the Correlation Energy of the Inhomogeneous Electron Gas. *Phys. Rev. B* **1986**, *33* (12), 8822–8824. <https://doi.org/10.1103/PhysRevB.33.8822>.

- (22) Yu, H. S.; He, X.; Li, S. L.; Truhlar, D. G. MN15: A Kohn–Sham Global-Hybrid Exchange–Correlation Density Functional with Broad Accuracy for Multi-Reference and Single-Reference Systems and Noncovalent Interactions. *Chem. Sci.* **2016**, 7 (8), 5032–5051. <https://doi.org/10.1039/C6SC00705H>.
- (23) Perdew, J. P.; Burke, K.; Ernzerhof, M. Generalized Gradient Approximation Made Simple. *Phys. Rev. Lett.* **1996**, 77 (18), 3865–3868. <https://doi.org/10.1103/PhysRevLett.77.3865>.
- (24) Zhao, Y.; Truhlar, D. G. A New Local Density Functional for Main-Group Thermochemistry, Transition Metal Bonding, Thermochemical Kinetics, and Noncovalent Interactions. *J. Chem. Phys.* **2006**, 125 (19), 194101. <https://doi.org/10.1063/1.2370993>.
- (25) Jiang, W.; DeYonker, N. J.; Wilson, A. K. Multireference Character for 3d Transition-Metal-Containing Molecules. *J. Chem. Theory Comput.* **2012**, 8 (2), 460–468. <https://doi.org/10.1021/ct2006852>.

Chapter 5

Exploring reactivity of nickel-imide species
derived from Ni-mediated activation of azo-
benzene

5.1 Introduction

Transition metal imides (also referred to as nitrenes) have been extensively studied,^{1,2} because of their involvement in a variety of organic reactions, such as C-H amination, formation of aziridines and various other reactions.^{3–6} The interest in transition metal imides also includes those based on nickel, both in stoichiometric^{7–11} and catalytic reactions.^{12,13}

The generation of a metal-imide species typically depends on activation of amines with iodine or bromamine-T (either *in situ* or *ex situ*), or the use of azides. While great progress in synthetic chemistry and mechanistic understanding has been made using these methods, they also have some downsides.

The use of amines activated by oxidants leads to a considerable production of waste byproducts (e.g., reduced forms of oxidants). Moreover, the strategy puts restraints on the type of N-H functionality that can be used in the reaction, as electron-withdrawing groups like sulfones or carbonyls are often needed to be connected directly to the activated nitrogen. Only recently has this strategy for nitrene formation been applied to simple anilines.¹⁴

Using azides allows for a wider substrate scope. The byproduct for imide formation from an azide, dinitrogen, is traceless, so the reaction itself provides better atom economy. However, the relatively facile and highly exergonic release of dinitrogen from the azide¹⁵ make them hazardous compounds to work with in terms of synthesis, storage and application. This means their application on industrial scale can only be done after considerable safety testing^{16,17} and may require additional safety measures,¹⁸ thus increasing the cost. It may also occur that no conditions can be found that allow the process to be sufficiently safe, forcing the search for an alternative reaction pathway.¹⁹

In chapters 3 and 4 we have provided evidence that azobenzene can serve as a precursor to a nickel imide. Azobenzene as an imide precursor would provide 100% atom efficiency from the perspective of the substrates. Moreover, azobenzene and its derivatives are stable solid compounds unassociated with any extraordinary hazards. These compounds are readily available through reduction of nitroarenes^{20,21} or oxidation of anilines^{22,23} and can be modified after their preparation.²⁴ Thus, expanding the application of an nickel imide intermediates generated from azobenzene could be highly impactful. This chapter outlines our attempts at a variety of metal imide based chemistry using azobenzene as starting material.

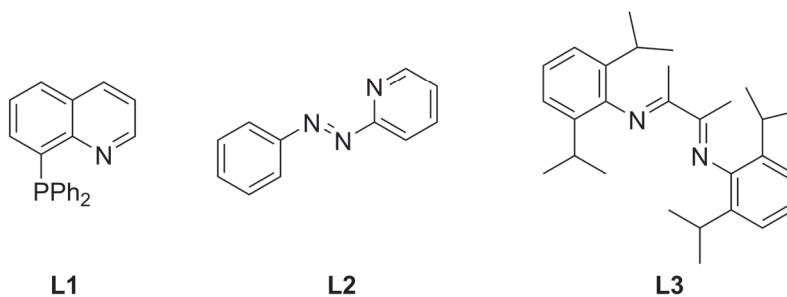
5.2 Ligand considerations

The reaction intermediate generated from **7^F**, (DME)NiCl₂, phenanthroline and Zn, proposed to be a nickel imide dimer **VI_2Zn**, reacts very poorly with carbon monoxide and *tert*-butylisonitrile, and is inert to trimethylphosphine and styrene, even though these reagents are generally good substrates for nickel imide reactivity.^{8,11}

One possible reason for this poor reactivity is the ligation on the nickel. In chapter 4 we demonstrated that Zn is unable to reduce (phen)Ni^ICl (**II**). This indicates that naked (phen)Ni(0) is highly unstable and should therefore also be difficult to generate from the nickel imide with a reducing substrate, like the ones described above. We have therefore considered several ligands besides 1,10-phenanthroline and 4,4'-bipyridine in our reactivity screening (Scheme 5.1).

Since Hillhouse's diphosphine nickel imide seems to favour elimination of azobenzene to form Ni(0)¹⁰ and 1,10-diphenanthroline seems to have difficulty facilitating a return to Ni(0) from a nickel imide, a mixed phosphine-imine ligand like **L1** might be a good mix between the two to facilitate both halves of the catalytic cycle. **L2**²⁵ and **L3**²⁶ are known to be capable of redox non-innocent behaviour. This may attenuate the difficulty of returning to low-valent nickel from the imide complex by allowing excess electron density to be stored on the ligand.

Scheme 5.1: Ligands used in this chapter to ease formation of Ni(0) from the nickel imide

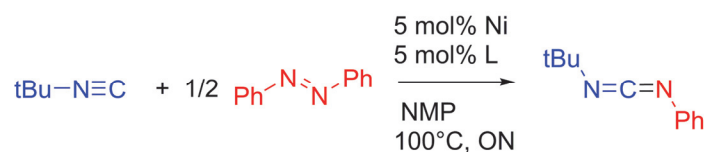


5.3 Reaction with isonitrile

The reaction between imides and isocyanides can lead to carbodiimides (Scheme 5.2). This compound class is useful because they can function as useful precursors in both small molecule²⁷ and polymer synthesis.²⁸ The reactivity was screened with phen, **L1** and **L2** and with either Ni(COD)₂, or (DME)NiCl₂ combined with reductant Zn or CoCp₂, as nickel source. Under all these conditions, carbodiimide product was observed in trace quantities at best and

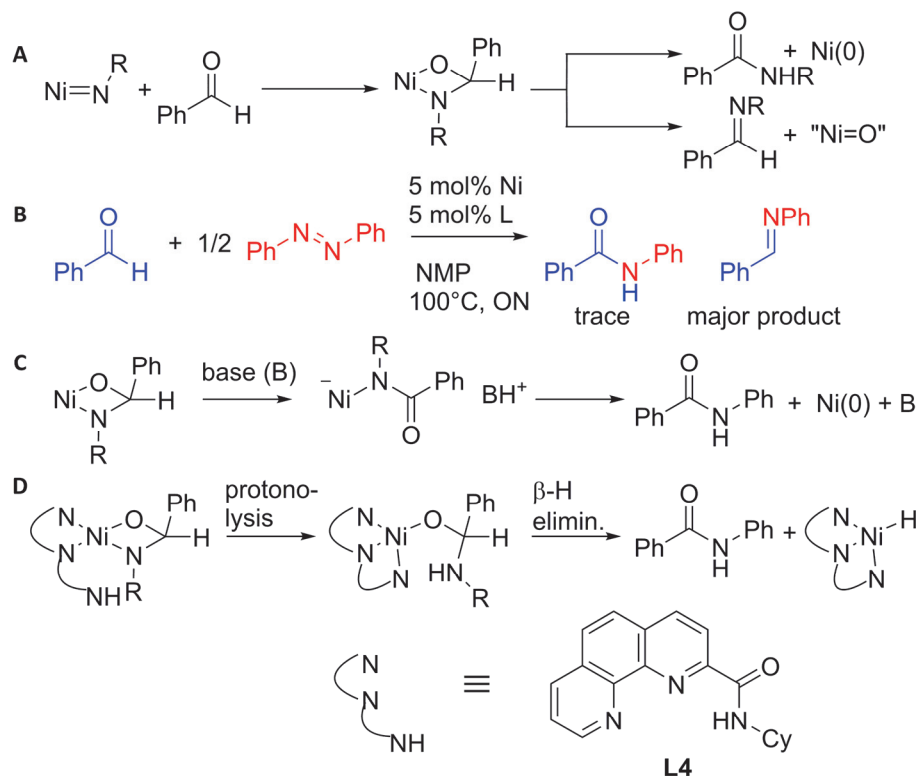
the azobenzene conversion was minimal. Although there are still plenty of options available for further screening, we consider it likely that the reason for the lack of reactivity is the poisoning of a low-valent nickel ion by a strongly pi-acidic isonitriles, rendering the nickel incapable of azobenzene activation. This poisoning is difficult to overcome and since the reaction has already been realized by titanium catalysis,²⁹ we abandoned the project.

Scheme 5.2: Tested reaction between tert-butylisonitrile and azobenzene



5.4 Amidation of aldehydes

Scheme 5.3: (A) Literature basis and (B-D) reaction design of C-H amination for aldehydes with azobenzene



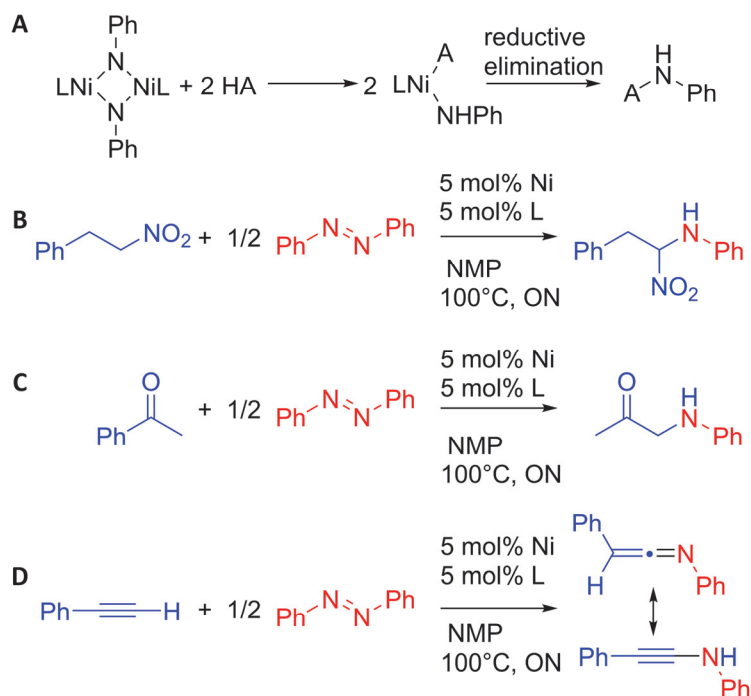
Addition of an aldehyde to nickel imide can lead to an aza oxy nickel cyclobutane.¹⁰ Such a species is capable of elimination of amide, or imine, depending on the conditions (Scheme 5.3A).³⁰ Thus, it may be possible to couple azoarenes with aldehydes to form amides. The direct

synthesis of amides from aldehydes is a widely explored field in organic chemistry. However, the methods for substituted amides generally require a stoichiometric amount of oxidant for reaction between an amine and an aldehyde. By employing azoarenes rather than amines, the oxidation of amine has already been done before the reaction, potentially increasing the substrate scope.

From reactions under the conditions we screened with either $\text{Ni}(\text{COD})_2$, or $(\text{DME})\text{NiCl}_2$ with substoichiometric Zn and phen, or **L1-3** as ligands, only trace amounts of the desired amide were detected. The major product was an imine (Scheme 5.3B). In principle, the selectivity might be influenced by a base (Scheme 5.3C). However, screening of several bases with 1,10-phenanthroline as ligand gave no observable change in selectivity for the amide formation. Finally, it was considered that a ligand design with proton shuttle could facilitate beta-hydride elimination by relieving the ring strain of the aza oxy nickel cyclobutane (Scheme 5.3D). Unfortunately, **L5** did not prove to be capable of steering the selectivity towards the desired amide.

5.5 C-H amination at acidic positions

Scheme 5.4: (A) Hypothetical mechanism and (B-D) test reactions for acidic C-H amination



The proposed nickel imide dimer intermediate proved too difficult to isolate (see Chapter 3). One of the frequently observed products in our attempts to synthesize this intermediate was aniline. This may indicate that the intermediate is easily protonated, so it may be considered rather basic. Possibly, this basicity can be taken advantage of, if the product of the acid base reaction can effect formation of a new bond through reductive elimination (Scheme 5.4A).

5.5.1 α -Amination of nitroalkane

The α -position of nitroalkanes is among the most acidic carbon groups. Hence, it may be suitable for our acidic C-H amination approach, forming underexplored α -nitroamines (Scheme 5.4B).

Unfortunately, the reaction between 1-phenyl-2-nitroethane and azobenzene yields no desired product and only limited azobenzene conversion. Among the products were 2-phenylacetaldehyde and 2-phenylacetaldehyde oxime, which are typical products from aliphatic nitroreduction.^{31,32} It therefore seems that the highly reductive nickel species used for the activation of azoarenes preferentially reduces the nitro moiety, making the desired α -amination unachievable.

5.5.2 Ketone α -amination

α -amino carbonyls are a useful moiety in medicinal chemistry, which has led to considerable effort in developing α -amination reactions.³³ The relatively acidic α -carbonyl protons could be a good candidate for C-H amination with the basic nickel imide dimer, thus facilitating a new route for α -amination (Scheme 5.4C).

However, under the studied conditions (either Ni(COD)₂ or (DME)NiCl₂ with zinc as nickel source and phen, or **L1-3** as ligand), no formation of the target product was observed. Instead, various products resulting from aldol condensation were observed. This reactivity is considerably hampered when the reaction is performed in absence of azobenzene. It therefore seems that the nickel imide intermediate might form and even act as a base, but that the resulting enolate reacts faster with a ketone than with the amide nitrogen on nickel.

5.5.3 Amination of terminal alkynes

If the nickel diimide is basic enough to deprotonate the terminal hydrogen of alkynes, it may be possible to generate aminoalkynes, which can tautomerize to ketenimines (Scheme 5.4D). Keteneimines are versatile reagents that can be trapped in a myriad of ways, but generally require decomposition of a stable precursor since they are too reactive to isolate.^{34,35} *In situ* formation of ketenimines by cross-coupling between terminal alkynes and azoarenes would therefore be a considerable advance in the field. Moreover, hydrolysis of ketenimines formed in the absence of trapping agents leads to the formation of an amide.³⁶ The azobenzene-acetylene cross coupling could therefore also be a pathway to amides from unorthodox precursors.

The reaction was attempted with both Ni(COD)_2 and $(\text{DME})\text{NiCl}_2$ with Zn as nickel sources and phenanthroline, **L1** and **L2** as ligands. In all cases, azobenzene conversion was low, while phenylacetylene was completely consumed. No product related to aminoalkynes were observed in GC/MS, but 2 isomers of triphenylbenzene were observed. Apparently, the well-established cyclotrimerization of alkynes³⁷ is more facile than the reductive splitting of azoarenes. The envisioned cross coupling between terminal alkynes and azoarenes therefore seems to be inaccessible.

5.6 Benzylic C-H amination

Arguably the most useful application of transition metal imides is their ability to affect C-H amination at relatively inert positions, which allows to build up molecular complexity from simple starting materials.⁴ DFT calculations predict that C-H amination with azoarene as nitrogen source is exergonic (Scheme 5.5A) and may therefore be attainable.

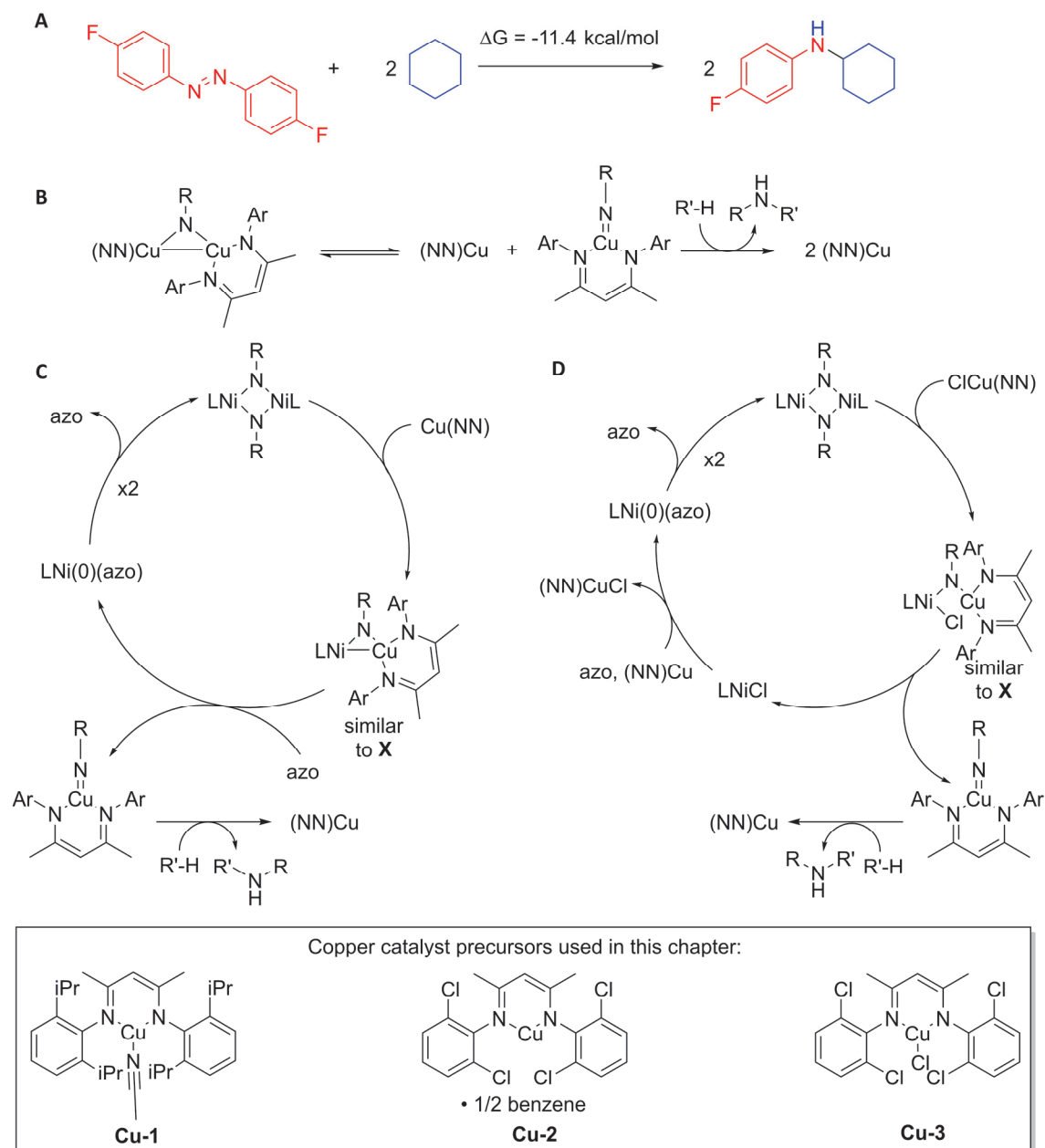
Since chapter 4 revealed that ZnCl_2 can bind the imide and reorganize to make nickel-zinc bimetallic imide complex (*e.g.* **X**). We reasoned that similar reactivity may occur with different metal complexes than ZnCl_2 and thereby create complexes capable of C-H amination.

Warren has developed copper(I) diketiminate complexes capable of C-H amination.³⁸ Mechanistic studies have shown a dicopper complex bridged by an imide is formed under catalytic conditions, which is in equilibrium with a copper imide monomer that is responsible for the C-H activation (Scheme 5.5B).

Such an equilibrium may also be envisioned for nickel-copper bimetallic imide complexes

similar to **X** to give the aminating copper nitrene complex and either the Ni(0) azobenzene adduct (Scheme 5.5C) or the Ni(I) chloride complex (Scheme 5.6D), depending on the copper ketimine precursor.

Scheme 5.5: (A) Calculated reaction free energy for C-H amination with azobenzene as nitrogen source. (B) mechanism of copper catalysed C-H amination reported by Warren. (C and D) envisioned mechanistic cycles for C-H amination with azobenzene as nitrogen source through nickel-copper cocatalysis.



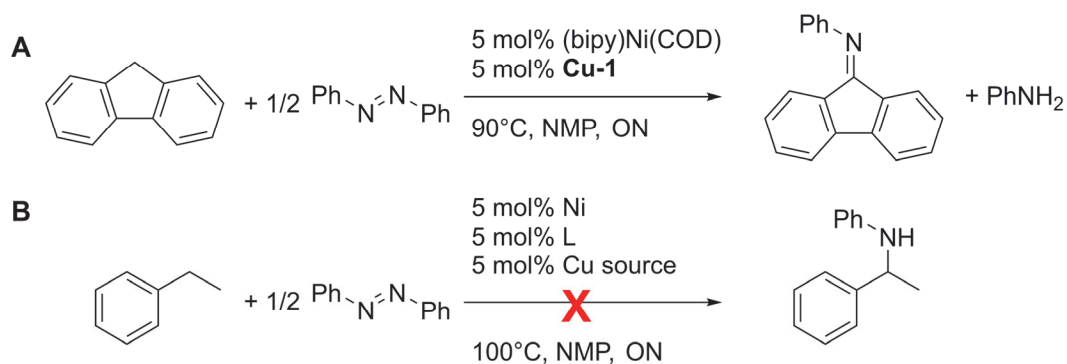
First, the amination of fluorene was attempted, as it has a particularly weak C-H bond strength (79.5 kcal/mol).³⁹ Both azobenzene and fluorene are converted to a considerable extent (respectively 93% and 87%) and N-phenyl-9H-fluoren-9-imine was observed as a product with GC/MS at an estimated 28% yield alongside aniline (Scheme 5.6A). Although an overoxidized imine was observed rather than the target amine, the successful C-H functionalization was encouraging.

Next, we considered the C-H amination of ethylbenzene. This substrate has a higher C-H bond strength (85.4 ± 1.5 kcal/mol),⁴⁰ which may help prevent the overoxidation observed for fluorene. Moreover, amination of substrates like ethylbenzene is more likely synthetically useful than the amination of fluorene.

Unfortunately, no conversion of ethylbenzene, or product formation was observed when **Cu-1** or **Cu-2** were used as catalysts. The failure with **Cu-2** is especially disappointing, since this is the best catalyst reported by Warren and is capable of amination of toluene with aryl azides.⁴¹ This indicates that no monometallic copper nitrene species can be formed under our conditions. The oxidation of fluorene may instead have been effected by a dimetallic complex that cannot react with substrates containing stronger C-H bonds.

Reasoning that the formation of a formally zerovalent nickel complex and a formally trivalent copper imide complex from the dimetallic complex (Scheme 5.5C) might be particularly difficult, we turned to **Cu-3** as spreading out the reduction of nickel over multiple steps (Scheme 5.6D) might lead to lower energy barriers. Unfortunately, no target product could be obtained with this precatalyst either. Thus, we were unable to find conditions for C-H amination of mildly activated positions with azobenzene as nitrogen source, despite the calculated favourable thermodynamics and the promising reaction with fluorene.

Scheme 5.6: Benzylic C-H amination using nickel-copper cocatalysis.



5.7 Discussion & Conclusion

In this chapter, we have explored several ways of converting azobenzene with nickel imides as catalytic intermediates in mind. Although our screening was somewhat superficial, some lessons may be drawn from our efforts.

On the one hand, it appears that there is a price to be paid for the highly reductive nature of the nickel catalyst that is required for the azobenzene splitting: several reactants appear to be incompatible with our system, either because they are prone to poison the electron rich nickel catalyst (isonitriles), or because they are preferentially reduced over azobenzene (alkynes, nitroalkanes), hindering the nickel imide formation.

On the other hand, two of the attempted reactions show some promise, although we failed to find reasonable conditions with our limited screening efforts. The reaction between benzaldehyde and azobenzene does generate some of the desired amide, but the reaction selectivity is towards imination. As imine formation does not regenerate the catalyst, it should be strongly suppressed. We suggest a better understanding of the factors influencing the selectivity should be obtained through studies with model complexes and theoretical calculations before further screening can be done.

The calculation of thermodynamics suggest that C-H amination could be feasible and our results with fluorene provide some reassurance that the bimetallic reaction design could be a fruitful strategy. However, synthetically useful substrates for C-H amination, like ethylbenzene, proved too inert for our catalytic system. Possibly, moving from copper to cobalt as the cocatalyst would be a useful future endeavour, as some Co(III) imides are known to be capable of C-H amination,^{42,43} and the more reductive nature of cobalt compared to copper might facilitate splitting the dimetallic complex as proposed in Scheme 5.5C and 5.5D.

Overall, it appears the activation of azobenzene by nickel does indeed have potential for application in a wider range of synthetic chemistry, but the realization of this potential will require a considerable amount of research effort.

5.8 Experimental

5.8.1 Computational details

Computations were performed using density functional theory (DFT) and the Gaussian 16 rev A03 program package.⁴⁴ Geometry optimization was performed employing the hybrid functional B3LYP⁴⁵ including the D3 empirical dispersion correction with Becke and Johnson damping D3BJ,⁴⁶ together with the 6-31g basis set⁴⁷ on all atoms. Vibrational frequency calculations were performed at the same level of theory as used for optimization and used to verify the nature of the stationary points as minima. Free energy corrections were applied to the electronic energy and calculated based on the calculated rotational constants and vibrational frequencies, using the quasi-harmonic correction for small vibrational frequencies, with the cut-off set at 100 cm⁻¹ (G_{corr}).⁴⁸ The final Gibbs free energy value is obtained by $G = E_{\text{elec}} + G_{\text{corr}}$, where E_{elec} is the energy obtained with B3LYP-D3BJ as described above.

5.8.2 Equipment

GC/MS was measured on an Agilent 7890B GC coupled to an Agilent 5977B Mass Spectrometer equipped with an Agilent J&W DB-5MS Ultra Inert column with 0.25 mm internal diameter. NMR spectra were recorded on a Bruker Avance 400 Spectrometer. ¹H and ¹³C{¹H} chemical shifts were referenced internally to residual solvent signals. HRMS measurements were performed at the EPFL ISIC Mass Spectrometry Service. Liquid chromatography was performed with a Biotage Isolera One flash purification system.

5.8.3 Materials

Anhydrous NMP stored over molecular sieves was purchased from Acros and stored in a glove box. Anhydrous 1,10-phenanthroline, (DME)NiCl₂, zinc, azobenzene, *tert*-butylisonitrile, benzaldehyde, acetophenone, phenylacetylene, fluorene and cyclohexylamine were purchased from commercial sources and used without further purification. Ethylbenzene was purchased from Fluka and degassed by bubbling through N₂ before storing it in the glove box. **L1**,⁴⁹ **L2**,⁵⁰

L3,⁵¹ 1-phenyl-2-nitroethane,⁵² (bipy)Ni(COD),⁵³ **Cu-1**,⁵⁴ **Cu-2**,⁵⁵ **Cu-3**⁵⁶ and 1,10-phenanthroline-carbonyl chloride⁵⁷ were prepared according to literature procedures.

5.8.4 Synthesis N-cyclohexyl-1,10-phenanthroline-2-carboxamide (**L4**)

1,10-phenanthroline-carbonyl chloride (761 mg, 3.14 mmol) was suspended in 21 mL DCM in the glove box in a heat-gun dried Schlenk flask. Outside of the glove box, cyclohexylamine (1.0 mL, 8.8 mmol) was added under nitrogen flow, quickly turning the mixture red-brown. The Schlenk flask was then closed and the mixture was heated to 40°C for 11 hours. A white solid was filtered off under air and washed with DCM. The filtrate was evaporated and the residue was purified by liquid chromatography with 4 CV DCM, then a ramp to 20% MeOH in DCM. The collected material was recrystallized from DCM/hexane to yield a light brown powder. Yield: 135 mg, 14%. ¹H NMR (400 MHz, Chloroform-*d*) δ 9.13 (dd, *J* = 4.5, 1.7 Hz, 1H), 9.08 (d, *J* = 8.6 Hz, 1H), 8.59 (d, *J* = 8.2 Hz, 1H), 8.39 (d, *J* = 8.3 Hz, 1H), 8.30 (dd, *J* = 8.0, 1.7 Hz, 1H), 7.86 (s, 2H), 7.69 (dd, *J* = 8.1, 4.4 Hz, 1H), 4.06 (qd, *J* = 11.1, 4.1 Hz, 1H), 2.19 – 2.04 (m, 2H), 1.81 (dd, *J* = 12.0, 4.5 Hz, 2H), 1.68 (d, *J* = 12.4 Hz, 1H), 1.61 – 1.33 (m, 4H), 1.31 – 1.16 (m, 1H). ¹³C NMR (101 MHz, CDCl₃) δ 163.78, 150.72, 150.03, 145.91, 144.45, 137.54, 136.78, 130.19, 129.24, 127.84, 126.76, 123.52, 121.81, 49.26, 33.16, 25.80, 25.52. HRMS (ESI/QTOF) *m/z*: [M + H]⁺ Calcd for C₁₉H₂₀N₃O⁺ 306.1601; Found 306.1595.

5.8.5 Screening with Ni(II)

In the glove box, (DME)NiCl₂ (2.7 mg, 5 mol%), ligand (5 mol%), Zn (4.9 mg, 30 mol%), 0.2 mL NMP and TMSCl (1 μL, 3.2 mol%) were added to an oven dried vial. After mixing for a couple of minutes, 0.3 mL of an NMP stock solution containing azobenzene (0.417 M, 0.5 eq.), the second substrate (0.833 M, 1 eq.) and naphthalene as internal standard (0.167 M, 0.2 eq.) was added. The vial was then closed with a PTFE-lined cap and set to stir on a pre-heated heating plate. After stirring overnight, the mixture was allowed to cool down, before taking an aliquot to analyse the mixture with GC/MS. The stock solution was freshly prepared every time

a new set of reactions was set up. Substrate conversion was determined by comparing the substrate to internal standard ratio between the reaction mixture sample and a sample made by diluting the remaining stock solution.

5.8.6 Screening with Ni(0)

In the glove box, Ni(COD)₂ (3.4 mg, 5 mol%), ligand (5 mol%) and 0.2 mL NMP were added to an oven dried vial. After mixing for a couple of minutes, 0.3 mL of an NMP stock solution containing azobenzene (0.417 M, 0.5 eq.), the second substrate (0.833 M, 1 eq.) and naphthalene as internal standard (0.167 M, 0.2 eq.) was added. The vial was then closed with a PTFE-lined cap and set to stir on a pre-heated heating plate. After stirring overnight, the mixture was allowed to cool down, before taking an aliquot to analyse the mixture with GC/MS. The stock solution was freshly prepared every time a new set of reactions was set up. Substrate conversion was determined by comparing the substrate to internal standard ratio between the reaction mixture sample and a sample made by diluting the remaining stock solution.

5.8.7 Screening nickel-copper cocatalysis

In the glove box, Ni(COD)₂ (3.4 mg, 5 mol%), ligand (5 mol%) and 0.2 mL NMP were added to an oven dried vial. After mixing for a couple of minutes, 0.3 mL of an NMP stock solution containing azobenzene (0.417 M, 0.5 eq.), the second substrate (0.833 M, 1 eq.) and naphthalene as internal standard (0.167 M, 0.2 eq.) was added. The copper precatalyst (5 mol%) was then added. The vial was then closed with a PTFE-lined cap and set to stir on a pre-heated heating plate. After stirring overnight, the mixture was allowed to cool down, before taking an aliquot to analyse the mixture with GC/MS. The stock solution was freshly prepared every time a new set of reactions was set up. Substrate conversion was determined by comparing the substrate to internal standard ratio between the reaction mixture sample and a sample made by diluting the remaining stock solution.

5.9 References

- (1) Ray, K.; Heims, F.; Pfaff, F. F. Terminal Oxo and Imido Transition-Metal Complexes of Groups 9–11. *Eur. J. Inorg. Chem.* **2013**, 2013 (22–23), 3784–3807. <https://doi.org/10.1002/ejic.201300223>.
- (2) Kawakita, K.; Parker, B. F.; Kakiuchi, Y.; Tsurugi, H.; Mashima, K.; Arnold, J.; Tonks, I. A. Reactivity of Terminal Imido Complexes of Group 4–6 Metals: Stoichiometric and Catalytic Reactions Involving Cycloaddition with Unsaturated Organic Molecules. *Coord. Chem. Rev.* **2020**, 407, 213118. <https://doi.org/10.1016/j.ccr.2019.213118>.
- (3) Kuijpers, P. F.; van der Vlugt, J. I.; Schneider, S.; de Bruin, B. Nitrene Radical Intermediates in Catalytic Synthesis. *Chem. - Eur. J.* **2017**, 23 (56), 13819–13829. <https://doi.org/10.1002/chem.201702537>.
- (4) Müller, P.; Fruit, C. Enantioselective Catalytic Aziridinations and Asymmetric Nitrene Insertions into CH Bonds. *Chem. Rev.* **2003**, 103 (8), 2905–2920. <https://doi.org/10.1021/cr020043t>.
- (5) Uchida, T.; Katsuki, T. Asymmetric Nitrene Transfer Reactions: Sulfimidation, Aziridination and C–H Amination Using Azide Compounds as Nitrene Precursors: Asymmetric Nitrene Transfer Reactions Using Azides. *Chem. Rec.* **2014**, 14 (1), 117–129. <https://doi.org/10.1002/tcr.201300027>.
- (6) Darses, B.; Rodrigues, R.; Neuville, L.; Mazurais, M.; Dauban, P. Transition Metal-Catalyzed Iodine(III)-Mediated Nitrene Transfer Reactions: Efficient Tools for Challenging Syntheses. *Chem. Commun.* **2017**, 53 (3), 493–508. <https://doi.org/10.1039/C6CC07925C>.
- (7) Laskowski, C. A.; Miller, A. J. M.; Hillhouse, G. L.; Cundari, T. R. A Two-Coordinate Nickel Imido Complex That Effects C–H Amination. *J. Am. Chem. Soc.* **2011**, 133 (4), 771–773. <https://doi.org/10.1021/ja1101213>.
- (8) Kogut, E.; Wiencko, H. L.; Zhang, L.; Cordeau, D. E.; Warren, T. H. A Terminal Ni(III)–Imide with Diverse Reactivity Pathways. *J. Am. Chem. Soc.* **2005**, 127 (32), 11248–11249. <https://doi.org/10.1021/ja0533186>.
- (9) Dong, Y.; Lukens, J. T.; Clarke, R. M.; Zheng, S.-L.; Lancaster, K. M.; Betley, T. A. Synthesis, Characterization and C–H Amination Reactivity of Nickel Iminyl Complexes. *Chem. Sci.* **2020**, 11 (5), 1260–1268. <https://doi.org/10.1039/C9SC04879K>.
- (10) Mindiola, D. J.; Waterman, R.; Iluc, V. M.; Cundari, T. R.; Hillhouse, G. L. Carbon–Hydrogen Bond Activation, C–N Bond Coupling, and Cycloaddition Reactivity of a Three-Coordinate Nickel Complex Featuring a Terminal Imido Ligand. *Inorg. Chem.* **2014**, 53 (24), 13227–13238. <https://doi.org/10.1021/ic5026153>.

-
- (11) Waterman, R.; Hillhouse, G. L. Group Transfer from Nickel Imido, Phosphinidene, and Carbene Complexes to Ethylene with Formation of Aziridine, Phosphirane, and Cyclopropane Products. *J. Am. Chem. Soc.* **2003**, *125* (44), 13350–13351. <https://doi.org/10.1021/ja0381914>.
- (12) Laskowski, C. A.; Hillhouse, G. L. Group-Transfer Reactions of Ni(II)–Ni(II) Bridging Imido Complexes. Catalytic Formation of Carbodiimides and Isocyanates via Nitrene Transfer from Organoazides. *Organometallics* **2009**, *28* (20), 6114–6120. <https://doi.org/10.1021/om900783u>.
- (13) Wiese, S.; Aguila, M. J. B.; Kogut, E.; Warren, T. H. β -Diketiminato Nickel Imides in Catalytic Nitrene Transfer to Isocyanides. *Organometallics* **2013**, *32* (8), 2300–2308. <https://doi.org/10.1021/om300909n>.
- (14) Deng, T.; Mazumdar, W.; Ford, R. L.; Jana, N.; Izar, R.; Wink, D. J.; Driver, T. G. Oxidation of Nonactivated Anilines to Generate *N*-Aryl Nitrenoids. *J. Am. Chem. Soc.* **2020**, *142* (9), 4456–4463. <https://doi.org/10.1021/jacs.9b13599>.
- (15) Tsuritani, T.; Mizuno, H.; Nonoyama, N.; Kii, S.; Akao, A.; Sato, K.; Yasuda, N.; Mase, T. Efficient Synthesis of 1,4-Diaryl-5-Methyl-1,2,3-Triazole, A Potential MGlur1 Antagonist, and the Risk Assessment Study of Arylazides. *Org. Process Res. Dev.* **2009**, *13* (6), 1407–1412. <https://doi.org/10.1021/op900062p>.
- (16) Wallace, D. J.; Baxter, C. A.; Brands, K. J. M.; Bremeyer, N.; Brewer, S. E.; Desmond, R.; Emerson, K. M.; Foley, J.; Fernandez, P.; Hu, W.; Keen, S. P.; Mullens, P.; Muzzio, D.; Sajonz, P.; Tan, L.; Wilson, R. D.; Zhou, G.; Zhou, G. Development of a Fit-for-Purpose Large-Scale Synthesis of an Oral PARP Inhibitor. *Org. Process Res. Dev.* **2011**, *15* (4), 831–840. <https://doi.org/10.1021/op2000783>.
- (17) González-Bobes, F.; Kopp, N.; Li, L.; Deerberg, J.; Sharma, P.; Leung, S.; Davies, M.; Bush, J.; Hamm, J.; Hrytsak, M. Scale-up of Azide Chemistry: A Case Study. *Org. Process Res. Dev.* **2012**, *16* (12), 2051–2057. <https://doi.org/10.1021/op3002646>.
- (18) Hagenbuch, J.-P. Opportunities and Limits of the Use of Azides in Industrial Production. Implementation of Safety Measures. *Chim. Int. J. Chem.* **2003**, *57* (12), 773–776. <https://doi.org/10.2533/000942903777678434>.
- (19) Wilson, R. D.; Cleator, E.; Ashwood, M. S.; Bio, M. M.; Brands, K. M. J.; Davies, A. J.; Dolling, U.-H.; Emerson, K. M.; Gibb, A. D.; Hands, D.; McKeown, A. E.; Oliver, S. F.; Reamer, R. A.; Sheen, F. J.; Stewart, G. W.; Zhou, G. X. Development of a Scaleable Synthesis of a Partial Nicotinic Acid Receptor Agonist. *Org. Process Res. Dev.* **2009**, *13* (3), 543–547. <https://doi.org/10.1021/op800290t>.
- (20) Sakai, N.; Fujii, K.; Nabeshima, S.; Ikeda, R.; Konakahara, T. Highly Selective Conversion of Nitrobenzenes Using a Simple Reducing System Combined with a Trivalent Indium Salt and a Hydrosilane. *Chem. Commun.* **2010**, *46* (18), 3173. <https://doi.org/10.1039/c000383b>.
- (21) Gund, S. H.; Shelkar, R. S.; Nagarkar, J. M. An Efficient Catalyst-Free and Chemoselective Synthesis of Azobenzenes from Nitrobenzenes. *RSC Adv* **2014**, *4* (81), 42947–42951. <https://doi.org/10.1039/C4RA06027J>.

- (22) Zhang, C.; Jiao, N. Copper-Catalyzed Aerobic Oxidative Dehydrogenative Coupling of Anilines Leading to Aromatic Azo Compounds Using Dioxygen as an Oxidant. *Angew. Chem. Int. Ed.* **2010**, *49* (35), 6174–6177. <https://doi.org/10.1002/anie.201001651>.
- (23) Antoine John, A.; Lin, Q. Synthesis of Azobenzenes Using *N*-Chlorosuccinimide and 1,8-Diazabicyclo[5.4.0]Undec-7-Ene (DBU). *J. Org. Chem.* **2017**, *82* (18), 9873–9876. <https://doi.org/10.1021/acs.joc.7b01530>.
- (24) Deng, H.; Li, H.; Wang, L. *Ortho* -Heteroarylation of Azobenzenes by Rh-Catalyzed Cross-Dehydrogenative Coupling: An Approach to Conjugated Biaryls. *Org. Lett.* **2016**, *18* (13), 3110–3113. <https://doi.org/10.1021/acs.orglett.6b01277>.
- (25) Matson, B. D.; McLoughlin, E. A.; Armstrong, K. C.; Waymouth, R. M.; Sarangi, R. Effect of Redox Active Ligands on the Electrochemical Properties of Manganese Tricarbonyl Complexes. *Inorg. Chem.* **2019**, *58* (11), 7453–7465. <https://doi.org/10.1021/acs.inorgchem.9b00652>.
- (26) Pappas, I.; Treacy, S.; Chirik, P. J. Alkene Hydrosilylation Using Tertiary Silanes with α -Diimine Nickel Catalysts. Redox-Active Ligands Promote a Distinct Mechanistic Pathway from Platinum Catalysts. *ACS Catal.* **2016**, *6* (7), 4105–4109. <https://doi.org/10.1021/acscatal.6b01134>.
- (27) Zhang, W.-X.; Hou, Z. Catalytic Addition of Alkyne C–H, Amine N–H, and Phosphine P–H Bonds to Carbodiimides: An Efficient Route to Propiolamidines, Guanidines, and Phosphaguanidines. *Org. Biomol. Chem.* **2008**, *6* (10), 1720. <https://doi.org/10.1039/b800135a>.
- (28) Kennemur, J. G.; Novak, B. M. Advances in Polycarbodiimide Chemistry. *Polymer* **2011**, *52* (8), 1693–1710. <https://doi.org/10.1016/j.polymer.2011.02.040>.
- (29) Beaumier, E. P.; McGreal, M. E.; Pancoast, A. R.; Wilson, R. H.; Moore, J. T.; Graziano, B. J.; Goodpaster, J. D.; Tonks, I. A. Carbodiimide Synthesis via Ti-Catalyzed Nitrene Transfer from Diazenes to Isocyanides. *ACS Catal.* **2019**, *9* (12), 11753–11762. <https://doi.org/10.1021/acscatal.9b04107>.
- (30) Desnoyer, A. N.; Chiu, W.; Cheung, C.; Patrick, B. O.; Love, J. A. Oxaziridine Cleavage with a Low-Valent Nickel Complex: Competing C–O and C–N Fragmentation from Oxazanicela(II)Cyclobutanes. *Chem. Commun.* **2017**, *53* (92), 12442–12445. <https://doi.org/10.1039/C7CC07690H>.
- (31) Johnson, Kenneth.; Degering, Ed. F. The Utilization of Aliphatic Nitro Compounds. (I) The Production of Amines and (II) The Production of Oximes. *J. Am. Chem. Soc.* **1939**, *61* (11), 3194–3195. <https://doi.org/10.1021/ja01266a061>.
- (32) Ohe, K.; Uemura, S. Sodium Arenetellurolate-Catalyzed Reduction of Nitroalkanes to Oximes. *Heteroat. Chem.* **1991**, *2* (4), 507–511. <https://doi.org/10.1002/hc.520020414>.
- (33) de la Torre, A.; Tona, V.; Maulide, N. Reversing Polarity: Carbonyl α -Aminations with Nitrogen Nucleophiles. *Angew. Chem. Int. Ed.* **2017**, *56* (41), 12416–12423. <https://doi.org/10.1002/anie.201702937>.

- (34) Alajarin, M.; Marin-Luna, M.; Vidal, A. Recent Highlights in Ketenimine Chemistry. *Eur. J. Org. Chem.* **2012**, 2012 (29), 5637–5653. <https://doi.org/10.1002/ejoc.201200383>.
- (35) Dodd, R. H.; Cariou, K. Ketenimines Generated from Ynamides: Versatile Building Blocks for Nitrogen-Containing Scaffolds. *Chem. - Eur. J.* **2018**, 24 (10), 2297–2304. <https://doi.org/10.1002/chem.201704689>.
- (36) Winter, H.-W.; Wentrup, C. N-Ethynylamines of the Type $R-NH-C\equiv C-H$. *Angew. Chem. Int. Ed. Engl.* **1980**, 19 (9), 720–721. <https://doi.org/10.1002/anie.198007201>.
- (37) Chopade, P. R.; Louie, J. [2+2+2] Cycloaddition Reactions Catalyzed by Transition Metal Complexes. *Adv. Synth. Catal.* **2006**, 348 (16–17), 2307–2327. <https://doi.org/10.1002/adsc.200600325>.
- (38) Gephart, R. T.; Warren, T. H. Copper-Catalyzed Sp^3 C–H Amination. *Organometallics* **2012**, 31 (22), 7728–7752. <https://doi.org/10.1021/om300840z>.
- (39) Bordwell, F. G.; Cheng, J. Pei.; Harrelson, J. A. Homolytic Bond Dissociation Energies in Solution from Equilibrium Acidity and Electrochemical Data. *J. Am. Chem. Soc.* **1988**, 110 (4), 1229–1231. <https://doi.org/10.1021/ja00212a035>.
- (40) Rumble, J. R., ed. Physical Constants of Organic Compounds. In *CRC Handbook of Chemistry and Physics, 100th Edition (Internet Version 2019)*; CRC press/Taylor&Francis, Boca Raton, FL; p Table 3, Entry 47.
- (41) Warren, T. H. C-H BOND AMINATION AND OLEFIN AZIRIDINATION WITH BETA-DIKETIMINATO COPPER CATALYSTS. WO2008/073781A3, June 19, 2008.
- (42) Du, X.; Huang, Z. Advances in Base-Metal-Catalyzed Alkene Hydrosilylation. *ACS Catal.* **2017**, 7 (2), 1227–1243. <https://doi.org/10.1021/acscatal.6b02990>.
- (43) Baek, Y.; Betley, T. A. Catalytic C–H Amination Mediated by Dipyrin Cobalt Imidos. *J. Am. Chem. Soc.* **2019**, 141 (19), 7797–7806. <https://doi.org/10.1021/jacs.9b01262>.
- (44) Frisch, M. J.; Trucks, G. W.; Schlegel, H. B.; Scuseria, G. E.; Robb, M. A.; Cheeseman, J. R.; Scalmani, G.; Barone, V.; Mennucci, B.; Petersson, G. A.; Nakatsuji, H.; Caricato, M.; Li, X.; Hratchian, H. P.; Izmaylov, A. F.; Bloino, J.; Zheng, G.; Sonnenberg, J. L.; Hada, M.; Ehara, M.; Toyota, K.; Fukuda, R.; Hasegawa, J.; Ishida, M.; Nakajima, T.; Honda, Y.; Kitao, O.; Nakai, H.; Vreven, T.; Montgomery, J. A., Jr.; Peralta, J. E.; Ogliaro, F.; Bearpark, M.; Heyd, J. J.; Brothers, E.; Kudin, K. N.; Staroverov, V. N.; Kobayashi, R.; Normand, J.; Raghavachari, K.; Rendell, A.; Burant, J. C.; Iyengar, S. S.; Tomasi, J.; Cossi, M.; Rega, N.; Millam, N. J.; Klene, M.; Knox, J. E.; Cross, J. B.; Bakken, V.; Adamo, C.; Jaramillo, J.; Gomperts, R.; Stratmann, R. E.; Yazyev, O.; Austin, A. J.; Cammi, R.; Pomelli, C.; Ochterski, J. W.; Martin, R. L.; Morokuma, K.; Zakrzewski, V. G.; Voth, G. A.; Salvador, P.; Dannenberg, J. J.; Dapprich, S.; Daniels, A. D.; Farkas, Ö.; Foresman, J. B.; Ortiz, J. V.; Cioslowski, J.; Fox, D. J. *Gaussian 09, Revision E.01*; Gaussian, Inc., Wallingford, CT, 2009.
- (45) Stephens, P. J.; Devlin, F. J.; Chabalowski, C. F.; Frisch, M. J. Ab Initio Calculation of Vibrational Absorption and Circular Dichroism Spectra Using Density Functional Force

- Fields. *J. Phys. Chem.* **1994**, *98* (45), 11623–11627. <https://doi.org/10.1021/j100096a001>.
- (46) Grimme, S.; Ehrlich, S.; Goerigk, L. Effect of the Damping Function in Dispersion Corrected Density Functional Theory. *J. Comput. Chem.* **2011**, *32* (7), 1456–1465. <https://doi.org/10.1002/jcc.21759>.
- (47) Ditchfield, R.; Hehre, W. J.; Pople, J. A. Self-Consistent Molecular-Orbital Methods. IX. An Extended Gaussian-Type Basis for Molecular-Orbital Studies of Organic Molecules. *J. Chem. Phys.* **1971**, *54* (2), 724–728. <https://doi.org/10.1063/1.1674902>.
- (48) Balabanov, N. B.; Peterson, K. A. Systematically Convergent Basis Sets for Transition Metals. I. All-Electron Correlation Consistent Basis Sets for the 3d Elements Sc–Zn. *J. Chem. Phys.* **2005**, *123* (6), 064107. <https://doi.org/10.1063/1.1998907>.
- (49) Pullmann, T.; Engendahl, B.; Zhang, Z.; Hölscher, M.; Zanotti-Gerosa, A.; Dyke, A.; Franciò, G.; Leitner, W. Quinaphos and Dihydro-Quinaphos Phosphine-Phosphoramidite Ligands for Asymmetric Hydrogenation. *Chem. - Eur. J.* **2010**, *16* (25), 7517–7526. <https://doi.org/10.1002/chem.201000063>.
- (50) Dougan, S. J.; Melchart, M.; Habtemariam, A.; Parsons, S.; Sadler, P. J. Phenylazo-Pyridine and Phenylazo-Pyrazole Chlorido Ruthenium(II) Arene Complexes: Arene Loss, Aquation, and Cancer Cell Cytotoxicity. *Inorg. Chem.* **2006**, *45* (26), 10882–10894. <https://doi.org/10.1021/ic061460h>.
- (51) Dieck, H. tom; Svoboda, M.; Greiser, T. Bis(Diazadien)Metall(O)-Komplexe, IV. Nickel(O)-Bis(Chelate) Mit Aromatischen N-Substituenten/ Bis(Diazadiene)Metal(O) Complexes, IV. Nickel(O)-Bis(Chelates) with Aromatic N-Substituents. *Z. Für Naturforschung B* **1981**, *36* (7), 823–832. <https://doi.org/10.1515/znB-1981-0709>.
- (52) Vojáčková, P.; Chalupa, D.; Prieboj, J.; Nečas, M.; Švenda, J. Enantioselective Conjugate Additions of 2-Alkoxy carbonyl-3(2*H*)-Furanones. *Org. Lett.* **2018**, *20* (22), 7085–7089. <https://doi.org/10.1021/acs.orglett.8b03039>.
- (53) Dinjus, E.; Gorski, I.; Uhlig, E.; Walther, H. Nickel(0)-Komplexe mit der zentralen Koordinationseinheit NiN₂P₂. *Z. Für Anorg. Allg. Chem.* **1976**, *422* (1), 75–79. <https://doi.org/10.1002/zaac.19764220110>.
- (54) Spencer, D. J. E.; Aboelella, N. W.; Reynolds, A. M.; Holland, P. L.; Tolman, W. B. β -Diketiminato Ligand Backbone Structural Effects on Cu(I)/O₂ Reactivity: Unique Copper-Superoxo and Bis(μ -Oxo) Complexes. *J. Am. Chem. Soc.* **2002**, *124* (10), 2108–2109. <https://doi.org/10.1021/ja017820b>.
- (55) Badiei, Y. M.; Dinescu, A.; Dai, X.; Palomino, R. M.; Heinemann, F. W.; Cundari, T. R.; Warren, T. H. Copper-Nitrene Complexes in Catalytic C–H Amination. *Angew. Chem. Int. Ed.* **2008**, *47* (51), 9961–9964. <https://doi.org/10.1002/anie.200804304>.
- (56) Wiese, S.; Badiei, Y. M.; Gephart, R. T.; Mossin, S.; Varonka, M. S.; Melzer, M. M.; Meyer, K.; Cundari, T. R.; Warren, T. H. Catalytic C–H Amination with Unactivated Amines through Copper(II) Amides. *Angew. Chem. Int. Ed.* **2010**, *49* (47), 8850–8855. <https://doi.org/10.1002/anie.201003676>.

- (57) Mazik, M.; Hartmann, A.; Jones, P. G. Highly Effective Recognition of Carbohydrates by Phenanthroline-Based Receptors: α - versus β -Anomer Binding Preference. *Chem. - Eur. J.* **2009**, *15* (36), 9147–9159. <https://doi.org/10.1002/chem.200900664>.

Chapter 6

Mechanistic Investigations of Nickamine-Catalyzed Hydrosilylation of Alkenes

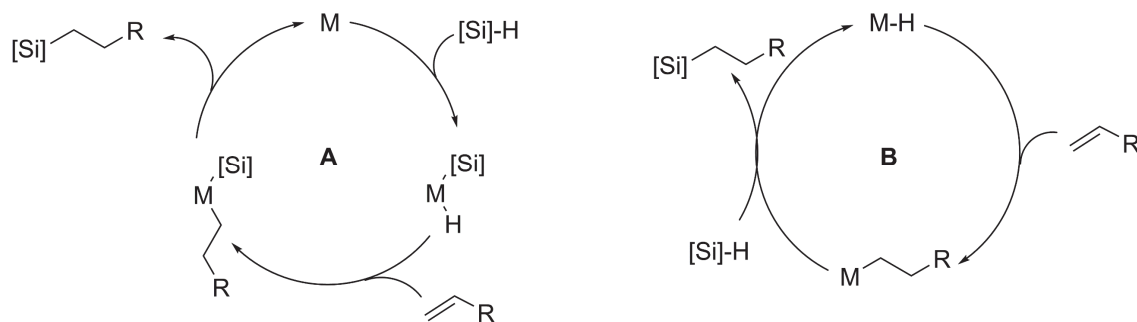
6.1 Introduction

Hydrosilylation of unsaturated carbon-carbon bonds is an important industrial process for the synthesis of organo silanes, as well as for the production of silicone polymers.¹ Typically, the reaction is catalysed by platinum complexes, such as Speier's catalyst² or Karstedt's catalyst.³ However, because of the scarcity of platinum, efforts have been made to develop hydrosilylation catalysts based on more abundant metals,^{4,5} including nickel.⁶

For platinum, the most widely accepted mechanism is the model proposed by Chalk and Harrod.^{7,8} It consists of oxidative addition of the hydrosilane, followed by hydride insertion into the alkene and reductive elimination of the product silane to close the catalytic cycle (Scheme 6.1A). For various catalysts, a modified Chalk-Harrod mechanism has been proposed, wherein silyl insertion occurs rather than hydride insertion,⁹ or a different resting state is observed.¹⁰ Despite these small differences, these models still follow a general scheme of oxidative addition of the H-Si bond and subsequent addition of the fragments to the alkene through insertion and reductive elimination.

A fundamentally different mechanism is often observed for early transition metals¹¹ and rare earth metals,¹² but also proposed for later transition metals.¹³ It consists of a metal hydride species that undergoes migratory insertion with the alkene. The resulting metal alkyl species then undergoes sigma-bond metathesis with the hydrosilane, releasing the product and regenerating the metal hydride (Scheme 6.1B).

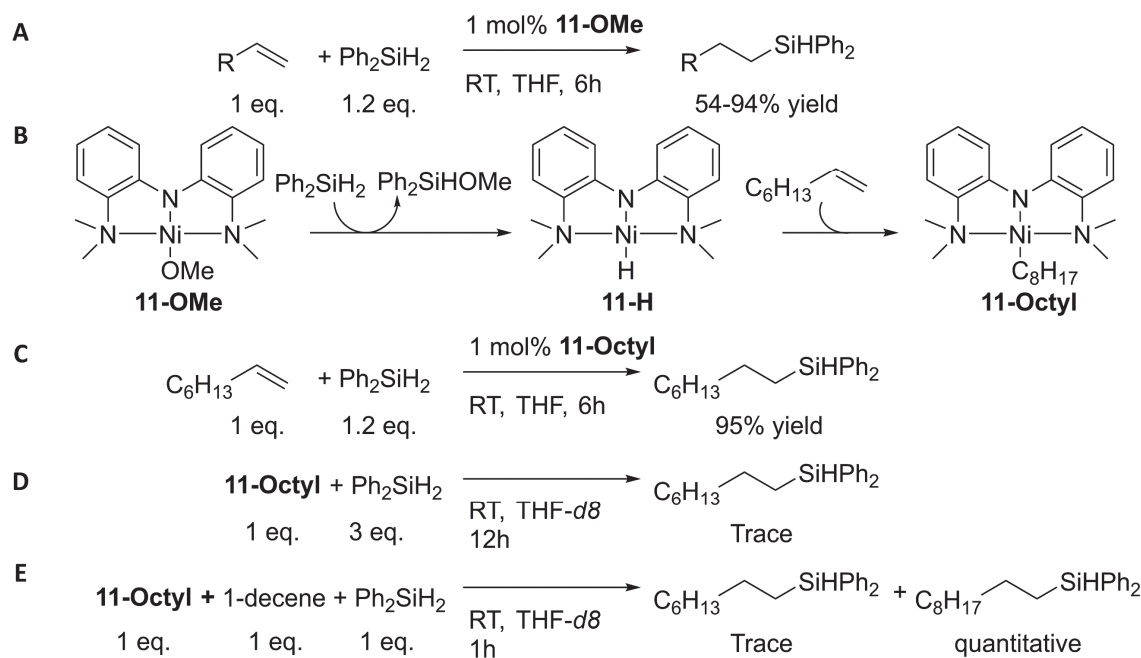
Scheme 6.1: Common catalytic cycles for hydrosilylation. A: Chalk-Harrod. B: sigma bond metathesis.



Recently, different mechanisms have been proposed involving silyl radical formation and radical addition to the alkene.^{14,15} These findings indicate that the full scope of mechanistic possibilities for hydrosilylation is yet to be uncovered. Another potential blind spot in the mech-

anistic landscape could be metal-ligand cooperativity, which has been observed for Si-H activation¹⁶ and in carbonyl hydrosilylation,^{17,18} but is not yet demonstrated for alkene hydrosilylation to the best of our knowledge.

Scheme 6.2: Preliminary mechanistic experiments presented in the thesis of Dr. Buslov



Recently, our group developed alkene hydrosilylation with high regio- and chemoselectivity using a nickel pincer complex **11-OMe** as catalyst (Scheme 6.2A).¹⁹ Although the data were not published in the article, Dr. Ivan Buslov performed preliminary mechanistic studies on this catalytic system and presented the following key findings in his doctoral thesis.²⁰ (1) As previously reported,²¹ **11-OMe** is readily converted to **11-H** in the presence of diphenylsilane, which is in turn readily converted to **11-octyl** in the presence of 1-octene (Scheme 6.2B). Under catalytic conditions, **11-H** is observed in the initial stages, but then decays over time, while **11-octyl** builds up initially and then reaches a plateau. (2) **11-octyl** can be used as catalyst in lieu of **11-OMe**, with excellent yields (Scheme 6.2C) and **11-octyl** is still observable at the end of the reaction under these conditions. (3) A reaction between **11-octyl** and diphenylsilane yields only trace amounts of product over a duration twice as long as double the standard time for catalysis (Scheme 6.2D). (4) A stoichiometric reaction between **11-octyl**, diphenylsilane and 1-decene formed diphenyldecylsilane, without only traces of diphenyloctylsilane (Scheme 6.2E).

Combined, these findings point towards **11-octyl** as the resting state, but with the octyl group

as a spectator ligand, rather than a reactive moiety that is converted into the product. This indicates a mechanism different from any Chalk-Harrod variations, or models containing sigma bond metathesis. In this chapter, a more in-depth analysis of the hydrosilylation mechanism by **11-octyl** was performed, in search of a heretofore undiscovered mechanistic pathway for alkene hydrosilylation.

6.2 Reaction progress monitoring by *in situ* ^1H NMR

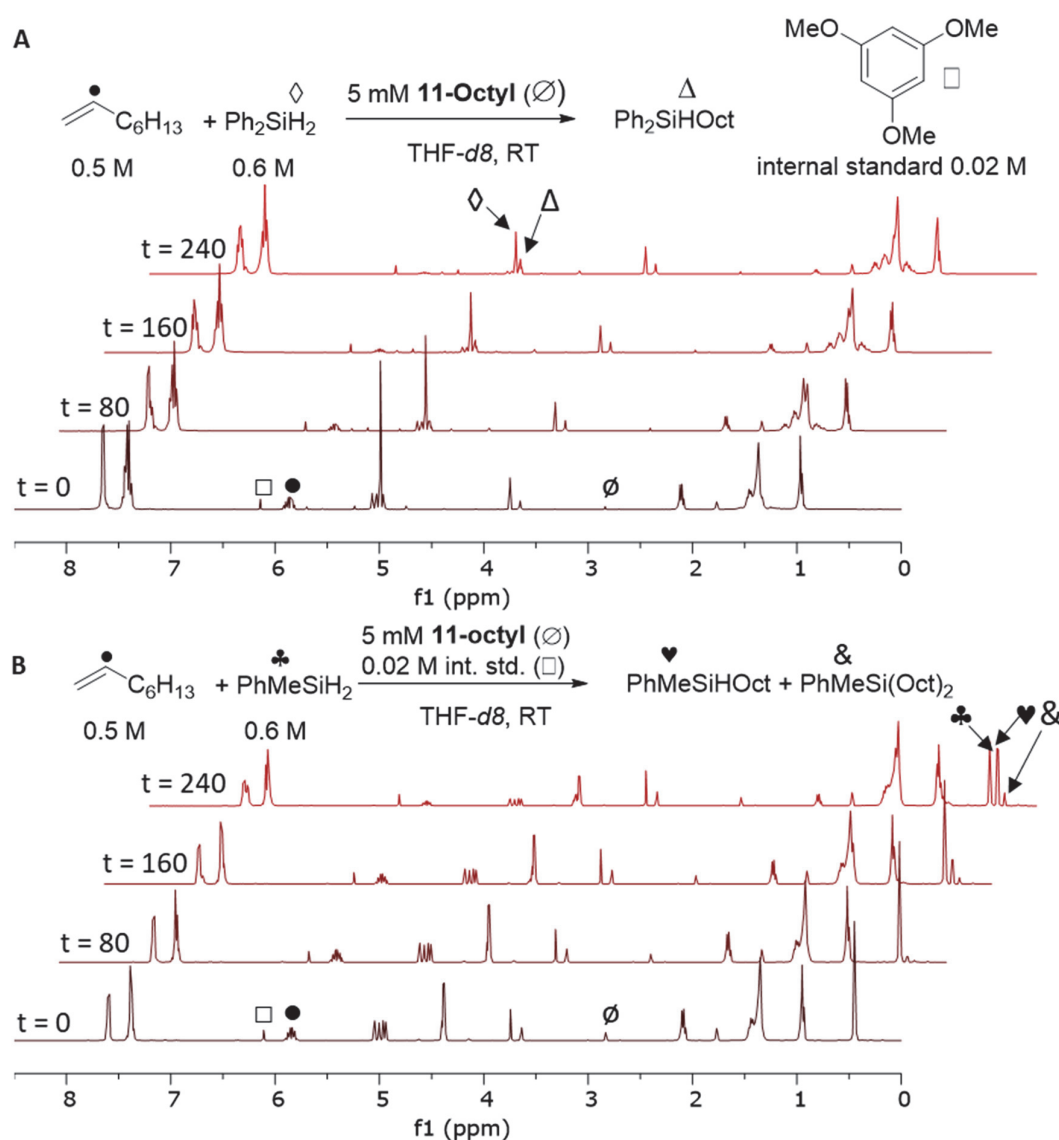


Figure 6.1: (A) Reaction scheme and selected spectra from reaction monitoring with ^1H NMR for the reaction between 1-octene and diphenylsilane. (B) Reaction scheme and selected spectra from reaction monitoring with ^1H NMR for the reaction between 1-octene and phenylmethylsilane. The symbols indicate which protons were used for quantification. Time is indicated in minutes.

NMR is a useful technique for studying the course of a reaction *in situ* if both starting material and products can be quantified independently. Unfortunately, using the standard substrates used in Buslov's study led to overlapping peaks of the silane protons of the starting material and product, complicating their accurate quantification and kinetic analysis (Figure 6.1A).

Therefore, phenylmethylsilane was used for the hydrosilylation instead. While the Si-H signals of starting material and product still overlap, the Si-Me hydrogen shifts are well-resolved (Figure 6.1B). The overalkylation byproduct can also be quantified. Moreover, despite the 1 mol% loading, the catalyst can be readily quantified using the 12-proton signal of the dimethylamino moiety.

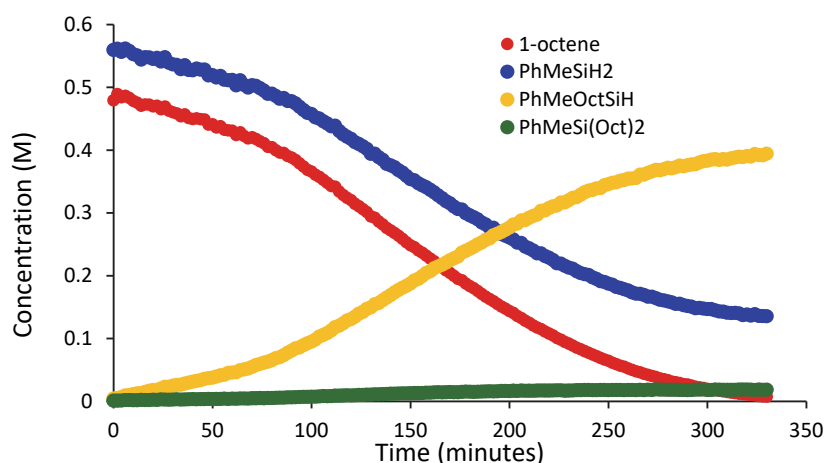


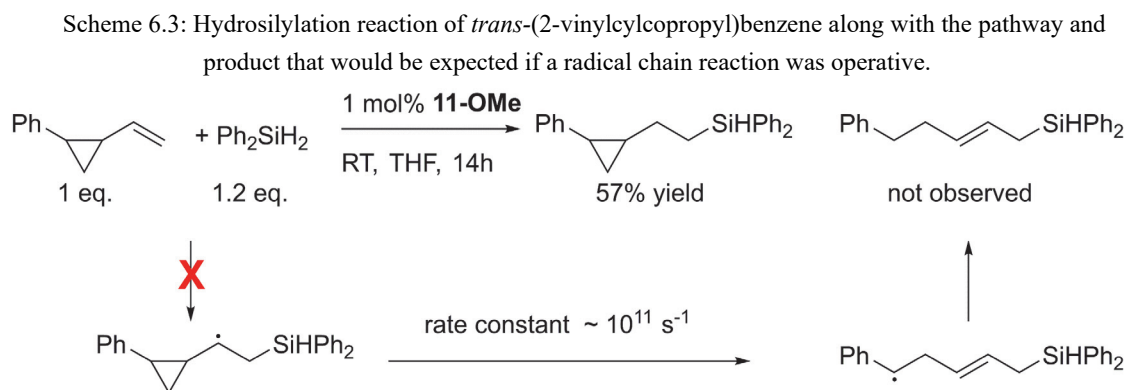
Figure 6.2: Concentration of starting materials and products over time. Conditions as in figure 6.1B.

Figure 6.2 shows the concentration of different species versus reaction time. Over the course of the NMR experiment, the yield of desired product phenylmethyloctylsilane is 84% based on converted 1-octene. By considering the overalkylated byproduct, 92% of the converted 1-octene can be accounted for. Various other products could be observed in GC-MS, but they could not be reliably quantified by NMR. Nonetheless, the vast majority of relevant species, including the catalyst, can be tracked, which allows for kinetic analysis of the reaction.

Interestingly, the reaction has an initial slow period of around 80 minutes, after which both the consumption of starting materials and the formation of product accelerate (Figure 6.2). An induction period like this could be an indication of catalyst activation,²² auto-catalysis,²³ or a radical chain reaction with slow initiation.²⁴

A radical chain reaction could be excluded by the hydrosilylation reaction of *trans*-(2-vinylcyclopropyl)benzene. The reaction leads to anti-markovnikov hydrosilylation with a 57% yield

(Scheme 6.3). No ring opening product was observed, despite the high ring opening rate for a radical alpha to the cyclopropyl ring.²⁵



A closer look at the concentration of **11-octyl** over time is given in Table 6.1 and Figure 6.3A. The minimal difference in [**11-octyl**] at the beginning and end of the reaction explains why the decay had remained unnoticed in previous mechanistic studies. However, following the reaction over time reveals a small, but statistically significant downward slope. The decay rate follows the qualitative trend of conditions with double [phenylmethylsilane] > conditions with double [**11-octyl**] > conditions with double [1-octene] > standard conditions (Figure 3A). Interestingly, this is the inverse of a qualitative trend in the length of induction period for the hydrosilylation reaction under these conditions (conditions with double [phenylmethylsilane] < conditions with double [**11-octyl**] < conditions with double [1-octene] \approx standard conditions, Figure 6.3B). These data indicate that the decay of **11-octyl** is an activation pathway towards the real catalyst.

Table 6.1: Fate of [**11-octyl**] during catalysis

Deviation from standard conditions ^a	[11-octyl] remaining after 6 hours ^b	Linear regression ^c	
		Slope (M min ⁻¹)	R ²
None	94%	-6.8(1)*10 ⁻⁷	0.955
Double [1-octene] ₀	95%	-7.8(2)*10 ⁻⁷	0.891
Double [PhMeSiH ₂] ₀	80%	-2.78(3)*10 ⁻⁶	0.912
Double [11-octyl] ₀	93%	-2.35(3)*10 ⁻⁶	0.980

^aStandard conditions are as in figure 6.1B. ^bPercentage relative to first measured concentration. ^cDecay of [**11-octyl**] modelled linearly. Value in parentheses denotes the standard error of the slope

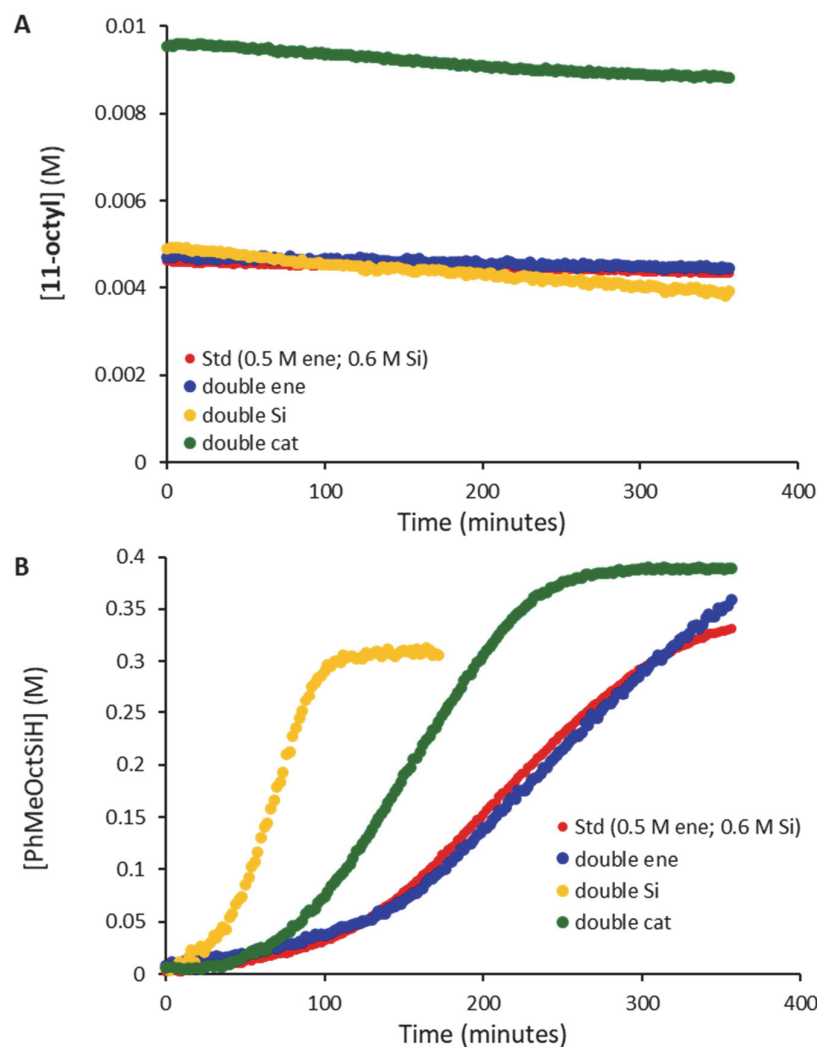


Figure 6.3: (A) Catalyst concentration versus time under different catalytic conditions. (B) Product formation versus time under different catalytic conditions. Standard conditions are as in figure 6.1B.

6.3 Determination of true catalyst

Due to the low concentration of the catalyst and the minimal conversion of it during catalysis, the identity of the decay product from the catalyst is difficult to determine. One possibility would be the formation of nickel particles. This is not unprecedented for compounds this type of complex, since it is known to occur for **11-H**.^{20,21}

6.3.1 Ex situ TEM

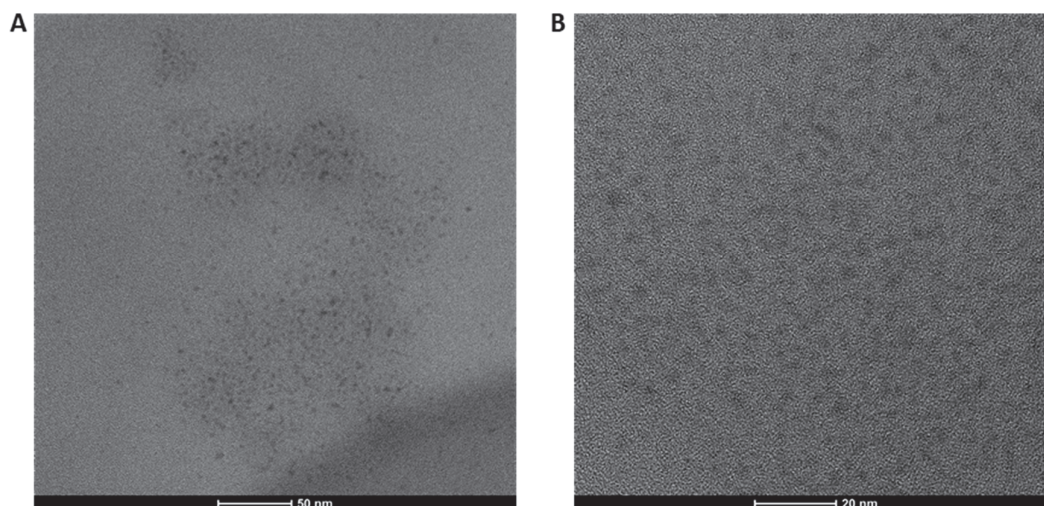


Figure 6.4: Dark field TEM images of samples prepared from N-allylcarbazole versus 1-octene hydrosilylation competition experiments (see figure 6.5) with (A) 3.5 mM nickel and (B) 8.75 mM nickel.

Transmission electron microscopy (TEM) samples were prepared from competition reaction mixtures (*vide infra*) after 6 hours reaction time. Some particle formation could be observed in samples with different concentrations of nickel (figure 6.4). Importantly, such particles were not observed in a sample prepared with pure **11-octyl**, indicating the particles are not formed from the remaining **11-octyl** in the reaction mixture under the electron beam or during sample preparation. Unfortunately, the large amount of organic residues, derived from the hydrosilylation products and starting materials led to a low quality of the images and precluded energy dispersive X-ray spectroscopy (EDX) elemental mapping and statistical analysis for determination of the size distribution of the particles.

While the TEM images indicate that particulate nickel may be formed, the *ex situ* nature of the experiment does not allow to make any statements about whether these are catalytically active, or merely inactive decomposition products.

6.3.2 Mercury test

A hydrosilylation reaction in the presence of 1600 equivalents of mercury with respect to total nickel concentration gave an NMR yield of only 1.5% over 6 hours. **11-octyl** was still present at a concentration approximately 90% of the starting concentration. Moreover, the colour of the

THF solution at the end of the reaction was the same dark red colour as **11-octyl**, whereas reaction mixtures in absence of mercury turn brown over time. The observations support the hypothesis that **11-octyl** is partially transformed to nickel particles, which are responsible for catalysis and the colour change. When the mercury droplets sequester these particles, catalysis is inhibited and the colour remains red.

The observed inhibition by Hg is contradictory to the findings reported in Buslov's thesis: he observed the same yield in absence of Hg and in presence of 100 equivalents of Hg with respect to total nickel concentration.²⁰ One explanation for this would be that the mercury test is sensitive to both the Hg to catalyst ratio and the stirring rate.²⁶ 100 Equivalents of Hg could therefore simply not be enough to observe the sequestration effect, leading to a false negative.

On the other hand, the mercury test can also lead to false positives, as certain metal complexes are known to react directly with mercury.^{26–28} Although **11-octyl** itself does not react with mercury to a significant extent, as 90% of it is still remaining after 6 hours reaction time with 1600 equivalents of Hg, it is possible that its unidentified decomposition product is a mercury-sensitive nickel complex. In addition, there is the possibility of equilibration between molecular catalytic nickel species and inactive nickel clusters²⁹ at a higher rate than catalysis. Under such circumstances, even if the catalytic metal complex is itself inert to mercury, sequestration of the clusters by Hg still leads to a decrease of the complex concentration via Le Chatelier's principle. Both false positive inhibition pathways (via mercury-sensitivity and via depletion of species connected to the active catalyst through equilibration) should be sensitive to the amount of mercury added, which would explain why such a false positive is only observed under the conditions presented here and not under conditions reported by Buslov.

6.3.3 Competition experiments

To better differentiate between catalysis by nickel particles and catalysis by a heretofore unidentified nickel complex derived from **11-octyl**, substrate competition experiments were performed. This tool has already proven useful to differentiate molecular catalysis from cluster catalysis for reactions catalysed by palladium.³⁰ In principle, when two substrates compete for reactivity with the same catalytic species, the outcome should be dependent on the respective rate constants and the concentrations of different substrates, but not on the concentration of the catalytic species. However, agglomeration rates change non-linearly with the concentration of available metal atoms.^{31–33} Therefore, the shape and size of particulate nickel should change

with total nickel concentration (or factors influencing reduction of precursors to Ni(0)). Different sizes and shapes of particles lead to different reactivity and therefore could lead to a different selectivity pattern in competition experiments. Thus, the selectivity between two substrates should be unaffected by concentration for molecular catalysis, but may change for particulate catalysis.

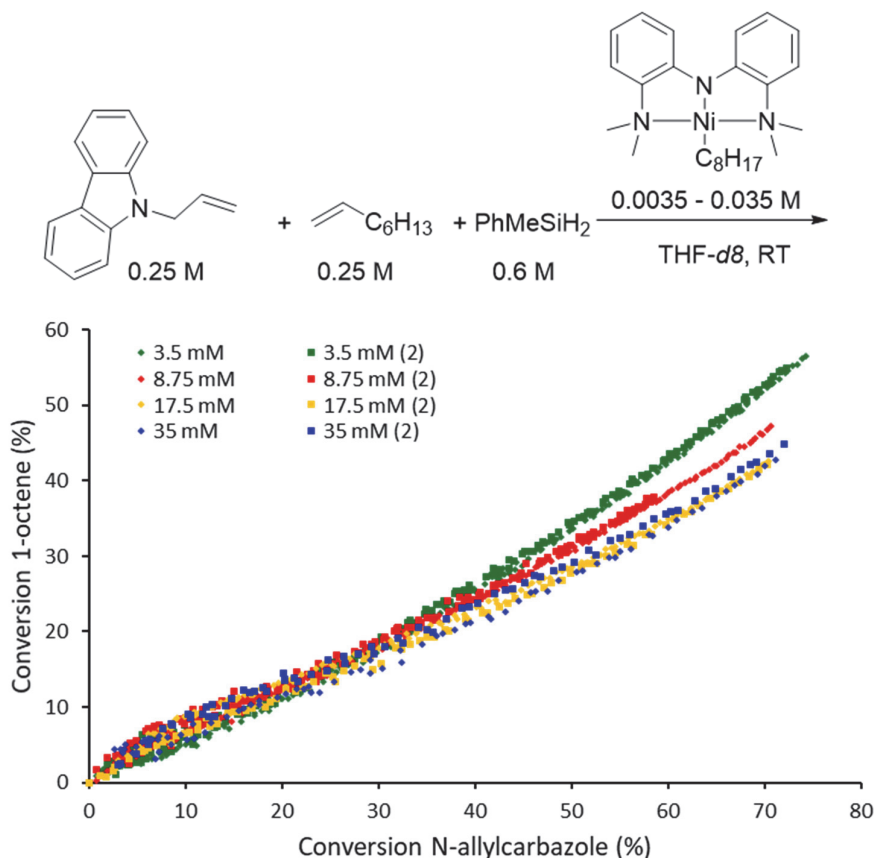


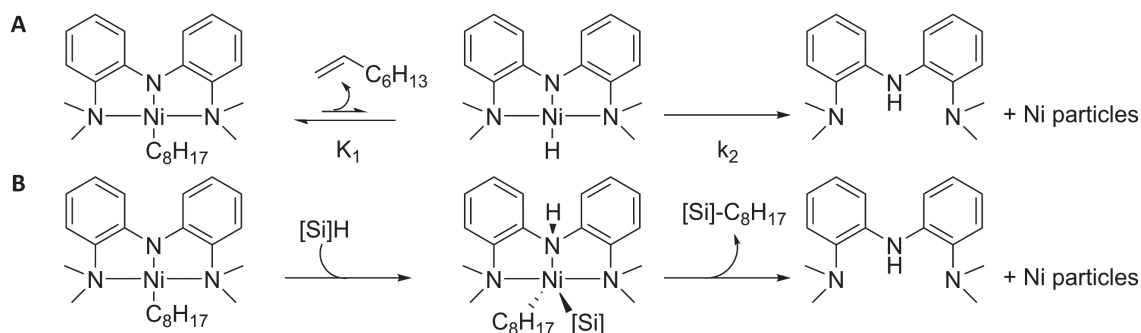
Figure 6.5: Competition experiments between N-allylcarbazole and 1-octene at different concentrations of catalyst precursor **11-octyl**. Conversions determined by NMR (see methods section for details). Two runs of each condition are plotted to show the good agreement between them.

Figure 6.5 shows a plot of conversion of 1-octene versus the conversion of N-allylcarbazole at different concentrations of nickel. A plot like this allows for a direct visual comparison of catalyst selectivity under different conditions. From the graph it is clear that the selectivity changes as the nickel concentration is increased from 3.5 mM to 17.5 mM (0.7 – 3.5 mol% with respect to total alkene concentration). The difference between the conditions is especially noticeable at a high alkene conversion level. The difference between conditions is also larger than the difference between two runs under the same conditions. At the even higher concentration

of 35 mM (7 mol%), the error becomes too large to clearly differentiate between this concentration and 17.5 mM. Nonetheless, the difference in selectivity between conditions closest to those applied in standard catalysis (1 mol% Ni) supports the hypothesis of particulate nickel being responsible for catalysis.

6.4 Mechanism of decomposition **11-octyl**

Scheme 6.4: Potential pathways for decomposition of **11-octyl**.



Two possible pathways for the decomposition of **11-octyl** may be considered. On the one hand, it is possible that beta-hydride elimination occurs, releasing 1-octene and generating a nickel hydride complex (Scheme 6.4A). Although this is an uphill process, it has been indirectly demonstrated to occur through isomerization reactions.³⁴ The nickel hydride formed in this manner is known to decompose to nickel particles either by itself,²¹ or in presence of a silane.²⁰ Alternatively, **11-octyl** may react with the silane directly in a metal-ligand cooperative pathway (Scheme 6.4B). Following reductive elimination of the alkylsilane, Ni(0) can release the ligand and agglomerate. Both pathways can account for the results of hydrosilylation of 1-decene with stoichiometric **11-octyl** reported by dr. Buslov (Scheme 6.2E): there is either just a small amount of 1-octene generated during catalyst activation to compete with 1-decene (scheme 6.4A), or only a small amount of octylsilane is generated before enough active catalyst is generated to consume all silanes with 1-decene (Scheme 6.4B).

To probe the mechanism of decomposition of the catalyst precursor, its decomposition was monitored by NMR. Since the decomposition is too slow under standard conditions (see Figure 6.3A) for extraction of kinetic parameters from the decay trace, these studies were performed at 40°C.

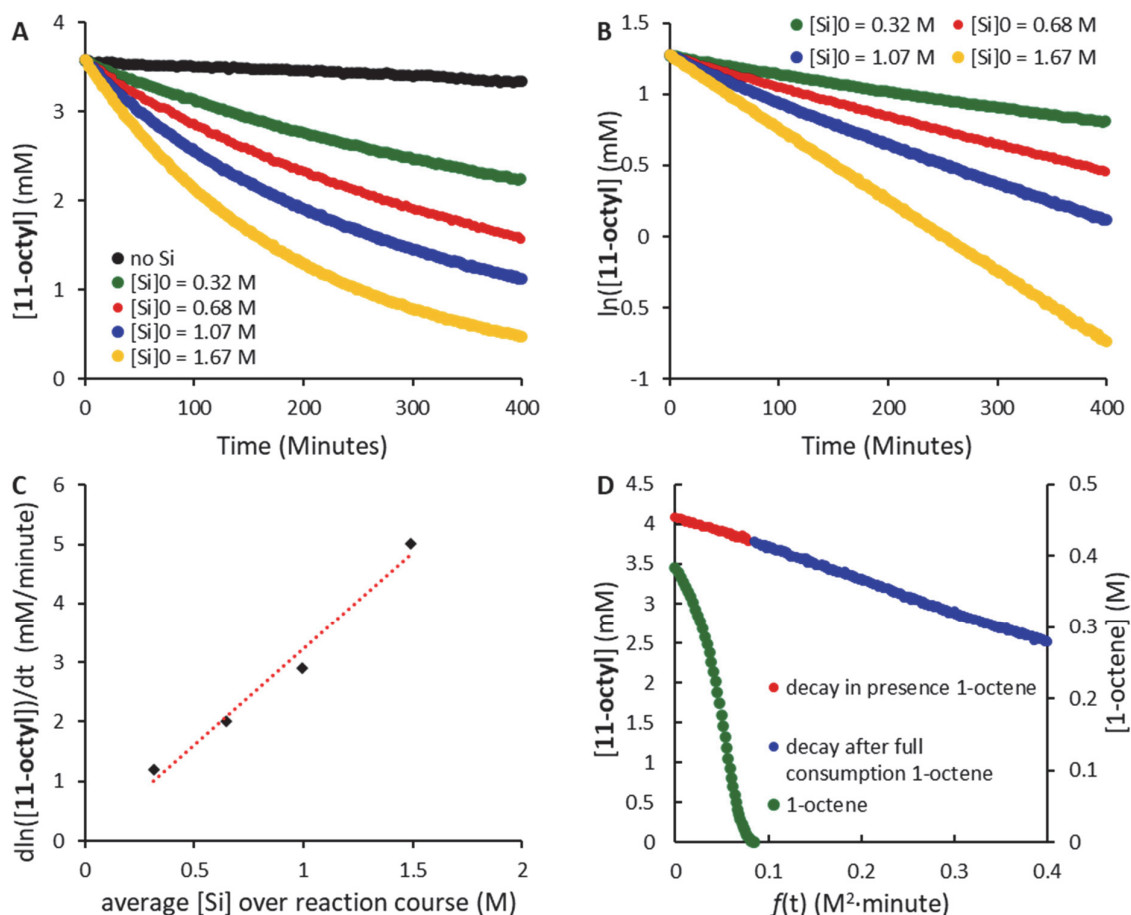


Figure 6.6: Decay of **11-octyl** at 40°C in THF-*d*8 followed by ¹H NMR. Si means PhMeSiH₂. (A) Concentration of **11-octyl** versus time with various amounts of starting concentration of silane. (B) Same data of A, but $\ln([11\text{-octyl}])$ now plotted to demonstrate first order in nickel. (C) Slopes of the traces in B plotted against the silane concentration to demonstrate first order in silane. The average concentration over time of the silane is taken, as a slight decrease in concentration is observed during the reaction. (D) Hydrosilylation reaction of 1-octene with excess PhMeSiH₂ followed by ¹H NMR. **11-octyl** is plotted on the left y-axis, while $[1\text{-octene}]$ is plotted on the right y-axis. The x-axis is equation 6.1

Under these conditions, **11-octyl** still decomposes slowly by itself (Figure 6.6A, black trace). However, in presence of phenylmethylsilane, the decomposition speeds up considerably. Figure 6.6B shows the natural logarithm of **11-octyl** decreases linearly in time with all the tested concentrations of phenylmethylsilane, indicating a pseudo-first order reaction. The observed rate constant for this reaction shows a linear relation with the concentration of silane (Figure 6.6C). Finally, when a hydrosilylation reaction of 1-octene was set up at 40°C with excess phenylmethylsilane, there is no difference in decay rate of **11-octyl** in presence or absence of 1-octene (Figure 6.6 D). Moreover, the concentration of **11-octyl** shows a linear relation with $f(t)$ (equation 6.1).

$$f(t) = \sum_{i=1}^n \left(\frac{[\mathbf{11-octyl}]_i + [\mathbf{11-octyl}]_{i-1}}{2} \right)^1 \left(\frac{[\text{PhMeSiH}_2]_i + [\text{PhMeSiH}_2]_{i-1}}{2} \right)^1 (t_i - t_{i-1}) \quad (6.1)$$

This linearity indicates all variables that influence the decay rate of **11-octyl** are included in $f(t)$.³⁵ Thus, with the data from Figure 6.6 a rate law for the decomposition of **11-octyl** can be formulated (equation 6.2). This rate law is incompatible with scheme 6.4A, since that should lead to equation 6.3, or either of its simplifications, equations 6.4 or 6.5, none of which is equivalent to equation 6.2.

$$\frac{-d[\mathbf{11-octyl}]}{dt} = k[\mathbf{11-octyl}][\text{PhMeSiH}_2] \quad (6.2)$$

$$\frac{-d[\mathbf{11-octyl}]}{dt} = \frac{k_1 k_2 [\mathbf{11-octyl}][\text{PhMeSiH}_2]}{k_{-1}[\mathbf{1-octene}] + k_2[\text{PhMeSiH}_2]} \quad (6.3)$$

$$\frac{-d[\mathbf{11-octyl}]}{dt} = K_1 \frac{k_2 [\mathbf{11-octyl}][\text{PhMeSiH}_2]}{[\mathbf{1-octene}]} \quad (k_2[\text{PhMeSiH}_2] \ll k_{-1}[\mathbf{1-octene}]) \quad (6.4)$$

$$\frac{-d[\mathbf{11-octyl}]}{dt} = k_1[\mathbf{11-octyl}] \quad (k_2[\text{PhMeSiH}_2] \gg k_{-1}[\mathbf{1-octene}]) \quad (6.5)$$

Additional evidence against the pathway of Scheme 6.4A can be obtained from performing catalytic hydrosilylation of styrene with **11-octyl** as precatalyst. The equilibrium depicted in scheme 6.4A would suggest some conversion from **11-octyl** to **11-(2-phenylethyl)**. A reaction between **11-OMe**, phenylmethylsilane and styrene in THF-*d*8 leads to a peak at -0.20 ppm with a coupling pattern reminiscent of **11-octyl**, so we assign it to **11-(2-phenylethyl)** (Figure 6.7A). This shift is distinct enough from **11-octyl** (-0.48 ppm) for a shift due to equilibration according to Scheme 6.4A to be observable. However, when hydrosilylation of styrene with **11-octyl** as pre-catalyst was followed by ¹H NMR, only **11-octyl** could be observed (see Figure 6.7B).

Thus, on the basis of kinetics and the styrene hydrosilylation experiment, the decay mechanism depicted in Scheme 6.4A can be excluded. We therefore consider the mechanism depicted in Scheme 6.4B the most likely mechanism for the activation of the catalyst.

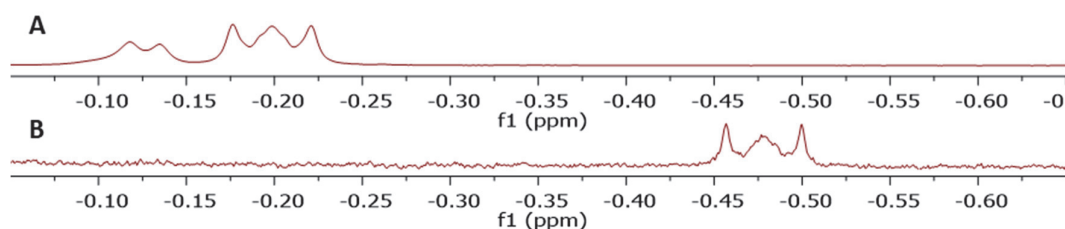


Figure 6.7: (A) Section of ¹H NMR of reaction mixture containing **11-OMe**, PhMeSiH₂ and styrene in THF-*d*8. (B) Section of ¹H NMR measured at the end of a hydrosilylation reaction of styrene with **11-octyl** as precatalyst.

6.5 Discussion on TOF

The turnover frequency was previously determined at 83000 h^{-1} , which made the catalytic system already among the most active catalysts for alkene hydrosilylation.¹⁹ In this perspective, the finding that only a small amount of the added nickel complex is converted to the true catalyst would mean that the true TOF is an incredibly high number, particularly compared to that observed for other nickel nanoparticles (1700 h^{-1}).³⁶ However, a few nuances should be considered.

Firstly, the TOF was measured in neat conditions. With 1.2 equivalents of diphenylsilane to 1-octene, this would lead to a silane concentration of roughly 3.2 M (ignoring any changes in volume upon mixing the 1-octene and silane). This is considerably higher than any of the concentrations used in this chapter. Therefore, the decay of **11-octyl** should be faster than what is reported herein.

Secondly, the hydrosilylation reaction is exothermic and the reaction mixture is reported to heat up considerably under the neat reaction conditions. This is another difference with the conditions used in this chapter that should increase the decay rate of **11-octyl**.

Finally, the pre-catalyst used in the TOF experiment was **11-OMe**, rather than **11-octyl**. Although the conversion from one to the other was reported to occur cleanly, this was studied in THF solution. The higher concentration of silane and the increased temperature may well lead to the direct formation of nickel nanoparticles from the sensitive **11-H** intermediate to some extent, rather than clean formation of **11-octyl**, which then has to decay. Thus, the error in the reported TOF due to incomplete pre-catalyst activation may be smaller than initially apparent from Figure 6.3 and 6.6.

Regarding the large difference in TOF with the other reported nickel nanoparticle catalyst, it should be considered that a different reaction is studied (1-decene rather than 1-octene and trimethoxysilane rather than diphenylsilane). Not only should this change kinetics to some extent, but factors such as exothermicity of the reaction and heat capacity of the medium also play a role because of the neat setup. Finally, it should be noted that the environment of nickel nanoparticles can have a strong influence on their reactivity,³⁷ so the manner in which they are generated could be an important factor.

6.6 Conclusions

Through a detailed mechanistic study, we have revealed that a hydrosilylation reaction previously believed to occur with a molecular nickel catalyst, is in reality catalysed by nickel nanoparticles. In addition, we propose a mechanism for the conversion of the pre-catalyst to nickel(0) that is consistent with both our results and previously reported experiments.

The results presented in this study underline the importance of thorough mechanistic research, since changes in the nature of the catalytic species can be subtle and may be easily missed with superficial mechanistic probes.

6.7 Experimental

6.7.1 General experimental methods

All reactions were set up and performed under inert nitrogen atmosphere using standard glove box techniques. Deuterated solvents were subjected to three freeze-pump-thaw cycles before storage on 4Å molecular sieves in the glove box. After 24 hours, the solvent was decanted onto fresh 4Å molecular sieves and stored for at least an additional 24 hours prior to usage. The other solvents were purified using a two-column solid-state purification system (Innovative Technology, NJ, USA) and transferred to the glovebox after three freeze-pump-thaw cycles. 1-octene (GC standard) was purchased from TCI and stored on 4Å molecular sieves at -30°C in the glove box. Phenylmethylsilane was purchased from Aldrich and distilled and subjected to three freeze-pump-thaw cycles before storage on 4Å molecular sieves at -30°C in the glove box. **11-Cl**,³⁸ **11-OMe**,³⁹ N-allylcarbazole⁴⁰ and *trans*-(2-vinylcyclopropyl)benzene⁴¹ were prepared according to literature procedures. NMR spectra were recorded on a Bruker Avance 400 Spectrometer. ¹H and ¹³C{¹H} chemical shifts were referenced internally to residual solvent signals. Elemental analyses were performed on a Carlo Erba EA 1110 CHN instrument at EPFL. HRMS measurements were performed at the EPFL ISIC Mass Spectrometry Service. TEM was measured on a FEI Talos instrument. Liquid chromatography was performed with a Biotage Isolera One flash purification system.

6.7.2 Synthesis **11-octyl**

11-Cl (376 mg, 1.08 mmol) was dissolved in 5.5 mL THF in the glove box. The solution was cooled down to -47°C with a toluene cooling bath. 0.68 mL of a solution of *n*-BuLi in hexanes (1.6 M, 1.1 mmol) was added slowly. The conversion of **11-Cl** was periodically checked by taking an aliquot for NMR. If the conversion was not complete after 12 hours, additional *n*-BuLi solution was added. After complete conversion, the cooling bath was removed and volatiles were removed in vacuo. The residue was extracted with *n*-pentane and filtered over celite. Evaporation of the filtrate yielded a viscous dark red oil. Yield: 409 mg (89%). **^1H NMR** (400 MHz, Benzene- d_6): δ 7.61 (d, $J = 8.3$ Hz, 2H), 7.06 (t, $J = 7.8$ Hz, 2H), 6.63 (d, $J = 8.0$ Hz, 2H), 6.44 (t, $J = 7.6$ Hz, 2H), 2.41 (s, 12H), 1.62-1.30 (m, 12H), 0.94 (t, $J = 5.4$ Hz, 3H), -0.43 - -0.53 (m, 2H). **^{13}C NMR** (101 MHz, C_6D_6): δ 149.24, 147.58, 128.24, 119.43, 114.07, 113.84, 49.60, 35.22, 32.54, 30.16, 30.15, 29.99, 23.24, 14.44, 10.53. **Elemental Analysis:** Anal. Calcd for $\text{C}_{24}\text{H}_{37}\text{N}_3\text{Ni}$: C, 67.62; H, 8.75; N, 9.86. Found: C, 67.56; H, 8.72; N, 10.05. The compound is thermally labile, but is stable for at least three months when stored at -30°C in the glove box.

6.7.3 NMR-followed hydrosilylation of 1-octene

Three stock solutions in THF- d_8 were prepared in oven dried 1 mL volumetric flasks: (1) **11-octyl** (13.3 mg, 0.0312 mmol) with 1,3,5-trimethoxybenzene (21.0 mg, 0.125 mmol); (2) methylphenylsilane (520 μL , 3.74 mmol) and (3) 1-octene (490 μL , 3.12 mmol). For preparation of the reaction mixtures, the required amount of the three stock solutions was mixed (for standard conditions, this is 80 μL of each stock solution) with an amount of THF- d_8 to make the total amount of added liquid 500 μL . The silane stock solution was always the final addition. The mixture was then immediately transferred to an oven dried J-young's NMR tube. After locking and shimming the sample, the NMR machine was programmed to perform a single scan ^1H experiment every 2 minutes. The program was generally started 7-9 minutes after the addition of the silane stock solution to the reaction mixture. Concentrations of the observed species were determined by normalizing against the aryl-CH peak of 1,3,5-trimethoxybenzene (6.06 ppm). The volume was always presumed to be 0.5 mL, neglecting any changes in volume due to mixing. Stock solutions were stored at -30°C in the glove box in between measurements.

6.7.4 Hydrosilylation of *trans*-(2-vinylcyclopropyl)benzene

Trans-(2-vinylcyclopropyl)benzene (75.1 mg, 0.521 mmol) and **11-OMe** (1.9 mg, 0.0055 mmol) were dissolved in 0.5 mL THF. Diphenylsilane (114 mg, 0.619 mmol) was added and the reaction was stirred for 16 hours. The solution was then loaded onto silica with hexane and volatiles were evaporated. Liquid Chromatography was done with 100% hexane as eluent. Diphenyl(*trans*-2-phenylcyclopropyl)ethyl)silane was obtained as a colourless oil (98 mg, 0.298 mmol, 57% yield). **¹H NMR** (400 MHz, Chloroform-*d*): δ 7.88 – 7.56 (m, 4H), 7.53 – 7.40 (m, 6H), 7.34 (t, J = 7.6 Hz, 2H), 7.26 – 7.19 (m, 1H), 7.15 – 7.08 (m, 2H), 5.01 (t, J = 3.7 Hz, 1H), 1.79 – 1.60 (m, 3H), 1.48 – 1.41 (m, 2H), 1.28 – 1.18 (m, 1H), 0.97 (dt, J = 8.4, 4.9 Hz, 1H), 0.85 (dt, J = 8.6, 5.2 Hz, 1H). **¹³C NMR** (101 MHz, CDCl₃): δ 143.98, 135.25, 134.56, 129.70, 128.35, 128.14, 125.73, 125.31, 29.43, 26.71, 23.55, 16.55, 12.08. **HRMS (APPI/QTOF)**: calculated for (M^{+} : C₂₃H₂₄Si⁺) 328.1642, found 328.1638.

6.7.5 Mercury test

To an oven dried scintillation vial was added 800 mg Hg (3.99 mmol). 260 μ L THF-*d*8 and 80 μ L of each stock solution from section 6.7.3 were added and the mixture was stirred (800 rpm) at RT in the glove box for 6 hours. The mixture was then allowed to settle and the THF-*d*8 solution was carefully transferred to an NMR tube, making sure no mercury was transferred. The mixture was analysed with ¹H NMR, determining the concentrations by normalization against 1,3,5-trimethoxybenzene.

6.7.6 Alkene competition

Three stock solutions in THF-*d*8 were prepared in oven dried 1 mL volumetric flasks: (1) **11-octyl** (37.3 mg, 0.0875 mmol) with 1,3,5-trimethoxybenzene (23.0 mg, 0.137 mmol); (2) methylphenylsilane (520 μ L, 3.74 mmol) and (3) 1-octene (250 μ L, 1.59 mmol) and N-allylcarbazole (327 mg, 1.58 mmol). For preparation of the reaction mixtures, the required amount of the three stock solutions was mixed with an amount of THF-*d*8 to make the total amount of added liquid 500 μ L. The silane stock solution was always the final addition. The mixture was then immediately transferred to an oven dried J-young's NMR tube. After locking and shimming the sample, the NMR machine was programmed to perform a single scan ¹H

experiment every 2 minutes (every 5 minutes for the 3.5 mM traces). The program was generally started 7-9 minutes after the addition of the silane stock solution to the reaction mixture. Concentrations of the observed species were determined by normalizing against the aryl-CH peak of 1,3,5-trimethoxybenzene (6.06 ppm). The volume was always presumed to be 0.5 mL, neglecting any changes in volume due to mixing. The concentration at the first measured point was taken as 0% conversion for both alkene substrates. Stock solutions were stored at -30°C in the glove box in between measurements.

6.7.7 TEM sample preparation

At the end of the reaction competition NMR experiment, three drops of the reaction mixture were placed onto a TEM grid. The grid was then allowed to dry in the glove box overnight. For the sample of pristine **11-octyl**, 5 mg was dissolved in 100 μ L pentane. From this solution, 3 drops were placed onto a TEM grid. The grid was then allowed to dry in the glove box overnight.

6.7.8 Study of **11-octyl** decomposition

Two stock solutions in THF-*d*8 were prepared in oven dried 1 mL volumetric flasks: (1) **11-octyl** (11.0 mg, 0.0258 mmol) with 1,3,5-trimethoxybenzene (18.4 mg, 0.109 mmol) and (2) methylphenylsilane (420 μ L, 3.02 mmol). For preparation of the reaction mixtures, the required amount of the two stock solutions was mixed with an amount of THF-*d*8 to make the total amount of added liquid 500 μ L. The silane stock solution was always the final addition. The mixture was then immediately transferred to an oven dried J-young's NMR tube. After locking and shimming the sample, the NMR probe temperature was set to 313K and the NMR machine was programmed to perform a single scan ^1H experiment every 2 minutes for the two highest silane concentrations and every 3 minutes for the two lowest silane concentrations. After the probe temperature had stabilized, the shimming generally needed to be corrected manually. Any spectra with mis-shapen peaks due to non-equilibrated temperature or bad shimming were ignored. Concentrations of the observed species were determined by normalizing against the aryl-CH peak of 1,3,5-trimethoxybenzene (6.06 ppm). The volume was always presumed to be 0.5 mL, neglecting any changes in volume due to mixing. For the 1-octene experiment (Figure

6.6D), the 1-octene was added neat and its volume was assumed to be 0. Stock solutions were stored at -30°C in the glove box in between measurements.

6.7.9 Spectroscopic characterisation **1-(2-phenylethyl)**

11-OMe (34.7 mg, 0.101 mmol) was dissolved in 500 μ L THF-*d*8. 58 μ L styrene (0.503 mmol) was added. While stirring, 14 μ L phenylmethylsilane (0.101 mmol) was then added. The mixture immediately turned brown-orange. After stirring for 5 minutes, the mixture was transferred to an NMR tube to record the ^1H spectrum.

6.7.10 NMR-followed hydrosilylation of styrene

200 μ L of the **11-octyl** stock from section 6.7.8. was mixed with 150 μ L THF-*d*8 and 29 μ L styrene (0.252 mmol). 150 μ L silane stock from section 6.7.8. was added and the mixture was transferred to an oven dried J-Young' s NMR tube. The NMR probe temperature was set to 313K. The NMR machine was then programmed to measure a single-scan ^1H spectrum every minute. No negative-shift peaks were observed during the reaction other than the one assigned to **11-octyl**. The spectrum displayed in Figure 6.7B is measured at a point where the concentration of styrene is estimated at less than 1 mM, at the very end of the hydrosilylation reaction.

6.8 References

- (1) Troegel, D.; Stohrer, J. Recent Advances and Actual Challenges in Late Transition Metal Catalyzed Hydrosilylation of Olefins from an Industrial Point of View. *Coordination Chemistry Reviews* **2011**, *255* (13–14), 1440–1459. <https://doi.org/10.1016/j.ccr.2010.12.025>.
- (2) Speier, J. L.; Webster, J. A.; Barnes, G. H. The Addition of Silicon Hydrides to Olefinic Double Bonds. Part II. The Use of Group VIII Metal Catalysts. *J. Am. Chem. Soc.* **1957**, *79* (4), 974–979. <https://doi.org/10.1021/ja01561a054>.
- (3) Karstedt, B. D.; General Electric Company. Platinum Complexes of Unsaturated Siloxanes and Platinum Containing Organopolysiloxanes. US3775452A, 1973.
- (4) Obligation, J. V.; Chirik, P. J. Earth-Abundant Transition Metal Catalysts for Alkene Hydrosilylation and Hydroboration. *Nat Rev Chem* **2018**, *2* (5), 15–34. <https://doi.org/10.1038/s41570-018-0001-2>.
- (5) Du, X.; Huang, Z. Advances in Base-Metal-Catalyzed Alkene Hydrosilylation. *ACS Catal.* **2017**, *7* (2), 1227–1243. <https://doi.org/10.1021/acscatal.6b02990>.
- (6) Nakajima, Y.; Sato, K.; Shimada, S. Development of Nickel Hydrosilylation Catalysts. *The Chemical Record* **2016**, *16* (5), 2379–2387. <https://doi.org/10.1002/tcr.201600056>.
- (7) Chalk, A. J.; Harrod, J. F. Homogeneous Catalysis. II. The Mechanism of the Hydrosilylation of Olefins Catalyzed by Group VIII Metal Complexes ¹. *J. Am. Chem. Soc.* **1965**, *87* (1), 16–21. <https://doi.org/10.1021/ja01079a004>.
- (8) Meister, T. K.; Riener, K.; Gigler, P.; Stohrer, J.; Herrmann, W. A.; Kühn, F. E. Platinum Catalysis Revisited—Unraveling Principles of Catalytic Olefin Hydrosilylation. *ACS Catal.* **2016**, *6* (2), 1274–1284. <https://doi.org/10.1021/acscatal.5b02624>.
- (9) A. Schroeder, M.; S. Wrighton, M. Pentacarbonyliron(0) Photocatalyzed Reactions of Trialkylsilanes with Alkenes. *Journal of Organometallic Chemistry* **1977**, *128* (3), 345–358. [https://doi.org/10.1016/S0022-328X\(00\)92207-1](https://doi.org/10.1016/S0022-328X(00)92207-1).
- (10) Duckett, S. B.; Perutz, R. N. Mechanism of Homogeneous Hydrosilylation of Alkenes by (η⁵-Cyclopentadienyl)Rhodium. *Organometallics* **1992**, *11* (1), 90–98. <https://doi.org/10.1021/om00037a022>.
- (11) Jia, L.; Zhao, J.; Ding, E.; Brennessel, W. W. Synthesis, Structures, and Alkene Hydrosilylation Activities of Neutral Tripodal Amidozirconium Alkyls. *J. Chem. Soc., Dalton Trans.* **2002**, No. 13, 2608–2615. <https://doi.org/10.1039/b200789d>.
- (12) Fu, P.-F.; Brard, L.; Li, Y.; Marks, T. J. Regioselection and Enantioselection in Organolanthanide-Catalyzed Olefin Hydrosilylation. A Kinetic and Mechanistic Study. *J. Am. Chem. Soc.* **1995**, *117* (27), 7157–7168. <https://doi.org/10.1021/ja00132a015>.

- (13) Brookhart, M.; Grant, B. E. Mechanism of a Cobalt(III)-Catalyzed Olefin Hydrosilylation Reaction: Direct Evidence for a Silyl Migration Pathway. *J. Am. Chem. Soc.* **1993**, *115* (6), 2151–2156. <https://doi.org/10.1021/ja00059a008>.
- (14) Vijaykumar, G.; Pariyar, A.; Ahmed, J.; Shaw, B. K.; Adhikari, D.; Mandal, S. K. Tuning the Redox Non-Innocence of a Phenalenyl Ligand toward Efficient Nickel-Assisted Catalytic Hydrosilylation. *Chem. Sci.* **2018**, *9* (10), 2817–2825. <https://doi.org/10.1039/C7SC04687A>.
- (15) Zhou, R.; Goh, Y. Y.; Liu, H.; Tao, H.; Li, L.; Wu, J. Visible-Light-Mediated Metal-Free Hydrosilylation of Alkenes through Selective Hydrogen Atom Transfer for Si–H Activation. *Angew. Chem. Int. Ed.* **2017**, *56* (52), 16621–16625. <https://doi.org/10.1002/anie.201711250>.
- (16) Higashi, T.; Kusumoto, S.; Nozaki, K. Cleavage of Si–H, B–H, and C–H Bonds by Metal–Ligand Cooperation: Focus Review. *Chem. Rev.* **2019**, *119* (18), 10393–10402. <https://doi.org/10.1021/acs.chemrev.9b00262>.
- (17) Hesp, K. D.; McDonald, R.; Ferguson, M. J.; Stradiotto, M. New Cationic and Zwitterionic $\text{Cp}^*\text{M}(\kappa^2\text{-P,S})$ Complexes (M = Rh, Ir): Divergent Reactivity Pathways Arising from Alternative Modes of Ancillary Ligand Participation in Substrate Activation. *J. Am. Chem. Soc.* **2008**, *130* (48), 16394–16406. <https://doi.org/10.1021/ja8062277>.
- (18) Fuchs, J.; Irran, E.; Hrobárik, P.; Klare, H. F. T.; Oestreich, M. Si–H Bond Activation with Bullock’s Cationic Tungsten(II) Catalyst: CO as Cooperating Ligand. *J. Am. Chem. Soc.* **2019**, *141* (47), 18845–18850. <https://doi.org/10.1021/jacs.9b10304>.
- (19) Buslov, I.; Becouse, J.; Mazza, S.; Montandon-Clerc, M.; Hu, X. Chemoselective Alkene Hydrosilylation Catalyzed by Nickel Pincer Complexes. *Angewandte Chemie International Edition* **2015**, *54* (48), 14523–14526. <https://doi.org/10.1002/anie.201507829>.
- (20) Buslov, I. Chapter 2: Chemoselective Alkene Hydrosilylation Catalyzed by Nickel Pincer Complexes. In *Nickel-Catalyzed Hydrosilylation of Alkenes and Transition-Metal-Free Intermolecular α -C-H Amination of Ethers*; École Polytechnique Fédérale de Lausanne, 2016; pp 47–80.
- (21) Breitenfeld, J.; Scopelliti, R.; Hu, X. Synthesis, Reactivity, and Catalytic Application of a Nickel Pincer Hydride Complex. *Organometallics* **2012**, *31* (6), 2128–2136. <https://doi.org/10.1021/om201279j>.
- (22) Martínez-Carrión, A.; Howlett, M. G.; Alamillo-Ferrer, C.; Clayton, A. D.; Bourne, R. A.; Codina, A.; Vidal-Ferran, A.; Adams, R. W.; Burés, J. Kinetic Treatments for Catalyst Activation and Deactivation Processes Based on Variable Time Normalization Analysis. *Angew. Chem. Int. Ed.* **2019**, *58* (30), 10189–10193. <https://doi.org/10.1002/anie.201903878>.
- (23) Sankaralingam, M.; Lee, Y.-M.; Nam, W.; Fukuzumi, S. Selective Oxygenation of Cyclohexene by Dioxygen via an Iron(V)-Oxo Complex-Autocatalyzed Reaction. *Inorg. Chem.* **2017**, *56* (9), 5096–5104. <https://doi.org/10.1021/acs.inorgchem.7b00220>.

- (24) Sy Piecco, K. W. E.; Aboelenen, A. M.; Pyle, J. R.; Vicente, J. R.; Gautam, D.; Chen, J. Kinetic Model under Light-Limited Condition for Photoinitiated Thiol–Ene Coupling Reactions. *ACS Omega* **2018**, *3* (10), 14327–14332. <https://doi.org/10.1021/acsomega.8b01725>.
- (25) Newcomb, M.; Johnson, C. C.; Manek, M. B.; Varick, T. R. Picosecond Radical Kinetics. Ring Openings of Phenyl-Substituted Cyclopropylcarbinyl Radicals. *J. Am. Chem. Soc.* **1992**, *114* (27), 10915–10921. <https://doi.org/10.1021/ja00053a031>.
- (26) Chernyshev, V. M.; Astakhov, A. V.; Chikunov, I. E.; Tyurin, R. V.; Eremin, D. B.; Ranny, G. S.; Khrustalev, V. N.; Ananikov, V. P. Pd and Pt Catalyst Poisoning in the Study of Reaction Mechanisms: What Does the Mercury Test Mean for Catalysis? *ACS Catal.* **2019**, *9* (4), 2984–2995. <https://doi.org/10.1021/acscatal.8b03683>.
- (27) Gorunova, O. N.; Novitskiy, I. M.; Grishin, Y. K.; Gloriov, I. P.; Roznyatovsky, V. A.; Khrustalev, V. N.; Kochetkov, K. A.; Dunina, V. V. When Applying the Mercury Poisoning Test to Palladacycle-Catalyzed Reactions, One Should Not Consider the Common Misconception of Mercury(0) Selectivity. *Organometallics* **2018**, *37* (17), 2842–2858. <https://doi.org/10.1021/acs.organomet.8b00363>.
- (28) Ehara, K.; Kumagaya, K.; Yamamoto, Y.; Takahashi, K.; Yamazaki, H. Unusual Reductive Behaviour of a Trans-NiI₂(RNC)₂ Complex at Mercury and Platinum Electrodes. *Journal of Organometallic Chemistry* **1991**, *410* (3), C49–C53. [https://doi.org/10.1016/0022-328X\(91\)83017-X](https://doi.org/10.1016/0022-328X(91)83017-X).
- (29) Eremin, D. B.; Ananikov, V. P. Understanding Active Species in Catalytic Transformations: From Molecular Catalysis to Nanoparticles, Leaching, “Cocktails” of Catalysts and Dynamic Systems. *Coordination Chemistry Reviews* **2017**, *346*, 2–19. <https://doi.org/10.1016/j.ccr.2016.12.021>.
- (30) Schmidt, A. F.; Kurokhtina, A. A.; Larina, E. V. Differential Selectivity Measurements and Competitive Reaction Methods as Effective Means for Mechanistic Studies of Complex Catalytic Reactions. *Catal. Sci. Technol.* **2014**, *4* (10), 3439–3457. <https://doi.org/10.1039/C4CY00479E>.
- (31) Bhattacharyya, K. X.; Pradel, C.; Lecante, P.; Mézailles, N. Mechanistic Investigations of the Synthesis of Size-Tunable Ni Nanoparticles by Reduction of Simple Ni^{II} Diamide Precursors. *Chem. Eur. J.* **2017**, *23* (39), 9352–9361. <https://doi.org/10.1002/chem.201701258>.
- (32) Schmidt, A. F.; Al-Halalqa, A.; Smirnov, V. V. Effect of Macrokinetic Factors on the Ligand-Free Heck Reaction with Non-Activated Bromoarenes. *Journal of Molecular Catalysis A: Chemical* **2006**, *250* (1–2), 131–137. <https://doi.org/10.1016/j.molcata.2006.01.051>.
- (33) Aiken, J. D.; Finke, R. G. Nanocluster Formation Synthetic, Kinetic, and Mechanistic Studies. [†] The Detection of, and Then Methods To Avoid, Hydrogen Mass-Transfer Limitations in the Synthesis of Polyoxoanion- and Tetrabutylammonium-Stabilized, Near-Monodisperse 40 ± 6 Å Rh(0) Nanoclusters. *J. Am. Chem. Soc.* **1998**, *120* (37), 9545–9554. <https://doi.org/10.1021/ja9719485>.

- (34) Breitenfeld, J.; Vechorkin, O.; Corminboeuf, C.; Scopelliti, R.; Hu, X. Why Are (NN₂)Ni Pincer Complexes Active for Alkyl–Alkyl Coupling: β -H Elimination Is Kinetically Accessible but Thermodynamically Uphill. *Organometallics* **2010**, *29* (17), 3686–3689. <https://doi.org/10.1021/om1007506>.
- (35) Burés, J. Variable Time Normalization Analysis: General Graphical Elucidation of Reaction Orders from Concentration Profiles. *Angewandte Chemie International Edition* **2016**, *55* (52), 16084–16087. <https://doi.org/10.1002/anie.201609757>.
- (36) Buslov, I.; Song, F.; Hu, X. An Easily Accessed Nickel Nanoparticle Catalyst for Alkene Hydrosilylation with Tertiary Silanes. *Angew. Chem. Int. Ed.* **2016**, *55* (40), 12295–12299. <https://doi.org/10.1002/anie.201606832>.
- (37) Galeandro-Diamant, T.; Suleimanov, I.; Veyre, L.; Bousquié, M.; Meille, V.; Thieuleux, C. Alkene Hydrosilylation with Supported and Unsupported Ni Nanoparticles: Strong Influence of the Ni Environment on Activity and Selectivity. *Catal. Sci. Technol.* **2019**, *9* (7), 1555–1558. <https://doi.org/10.1039/C8CY01487F>.
- (38) Csok, Z.; Vechorkin, O.; Harkins, S. B.; Scopelliti, R.; Hu, X. Nickel Complexes of a Pincer NN₂ Ligand: Multiple Carbon–Chloride Activation of CH₂Cl₂ and CHCl₃ Leads to Selective Carbon–Carbon Bond Formation. *J. Am. Chem. Soc.* **2008**, *130* (26), 8156–8157. <https://doi.org/10.1021/ja8025938>.
- (39) Vechorkin, O.; Csok, Z.; Scopelliti, R.; Hu, X. Nickel Complexes of a Pincer Amidobis(Amine) Ligand: Synthesis, Structure, and Activity in Stoichiometric and Catalytic C–C Bond-Forming Reactions of Alkyl Halides. *Chem. Eur. J.* **2009**, *15* (15), 3889–3899. <https://doi.org/10.1002/chem.200802059>.
- (40) Milen, M.; Grün, A.; Bálint, E.; Dancsó, A.; Keglevich, G. Solid–Liquid Phase Alkylation of *N*-Heterocycles: Microwave-Assisted Synthesis as an Environmentally Friendly Alternative. *Synthetic Communications* **2010**, *40* (15), 2291–2301. <https://doi.org/10.1080/00397910903226166>.
- (41) Baik, J.-S.; Lee, N.-H. Mechanistic Studies on the O₂-Mediated Oxidation of Olefins in the Presence of (Schiff-Base)Mn(III) Catalyst and NaBH₄. *Bulletin of the Korean Chemical Society* **2006**, *27* (5), 765–768. <https://doi.org/10.5012/BKCS.2006.27.5.765>.

Curriculum Vitae

Name: Marten Leendert Ploeger
Date of birth: 06/07/1991
Place of birth: Hoorn NH, The Netherlands
Nationality: Dutch

Degrees

MSc (Chemistry) Molecular Design, Synthesis & Catalysis track; VU University Amsterdam and University of Amsterdam, 27th of January 2016

BSc (Pharmaceutical Sciences) VU University, Amsterdam 25th of April 2012

Research positions

01-06-2016 - present PhD student in group of prof. dr. Xile Hu at the EPFL. Mechanistic investigations of homogeneous nickel catalysis.¹⁻⁴ My PhD track is part of the EU-funded Innovative Training Network NoNoMeCat. The network allowed me to obtain experience beyond my own laboratory through temporary research stays in the laboratories of prof. dr. Bert Klein-Gebink at the University of Utrecht (design and synthesis of non-innocent ligands) and prof. dr. Jeremy Harvey at the KU Leuven (DFT calculations) as well as at the pharmaceutical production site of Abbvie Inc. in Sligo, Ireland. I have also maintained a strong scientific collaboration within the context of the network.

May - August 2013 Internship in the group of prof. dr. Paul Pringle at the University of Bristol; research towards the synthesis of borylphosphines and to their application as ligands for transition metals.⁵

June 2012 - March 2013 Internship in the group of prof. dr. Joost Reek at the University of Amsterdam: selective isomerization-hydroformylation for access to internal aldehydes.⁶

June 2011 - August 2011 Internship in the group of prof. dr. Romano Orru: Multi-component reactions in organic synthesis.⁷

Core Competences

- Synthesis and analysis of sensitive compounds
- Analysis of complex reaction mixtures and isolated compounds with GC/MS, NMR, FTIR, EPR and HRMS.
- Experience with complex mechanistic analysis through kinetic analysis, Hammett plots, differential selectivity experiments and designing tailor-made experiments for testing hypotheses.
- Maintaining a strong research collaboration with researchers from a field outside of my expertise.
- Basic understanding of DFT calculations.

Publications

- (1) Ploeger, M.L.; Darù, A.; Harvey, J.N.; Hu, X. *ACS Catalysis*. 2020, 10, 2845-2854
- (2) Cheung, Chi Wai; Ploeger, Marten L.; Hu, Xile *Chem. Sci.* **2018**, 9, 655-659
- (3) Cheung, Chi Wai; Ploeger, Marten L.; Hu, Xile *ACS Catalysis* **2017**, 7, 7092-7096
- (4) Cheung, Chi Wai; Ploeger, Marten L.; Hu, Xile *Nat. Commun.* **2016**, 8, 14878
- (5) Bailey, Jonathan A.; Ploeger, Marten; Pringle, Paul G. *Inorg Chem* **2014**, 53(14) 7763-7769

(6) Dydio, Pawel; Ploeger, Marten; and Reek, Joost N.H. *ACS Catalysis* **2013**, 3(12) 2939-2942
(7) Kruithof, Art; Ploeger, Marten L.; Janssen, Elwin; Helliwell, Madeleine; de Kanter, Frans J.J.; Ruijter, Eelco; and Orru, Romano V.A. *Molecules* **2012**, 17(2) 1675-1685

Awards

SCGC teaching excellence award EPFL, 2018

Academic presentations

Poster presentation: Summer school “Physical Methods in Molecular and Heterogeneous Catalysis”
September 2017, Gelsenkirchen, Germany

Poster presentation: SCS Fall meeting, September 2018, Lausanne, Switzerland

Poster presentation: XX1st The Netherlands’ Catalysis and Chemistry Conference, March 2019,
Noordwijkerhout, The Netherlands

Language skills

Dutch – mother tongue

English– fluent

French – conversational

Activities outside of research

May 2012 - April 2013 Board member of PAC foundation. The PAC foundation is tasked with the organisation of a yearly chemistry symposium organised for and by students.

<https://www.pacsymposium.nl/>